# Inkjet Printing of Solid Oral Dosage Forms

Hatim Khuzemah Cader

Doctoral Thesis

Submitted to the University of Nottingham for the degree of Doctor of Philosophy

December 2018

# Abstract

Inkjet printing is a form of additive manufacturing where liquid droplets are selectively deposited onto a substrate, followed by solidification. This process can potentially be used to address limitations for the manufacturing of solid oral dosage forms or tablets. Conventional processes can be long and complex, making personalisation a major challenge.

The main aim of this thesis was to wholly inkjet a tablet capable of delivering drug with a controlled release. To achieve this a multi-material reservoir system was designed for one-directional drug release. It consisted of three components: (i) a rapidly dissolving core, (ii) an impermeable shell (base and walls) and (iii) a release controlling membrane.

The first component of the reservoir system that was developed was the rapidly dissolving core, which on its own was presented as a standalone tablet, using thiamine hydrochloride (HCl). Using a water-based ink, which was presented as a potential universal formulation for water soluble drugs, it was shown that consistent and reliable jetting behaviour was achieved. The tablet was easily removed from its substrate and could be handled without any indication of damage. Printed drug was determined to be in its desired polymorphic form and was distributed homogenously across its top and bottom surfaces, as well as across its cross-section. Rapid drug release was achieved, with 90 % of drug released within seven minutes.

The impermeable shell was printed using polycaprolactone (PCL) and N, N–dimethylacetamide (DMAC) as a solvent. The prints were seen to be very sensitive to substrate temperature. A final substrate temperature of 60 °C was selected resulting in molten PCL to form on the substrate. However, when the substrate heat was turned off, a uniform solid film formed without cracking or delamination, hence it was selected. The impermeable nature of the material was demonstrated by testing systems consisting of the rapid releasing core surrounded by printed PCL. Unless the top surface of PCL broke, PCL was effective in preventing release.

The release controlling membrane was developed with a blend of PCL and water-soluble polyvinylpyrrolidone (PVP). Surface characterisation techniques illustrated

phase separation between the materials. PVP domains were seen to be dispersed in a PCL matrix. When exposed to water, the PVP dissolved providing a pathway for drug release. With the application of this release controlling membrane (25 printed layers) controlled release was achieved and zero-order kinetics were exhibited. By varying not just the PVP loadings in the ink, but also different printing parameters, the thickness of the membrane and its pore area sizes were controlled, influencing releasing. Several different drug release profiles were achieved in this thesis including rapid, controlled extended, delayed and a bimodal (fast to slow) drug release.

# Acknowledgements

I would like to sincerely thank my supervisors Professors Ricky Wildman, Clive Roberts, Chris Tuck and Morgan Alexander. I am extremely appreciative for their guidance, support and patience in completing this PhD.

Special thanks to Dr. Andrea Domingues Gonçalves for arranging my visits to GSK and access to equipment as well as feedback on results and this thesis.

I would like to thank Dr. Graham Rance for conducting confocal Raman spectroscopy experiments and processing and analysing data. For ToF-SIMS, I would like to thank Dr. David Scurr for running a significant number of samples as well as his help in processing and understanding results. Both have provided me with a greater understanding of the work presented here.

I also would like to thank Dr. Elisabeth Steer for microtoming samples, Dr. Jane McLaren for CT scanning assistance, Dr. Long Jiang for additional ToF-SIMS help and Mr. Adrian Quinn for running samples for elemental analysis by combustion.

I thank all academic, technical, administrative and research members of the Centre for Additive Manufacturing for their help over the last few years.

I acknowledge funding from the EPSRC and GSK.

I am especially grateful to ‘Cohort 1’ of the CDT in Additive Manufacturing and 3D Printing for their support and for making my time at the University of Nottingham an enjoyable experience.

# Table of Contents

Abstract ..... i

Acknowledgements ..... iii

List of Symbols ..... ix

List of Abbreviations ..... x

List of Figures ..... xii

List of Tables ..... xxiv

1 Introduction ..... 1

1.1 Technical Background ..... 1

1.1.1 Additive manufacturing ..... 1

1.1.2 Inkjet printing ..... 3

1.1.3 Solid oral dosage forms ..... 8

1.2 Aims of Thesis ..... 14

1.3 Thesis Chapters ..... 15

1.4 Statement of Novelty ..... 16

2 Literature Review ..... 18

2.1 Introduction to Chapter ..... 18

2.1.1 Aims of chapter ..... 18

2.1.2 Background ..... 18

2.2 Inkjet Printing of Oral Pharmaceutical Dosage Forms ..... 18

2.2.1 Printing small structures and thin films for drug delivery ..... 18

2.2.2 Inkjet printing with quality control and screening processes ..... 24
2.2.3 Combining and comparing other manufacturing processes ..... 27
2.2.4 Jetting into containers for oral delivery ..... 31
2.2.5 Multi-material printing ..... 34
2.2.6 Freestanding and wholly inkjet printed tablets ..... 36
2.3 Other Additive Manufacturing Techniques for Tablet Manufacturing ..... 39
2.3.1 Binder jetting ..... 39
2.3.2 Material extrusion ..... 40
2.3.3 Stereolithography ..... 40
2.3.4 Selective laser sintering ..... 41
2.4 Identification of Gaps in State of the Art ..... 42
2.4.1 Wholly inkjet printed tablets with a non-toxic solvent evaporation solidification mechanism ..... 42
2.4.2 Multi-material inkjet printed reservoir system tablets for controlled release 43
2.5 Conclusion ..... 43
3 Inkjet Printing of Tablets with a Rapid Drug Release ..... 45
3.1 Introduction ..... 45
3.1.1 Aims of chapter ..... 45
3.1.2 Background ..... 45
3.2 Materials and Methods ..... 47
3.2.1 Materials ..... 47

3.2.2 Methods ..... 47
3.3 Results and Discussion ..... 52
3.3.1 Additives for ink formulation ..... 52
3.3.2 Jetting parameters ..... 55
3.3.3 Substrate selection ..... 56
3.3.4 Print formation ..... 56
3.3.5 Observed phase separation ..... 58
3.3.6 Investigation of ink jet printing's reliability ..... 63
3.3.7 Polymorph investigation ..... 64
3.3.8 Drug spatial distribution ..... 66
3.3.9 Investigating the hygroscopic nature of the tablet ..... 67
3.3.10 Drug release studies ..... 69
3.4 Conclusions ..... 71
3.5 Chapter Appendix: Supplementary Information ..... 72
4 Inkjet Printing of a Reservoir System: The Impermeable Shell ..... 77
4.1 Introduction ..... 77
4.1.1 Aims of chapter ..... 77
4.1.2 Background ..... 77
4.2 Materials and Methods ..... 80
4.2.1 Materials ..... 80
4.2.2 Methods ..... 80

4.3 Results and Discussion ..... 83
4.3.1 Ink formulation ..... 83
4.3.2 Selection of printing parameters ..... 84
4.3.3 Printing an impermeable reservoir system ..... 90
4.3.4 Illustrating the impermeable nature of the material ..... 93
4.4 Conclusions ..... 97
4.5 Chapter Appendix: Supplementary Information ..... 99
5 Inkjet Printing Reservoir Systems with a Controlled Drug Release ..... 101
5.1 Introduction ..... 101
5.1.1 Aims of chapter ..... 101
5.1.2 Background ..... 101
5.2 Materials and Methods ..... 104
5.2.1 Materials ..... 104
5.2.2 Methods ..... 104
5.3 Results and Discussion ..... 107
5.3.1 Ink formulation and printing parameters ..... 107
5.3.2 Initial characterisation of the release controlling membrane ..... 108
5.3.3 Testing the functionality of the release controlling membrane ..... 110
5.3.4 Controlling drug release behaviour ..... 117
5.3.5 Limitations of the current reservoir system ..... 130
5.4 Conclusions ..... 135

5.5 Chapter Appendix: Supplementary Information ..... 138

6 Conclusions and Future Work ..... 144

6.1 Conclusions ..... 144

6.1.1 Rapid releasing tablets ..... 144

6.1.2 Controlled release tablets ..... 146

6.2 Future work ..... 148

6.2.1 Short term considerations ..... 148

6.2.2 Long term considerations ..... 150

7 References ..... 154

# List of Symbols

| | | | |
|---|---|---|---|
| $a$ | Nozzle diameter | $W_A$ | Work of adhesion |
| $Bo$ | Bond number | $We$ | Weber number |
| $g$ | Gravitational force | $Z$ | Printability factor |
| $M_w$ | Molecular weight | $\gamma$ | Surface tension |
| $Oh$ | Ohnesorge number | $\Delta G_m$ | Gibbs free energy of melting |
| $Re$ | Reynolds number | $\Delta H_f$ | Enthalpy of fusion |
| $S_m$ | Entropy of mixing | $\Delta H_m$ | Enthalpy of melting |
| $T$ | Temperature | $\eta$ | Viscosity |
| $u$ | Ion fragment mass | $\theta$ | Contact angle |
| $v$ | Velocity | | |

# List of Abbreviations

| | |
|---|---|
| 2D | Two-dimensional |
| 3D | Three-dimensional |
| AFM | Atomic force microscopy |
| AH | Anhydrate |
| API | Active pharmaceutical ingredient |
| ASTM | American society for testing and materials |
| ATR | Attenuated total reflectance |
| CAD | Computer aided design |
| CLS | Classic least square |
| CT | Computed tomography |
| DMAC | N, N - dimethylacetamide |
| DMSO | Dimethyl sulfoxide |
| DSA | Drop shape analyser |
| DSC | Differential scanning calorimetry |
| FDA | Food and Drug Administration |
| FTIR | Fourier transform infrared spectroscopy |
| HCl | Hydrochloride |
| HH | Hemihydrate |
| HPLC | High performance liquid chromatography |
| HPMC | Hydroxypropyl methylcellulose |
| L | Layers |
| MM | Monomethanolate |
| NIR | Near-infrared |
| NMR | Nuclear magnetic resonance |

| | |
|---|---|
| NSH | Non-stoichiometric hydrate |
| ODF | Orodispersible films |
| PCL | Polycaprolactone |
| PEG | Polyethylene glycol |
| PEGDA | Polyethylene glycol diacrylate |
| PET | Polyethylene terephthalate |
| PLGA | Polylactic-co-glycolic acid |
| PVP | Polyvinylpyrrolidone |
| QR | Quick response |
| SAXS | Small angle X-ray scattering |
| SEM | Scanning electron microscopy |
| SLA | Stereolithography (additive process) |
| SLS | Selective laser sintering |
| STL | Stereolithography (file type) |
| ToF-SIMS | Time-of-flight secondary ion mass spectroscopy |
| USP | United States Pharmacopeia |
| UV | Ultra-violet |
| UV-Vis | Ultraviolet-visible |
| XRD | X-ray diffraction |

# List of Figures

Figure 1.1 - Continuous inkjet printer schematic (taken from Martin et al. 2008) [7].4

Figure 1.2 - Drop-on-demand inkjet printer with a thermal resistor controlling drop ejection (taken from Cummins and Desmulliez 2012) [8].....4

Figure 1.3 - Various DoD inkjet printer schematic with piezoelectric material controlling drop ejection (taken from Wijshoff 2010) [9]. .....5

Figure 1.4 – Visual representation of the relation between the Weber and Reynolds numbers and what values would be required for suitable jetting characteristics (taken from Derby 2010) [6].....7

Figure 1.5 - A summary overview of different manufacturing routes for solid oral dosage form production (taken from Zhang et al. 2004) [15].....9

Figure 1.6 - Some of the advantages of utilising inkjet printing for tablet production. .....14

Figure 2.1 - Thermal inkjet printed prednisolone on coated substrates after vacuum drying (taken from Meléndez et al. 2008) [36].....19

Figure 2.2 - The proposed manufacturing process by Sandler et al. 2011 with the use of an (a) inkjet printer, (b) accurate drug deposition, (c) paper substrates which can be cut which are then (d) placed in capsules (taken from Sandler et al. 2011) [40]. .21

Figure 2.3 – Fluorescence microscopy images of drug loaded PLGA microspheres with varying geometries: (a) circles, (b) grids, (c) honeycomb and (d) rings (taken from Lee et al. 2012). Scale bar = 500 μm. [41].....22

Figure 2.4 - Inkjet printed rasagiline mesylate on transparency films with increasing number of layers (taken from Genina et al. 2013a) [43].....23

Figure 2.5 - Inkjet printed theophylline formulation on a paper substrate (left) and its hyperspectral image generated with principal component analysis (right) (taken from Vakili et al. 2014) [50].....25

Figure 2.6 - Change in colour intensity as more drug containing layers were printed (taken from Wickström et al. 2016) [52]. .....26

Figure 2.7 - Printed QR code containing drug on an edible HPMC substrate (taken from Edinger et al. 2018) [54]. .....27

Figure 2.8 - Schematic representing the combination of inkjet and flexographic printing (taken from Genina et al. 2012) [55]. .....28

Figure 2.9 - A suggested work flow process presenting the key stages of inkjet printing for tablets from formulation to post printing analysis (taken from Raijada et al. 2013) [56] .....28

Figure 2.10 - Manufacturing process combining electrospinning and inkjet printing to create oromucosal dosage forms (taken from Palo et al. 2017) [58]. .....29

Figure 2.11 – Confocal Raman map showing that the inkjet printed enalapril maleate (red) did not penetrated through the ODF containing hydrochlorothiazide (green) (taken from Thabet et al. 2018a) [63]. .....30

Figure 2.12 – Schematic of the continuous coating machine and modified inkjet printing system used to create ODFs (taken from Thabet et al. 2018b) [64]. .....31

Figure 2.13 - Overview of the inkjet process for deposition of drugs into micro-devices (taken from Fox et al. 2017) [60]. .....32

Figure 2.14 - Preformed tablets cap and base (top row), base of preform tablet with inkjet printed formulation (bottom left )and the closed tablet (bottom right) (taken from Acosta-Vélez et al. 2017) [61] .....33

Figure 2.15 – Hydrophobic drug formulation was jetted into preform tablets and cured. They were then removed for characterisation (taken from Acosta-Vélez et al. 2018) [62]. .....34

Figure 2.16 - The three-layer film containing three antihypertensive drugs (taken from Scoutaris et al. 2018) [66]. .....35

Figure 2.17 - The internal solid and honeycomb structures printed. Spacing between honeycomb cells were varied (taken from Kyobula et al. 2017) [67].....36

Figure 2.18 - The different release profiles achieved as the internal honeycomb structure is varied (taken from Kyobula et al. 2017) [67].....38

Figure 2.19 - UV-cured inkjet printed tablets containing ropinirole HCl (taken from Clark et al. 2017) [68].....39

Figure 2.20 – The ZipDose process involved the layering of powder material and the jetting of a binder (taken from Aprecia, “ZipDose Technology”) [74].....39

Figure 2.21 – The material extrusion printer that was used to create paracetamol containing tablets with varying geometry to control drug release (taken from Khaled et al. 2018) [77].....40

Figure 2.22 – The stages of printing tablets using SLA with a Formlabs printer. Tablet designs are created on a computer, loaded on to the printer and final product is printed (taken from Wang et al. 2016) [80].....41

Figure 2.23 – Design, print and post-print analysis for SLS printed tablets with different structures and their significantly different release profiles (taken from Fina et al. 2018) [83].....42

Figure 3.1 - Molecular structure of thiamine HCl [88].....46

Figure 3.2 - Molecular structure of PVP [94].....46

Figure 3.3 - Molecular structure of polysorbate 20 [102].....53

Figure 3.4 - Printed tablets without glycerol. Some samples showed extensive cracking while others delaminated substantially. The delamination resulted in the print head to crash into some tablets, damaging or moving their position on the print bed.....53

Figure 3.5 - Molecular structure of glycerol [105].....54

Figure 3.6 - 3D printed tablets with glycerol.....54

Figure 3.7 - The standard and selected waveform applied during the jetting process. .....55

Figure 3.8 - The jetting of droplets. Here, 6 of the 16 nozzles of the printer are jetting simultaneously. Spherical droplets were seen consistently.....56

Figure 3.9 - Individual drops of the ink printed on PET film. .....57

Figure 3.10 - Single line (top) and film (bottom) formation of the formulation. Scale bar = 500 µm.....58

Figure 3.11 - Optical reflection images of printed films on glass slide. a) 30 minutes after printing, b) 1 day, c) 4 days, d) 8 days, e) 12 days, f) 12 days after orienting confirm the formation of a crystalline phase (cross polarised transmission OM). Scale bar = 500 µm. .....59

Figure 3.12 - Films of thiamine HCl formulation printed with varying number of layers. As additional layers are printed regions of white growth are observed. .....59

Figure 3.13 - AFM height sensor image of the top surface of 10 layers of the printed thiamine formulation. The ‘clear’ region with no white crystal growth was scanned. .....60

Figure 3.14 - AFM height sensor image of the top surface of a 100 layer printed tablet. A greater density of crystals was observed. .....61

Figure 3.15 - ToF-SIMS maps of 1layer (top) and 10 layers (bottom). The total ion intensity (left) is shown and compared to the HS- ion (right) indicative of the drug.62

Figure 3.16 - Optical profile (left) in reference optical image (right). The yellow line indicates the horizontal measurement line (from left to right) along which a Z height was measured. Scale bar (red) = 69 µm.....63

Figure 3.17 - Relation between the number of printed layers and dose of drug detected with UV-Vis spectroscopy (n=3, for layer 7 n=2).....64

Figure 3.18 - Raman spectra of the thiamine HCl powder and different printed samples all showing peak positions indicative of the NSH phase. Also shown is the drug powder exposed to the ambient environment with features of the HH phase. ..65

Figure 3.19 - Optical image (a) and CLS score map for thiamine HCl (b) from the top surface. Optical image (c) and CLS score map for thiamine HCl (d) from the bottom surface. Scale bar = 500 µm. .....67

Figure 3.20 – Mean spectra generated from the top and bottom surface lateral maps and the cross-section line measurement. .....67

Figure 3.21 - Mass variation over time of tablets in three different batches (i) an ambient uncontrolled environment, (ii) non-vacuum oven at 50 °C and (iii) a non-vacuum desiccator (n=5, for each batch, n=4 for samples in non-vacuum oven at 50 °C for day 21.).....68

Figure 3.22 - Release profiles of tablets with varying printed layers. The printed pattern's dimensions were set at 5 x 5 mm (n=3 except for 375L where n=2). .....70

Figure 3.23 - Release profiles of tablets with varying pattern dimensions. The number of layers for each print were kept at 250 layers (n=3). .....70

Figure S3.24 - Rheological flow curve of the final formulated ink (n=3). Newtonian behaviour is seen from 10 to 100 $s^{-1}$. Measurements below 3.981 $s^{-1}$ did not achieve steady state and the increase in viscosity seen at shear rates above 100 $s^{-1}$ was caused by the geometry used for measuring viscosity [113]. .....72

Figure S3.25 - ToF-SIMS spectra of pure thiamine HCl and PVP. .....72

Figure S3.26 – UV-Vis spectroscopy calibration line for thiamine dissolved in deionised water (n=3).....73

Figure S3.27 - Raman spectra of the individual components of the formulation. .....74

Figure S3.28 – Top surface of tablet CLS score map for thiamine (A), PVP (B), glycerol (C) and polysorbate 20 (D). Scale bar = 20µm. .....75

Figure S3.29 - Bottom surface of tablet CLS score map for thiamine (A), PVP (B), glycerol (C) and polysorbate 20 (D). Scale bar = 20µm. .....75

Figure S3.30 - Raman scores generated with the CLS analysis method to show the relative location of individual components of the tablet across its cross-section. Mid-point of tablet at 0 µm. .....76

Figure 4.1 - Molecular structure of PCL [118]. .....77

Figure 4.2 - Molecular structure of DMAC [130].....80

Figure 4.3 - Cross-sectional schematic of the proposed reservoir system. Black represents the impermeable shell (base and walls of device). Yellow represent the rapid releasing core of the system. Blue represents the release controlling membrane through which drug release would occur. .....81

Figure 4.4 - Optical images of the three morphologies observed when printing the PCL ink at different temperatures: 28 °C (left), 44 °C (40 °C was not observed with optical microscopy) (centre) and 60 °C (right). Scale bar = 500 µm. .....84

Figure 4.5 - The weak, 'powder-like' structure that from when 100 layers of PCL was printed at 28 °C. .....85

Figure 4.6 - PCL films printed at 40 °C. Cracking and delamination occurs during the printing process. .....85

Figure 4.7 - PCL ink being printed at 60 °C. A single layer showed good film forming characteristics but as additional layers are printed, 'islands' of molten PCL form. .....86

Figure 4.8 - 100 layers of PCL ink printed at 60 °C. After a certain number of layers (approximately 50) uniform films of molten PCL form. .....86

Figure 4.9 - 100 printed layers of PCL after the substrate temperature was reduced from 60 °C to 28 °C. Uniform solid films were formed. .....86

Figure 4.10 – Single layer of PCL film printed at 60 °C crystallising (from melt) at room temperature over time: (A) immediately removed from heated print bed, (B) 30

s, (C) 60 s, (D) 90 s, (E) 120 s, (F) 180 s. Spherultic growth was clearly observed. Scale bar = 500 µm. .....87

Figure 4.11 - First heating cycle DSC thermographs (endo down). The melting peak of PCL is observed. .....87

Figure 4.12 - First cooling cycle DSC thermographs (endo down). The crystallisation peak of PCL is observed. .....88

Figure 4.13 - The PCL ink jetted at 28 °C (left), ink jetted at 70 °C (centre) and ink jetted at 70 °C with an edited waveform (right). .....90

Figure 4.14 - The general waveform applied during the printing process. To prevent tailing and satellite drops that occur due to the higher temperatures, the initial stage of the jetting process, which relates to ink uptake before jetting, is reduced. .....90

Figure 4.15 - Satellite drops and tailing of droplets that were seen while printing the water-based ink at elevated temperatures, before the nozzles completely block and stop working. .....92

Figure 4.16 - Printed PVP-thiamine formulation on the PCL printed base of the reservoir system. .....92

Figure 4.17 - Reservoir devices after the PCL walls were printed at 60 °C. Some loss of shape is observed due to the spreading of the molten PCL, but closer visual examination showed the edges were sufficiently encapsulated. .....92

Figure 4.18 - Completed reservoir systems with PVP-thiamine completely encapsulated in printed PCL. .....93

Figure 4.19 - The manufacturing process for inkjet printed reservoir systems. .....93

Figure 4.20 - Optical images of one the reservoir devices. The top surface (left) appeared to be rough in contrast to the bottom surface (right), where a very flat and smooth surface was observed. Scale bar = 500 µm. .....94

Figure 4.21 - Release profile of PCL encapsulated reservoir tablets. .....94

Figure 4.22 - Tablet after dissolution. .....95

Figure 4.23 - The top surface of the tablet (PCL only) that has not undergone dissolution .....96

Figure 4.24 - SEM images of tablets that underwent dissolution. The tablet that showed no significant drug release (left) showed no indication of physical loss of membrane on the top (top) or bottom (bottom) surfaces. The tablet that did show a release (right) clearly showed a significant physical loss on the top surface. No indication of mass loss was seen on the bottom surface (although some dirt is seen). .....96

Figure S4.25 - Rheological flow curves of the PCL-DMAC ink measured at 28 °C and 60 °C.....99

Figure S4.26 - The second heating cycle DSC thermographs (endo down). Melting peak of PCL is observed. .....99

Figure S4.27 - Second cooling cycle DSC thermographs (endo down). Crystallisation peak of PCL is observed. .....100

Figure 5.1 – Films of PCL-PVP ink printed on PET at 40 °C with cracking. .....108

Figure 5.2 - Raman image mapping of the top surface of a reservoir device. Regions of PVP (blue) are seen as individual domains in a continuous phase of PCL (green) (left). After the device was exposed to water for 1 hour (right), the same region was mapped. Nearly all indication of PVP was removed, suggesting PVP would act as a pore-forming agent in the printed reservoir systems. Scale bar = 4 µm. .....109

Figure 5.3 - ToF-SIMS map of a PCL (green) – PVP (blue) film's cross section. ..109

Figure 5.4 – ToF-SIMS drop and line of the PCL (green) – PVP (blue) formulation printed on PET substrate. .....110

Figure 5.5 - Completed reservoir system tablets.....111

Figure 5.6 - Optical microscope images of the tablets (25 L release controlling membrane). The top and bottom surfaces of the tablets were inspected for flaws. Scale bar = 500 µm. .....112

Figure 5.7 - Release profile of a reservoir system with a 25 layer release controlling membrane (n=3). ..... 113

Figure 5.8 - Top and bottom surfaces (centre region) of tablets after dissolution. Scale bar = 500 µm. ..... 114

Figure 5.9 - Possible fracture of the release controlling membrane (at the edge of the core region). Since no similar features were seen on the tablets tested, it was thought that it did not play a significant role in drug release. Damage may have been caused during handling of the tablet post-dissolution. Scale bar = 500 µm. ..... 115

Figure 5.10 - Release profiles of reservoir systems with different number of printed layers for the release controlling membrane. (n=3) ..... 118

Figure 5.11 - 100 layer reservoir system after dissolution. ..... 118

Figure 5.12 - CT scan of a reservoir system before dissolution (left) and after dissolution (right). Before dissolution the PVP-thiamine HCl core was distinctively seen, in contrast to the sample after dissolution where a void space was observed. 119

Figure 5.13 - SEM images of the top surface of the reservoir system. As the number of printed layers increased, the size of pores appeared to decrease. ..... 120

Figure 5.14 - Release profile of reservoir systems with different PVP loadings in the release controlling membrane. (n = 3 for 38 wt% and n = 2 for 43 wt%) ..... 121

Figure 5.15 – Optical microscope images of one of the reservoir tablets tested before (left) and after (right) dissolution. Scale bar = 500 µm. ..... 122

Figure 5.16 - SEM images of the release controlling membrane of reservoir systems with 100 layers and a 38 wt% (left) and 43 wt% (right) PVP loading. A large crack was observed with the 43 wt% membrane. ..... 122

Figure 5.17 - ToF-SIMS maps of the top surface of reservoir systems that did not undergo dissolution. With a higher PVP loading, the PVP domains appear to be larger, which would account for the faster drug release observed. PCL is mapped in green and PVP is mapped in blue. ..... 123

Figure 5.18 - Illustration of the effect of varying the drop spacing has on drop overlap and the number of drops required to complete a single layer of an 8 x 8 mm square pattern. .....124

Figure 5.19 - ToF-SIMS maps of single layer prints of the PCL-PVP ink on a glass slide. As drop spacing increases, PVP regions appear to be smaller in size. PCL is mapped in green and PVP is mapped in blue.....124

Figure 5.20 - Drug release profiles of reservoir systems with 50 printed layers of the release controlling membrane, with varied drop spacing. (n=3).....125

Figure 5.21 - 50 layers of the release controlling membrane printed with a 30 µm drop spacing. .....126

Figure 5.22 - Release profiles of reservoir systems with a different number of layers and drop spacing. The amount of material and drop density were comparable. (n=3) .....127

Figure 5.23 - Optical microscope images of a 10 layer and 10 µm drop spacing reservoir system before (left) and after (right) dissolution. .....128

Figure 5.24 - ToF-SIMS maps of a 10 layer, 10 µm drop spacing (left) and a 90 layer, 30 µm drop spacing (right) reservoir system. PCL is mapped in green and PVP is mapped in blue. .....128

Figure 5.25 - Reservoir system tablets with 10 layers, 10 µm and 38wt% PVP release controlling membrane. .....129

Figure 5.26 - Cross sectional schematic of a multi-core reservoir system. Black represents the impermeable PCL shell, yellow represents the PVP-thiamine HCl core and blue represents the PCL-PVP release controlling membrane. .....129

Figure 5.27 - Printed multi-core reservoir systems. .....130

Figure 5.28 - Release profile of a multi-core reservoir system. Initial drug release occurs at a faster rate and transitions into a more sustained drug release. .....130

Figure 5.29 - Reservoir systems with a reduced surface area for the release controlling membrane. Black represents the impermeable PCL shell, yellow represents the PVP-thiamine HCl core and blue represents the PCL-PVP release controlling membrane. .....133

Figure 5.30 - Experimental release profile of reservoir systems with a reduced surface area for the release controlling membrane. .....133

Figure 5.31 - Optical microscope images of samples before and after dissolution. Scale bar = 500 µm. .....134

Figure 5.32 - Delaminated PCL with the release controlling membrane printed on top.....134

Figure 5.33 - Damaged and exposed reservoir system (left) and the delaminated release controlling membrane with a reduced pattern area (right). Scale bar = 500 µm. .....135

Figure S5.34 - Rheological flow curves of the release controlling membrane formulation.....138

Figure S5.35 - Raman spectra of pure PVP, PCL, the mean spectra for the surface of the release controlling membrane before and after exposure to water.....138

Figure S5.36 - ToF-SIMS spectra of pure PCL and PVP material. .....139

Figure S5.37 - Dissolution models applied to data of drug release for a 25 layer reservoir system. .....139

Figure S5.38 - SEM images of different number of printed layers of the release controlling membrane of reservoir systems at different magnifications after dissolution. A 20 µm drop spacing and 38 wt% PVP loading was used for all samples.....140

Figure S5.39 - SEM images of 100 layers of the release controlling membrane (20 µm drop spacing and 43 wt% PVP loading). This specific sample was not used in actual dissolution testing but used to measure pore sizes. This specific sample was however made in the exact same batch of tablets used in dissolution testing. .....140

Figure S5.40 - SEM images of 50 layers of the release controlling membrane (30 µm drop spacing and 38 wt% PVP loading). .....141

Figure S5.41 - Areas of SEM images analysed, thresholded images, with despeckling and the outlines of particles analysed at a 100 X magnification. .....142

Figure S5.42 - Reservoir system tablets with 50 layer, 30 µm and 38wt% PVP release controlling membrane. .....143

Figure S5.43 - Reservoir system tablets with 50 layer, 30 µm and 38wt% PVP release controlling membrane after dissolution. .....143

Figure S5.44 - Reservoir system tablets with 10 layers, 10 µm and 38wt% PVP release controlling membrane after dissolution. .....143

Figure S5.45 - Multi-core reservoir system after dissolution. .....143

# List of Tables

Table 3.1 - Tablet designs generated and printed in this investigation. ..... 47

Table 3.2 - Final ink formulation for tablet ..... 54

Table 3.3 - Ink and printer properties ..... 55

Table 3.4 - Measured contact angle and calculated work of adhesion of the ink on glass and PET substrates (n=5). ..... 56

Table 3.5 - Sulphur content (based on mass %) measured through elemental analysis by combustion (n=3) ..... 63

Table 3.6 - The pattern dimensions, number of layers and the theoretical doses of tablets printed. ..... 69

Table S3.7 - Sample details and drug release data. ..... 73

Table S3.8 - CLS fitting values for components from lateral maps and line cross-section. ..... 74

Table 4.1 - Ink formulation for the impermeable component. ..... 83

Table 4.2 - Ink properties of the impermeable component. Surface tension was taken at room temperature (23 °C) and the viscosity value presented below was taken at 28 °C. ..... 83

Table 4.3 - Crystallinity values calculated from DSC (n=1). ..... 88

Table S4.4 - Additional information regarding thickness of the PCL printed structures (n = 4). PET thickness was 0.110 ± 0.001 mm. ..... 99

Table S4.5 - Thermal properties of samples analysed with DSC. ..... 100

Table 5.1 - Formulation of the release controlling membrane. ..... 107

Table 5.2 - Ink properties of the release controlling membrane. ..... 107

Table 5.3 - Correlation values of the different kinetic models applied to dissolution data (the first 60% of drug release) of the 25 layer reservoir system. .....116

Table 5.4 - Average layer thickness of the PCL-PVP ink (38 wt% PVP). Films were printed on PET substrate and their layer thickness was calculated based on the number of layers printed (n =3). .....126

Table S5.5 - Ink formulation for a release controlling membrane with an increased PVP loading (43 wt% in release controlling membrane).....140

Table S5.6 – Additional information regarding thickness of the PCL-PVP (38 wt%) printed structures (n = 3). PET thickness was 0.136 ± 0.0 mm. .....141

Table S5.7 - Analysis of particles from Figure S5.41.....142

# 1 Introduction

## 1.1 Technical Background

### 1.1.1 Additive manufacturing

The American Society for Testing and Materials (ASTM) defines additive manufacturing as a method to create objects from three-dimensional (3D) model data layer-by-layer [1]. Commonly referred to as 3D printing by the general public and as rapid prototyping by its early proponents, additive manufacturing is radically changing manufacturing in many industries, through its unique characteristics.

Additive manufacturing has numerous advantages. The time taken to produce a part through additive manufacturing is relatively low, assuming all design data is available [2]. With products over the last four decades becoming more complex, additive manufacturing, with only a short period of time can investigate different physical models with the high levels of complexity [2]. Additive manufacturing can be described as a process where 'What You See Is What You Build' [3]. This is especially useful to product designers where the complexity of a part will have little effect on the build time and cost, allowing for high customer demands to be met [2]. Additive manufacturing processes can greatly reduce the cost of a supply chain and can greatly reduce the amount of waste produced during the manufacturing process. This is a key attribute of lean manufacturing, where key principles include delivering only value to the customer, through the removal of waste [4]. Forms of waste that additive manufacturing minimises include overproduction, excess raw materials, transportation, unnecessary inventory and motion [4]. Simplification of the manufacturing supply chain can occur as additive manufacturing machines are often operated by a single user (decreasing labour costs) and can be positioned near the rest of manufacturing line [2].

The ASTM classifies a total of seven processes of additive manufacturing. Names and definitions are listed below, taken from the ASTM standard terminology for additive manufacturing technologies [1].

1. *Binder jetting* – ‘liquid bonding agent is selectively deposited to join powder materials’.
2. *Direct energy deposition* – ‘focused thermal energy is used to fuse materials by melting as they are being deposited’.
3. *Material extrusion* – ‘material is selectively dispensed through a nozzle orifice’.
4. *Material jetting* - ‘droplets of build material are selectively deposited’
5. *Powder bed fusion* – ‘thermal energy fuses regions of a powder bed’
6. *Sheet lamination* – ‘sheets of material are bonded to form an object’
7. *Vat photopolymerisation* – liquid photopolymer in a vat is selectively cured by light-activated polymerisation’.

Regardless of the specific additive manufacturing process used, there is a general route for additive manufacturing to follow, from generation on a computer to its actual application [3]:

1. *Computer aided design (CAD)* – A description of the part’s geometry, either designed on computer software or from a reverse engineered scan.
2. *Conversion to stereolithography (STL) file* – A file format, which describes the external closed surfaces of the original CAD file (sliced and represented by triangles) and is generally accepted by many additive manufacturing systems.
3. *Transfer to additive manufacturing machine and STL file manipulation* – The transferring of the STL file from a computer to the additive manufacturing printer where manipulation can occur (e.g. changing size, position and build orientation).
4. *Machine setup* – Additional build parameters such as layer thickness, timing or material can be specified in this step.

5. *Build* – Automated process of the additive manufacturing machine building the part inputted.
6. *Removal* – Following successful printing of object, the part can be removed.
7. *Post-processing* – A stage of post-processing may be required such as removal of support materials
8. *Application* – The part's proposed function can now be executed, although there may be additional post processing to ensure the part is aesthetically suitable or has an acceptable level of strength.

### 1.1.2 Inkjet printing

Material jetting (or inkjet printing) is an additive technique where individual droplets are selectively deposited onto a substrate [5]. The jetting process consists of three phases [6]:

1. Droplet generation
2. Positioning and interaction of ink droplets with substrate used
3. Solidification mechanism to produce a solid deposit

Inkjet printing can be classified into two mechanisms of dispensing inks: (i) continuous inkjet printing and (ii) drop-on-demand inkjet printing.

In continuous inkjet printing (Figure 1.1), ink is forced through a nozzle and a piezoelectric transducer controls the frequency of drops by applying a disturbance at regular intervals. Inks used are usually conductive and therefore when passed through a charged electrode their placement can be controlled with the help of field plates. A catcher can be used to collect areas where no ink is required and those drops can be reused [7].

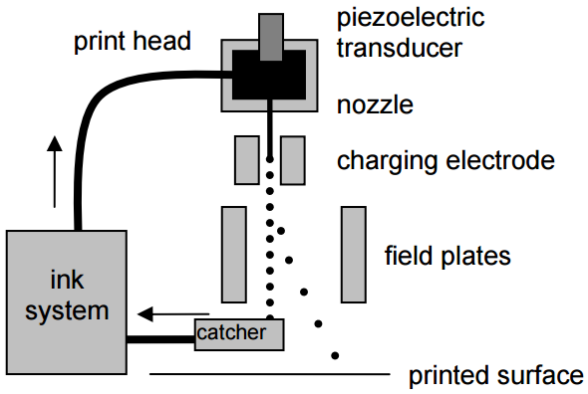



*Figure 1.1 - Continuous inkjet printer schematic (taken from Martin et al. 2008)* [7].

If greater control over placement for ink deposition is required, a drop-on-demand mechanism is used. As the name suggests, drops are only ejected when required. Droplet generation is done through the rapid heating of a thermal resistor (Figure 1.2). This results in the surrounding ink to be vapourised causing an air bubble to grow, forcing material out of the nozzles. When the heater is turned off, a transient pressure wave is generated allowing stable ink ejection [8].

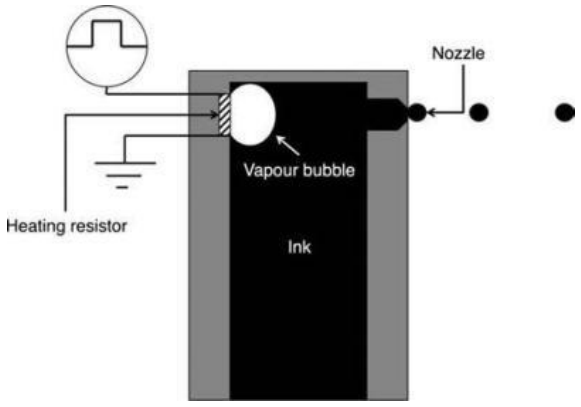



*Figure 1.2 - Drop-on-demand inkjet printer with a thermal resistor controlling drop ejection (taken from Cummins and Desmulliez 2012)* [8].

Alternatively, a piezoelectric material can be used to force the ejection of droplet (Figure 1.3). A voltage is applied to the material and the resultant mechanical deformation forces ink ejection. A specific waveform is applied to control the movement of the piezoelectric material that will affect jetting behaviour. This form of drop-on-demand inkjet printing may be preferred when investigating inks that are thermally sensitive or degrade due to heat [9].

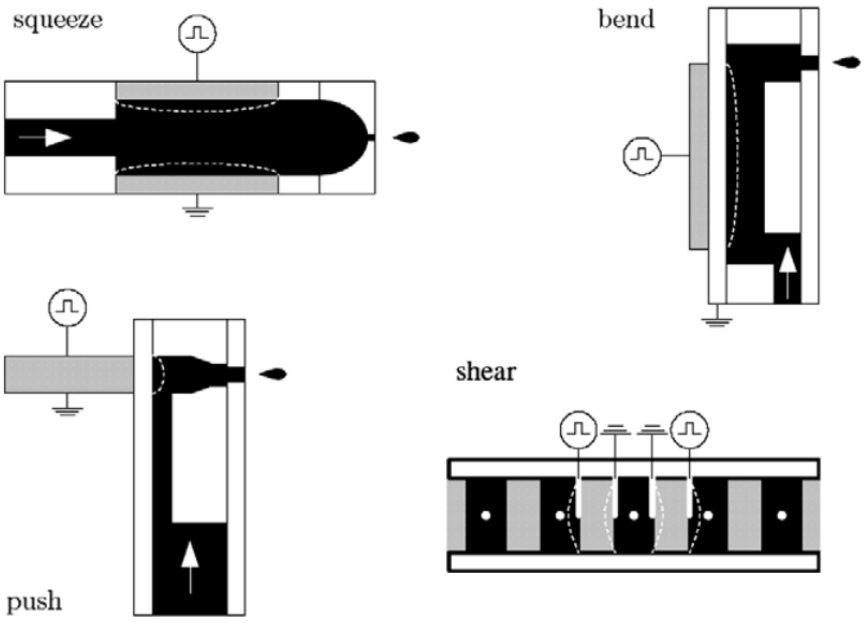



*Figure 1.3 - Various DoD inkjet printer schematic with piezoelectric material controlling drop ejection (taken from Wijshoff 2010)* [9].

The development of a printable ink is paramount for the stable and reliable jetting of an ink. A range of dimensionless physical constraints are used to characterise 'how well' an ink will print. This includes the Reynolds ($Re$) and Weber ($We$) numbers. The Reynolds number (Equation 1.1) is the ratio of fluid inertia to viscous forces and the Weber number (Equation 1.2) is the ratio of fluid inertia to surface forces [5]. From the ratio of these number the Ohnesorge (*Oh)* is derived, and its inverse value is known as the printability factor ($Z$) (Equation 1.3) [10]. These parameters take into account ink properties including the viscosity ($\rho$), surface tension ($\gamma$), density ($\rho$), the velocity of the droplet ($v$) and its diameter [6]. The diameter is a characteristic length which is dominated by the diameter of the nozzle used ($a$) [10].

$$Re = \frac{v\rho a}{\eta} \qquad 1.1$$

$$We = \frac{v^2 \rho a}{\gamma} \qquad 1.2$$

$$Z = Oh^{-1} = \frac{Re}{We^{\frac{1}{2}}} = \frac{(\gamma \rho a)^{\frac{1}{2}}}{\eta} \qquad 1.3$$

An ink's viscosity greatly affects the jetting and spreading behaviour of ink [10]. If viscosity is too high, the material would not be able to flow in the cartridge leading to

the blocking of nozzles [6]. Additives such as surfactants, pigments or active pharmaceutical ingredients (APIs) can have significant impact on viscosity values. Flocculation, aggregation or sedimentation of these additives can occur during increased storage time the inks [5]. A potential problem for ultra-violet (UV) curable inks is that polymerisation may occur leading to oligomer formation [5]. This would significantly increase the viscosity of the ink. As a temperature dependent property – heating the ink (by heating the substrate or cartridge) can allow for higher viscosity inks to be printed [11]. The material content of the ink (density) is a key parameter that is also dependent on the amount of additives or solvent in the ink. There is a very close relationship with viscosity, hence, it is not investigated as much as the other parameters.

The formation and spreading of droplets are greatly controlled by the ink's surface tension. When within an acceptable range, stable droplet formation occurs during printing, preventing drops to fall without intent, but also having the sufficient energy to overcome the barrier for ejection [6]. This material property is greatly dependent on the solvents and surfactants present in the ink [11]. The desired droplet spreading or wettability can be controlled through this parameter.

When it comes to developing an ink, the two easiest controlling parameters to influence will be surface tension and viscosity, through the use of additives such as surfactants [5]. It generally accepted that surface tension should be within the range of 20 and 50 $mN \cdot m^{-1}$ [10] and viscosity within 8 and 15 mPa·s [5], although this can vary significantly depending on the specific printer used. An 'ideal' value for $Z$ ranges between 1 and 10 as illustrated in Figure 1.4 [10].

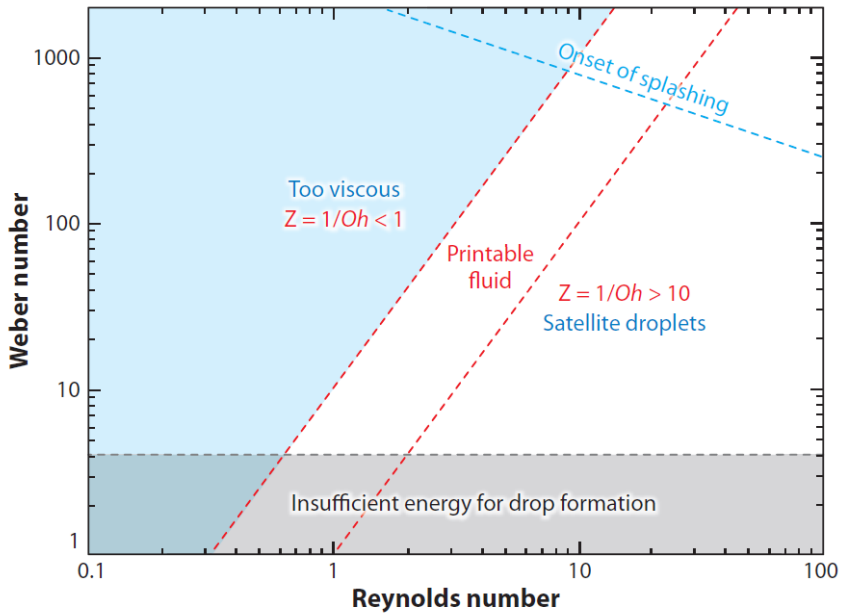



*Figure 1.4 – Visual representation of the relation between the Weber and Reynolds numbers and what values would be required for suitable jetting characteristics (taken from Derby 2010)* [6].

Substrate interactions with the ink and final solidification of material are also key areas of inkjet printing research. Initially after droplet impact, impact driven spreading will begin, controlled by the jetting parameters of the printing process. Over time, a shift to capillary driven spread or retraction can occur, due to substrate interactions. The Weber and Reynolds numbers influence ink-substrate interactions, in addition to the Bond number ($Bo$), which takes into account the effect of gravity ($g$) (Equation 1.4) [6].

$$Bo = \frac{\rho g a^2}{\gamma} \qquad 1.4$$

The Bond number is often found be negligible as density and surface energy of the inks are usually close to 1000 $kgm^{-3}$ and 0.1 $Jm^{-2}$ respectively [6]. Droplet diameters are also usually less than 100 µm. These characteristics lead to Bond number values much smaller 1, allowing gravitational forces to be neglected. This leads to inertial and capillary forces being dominant for influencing interactions between the ink and substrate [6].

The last stage of the inkjet process, solidification, can occur due to solvent evaporation, phase change (e.g. hot melt jetting) or by a reaction (e.g. UV curing, thermal curing or chemical reactions) [5].

### 1.1.3 Solid oral dosage forms

Numerous devices exist for the delivery of drugs for a therapeutic effect. The aim for any drug delivery system is to achieve a predictable therapeutic response to a drug, which would exist in a system ideally capable of being manufactured on a large scale and with high reproducibility [12]. A solid oral dosage form is a drug delivery device, such as a tablet or capsule, administered through ingestion [13]. Tablets are popular among patients as the route of delivery is the least invasive, easily understood by the patient and is administered by the patient themselves. For pharmaceutical manufacturers, tablets are a relatively cheap technology that allows the API to be in its most stable form [13].

Tablet manufacturing is a highly regulated process, which is required to follow current Good Manufacturing Practices (cGMP). This can require the preparation of tablets in completely enclosed systems that minimise handling [14].

The first phase of producing tablets begins with decreasing the physical size of the API and its excipients through milling processes (e.g. compressing and cutting). This improves the performance of the tablet through maximizing surface area and uniformity. Granulation of the ingredients is commonly the next step where characteristics of flowability and compressibility are achieved. Sizing and blending of granules occur, commonly through wet or dry granulation (other processes exist too). The process is a low energy process so that negative phase transformations can be detected (although chances of occurring are low). Further addition of excipients, such as lubricants, can be added. Compression and encapsulation of the dosages occur to form stable tablets. Applying a coating is the final step for modified drug release or aesthetic and taste alterations [15].

The standard practice of manufacturing tablets involves numerous steps. With each step, except for granulation sizing and blending, the probability of phase transformations of the drug can be significant. Transformations can refer to polymorphism, crystallisation, solvate and salt formations [16]. All can affect the tablet's physical, chemical and mechanical properties. Important properties including the solubility, bioavailability and stability of the tablet can be negatively impacted as

a results of these changes [17]. The potential routes of manufacturing are illustrated in Figure 1.5

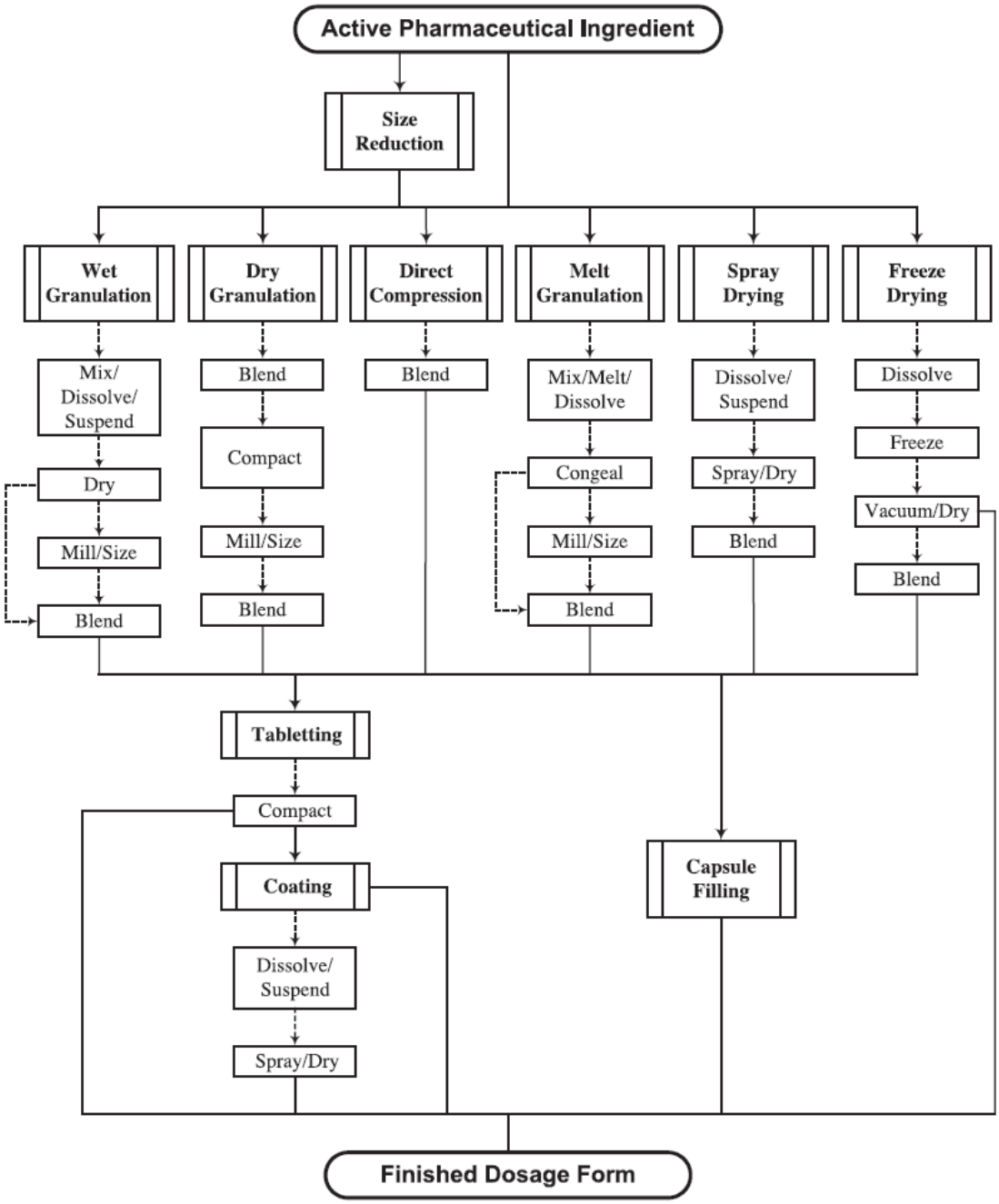



*Figure 1.5 - A summary overview of different manufacturing routes for solid oral dosage form production (taken from Zhang et al. 2004)* [15].

### *1.1.3.1 Controlled drug release*

The development of new drugs has become increasingly difficult and expensive; hence a great deal of research has gone into the development of new delivery systems, including oral controlled release formulations. Common controlled release behaviours

include delayed, sustained and repeat action therapies. These formulations are developed for drugs that are more therapeutically effective at a specific site or time after ingestion [18].

The main challenge for an effective controlled drug release for oral systems is the variation in environment and transit time in the gastrointestinal tract. Challenges included variation between patients in terms of gastric residence time and the conditions in which tablets have been ingested (e.g. if the patient is in a fasted or fed state) [19]. pH is another significant variable of the gastrointestinal tract. pH is usually low in the stomach (at least two in the fasted state but can increase to up to five after food) and increases to approximately 6.5 in the small intestine. The variation in pH can affect a drug's stability, absorption and solubility [19]. Changing the drug release behaviour such as onset and duration can address these problems, allowing the optimum amount of drug to be released at specific times or sites. There would be an improved efficiency by treating ailments with less amount of drug, which could also lead to reduced side effects [18]. In addition, controlled released tablets can improve patient compliance as the need for repeated doses are reduced, improving patient convenience [18].

Drug delivery devices have numerous mechanisms for drug release. These include [20]:

- *Dissolution* – the transfer of drug from a solid phase to the surrounding medium.
- *Partitioning* – delivery caused by the relative affinity for a drug between two phases.
- *Diffusion* – independent random walks of a drug's molecules from a region of high concentration to a region of low concentration.
- *Osmosis* – flow of water through a semi-permeable membrane to equalise concentrations of impermeable solutes on either side of a membrane.
- *Swelling* – the uptake of water by a delivery system causing an increase in volume of the device, allowing release of drug through dissolution or diffusion

- *Erosion and degradation* – release of drug as a polymer disintegrates
- *Regional delivery and targeting* – localised direct administration of a drug near or at the site or action

Often, several of the above mechanisms can occur in sequence during drug release. The slowest mass transport step – the rate-limiting step – will control the majority of drug release [21]. If these mechanisms can be influenced (e.g. by material choice or device design) a degree of control can be introduced into the system. The highly individualised nature that requires controlled drug release systems to be most effective, makes it an ideal candidate for additive manufacturing.

#### *1.1.3.2 Additive manufacturing for tablets*

There are numerous reasons why additive manufacturing is advantageous over the current manufacturing process for tablets. As discussed in the previous section, the route for manufacturing tablets is a long and multi-step process [15]. At each stage, the risk of a phase transformation (potentially causing a change in API behaviour in the body) exists. Different polymorphisms can alter drug properties, negatively affecting behaviour such as dissolution, stability and toxicity of the drug [22]. As the manufacturing route progresses, the danger of a phase transformation of the drug or an excipient remains and needs to be monitored. Through additive manufacturing, a shorter and more direct path to the final product is possible. With inkjet printing, there are potentially just three manufacturing points that may require polymorph screening: initial analysis of raw API, analysis of the ink and lastly the analysis of printed formulation. Similarly, there are just potentially three manufacturing steps for inkjet printed tablets: the formulation of the ink, jetting of the ink and the solidification process.

Personalised medicine is a key benefit of using additive manufacturing over the conventional process, which provide no route for personalisation. Medical professionals can take into account a patient's age, gender or existing ailments to create a specific dose for a more effective therapeutic treatment [23]. The geometric freedom that additive manufacturing provides, gives the ability to create complex tablet structures which can influence drug release behaviour [24]. Creating a specific

release profile for one or multiple drugs in a single tablet can uniquely be accomplished by additive manufacturing. The ease of which multiple materials can be incorporated into a printer is another advantage of additive manufacturing (inkjet printing and material extrusion in particular) [25]. Multiple API-loaded inks can be used to create tablets to treat multiple conditions of a patient, removing the need to take a cocktail of tablets [26]. The ability to print multiple inks for a single structure and by selecting the spatial location of the drug in the tablet, drug release could by modelled computationally. This would add to the prospect of a programmable drug release system.

Another incentive to print formulations, are the economic advantages. This includes a shortening of the current long, slow and expensive supply chains [27]. Time consumption would be an exceptional challenge in reference to unstable and quick-degrading drugs. With 3D printable formulations, liquid or paste filled cartridges could be delivered to or prepared in pharmacies or hospitals ready to be printed [28]. A major source of capital loss in this industry is in its inventory levels where large replenishment times requires greater stock productions with estimated losses of US$ 20-25 billion [27]. Additively manufacturing tablets could be printed on demand by a pharmacist or physician when required by a patient [28]. A greater reduction in wasted of materials also decreases the overall cost of production.

Contrary to popular belief, additive manufacturing can be utilised as a method of mass production for the pharmaceutical industry. Inkjet printing is inherently a scalable processes [29]. Their throughput can be increased by increasing the number of nozzles or print heads in the system.

One area that is often overlooked is the potential for additive manufacturing at the clinical trials levels Presently, the pharmaceutical industry takes advantage of micro-dosing systems for the fast and precise manufacturing of dosages to be used in clinical trials. An example of the current technology is Xcelodose (developed by Capsugel), a powder micro-dosing system where the API is filled into pre-made capsules for clinical testing [30]. For testing of controlled release products, technologies such as DiffCORE (by GSK) are used, where tablet template shells are used, with drug release controlled by coatings and apertures [31]. Additive manufacturing has the potential to

replace current systems with their precision and accuracy and potential for functionality testing of excipients.

Inkjet printing can deposit extremely small volumes of material, with accuracy and precision. For common drop-on-demand printer systems, cartridges exist where droplet volume is as low as 1 pL (this can result in droplet sizes of approximately 10 µm) [6] . Individual droplets can be used as dispensed doses, greatly reducing the risk in working with potent and toxic APIs. This can also be done with great speed and placement precision. Feature size is determined by a variety of print parameters (e.g. drop diameter, drop velocity, substrate interactions and more [6]) but it is possible to get feature size of as low as approximately 30 µm [6].

While simultaneously investigating the safety of new APIs and excipients, inkjet printing could allow for the investigation of different drug release profiles and mechanisms with relative ease (shape, position of API or ingredients of tablet can easily be modified). The benefit of combining the testing of both safety and functionality includes saving time and costs.

Some of the advantages of inkjet printing for tablet production are summarised in Figure 1.6. More specific advantages of inkjet printing for tablet manufacturing are discussed in Section 2.2, as part of the literature review of this thesis.

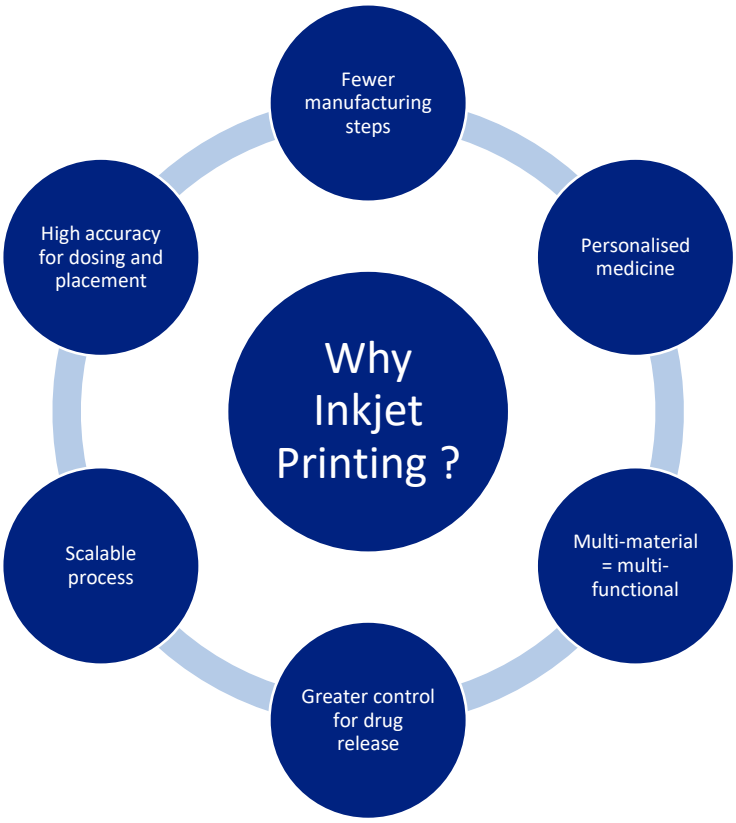



*Figure 1.6 - Some of the advantages of utilising inkjet printing for tablet production.*

## 1.2 Aims of Thesis

The main aim of this thesis was to wholly inkjet print a tablet capable of delivering its dose in a controlled manner.

It was decided to create a reservoir system where a drug-polymer core is surrounded by a membrane material. This would require multiple inks for its multiple components. A strategy of delivering one-directional drug release was pursued. The three components developed were (i) a drug-polymer core (which on its own could be used as a rapid releasing tablet), (ii) an impermeable shell (base and walls) and (iii) a release controlling membrane.

The production of this reservoir system was split into three sections, each with its own objectives:

1. The drug-polymer core:
    - Print a free-standing tablet with a rapid drug release that will act as the core for a reservoir device

- Show that inkjet printing can be used to deliver accurate doses reliably
- Show that the used API is in its desired polymorphic form
- Show the API is uniformly distributed throughout the tablet

2. The impermeable shell:
    - Design a reservoir system for a controlled drug releasing tablet
    - Formulate and develop a printable ink for the impermeable shell of a reservoir system
    - Illustrate functionality of an impermeable shell of a reservoir system
3. The release controlling membrane:
    - Formulate and develop a printable ink for the drug release controlling membrane a reservoir system
    - Characterise the formulated membrane
    - Investigate the influence printing and ink parameters have on drug release behaviour
    - Create specific drug release profiles

## 1.3 Thesis Chapters

In current Chapter 1, I have provided an overview of additive manufacturing, in particular inkjet printing. I have discussed, in general terms, the advantages that additive manufacturing can bring for tablet manufacturing. The aim, to wholly inkjet a multi-material tablet for controlled drug release, was broken down into smaller objectives, which are the stepping blocks to manufacture this novel device.

Chapter 2 provides an overview of the current state of the art for inkjet printing of tablets. Some discussion exists for other additive manufacturing processes for tablets and other drug delivery devices, but an emphasis was placed on inkjet printing. Gaps in the current state of research were identified.

Chapter 3 presents work to create wholly inkjet printed tablets with a single formulation for a rapid release. In addition, as a rapid releasing tablet, this system would then be used as a reservoir system's drug-polymer core. Using thiamine hydrochloride (HCl) as a model drug, a water-based formulation was developed, characterised and jetted to create freestanding tablets via a solvent evaporation inkjet printing process. Tablets were thoroughly investigated including drug release studies.

Chapter 4 focused on the development of an impermeable shell, which would be printed as the base and walls of a reservoir system. The material in focus was polycaprolactone (PCL). A significant part of experimental work in this chapter was focused on the printing and film forming behaviour of the PCL formulation. To illustrate the impermeable nature of the material, a reservoir system consisting of the core (discussed in Chapter 3) completed surrounded by printed PCL was tested. Aspects of printing a device with multiple materials were discussed.

Chapter 5 illustrates the creation of a release controlling membrane and how it was incorporated into the reservoir system. A blended polymer material was characterised with chemical mapping techniques to elucidate how controlled release would be achieved. From a simple reservoir design with a single direction for release, controlled drug release was achieved. By investigating different ink and printing parameters, their influence on release are observed. Different types of release profiles were achieved with a single formulation of the release controlling membrane.

Chapter 6 presents the conclusions and future work of this investigation. Discussion of the aims achieved and areas that are novel are highlighted as well as areas for future improvement.

## 1.4 Statement of Novelty

The novelty of this research lies in the two systems made in this investigation: rapid releasing tablets and controlled release reservoir systems.

As the literature review will illustrate, solvent-based inkjet printing has been extensively investigated although the use of substrates forming part of the dosage form is often present. Thin films for oral delivery have been produced, often with the use of organic solvents that would need to be tracked and quantified. Aqueous based formulations have been jetted, but are mainly used where the printing acts as a dosing method onto an edible substrate, rather than an individual manufacturing process. With the rapid releasing tablet developed in Chapter 3, I have inkjet printed a tablet without a substrate being part of the solid oral dosage form with solvent evaporation as the solidification mechanism. I also illustrate in the chapter that inkjet printing can be a water-based toxic-free method of manufacturing tablets that do not require the need of hazardous solvents or the need for post-curing. There was no need for high

temperatures (that hot-melt jetting could require) allowing for the use of thermally sensitive drugs. As the formulation developed was a water-based ink, it could be potentially used as an universal ink for any water-soluble drug.

With the reservoir system developed, I have created the first multi-material reservoir tablet manufactured solely with inkjet printing. With the use of a polymer-blend for the release controlling membrane, a degree of control was introduced into the system. In previous investigations, ink formulation has been the dominant method of varying and controlling release. In addition to this, this investigation illustrates the use of printing parameters to vary the morphologies of a release controlling membrane. It was illustrated with the use of a single formulation for the release controlling membrane, that a number of different release profiles could be created (extended, delayed and bimodal).

# 2 Literature Review

## 2.1 Introduction to Chapter

### 2.1.1 Aims of chapter

- Examine current literature regarding inkjet printing for tablet manufacturing, highlighting inkjet printing's advantages
- Identify gaps in current research that need to be addressed

### 2.1.2 Background

Inkjet printing has shown potential in a variety of applications in the medical and pharmaceutical industry. Literature has shown that inkjet printing has successfully manufactured drug delivery systems such as biodegradable microspheres [32] and coatings for stents [33] and microneedles [34]. It has also a great prospect in the manufacturing of tablets. This chapter reviews literature regarding inkjet printing for tablets and other oral pharmaceutical devices and potential advantages for this additive manufacturing method.

Literature is focused on oral pharmaceutical tablets where inkjet printing has played a role in the manufacturing process. Other additive techniques that have produced tablets are briefly highlighted.

## 2.2 Inkjet Printing of Oral Pharmaceutical Dosage Forms

### 2.2.1 Printing small structures and thin films for drug delivery

This section examines some of the early investigations of inkjet printing for potential oral delivery dosage forms. Examples include the jetting of small particles, individual drops and thin films. Most involve the use of edible substrates and involve a single ink.

An early patent submitted by the Hewlett-Packard Company in 2005 described how inkjet printing liposomes of APIs could be used to create tablets. Finely ground APIs were combined with an aqueous solution containing vesicle forming materials. Once liposomes had successfully formed, the solution was loaded into a material reservoir

and selectively jetted onto a substrate, where potentially they can be checked for defects [35].

Thermal inkjet printing was successfully used by Meléndez *et al.* 2008, where the effects of thermal inkjet printing on API polymorphism were investigated. Form I prednisolone was dissolved in a solution of ethanol, water and glycerol to form a jettable ink. The ink was printed on Teflon coated fiberglass substrates (Figure 2.1). It was found through powder x-ray diffraction (XRD) and Raman mapping that Form I and Form III of the API had formed. The polymorphs were also detected in samples that were micropipetted, suggesting that it was more likely that the solvent system or drying mechanism were the causes of drug polymorphism. The paper did not rule out that thermal inkjet printing had a role for encouraging polymorph formation [36].

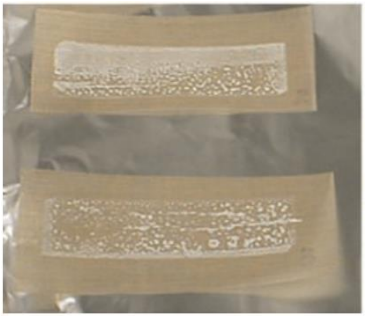


*Figure 2.1 - Thermal inkjet printed prednisolone on coated substrates after vacuum drying (taken from Meléndez et al. 2008)* [36].

Using rhodamine 6G as a model release agent, Desai *et al.* 2009 presented direct-write inkjet printing of calcium alginate microcapsules using a solidum alginate and calcium chloride-based formulation. Smaller microcapsules resulted in faster drug release, due to the higher surface area to volume ratio. Lower concentrations of sodium alginate resulted in less dye being entrapped in microcapsules, resulting in a decrease in release rate. The time of an initial burst which was observed was seen to decrease as both sodium alginate and calcium chloride content increased due to greater entrapment of the rhodamine dye. This highlighted the ability of inkjet printing as a means for tuning drug release by controlling size and surface area to volume ratios of the prints through ink formulation parameters [37].

Buanz *et al.* 2011 using a modified Hewlett-Packard printer cartridge to dose aqueous drug (salbutamol sulphate) solutions onto oral films (clear acetate films). In addition to water, glycerine was added to the formulation to increase viscosity and act as a

humectant which would slow the crystallisation of the drug and evaporation preventing nozzle blockage. The authors found that the inkjet process had dosed in good agreement drug content for the initial single pass of the print head (±5 % of the theoretical dose). When multiple passes were conducted, the measured dose was less than what was expected. This was attributed to shearing forces that may have had eroded the previous layer during handling of the paper when it moved through the rollers of the printer [38].

Scoutaris *et al.* 2011 also illustrated inkjet printing as a viable route for controlling drug release [29]. This paper used the poorly water-soluble API, felodipine, polymer excipient polyvinylpyrrolidone (PVP) and solvents: ethanol and dimethyl sulfoxide (DMSO). An array of printed microdots was produced and analysed after solvent evaporation. It was found that the level of interaction (measured with infrared spectroscopy) between the polymer and API was higher when inkjet printed and compared to previous investigations. Due to the very small amounts of material jetted, the solvents rapidly evaporated when compared to bulk solid dispersion methods. This allowed for closer interaction between PVP and felodipine. Drug release could be controlled by the loading of the droplets. With larger API loadings, there was less hydrogen bonding per unit mass of drug between the polymer and API and an increased rate of loss of polymer. The inkjet method here did show that high drug loadings were possible (up to 67 % by weight) while maintaining homogeneity. The authors also note that inkjet printing is a scalable manufacturing method, where single microdots can be made into larger delivery systems and the flexibility of inkjet printing can allow for multiple API loaded microdot arrays [29].

Further work involving poorly soluble APIs with inkjet printing has been done by Pardeike *et al.* 2011. High pressure homogenization of folic acid, resulted in a nanosuspension, which was inkjet printed. It was found that the nanosuspension were small enough to pass through the nozzles without clogging, excessive nozzle orifice wetting and build-up of solid material around the nozzles. Consistent droplet formation was observed. The nanosuspension was printed onto an edible substrate, which could then be folded into a pharmaceutical capsule [39].

The idea of jetting a polymer-drug formulation on edible substrates has been further investigated by Sandler *et al.* 2011 and their proposed manufacturing process in

illustrated in Figure 2.2. The paper aimed to investigate three APIs (paracetamol, theophylline and caffeine) that can be printed onto three different substrates which could then be inserted into capsule shells to form the final dosage form. It was found that different substrates can influence the crystallisation behaviour of APIs (in this case, due to different ink penetration behaviour) further allowing inkjet printing the ability to create complex drug delivery devices. Additional parameters such as surface energy, roughness, capillary action and chemical content of the substrate can potentially play a role. Drug release studies were not conducted [40].

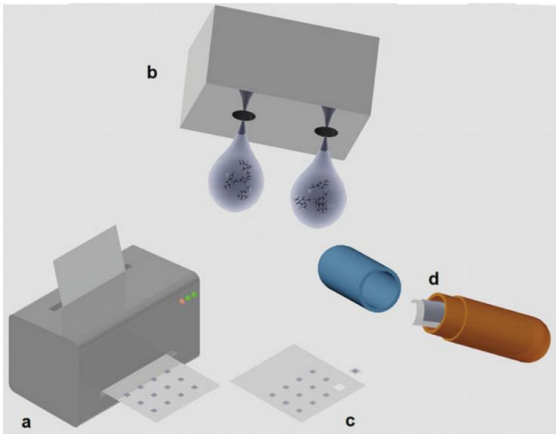



*Figure 2.2 - The proposed manufacturing process by Sandler et al. 2011 with the use of an (a) inkjet printer, (b) accurate drug deposition, (c) paper substrates which can be cut which are then (d) placed in capsules (taken from Sandler et al. 2011)* [40].

Inkjet printing complex shapes for drug delivery purposes was illustrated by Lee *et al.* 2012, where paclitaxel loaded polylactic-co-glycolic acid (PLGA) microspheres were inkjet printed. This investigation also highlighted inkjet printing's ability to produce extremely small designs with high accuracy (see Figure 2.3). Although the application of this materials would not be suited for a tablet (due to the long release over the course of days), it does show that by varying surface area of the complex geometries can affect the release profile of manufactured samples [41].

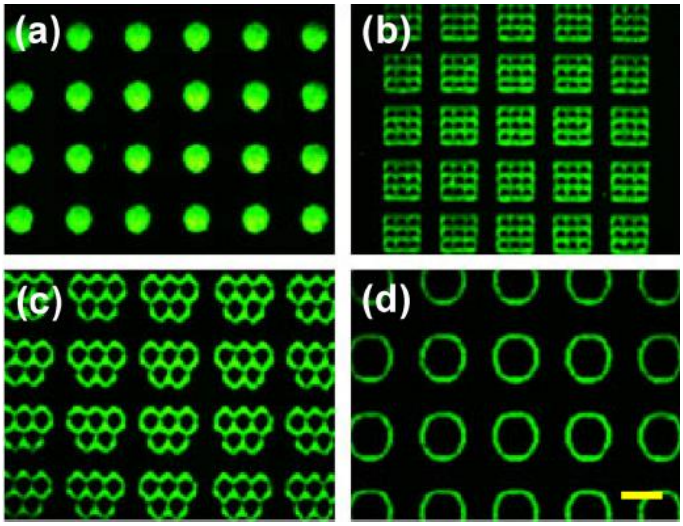



*Figure 2.3 – Fluorescence microscopy images of drug loaded PLGA microspheres with varying geometries: (a) circles, (b) grids, (c) honeycomb and (d) rings (taken from Lee et al. 2012). Scale bar = 500 µm. [41]*

Using hydrochlorothiazide and the polymer PVP, Scoutaris *et al.* 2012 highlighted inkjet printing's ability to create reproducible and uniform drug doses. This was done by printing a micro-array of droplets followed by analysis by time-of-flight secondary ion mass spectrometry (ToF-SIMS). With the PVP based formulation, clearly defined round spots with a uniform surface of dispersed drug was observed. The paper highlighted the need of an appropriate formulation to achieve this level of homogeneity. In contrast to the PVP formulation, a PLGA based formulation did not have the same level of drug uniformity and exhibited drug-polymer de-mixing. This may have been caused by different interactions between the API and polymer or due to the different drying kinetics caused by polymer solubility and formulation viscosity [42].

To further investigate the impact of substrates on printed doses, Genina *et al.* 2013a jetted rasagiline mesylate on three different substrates – orodispersible films (ODFs), porous copy paper and water impermeable transparency films (Figure 2.4). It was found that the drug recrystallised on the surface of the ODF and transparency film and no drug crystals were detected on the copy paper. This was attributed to the high absorption of the copy paper of the ink into the substrate matrix, caused by its high porosity. Due to the high absorption of ink, the copy paper also had the strongest linear correlation between printed layers and drug dose. The paper concludes that substrates with similar behaviour to the porous copy paper would be advantageous for accurate and precise drug delivery system [43].

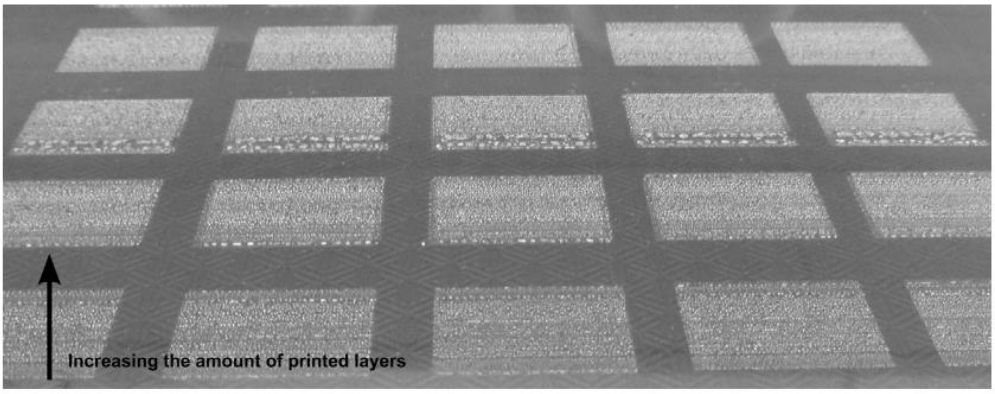



*Figure 2.4 - Inkjet printed rasagiline mesylate on transparency films with increasing number of layers (taken from Genina et al. 2013a)* [43].

The ability to vary the spacing between individual droplets on a substrate is a key advantage of inkjet printing for creating extremely small, but highly accurate doses. Genina *et al.* 2013b investigated the jetting of API inks on different substrates while varying dose strength by controlling drop spacing and the physical dimension of the printed pattern. It was found that by varying drop spacing, the theoretical doses matched more closely to what was actually printed when compared to the method of changing the size of the print, highlighting inkjet printing as a better method of producing flexible dose strengths[44].

The reproducibility of inkjet printing was again highlighted by Hirshfield *et al*. 2014 where the relative standard deviation of doses produced, were below 5 % (the limit defined by the Food and Drug Administration (FDA)). The authors also illustrated the ability of inkjet printing to control the crystallinity of the printed dosages by varying the print parameter of drop size. It was found that the smallest drop size resulted in the dosage being 33% crystalline whereas the largest drop size had a crystallinity of 77 %. The smaller drop sizes were found to be less crystalline due to the faster evaporation of the solvent (ethanol) used, giving less time for drug crystal nucleation and growth [45].

When it comes to developing a tablet for poorly soluble drugs, inkjet printing can be used to create novel systems. Cheow *et al.* 2015, successfully jetted a nanoparticle complex (termed by the authors as a ‘nanoplex’) using a printable nanosuspension ink. Drug release was successful from the printed dosage form on an edible substrate, but some issues were encountered. The correlation between jetted droplets and the actual drug dose was not as strong as expected, possibly due to spatial non-homogeneity in

the nanoplex suspension concentration, regardless of the size of nanoparticles. It was found however, that the doses created in the same batch had good dose uniformity, showing that inkjet printing is a reproducible method of creating tablets, even for poorly soluble APIs [46].

Poorly soluble APIs can also be formulated with a simple solvent ink as illustrated by Wickström *et al.* 2015. The drug indomethacin was formulated with PVP and L-arginine as excipients and with a propylene glycol and DMSO co-solvent system. It was illustrated that the dissolution rate was affected by a number of parameters including the spatial location of the ink, the amount of drug jetted, any remaining solvents of the ink, the drying phase and substrate characteristics [47].

To address issues of bitter tasting APIs, Scoutaris *et al.* 2015 used a jet dispensing system to create taste masked mucosal thin films. Ethanol based solutions with three bitter-tasting APIs (cetirizine HCl, diphenylhydramine HCl and ibuprofen) were formulated with eudragit. Films were measured with the use of a calliper and were seen to be accurate, reproducible and uniform. DSC studies showed the absence of drug melting peaks suggesting the drugs existed in an amorphous state in the polymer matrix. This resulted in a fairly rapid drug release from the printed formulations. *In vivo* taste masking tests were done with human volunteers. The films did not rapidly disintegrate in the mouth (due to the polymer) and no bitterness was reported by the volunteers [48].

Varan *et al.* 2017 used inkjet printing to dose paclitaxel and cidofovir drugs onto bio-adhesive films for the localised treatment of cervical cancer. A cyclodextrin inclusion was used in the PCL-based formulation to overcome paclitaxel's poor solubility. Although this dosage form was not for oral use, it was shown through inkjet printing that the process did not disrupt the structure of the nanoparticles (through scanning electron microscope (SEM) analysis) and the films produced showed an acceptable level of biocompatibility. The authors had successfully illustrated inkjet printing as a method of manufacturing dosage forms for mucosal administration [49].

### 2.2.2 Inkjet printing with quality control and screening processes

If inkjet printing were to be adopted by the pharmaceutical industry for large scale production, an appropriate quality control system will be needed. This section

highlights investigations where a screening process was incorporated or shown to have potential to incorporating with the inkjet printing process.

Vakili *et al*. 2015 used near-infrared (NIR) hyperspectral imaging to analyse printed doses to measure the API content (Figure 2.5), which showed a strong positive correlation to the theoretical dose strength. It was also able to provide spatial information of the printed ink even with low doses. Potential problems included substrate interference, extremely low doses may not be accurately detected and the presence of multiple APIs may make it harder for distinguishing drugs [50].

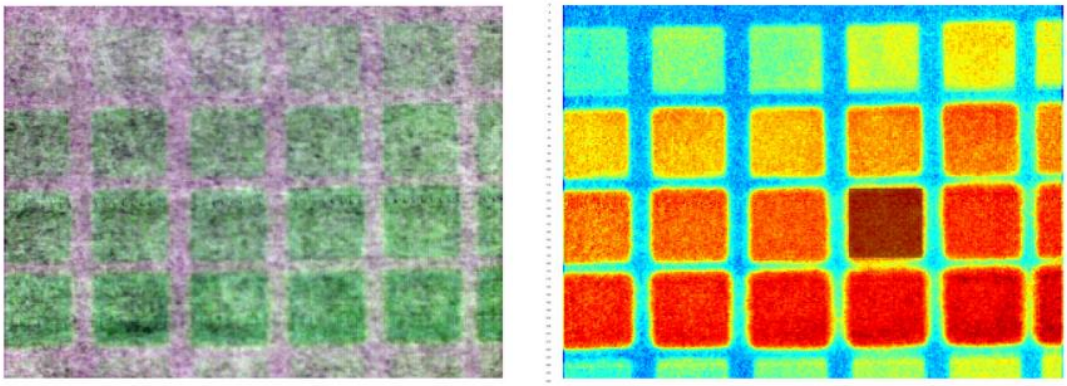


*Figure 2.5 - Inkjet printed theophylline formulation on a paper substrate (left) and its hyperspectral image generated with principal component analysis (right) (taken from Vakili et al. 2014)* [50].

Looking further into a quality control system for inkjet printing, Palo *et al.* 2016 investigated quantifying APIs (caffeine and loperamide HCl) using attenuated total reflectance (ATR) Fourier transform infrared (FTIR) spectroscopy. The dose strengths were varied by changing the drop spacing of the prints. It was found that a linear correlation exists between drop spacing and the height or area of an absorbance band and a logarithmic relation between drug content and absorbance band. ATR-FTIR was also seen to have good predictability when investigating drug content. With ATR-FTIR a quick, easy to use and non-destructive method of quality control can be incorporated into the manufacturing route of tablets [51].

Colorimetry as a quality control method was investigated by Wickström *et al.* 2016 for paediatric formulations made with thermal inkjet printing. With different Vitamin B types and a yellow edible ink, formulations were printed on different substrates (copy paper, sugar paper and rice paper) for the creation of ODFs. As more layers were printed, the yellow colour intensity increased (Figure 2.6). Colorimetry was seen

to be successful in detecting doses up to the fifth and sixth layers after which colour saturation of the yellow colour prevented further measurements. The authors did however show that handheld colorimetry could be used as a quality control process for the inkjet manufacturing of ODFs as long as colour saturation was not reached [52].

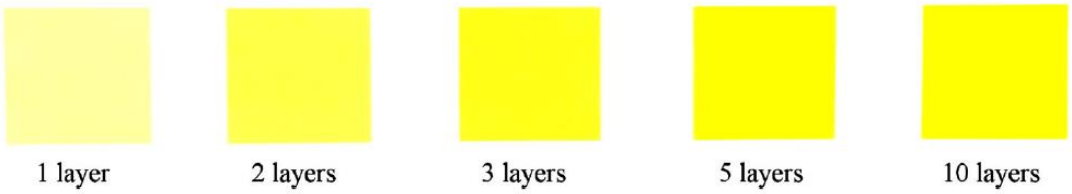



*Figure 2.6 - Change in colour intensity as more drug containing layers were printed (taken from Wickström et al. 2016)* [52].

Edinger *et al.* 2017 investigated Raman spectroscopy as a visualisation and quality control process for inkjet printed haloperidol. The drug was formulated with lactic acid and ethanol and jetted onto custom-made inorganic compacts (calcium hydrogen phosphate dihydrate), hydroxypropyl methylcellulose (HPMC) dry foam and paracetamol tablets. Principal components analysis and partial least squares regression were conducted to create Raman chemical maps and to quantify drug content in the printed dosage from respectively. These techniques were successful for samples printed on the inorganic compacts and paracetamol tablets but not on the foam due to the poor and fluctuating density of the material. The authors had shown that Raman spectroscopy is a viable process for drug visualisation and content measuring. However, some conditions must be met. The substrate used is homogenous and has poor Raman scattering (in contrast to the drug which must have significant scattering). As Raman spectroscopy in predominantly a surface characterisation technique, the drug should be at the surface of the substrate or evenly distributed through the substrate. Hence, porosity of the substrate and penetration of the ink must be taken into account [53].

Edinger *et al.* 2018 explored the use of inkjet printed quick response (QR) codes for labelling and quality control in pharmaceutical manufacturing. Using haloperidol as a model API, the drug containing solution was printed using a QR generated pattern on HPMC substrates (Figure 2.7). Actual drug content (measured with high performance liquid chromatography (HPLC)) was closely matched to the theoretical content (based

on ink composition and volume). High definition printing allowed the use of handheld smartphone devices to read the code accurately and extract data [54].




*Figure 2.7 - Printed QR code containing drug on an edible HPMC substrate (taken from Edinger et al. 2018)* [54].

### 2.2.3 Combining and comparing other manufacturing processes

Inkjet printing has the potential to be incorporated with other manufacturing processes of oral dosage production. Papers investigating this are reviewed here.

Inkjet printing has been combined with flexographic printing to create tablets for controlled released, as shown in Figure 2.8. Genina *et al.* 2012 investigated substrates for inkjet printing (with different porosities and levels of smoothness) and water insoluble polymer films (ethylcellulose) to be used in the flexographic printing process to act as a release controlling barrier. Different release profiles were achieved with different substrates and different thicknesses of the ethylcellulose, highlighting inkjet printing's ability to tune drug release [55].

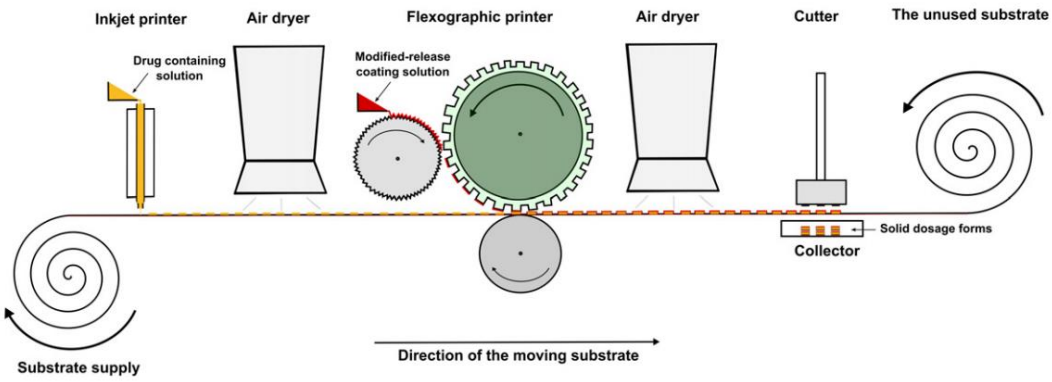



*Figure 2.8 - Schematic representing the combination of inkjet and flexographic printing (taken from Genina et al. 2012)* [55].

Raijada *et al.* 2013 compared inkjet printing to flexographic printing for the development of a formulation for poorly soluble drugs. Using a co-solvent system of polyethylene glycol (PEG) and ethanol for inkjet printing and only PEG for flexographic printing it was found that greater accuracy for drug deposition was found with inkjet printing [56]. The paper also discusses a generic approach for choosing a printing system with parameters when trying to create a printable drug formulation as well as potential characterisation methods, shown in Figure 2.9.

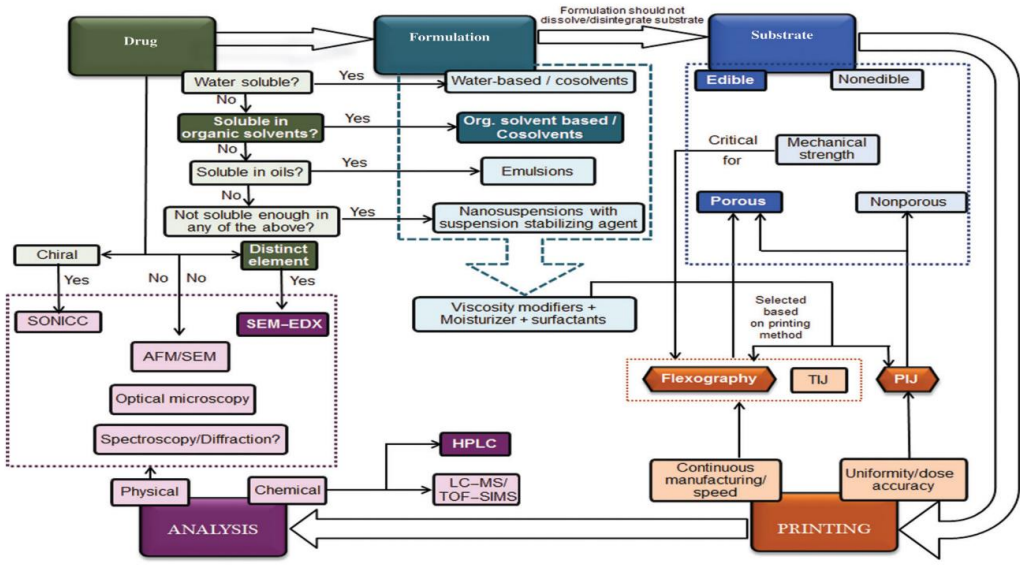



*Figure 2.9 - A suggested work flow process presenting the key stages of inkjet printing for tablets from formulation to post printing analysis (taken from Raijada et al. 2013)* [56] .

Inkjet printing has been compared to more traditional solvent casting methods to create ODFs by Buanz *et al.* 2015. Using a thermal inkjet process, clonidine HCl was printed in a formulation with methanol and glycerol. The ink was printed on polyvinyl alcohol

and carboxymethylcellulose films. Films prepared via solvent casting were more brittle. This was attributed to the drug exerting an anti-plasticising effect. The solvent casting process resulted in a molecular dispersion of the drug throughout the polymer, which caused this effect. The inkjet printed films however showed that the drug existed on the top layer or surface of the films, preventing any anti-plasticising effect to occur [57].

Inkjet printing has been combined with electrospinning to create oromucosal dosage forms by Palo *et al.* 2017. The authors illustrated the combination of two manufacturing processes to create dual drug delivery systems (process summarised in Figure 2.10). Piroxicam was incorporated into the electrospinning process to create drug loaded fibres. Lidocaine HCl was then jetted onto the fibres as well as cross-linked gelatin substrates. The accuracy of inkjet printing was highlighted by similar values of theoretical drug content. There was some evidence of drug degradation of the inkjet printed drug. After eight months in storages, significantly less amount of drug had been detected compared to the theoretical dose. The degradation of the drug was attributed to the hydrolysis of its amide functional group. Differential scanning calorimetry (DSC) and XRD showed that lidocaine HCl existed in a molecularly dispersed state. and a rapid drug release was observed (85 % in eight minutes) [58].

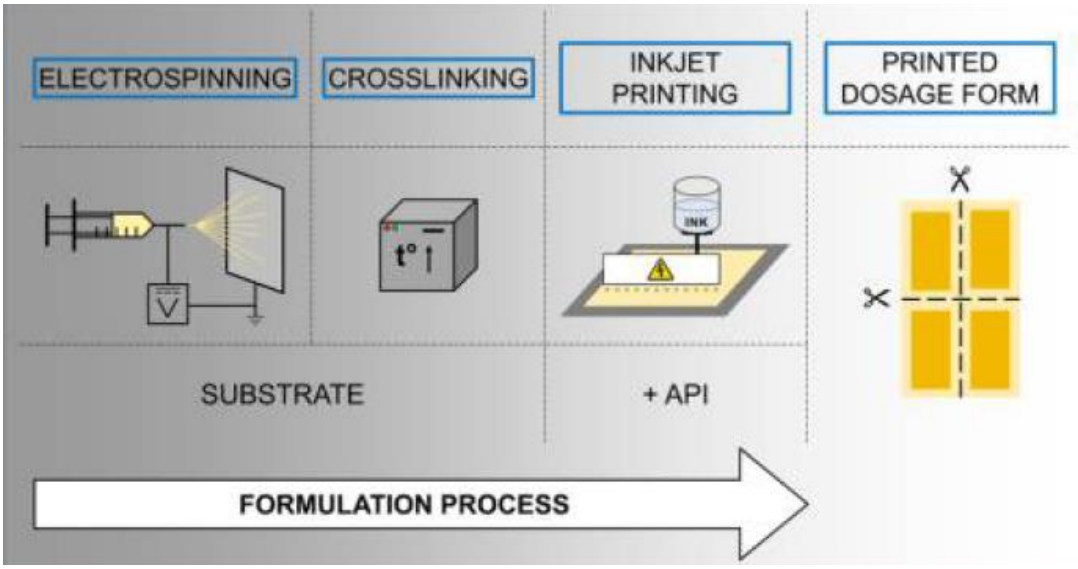



*Figure 2.10 - Manufacturing process combining electrospinning and inkjet printing to create oromucosal dosage forms (taken from Palo et al. 2017)* [58].

The printing of biologics (using lysozyme as a model) for a buccal drug delivery system was done by Montenegro-Nicolini *et al.* 2018. The biologic drug was printed

on previously solvent casted HPMC and chitosan films and PCL electrospun fibres. The jetting the biologic did not affect the mechanical or mucoadhesive (work of adhesion and detachment force) properties of the devices [59].

Printing combinations of drug were illustrated by Thabet *et al.* 2018a. Here the authors jetted enalapril maleate ink onto previously casted ODFs containing hydrochlorothiazide. The authors illustrated that no enalapril maleate migrated into the hydrochlorothiazide layers through the use of confocal Raman microscopy (Figure 2.11), highlighting the inkjet process as superior to solvent casting multi-layer films where migration of drug is a limitation [63].

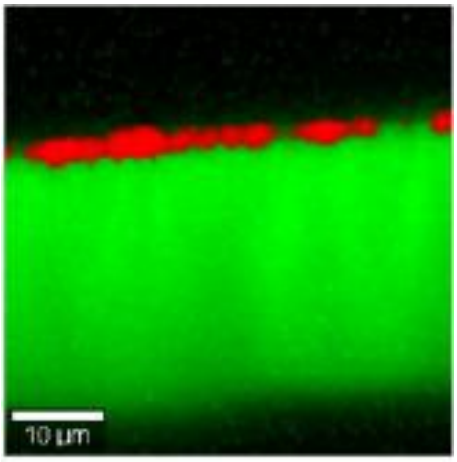



*Figure 2.11 – Confocal Raman map showing that the inkjet printed enalapril maleate (red) did not penetrated through the ODF containing hydrochlorothiazide (green) (taken from Thabet et al. 2018a)* [63].

Thabet *et al.* 2018b expanded on this investigation by moving on from small scale inkjet printer systems to a pilot scale process. A continuous ODF production process (Figure 2.12) was used to achieve this. Different printing parameters were investigated to ensure that the continuous process was a reliable manufacturing route including firing frequency, applied voltage and waveform. Image analysis was used as a process analytical technology using a standard computer scanner with the use of methylene blue dye [64].

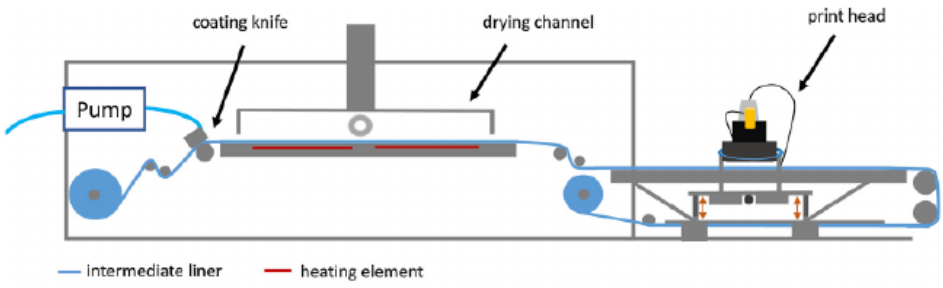



*Figure 2.12 – Schematic of the continuous coating machine and modified inkjet printing system used to create ODFs (taken from Thabet et al. 2018b)* [64].

### 2.2.4 Jetting into containers for oral delivery

In addition to printing of edible substrates, inkjet printing has been used to dose drug containing materials into containers for oral delivery.

Planar micro-devices for oral drug delivery were created and inkjet printed into (Figure 2.13) with the drug topotecan and biologic insulin by Fox *et al.* 2017. These devices were created to address issues such as low oral bioavailability due to the pH and enzymatic conditions that exist in gastrointestinal tract. Inkjet printing was used due to its high throughput while maintaining high efficiency. The method was seen to be relatively accurate (e.g. an average 21.5 µg of insulin was detected in contrast to the 19.2 µg of insulin expected), with differences in loadings attributed to variation in droplet size. As the inkjet system used was easily programmable (highlighting ease of potential of personalisation), experimental parameters such printing and drying cycles allowed large drug loading capacities in contrast to other techniques where the drug loading in limited due to solubility. The process did not require any UV light or heat which would not damage or degrade sensitive biologics and drugs. The authors highlight the use of inkjet printing for creating low-waste but high-capacity loading devices for different drug-containing micro-devices. Drug release studies were not examined by the authors [60].

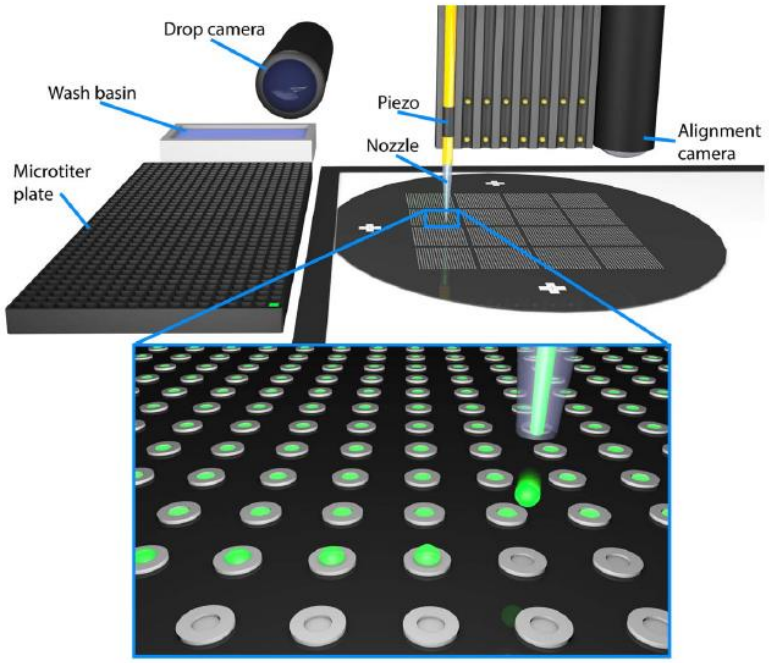



*Figure 2.13 - Overview of the inkjet process for deposition of drugs into micro-devices (taken from Fox et al. 2017)* [60].

Acosta-Vélez *et al.* 2017 used a photo-curable ink to inkjet print the hydrophilic drug ropinirole HCl into preformed tablets (see Figure 2.14). Norbornene moieties functionalised hyaluronic acid and was formulated with PEG dithiol and the drug. With Eosin Y acting as the photo-initiator a rapid step-growth polymerisation reaction via thiol-ene chemistry resulted in a drug loaded hydrogel when exposed to visible light. The tunability of mechanical properties was investigated by varying parameters such as the loading of functionalised hyaluronic acid, the crosslinking ratio and light exposure time. Dissolution from the preformed tablets showed that 60 % of ropinirole HCl is released within 15 minutes [61].



*Figure 2.14 - Preformed tablets cap and base (top row), base of preform tablet with inkjet printed formulation (bottom left )and the closed tablet (bottom right) (taken from Acosta-Vélez et al. 2017)* [61]

Inkjet printing a UV curable formulation for hydrophobic drugs was achieved by Acosta-Vélez *et al.* 2018. Individual inks were formulated with naproxen and ibuprofen. The bio-ink consisted of polyethylene glycol diacrylate (PEGDA) as the monomer, Eosin Y as the photo-initiator, methoxide-polyethylene glycol-amine as a co-initiator and PEG as a plasticiser. The ink was deposited into preformed tablets and capped off (illustrated in Figure 2.15). The cured tablets were then removed from the preformed templates for characterisation. The microstructure of the printed formulation's (with naproxen) cross section was characterised with SEM imaging. No naproxen crystals were seen suggested the drug had dissolved in the polymer. With samples with a lower PEGDA content, increased porosity was observed. The mesh size (an ambiguous characteristic length in polymer gels often referring to the distance between cross-linkers) within the polymer was determined to elucidate the potential effects on drug release. With a lower PEGDA loading, mesh size increased, which would lead to a faster drug release. This was proven to be true where tablets with a 20 wt% PEGDA loading had a significantly faster drug release compared with tablets with a 100 wt% PEGDA loading. In addition, it was found that decreasing the time for curing resulted in faster release [62].

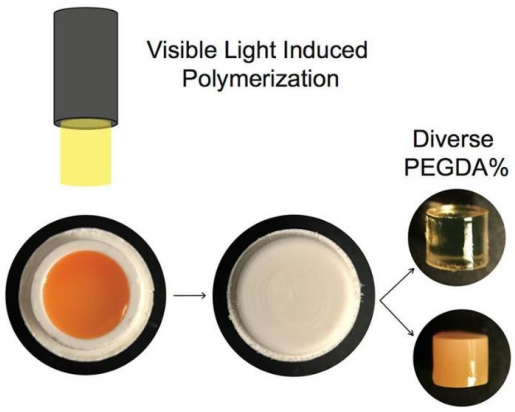



*Figure 2.15 – Hydrophobic drug formulation was jetted into preform tablets and cured. They were then removed for characterisation (taken from Acosta-Vélez et al. 2018)* [62].

### 2.2.5 Multi-material printing

This section reviews papers that use multiple inks for the manufacturing of dosages for oral delivery.

ODFs for the treatment of hypothyroidism were inkjet printed with oral drug combinations by Alomari *et al.* 2018. A two cartridge thermal inkjet printer was used to print separate solutions of triiodothyronine and thyroxine on HPMC gel substrates casted on polyester sheets. Dose control was achieved by varying the length of prints (i.e. pattern size). The authors have illustrated that inkjet printing is capable of dosing multiple drug-containing inks onto the same substrate [65].

The ability to create a single device with multiple drugs was illustrated by Scoutaris *et al.* 2018, where jet dispensing technology was used to create a three-layer film for three antihypertensive agents: hydrochlorothiazide, amiloride HCl and carvedilol (Figure 2.16). The first layer (layer 1) was printed with an ink formulated with ethylcellulose, copovidone and the APIs hydrochlorothiazide and carvedilol (dissolved in ethanol). The second layer (layer 2) was printed with only amiloride HCl, dissolved in an ethanol and water cosolvent system. The third and final layer (layer 3) consisted of 'dots' of carvedilol with copovidone dissolved in methanol. The authors note that organic solvents are not always advantageous due to their hazardous nature, however these were necessary due to the nature of the formulation. It was unclear if removal of the thin film from its substrate (not specified) had occurred for analysis including dissolution and if this caused any damage. It is also not clear if what is referred to as layers 1, 2 and 3 are actually single printed layers, or if they consisted

of multiple layers (based on the volume of ink it would suggest that it was made of multiple layers: e.g. layer 1 required 3.57 mL of ink to be jetted) [66].

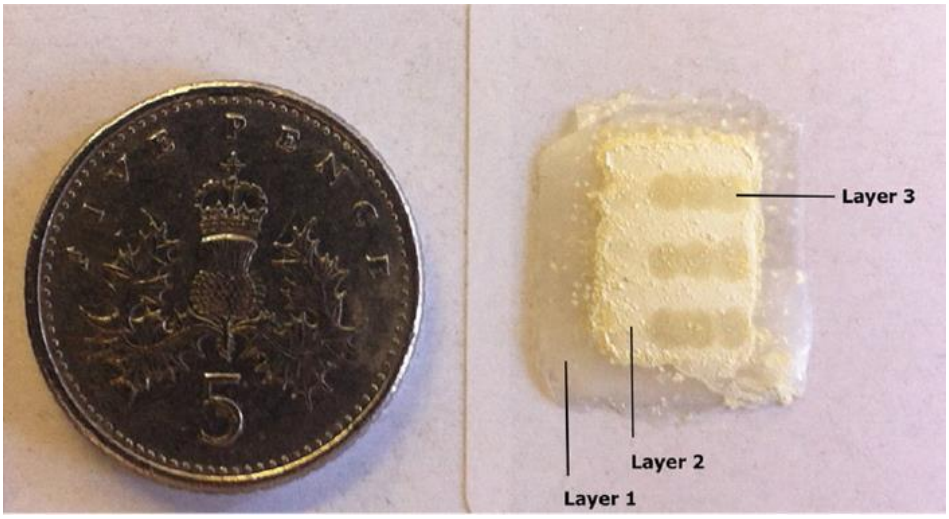



*Figure 2.16 - The three-layer film containing three antihypertensive drugs (taken from Scoutaris et al. 2018)* [66].

Analysis of the printed films with SEM showed that layers, where the drug is mixed with a polymer, are smooth and transparent. This indicated that the drugs are incorporated in the polymeric matrix. For layer 2, amiloride HCl existed as fine drug particles. XRD and DSC studies showed that all components in this formulation were amorphous, with the exception of hydrochlorothiazide, which was seen to be partially crystalline. The distribution of drug was investigated with confocal Raman mapping and principal component analysis. Analysis of layer 1 showed that both hydrochlorothiazide and carvedilol were distributed across the surface. There was no mention of the uniformity of distribution of drug (i.e. if there were there drug rich or poor regions) It was attempted to examine distribution of carvedilol in layer 3, however peaks from layer 2 (amiloride HCl) were dominant. This suggested that the layer 3's solution had been absorbed by layer 2 [66].

Drug content, measured with HPLC, was seen to closely match the film's nominal values. Dissolution of the films was also conducted. A degree of controlled release was achieved by varying the ratios of copovidone and ethylcellulose in layer 1. By increasing copovidone content, drug release was faster. This was attributed to copovidone's potential function as a pore forming agent (although this was not experimentally confirmed by the authors), allowing a faster release of hydrochlorothiazide and carvedilol. Release of amiloride HCl was fastest as this drug

was not embedded in any polymer matrix, whereas hydrochlorothiazide and carvedilol release was more sustained. For carvedilol in particular, a biphasic drug release was observed. An initial burst release from layer 3 was followed by a more sustained release from layer 1 [66].

### 2.2.6 Freestanding and wholly inkjet printed tablets

The first wholly inkjet printed tablet was manufactured by Kyobula *et al.* 2017 using a hot-melt inkjet system. A mixture consisting of 5 wt% fenofibrate in beeswax was created by melting and mixing the components. Using a hot-melt chamber, the mixture was loaded onto a LP50 PiXDRO (Meyer Burger) printer and heated to 90 °C for optimal printing. The tablets were printed on a polyethylene terephthalate (PET) substrate at 40 °C with different internal structures (shown in Figure 2.17) and were thoroughly characterised [67].

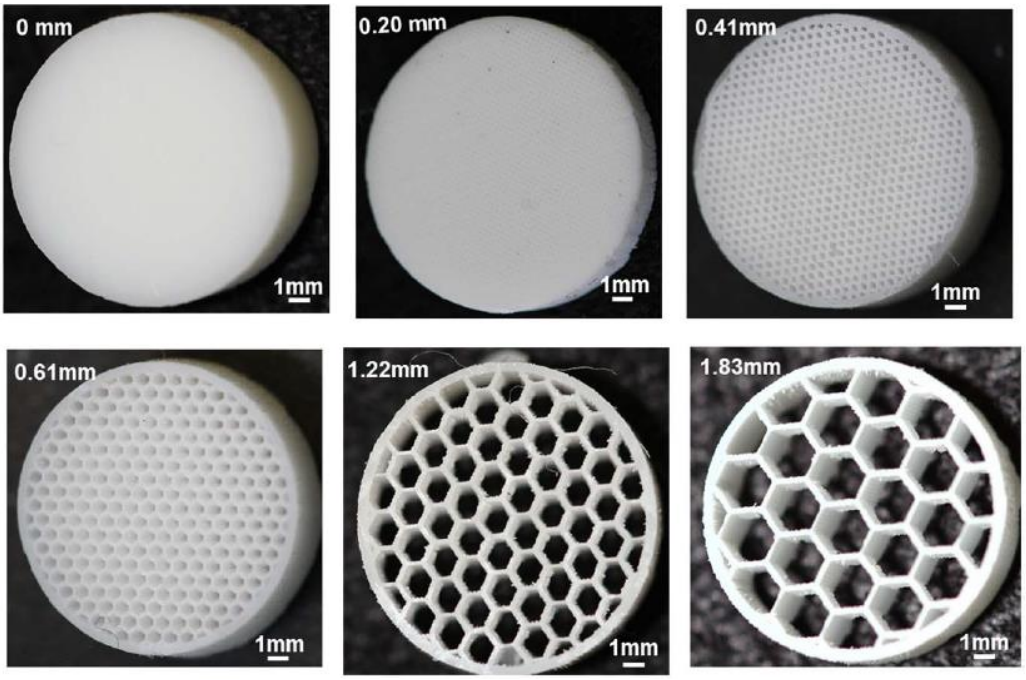



*Figure 2.17 - The internal solid and honeycomb structures printed. Spacing between honeycomb cells were varied (taken from Kyobula et al. 2017)* [67].

DSC thermograms showed that the mixture did not have the melting peak of Form 1 fenofibrate (the initial state of the drug) at 81 °C and closely followed the thermogram of pure beeswax. This suggested that fenofibrate exists in the formulation in an amorphous state. ToF-SIMS was conducted on the tablet to investigate drug distribution. Examination of the drug at the surface of the tablet showed that drug was

heterogeneously distributed at the surface. In contrast, when the bulk of the tablet was investigated (up to 10 µm deep) the drug ion intensity was seen to increase as depth increased until plateauing at approximately 2.5 µm. The lack of drug at the surface of the tablet was thought to be a result of the formation of crystalline regions of the beeswax material during cooling and solidification. The presence of drug particles may have exasperated an efflorescence phenomenon, where the drug was thought to be excluded from the crystalline regions. Drug distribution was further investigated with Raman spectroscopy. No significant peak shift was observed when compared to the pure components suggesting no major changes to the beeswax and drug structurally. Raman mapping of the tablet (with a 20 µm penetration depth of the laser) showed that fenofibrate was homogenously distributed in the bulk [67].

Drug release behaviour was investigated by printing tablets with varying internal structures. As illustrated in Figure 2.17, a solid tablet was printed, and then different honeycomb structures were created with varying spacing size. The ability to create and control the complex internal structures, done easily with inkjet printing, highlights the process as a viable manufacturing route for highly customised drug delivery devices. The solid tablet was seen to have the slowest and most incomplete drug release after 12 hours with faster drug release seen with tablets with the honeycomb internal structure (profiles shown in Figure 2.18). The drug release mechanism was determined to be a Fickian diffusion-controlled drug release mechanism, through the application of different dissolution kinetic models. Predictive release models were mathematically generated and showed similar profiles to what was seen experimentally, except for one batch of tablets where spacing was 0.2 mm (where release was slower than expected), attributed to a poor wetting effect [67].

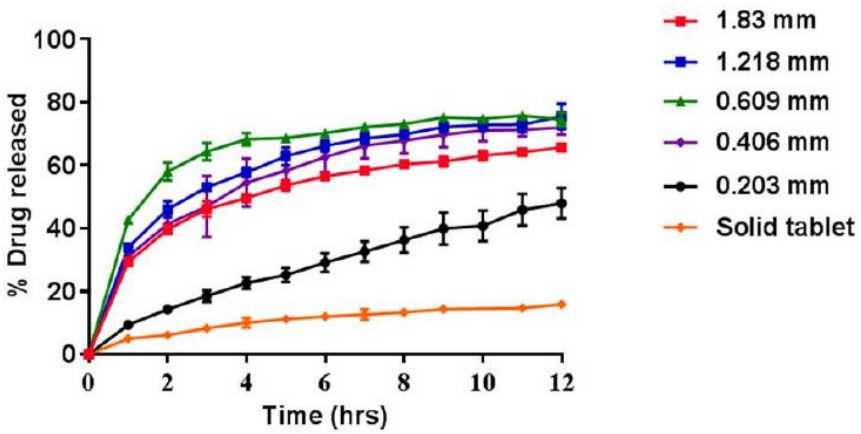



*Figure 2.18 - The different release profiles achieved as the internal honeycomb structure is varied (taken from Kyobula et al. 2017)* [67].

Using a UV curable inkjet process, Clark *et al.* 2017 manufactured free-standing tablets (Figure 2.19). Using Irgacure 2959 as a photo-initiator, the drug ropinirole HCl was formulated with PEGDA and water (used as a solvent for the drug). FTIR had shown that the printed tablet had been cured to a high degree as the peaks associated with the acrylate were not observed. Confocal Raman spectroscopy was used to investigate the drug on the top surface of the tablet. Chemical imaging illustrated the presence of drug rich and poor regions at the micron scale. The drug was thought to exist as a solid dispersion as no evidence of drug crystallinity was observed. Transmission cross-polarised optical microscopy of the tablets also suggested this. Swelling and leaching experiments were carried out. Tablets with drug were seen to swell 48 % and 97 % of drug was detected. This suggested that some of the drug release was incomplete or that some drug had degraded. The tablets remained intact throughout the process. Dissolution testing showed that 89 % of drug was released over four hours (60 % within the first hour). Application of dissolution models suggested that Fickian diffusion was the predominant mechanism for release [68].

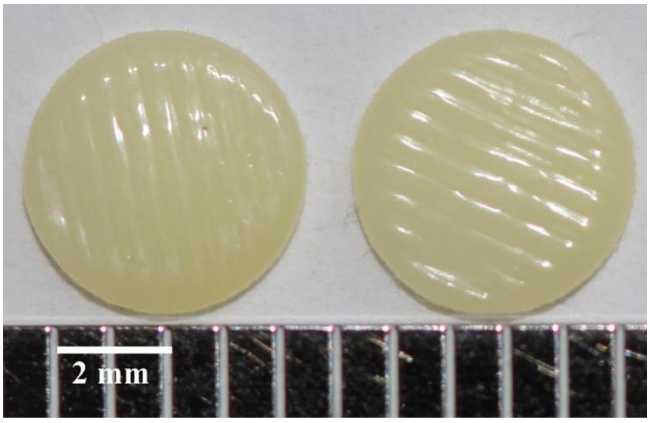



*Figure 2.19 - UV-cured inkjet printed tablets containing ropinirole HCl (taken from Clark et al. 2017)* [68].

## 2.3 Other Additive Manufacturing Techniques for Tablet Manufacturing

### 2.3.1 Binder jetting

One of the earliest additive processes to create tablets was done with binder jetting [69]. There has been significant work into the creation of controlled release devices including immediate-to-extended release, enteric dual pulse tablets [70] as well as devices capable of delivering a zero-order drug release [71]. Functionally graded tablets have also been printed by varying the composition of a release retarding material, resulting in an erosion controlled linear release [72]. Binder jetting has so far been the only additive process where FDA has approved a 3D printed tablet. Using their ZipDose Technology, Aprecia Pharmaceuticals have manufactured tablets with a highly porous structure allowing for rapid dispersion with taste masking properties [73]. The process is illustrated in Figure 2.20.

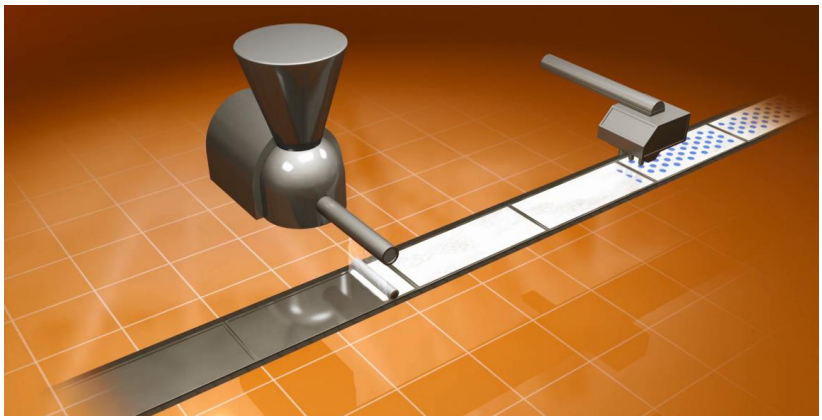


*Figure 2.20 – The ZipDose process involved the layering of powder material and the jetting of a binder (taken from Aprecia, "ZipDose Technology")* [74].

### 2.3.2 Material extrusion

Material extrusion has been investigated extensively for the creation of tablets. Both paste-based methods of extrusion as well as fused deposition modelling (FDM) have been used to show how to influence release rates by changing ink composition [75], geometry [24] and internal structures by varying infill structures [76] [77] (e.g. Figure 2.21) or by creating multi-layered tablets [78]. Multi-material printing has been highlighted by printed multiple APIs into a single tablet (polypills), with each drug released in individual controlled mechanisms [26].

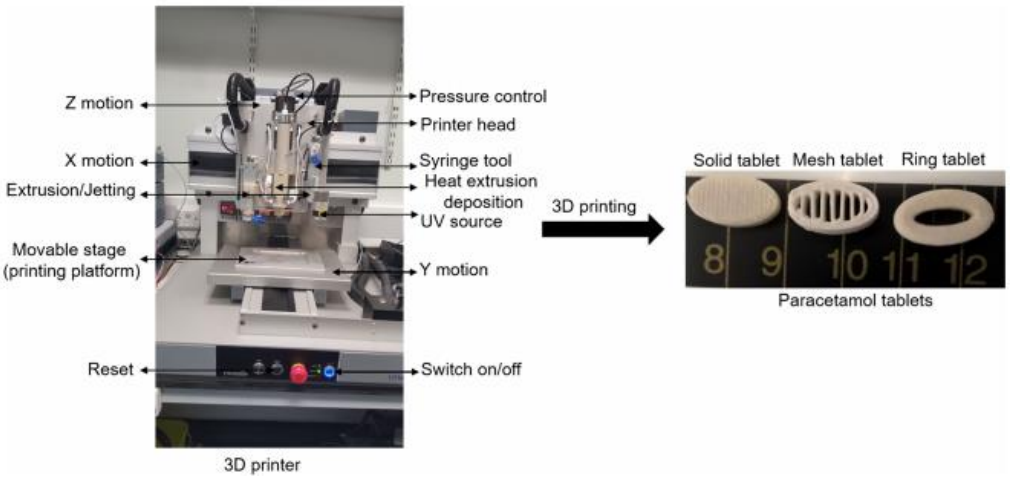



*Figure 2.21 – The material extrusion printer that was used to create paracetamol containing tablets with varying geometry to control drug release (taken from Khaled et al. 2018)* [77]

Goyanes *et al.* 2017 used FDM printed tablets to investigate patient acceptability of the additively manufactured tablets. Patient acceptability must be a key criterion for 3D printed tablets to meet if they are to be a truly patient centric method for personalised medicine. Different shapes, sizes and colours were presented to patients and their likelihood to take the medicine was recorded as well as their swallowability. The highest novel shape was the torus structure. Size choice was influenced by geometry and colour choice required further data, although darker colours were deemed to less favourable [79].

### 2.3.3 Stereolithography

Stereolithography (SLA) is a relatively new additive process for the 3D printing of tablets. Wang *et al.* 2016, used SLA with PEGDA as a monomer to illustrate its used for the manufacturing of tablets with paracetamol and aminosalicylic acid as model

drugs. The authors showed SLA's ability to control drug release by varying ratios of PEGDA with PEG 300. Lower PEGDA content resulted in faster release times as there would be less crosslinking within the tablet matrix. This results in greater mobility for PEG 300 and increased dissolution with drug release. Further controls such as the power of light used, scanning speed and duration of curing need to be further investigated for greater control [80].

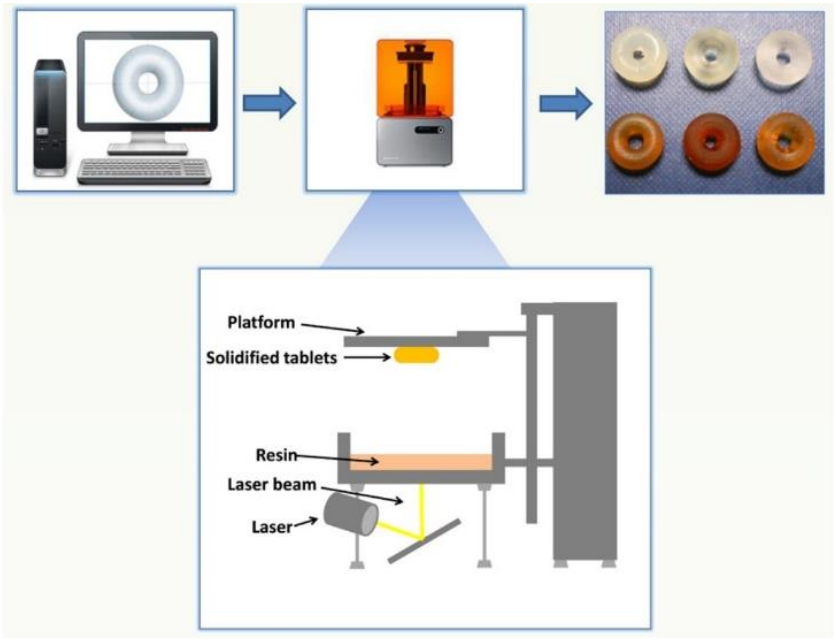



*Figure 2.22 – The stages of printing tablets using SLA with a Formlabs printer. Tablet designs are created on a computer, loaded on to the printer and final product is printed (taken from Wang et al. 2016)* [80].

### 2.3.4 Selective laser sintering

Selective laser sintering (SLS) is another additive process that has shown potential for tablet manufacture. SLS has illustrated different release profiles including sustained releases (over hours) [81] and rapid releasing oral disintegrating tablets [82] by investigating print and material parameters. Complex geometrical tablets were printed using computer generated lattice structures to illustrate major influence geometry can play in drug release [83]. The use of the food additive Candurin Gold Sheen was incorporated into the powder bed to aid the sintering process by enhancing energy absorption from the laser [81].

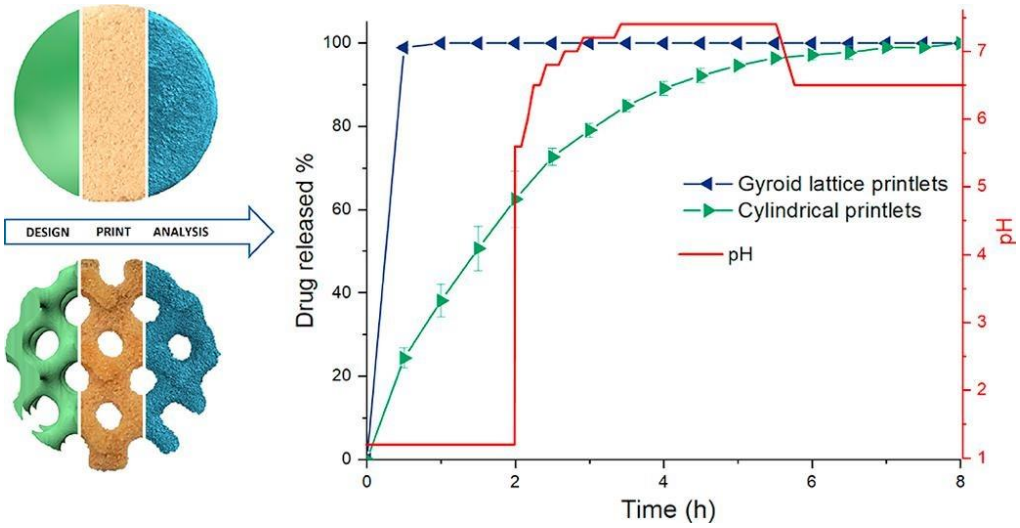



*Figure 2.23 – Design, print and post-print analysis for SLS printed tablets with different structures and their significantly different release profiles (taken from Fina et al. 2018)* [83].

## 2.4 Identification of Gaps in State of the Art

### 2.4.1 Wholly inkjet printed tablets with a non-toxic solvent evaporation solidification mechanism

Literature regarding the solvent-based inkjet printing for tablet production mostly used a sort of substrate that forms part of the dosage form. Jetting has involved the use of solvents, nanosuspensions and nanoplexes for both poorly water soluble and highly water-soluble drugs. Thin films, printed with the use of organic solvents, have also been manufactured, however they have used organic solvents that would require tracking and quantification post-manufacturing. In instances where inkjet printing results in tablets that are not attached to an edible substrate or a preformed tablet, UV curing and or a phase change (from molten material) is the solidification mechanism. The complete inkjet printing of a solid oral dosage form with the use of a non-toxic solvent, such as water has not been previously investigated. There have been instances where aqueous formulations have been used, but only where the printing process is used as a dosing technology. Non-toxic solvents can be advantageous as it would negate the need of post-printing curing and the need for checking all material had been fully cured or removed. Avoiding the use of a hot-melt inkjet system would also allow for thermally sensitive drugs to be used for inkjet printing.

### 2.4.2 Multi-material inkjet printed reservoir system tablets for controlled release

Controlled releasing tablets have been manufactured with the use of a single ink. Parameters such as geometry, ink formulation and curing time have been used to influence drug release. Scoutaris *et al.* 2018 created a three-layer film structure with multiple APIs for oral delivery solely with inkjet printing. The ability to control drug release was mainly achieved for one of the dosage's components but varying the ink formulation. So far, there have not been investigations of multi-material inkjet printing to create freestanding reservoir tablets where drug release is controlled by influencing the physical structure of a release controlling membrane. This could be achieved by not only varying the ink formulation, but by changing the parameters of the inkjet printing process (e.g. drop spacing). This would highlight inkjet printing's versatility and ability to customise release using an easily accessed and programmable manufacturing process.

## 2.5 Conclusion

Inkjet printing has successfully been used in the past to create oral pharmaceutical tablets. Various literature has been examined and their key findings and novelty highlight the different products that inkjet printing have produced and the process' advantages:

- Drug and biologic containing microspheres, liposomes, nanosuspensions and solutions have been jetted with the use of solvent-based and UV-curable formulations.
- Most inkjet printing for oral delivery occurred using variety of substrates that form part of the solid oral dosage form. Preformed tablets and planar micro-devices have also been used.
- Controlled drug release has been achieved by controlling the substrates on which they have been printed, the component loadings in the formulation, geometry of the devices printed, and the printing parameters used.
- Inkjet printing has been combined with electrospinning and flexographic printing to create solid oral dosage forms capable of controlled drug release.
- Both poorly water soluble and highly water-soluble drugs have been developed into inkjet printable formulations.

- High drug loadings have been achieved for inkjet formulations.
- Drug loadings have been proven their potential for highly reproducible, uniform and accurate applications.
- Numerous characterisation methods (such as Raman spectroscopy and colorimetry) have been investigated and proven to be potential method of quality control for dose quantification and location if inkjet printing were to be adopted for tablet manufacturing.
- It has been illustrated that the inkjet process can be easily programmed highlighting the potential for its manufacturing process to be easily to manipulated leading to personalised medicine.
- Multi-material inkjet printing has been used to create dosages containing different APIs and well as creating multi-layered thin film structures, capable of delivering a controlled drug release.
- Wholly inkjet printed tablets have been created using hot-melt and UV curable inkjet printing setups.

Other additive manufacturing technologies have also been used to create tablets. Controlled release from these tablets had been achieved by varying materials, ink formulations, geometry and printing parameters. The technologies included binder jetting, material extrusion, SLA and SLS.

Through the review of literature, two gaps in the research were identified.

- Wholly inkjet printed tablets have not been produced where a non-toxic water-based formulation was used, and evaporation was the main solidification mechanism.
- Multi-material wholly inkjet printed reservoir tablets have also not been produced in the past. By investigating different printing parameters, the physical structure of a release controlling membrane could be varied, potentially resulting in controlled drug release.

# 3 Inkjet Printing of Tablets with a Rapid Drug Release

Parts of this chapter have been submitted for publication: *H.K. Cader, G.A. Rance, M.R. Alexander, A.D. Gonçalves, C.J. Roberts, C.J. Tuck and R.D. Wildman, "Water-Based 3D Inkjet Printing of an Oral Pharmaceutical Dosage Form" International Journal of Pharmaceutics 2018.*

## 3.1 Introduction

### 3.1.1 Aims of chapter

- Print a free-standing tablet with a rapid drug release that will act as the core for a reservoir device
- Show that inkjet printing can be used to deliver accurate doses reliably
- Show that the used API is in its desired polymorphic form
- Show the API is uniformly distributed throughout the tablet

### 3.1.2 Background

To ensure a printed tablet would have a very rapid release (to highlight control when it is introduced), an ink around only water-soluble components was formulated. This would also provide the opportunity to use water as the solvent for an ink, illustrating the method of using solvent inkjet printing as a safe and toxic-free method of 3D printing tablets. Although there have been publications using a water-based formulation [39] for jetting drug-loaded inks, most use traditional organic and sometimes toxic solvents [41] and use inkjet printing as a method for dosing, rather than an individual manufacturing process.

As a model API, thiamine HCl was selected. This small organic molecule (structure shown in Figure 3.1) is vital for chemical functions such as enzyme catalysis as they cannot be performed by ordinary amino acids, lipids and sugars [84]. This water soluble (50 mg/mL [85]) vitamin (B1) is specifically used for carbohydrate metabolism and for the development and function of the brain and nerves [86]. The drug is also known to be effective in the treatment of diseases including beriberi and tuberculosis [87].

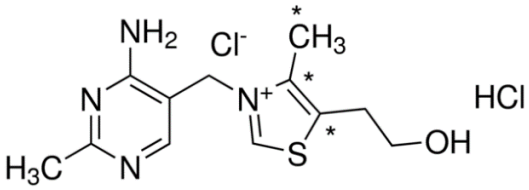



*Figure 3.1 - Molecular structure of thiamine HCl* [88].

There has been significant work in identifying the different polymorphic forms of thiamine HCl. The phases included a non-stoichiometric hydrate (NSH), a hemihydrate (HH) and an anhydrate (AH). When exposed to methanol, thiamine HCl can also form a monomethanolate (MM) and a desolvated MM [89]. In this investigation the two possible hydration states of thiamine HCl are the NSH and HH phase. The NSH is the starting phase for manufacturing and the preferred state for tablets [90]. NSH can readily transform to the HH state when in contact with water, often in high humidity environments. The phase change begins with moisture adsorption on the NSH crystal surface. This causes some of the NSH crystals to dissolve or deliquesce. Recrystallisation of the HH crystals then occur as they have a lower water solubility [91]. Even though the HH is exceptionally stable, it has lower aqueous solubility [92] and has poorer powder flow characteristics [91].

PVP (Figure 3.2) is a water-soluble polymer that is widely used in drug delivery applications. Due to its broad properties including good biocompatibility, chemical stability, solubility in a wide range of solvents it is widely used as an excipient in tablet manufacturing [93]. PVP would be used as the main polymer carrier for a rapid releasing tablet.

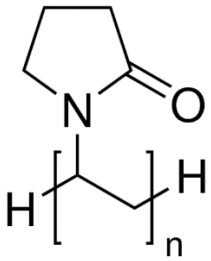



*Figure 3.2 - Molecular structure of PVP* [94].

## 3.2 Materials and Methods

### 3.2.1 Materials

Polyvinylpyrrolidone ($M_w$ ~ 10,000), thiamine HCl (reagent grade, > 99%), polysorbate 20 (TWEEN20) and glycerol were used with deionised water to form the required ink formulation. All chemicals were purchased from Sigma Aldrich. Polyethylene terephthalate films and Glass slides and (ThermoScientific) were provided by the University of Nottingham.

### 3.2.2 Methods

#### *3.2.2.1 Tablet design*

Using the Fujifilm Dimatix pattern editor software, two-dimensional (2D) bitmap patterns were generated. The drop spacing of patterns was set using the pattern edit software too. To illustrate dose variation with a single formulation, different patterns were created and are shown in Table 3.1.

*Table 3.1 - Tablet designs generated and printed in this investigation.*

| Pattern dimensions (mm) | No. of layers |
|---|---|
| 5 x 5 | 125 |
| 5 x 5 | 250 |
| 5 x 5 | 375 |
| 2.5 x 5 | 250 |
| 10 x 5 | 250 |

#### *3.2.2.2 Ink preparation*

All materials were weighed and placed in glass vials. The components were placed on a hot plate and heated (60 °C) and stirred (with a magnetic stirrer) until all components were dissolved.

#### 3.2.2.3 *Surface tension and contact angle measurement*

A Krüss Drop Shape Analyser (DSA100) was used for surface tension and contact angle measurements. For surface tension measurements, 1 mL of the ink was syringed and loaded onto the DSA. Small volumes of the ink were dosed through the syringe and an attached needle until a stable droplet had formed. Just before the droplet was dispensed, a profile of the droplet was taken from which surface tension was computationally calculated. To measure the ink's contact angle (θ), the substrate was raised to collect a drop from the syringe, minimising the effect of impact. The contact angle measurement was taken as soon the drop separated from the needle. Work of adhesion ($W_A$) values were calculated using the Young-Dupre equation (Equation 3.1) with the contact angle and ink's surface tension values (γ) [95]. Measurements were taken at the ambient room temperature, which at the time was 23 °C.

$$W_A = \gamma(1 + \cos\theta) \qquad 3.1$$

#### 3.2.2.4 *Viscosity*

Shear viscosity was measured using a Malvern Instruments Kinexus Pro Research Rheometer. A cup and bob set up was used to prevent solvent evaporation during the process. 3.09 mL of ink was syringed into the lower geometry (the cup) and the bob was automatically lowered into the cup. Shear viscosity was measured at shear rates between 1 $s^{-1}$ and 1000 $s^{-1}$. The measurements at 100 $s^{-1}$ were taken as a guide to the ink's viscosity during deposition. This is a widely accepted practice for determining the viscosity of Newtonian inks for jetting. In reality, shear rates during the jetting process can reach $10^5$ – $10^6$ $s^{-1}$ [10]. The temperature was fixed to 28 °C.

#### 3.2.2.5 *Density*

0.5 mL of the ink was syringed into a vial on a mass balance. The ratio between mass and volume was used to calculate the density of the ink.

#### 3.2.2.6 *Printing*

Printing was conducted using a Fujifilm Dimatix Materials Printer DMP-2850 Series. 3 mL of ink was loaded into a cartridge through a 0.45 µm filter (preventing any large particles from blocking the 21 µm nozzles [96]). A print head (10 pL drop volume)

with 16 nozzles was then attached to the printer cartridge. The parameters for jetting that can be controlled were the jetting voltage, waveform, frequency and cartridge heating. Jetting behaviour can be observed by using the system's drop watcher feature. For print formation, parameters such as substrate heating and distance between the print head and substrate could be varied. Drop spacing was set and calibrated using the calliper system on the Dimatix printer (based on what was set in the pattern editor).

#### *3.2.2.7 Optical microscopy*

A Nikon Eclipse LV100ND Optical Microscope was used to analyse the printed materials.

#### *3.2.2.8 Atomic force microscopy*

Atomic force microscopy (AFM) was conducted with Bruker Dimension FastScan Bio ICON. Mechanical properties mode was used with tapping in air. 16 x 16 µm maps were generated with a scan rate of 1.93 Hz. Peak force amplitude was set at 150 nm. Bruker RTESPA-300 probes were used. Nanoscope Analysis 1.7 was used for data analysis. 2$^{nd}$ order flattening was applied to remove tilt and bow features of the scans.

#### *3.2.2.9 Time-of-flight secondary ion mass spectrometry*

ToF-SIMS was conducted with a ToF-SIMS IV instrument (ION-TOF GmbH). $Bi^{3+}$ primary ion beam was used with an energy of 25000 eV. Pure thiamine HCl and PVP spectra were generated by dissolving each component in water and drop casting solutions on glass slides. Samples were analysed after being dried in air. Only negative spectra were generated. 6 x 6 mm mapping was done of films with a raster size of 600 x 600 pixels. Mapped images were generated after one scan. ION-TOF SurfaceLab 6 was used for data processing and analysis.

Experimental work was done by Dr. David Scurr (University of Nottingham).

#### *3.2.2.10 Optical Profilometry*

A Zeta ZDot Optical Profilometer was used to conduct profilometry. Upper level and lower level limits were set based on the samples. 3D images were generated with 800 steps per image. Levelling was done by subtraction of the centre points of cursors.

#### *3.2.2.11 Determining drug theoretical content*

Using the Dimatix pattern editor software, the number of drops per layer for each pattern was calculated. With a known number of printed layers, the total number of droplets for each tablet was calculated.

Using the printer's drop watcher feature and ImageJ software, it was possible to measure the diameter of the individual droplets. The diameter of the cartridge's nozzle was known and used for converting the pixel units to a unit of length.

The droplet diameter allowed volume calculations. After the ink's density measurement, it was possible to calculate the mass of each droplet. Knowing the ink's composition, it was possible to calculate the content of thiamine HCl.

#### *3.2.2.12 Validation of drug content*

Elemental analysis by combustion was conducted with a LECO 628 Series Carbon/Hydrogen/Nitrogen determinator with a Sulphur add-on module. The furnace was set at 1350 °C with oxygen at 40 PSI.

Samples were run by Mr. Adrian Quinn (University of Nottingham).

#### *3.2.2.13 Determination of drug content in individual layers*

An array of 5 x 5 mm squares was printed on PET film with varying layers. Each square was cut and placed in a vial of 10 mL of deionised water maintained at 37 °C using a hotplate for 10 minutes. Vials were manually shaken and solutions were filtered (0.45 µm). Ultraviolet-visible (UV-Vis) spectroscopy, done with a Varian Cary 50 UV-Vis Spectrophotometer, was used to determine the absorbance at 266 nm, from which the drug content could be calculated.

Calibration standards were also prepared by dissolving thiamine HCl in deionised water and by preparing serial dilutions. Standard solutions were analysed using UV-Vis spectroscopy and a calibration line was plotted based on the absorbance detected at 266 nm. The intensity of the diagnostic peak for thiamine HCl at 266 nm was used to calculate the amount of drug released using the Beer-Lambert law [97].

#### *3.2.2.14 Polymorph identification*

A ThermoElectron FT-Raman NXR 9650 spectrometer was used to investigate the polymorphic phase of thiamine HCl. Spectra were acquired using a 1064 nm laser (at a power of 0.6 mW) over the range 100-3701 $cm^{-1}$. The spectral resolution in this configuration was 4 $cm^{-1}$. 128 accumulations were used for each measurement. The laser spot size was 50 µm.

#### *3.2.2.15 Drug distribution investigation*

To investigate the drug and other components' distribution in the printed formulation, a Horiba Jobin Yvon LabRAM HR Raman spectrometer was used with an automated xyz stage (Märzhäuser). Spectra were acquired Using a 786 nm laser with a power of 24 mW. A 100 X objective lens with a 300 µm confocal pinhole was used. A 600 lines $mm^{-1}$ rotatable diffraction grating with a path length of 800 nm was used to simultaneously scan a range of Raman shifts. A thermoelectrically cooled (-60 °C) Synapse CCD detector (1024 pixels) was used to acquire spectra.

Individual components of the formulation were first analysed with single point measurements acquiring a spectrum over the range of 50 – 4000 $cm^{-1}$, with an acquisition time of 15 seconds and 4 accumulations.

The top and bottom surface of the tablets were analysed, and lateral spectroscopic maps were generated by collecting a spectrum over 460 – 1760 $cm^{-1}$ in 10 µm steps. A 230 x 230 µm map with a total of 576 spectra was generated. An acquisition time of 16 hours was needed as each spectrum was collected for 20 seconds. To confer a spatial resolution of approximately 10 µm in all directions, the DuoScan functionality was used.

The cross-section of the tablet was also analysed with the generation of an analogous spectroscopic line map in 1 µm steps leading to a total of 668 spectra. The AutoFocus function was used to correct for uneven surface topography.

Classical Least Squares (CLS) regression analysis was done with Labspec 6.4.3 software, allowing the spatial location of individual components to be evaluated.

Instrument calibration was conducted using the zero-order line and a standard Si(100) reference band at 520.7 $cm^{-1}$ with spectral resolution at < 0.8 $cm^{-1}$.

Experimental and data processing in this section was conducted by Dr. Graham Rance (University of Nottingham).

#### *3.2.2.16 Tracking moisture uptake of tablets*

A total of 15 tablets were printed (100 layers) and were split into three batches: (i) kept in the ambient environment (temperature varied 25- 30 °C between and relative humidity between 46 – 58 %), (ii) non-vacuum air oven at 50 °C and (iii) in a non-vacuum air desiccator (temperature varied between 25 - 30 °C and relative humidity between 19 – 20 %). At specific times, the tablets were removed from their environment and weighed.

#### *3.2.2.17 Drug release studies*

A Copley dissolution tester (DIS 8000) was used for dissolution studies. For thiamine HCl, 500 mL volume of deionised water was used (specified in United States Pharmacopeia (USP) [98]). Media were heated to 37 °C using a water bath and paddles used for stirring (50 rpm). Samples were placed in media and at pre-determined time intervals a 1.5 mL aliquot was extracted and replaced by fresh solution. The extracted aliquots were filtered (0.45 µm) and then analysed with UV-Vis spectroscopy (Varian Cary 50 UV-Vis Spectrophotometer). Solutions were syringed into a silica (quartz) cuvette (Sigma S-10SM) and scanned. Absorbance at 266 nm was used to calculate the amount of drug released.

## 3.3 Results and Discussion

### 3.3.1 Additives for ink formulation

With the two main components of the formulation (PVP and thiamine HCl) being water soluble, water could be readily used as the solvent. Water has a relatively high surface tension for inkjet printing, reported to be 73 $mN \cdot m^{-1}$ at 20 °C [99]. Hence, a surfactant was needed to reduce this to an appropriate level. Polysorbate 20 (Figure 3.3) is a non-ionic surfactant that is widely used in the pharmaceutical industry, as well as in cosmetics, skin care and food products [100]. Polysorbates are known to

have extremely low toxicity for oral and topical delivery systems [101]. When the surfactant polysorbate 20 was added to the formulation, a reduction in the surface tension of the ink to 37.05 $mN \cdot m^{-1}$ from 65.55 $mN \cdot m^{-1}$ was seen. When the surfactant is dissolved in water, it orientates itself so that its hydrophobic region is positioned away from the water environment. Water molecules are replaced by the surfactant molecules that adsorb at the surface of the water. The surface tension is then reduced as the attraction between the water molecules and surfactant molecules is weaker.

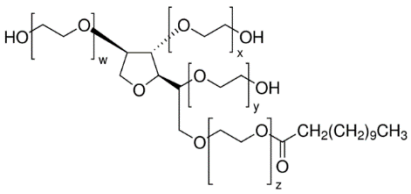



*Figure 3.3 - Molecular structure of polysorbate 20* [102].

It was attempted to print substantial 3D structures with the ink, however it was found the printed tablets were brittle and susceptible to fracture during both the printing process and subsequent substrate removal **(**Figure 3.4). To address this problem, a plasticiser was added. Glycerol or glycerine (Figure 3.5), is a hydrophilic plasticiser that is acceptable for use in pharmaceutical products [103]. With its addition, substantial 3D printed tablets were manufactured with no signs of delamination or cracking (Figure 3.6). Handling the tablets was much easier. The incorporation of plasticisers is well known to decrease the glass transition temperature and elastic modulus of the polymer they are mixed with. It is achieved by increasing the separation of polymer chains [104]. With this increased flexibility, the material resisted the drying stresses that can cause cracking and delamination.

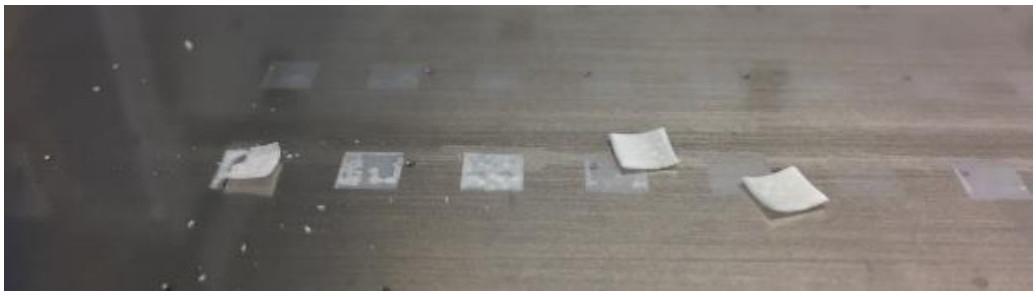


*Figure 3.4 - Printed tablets without glycerol. Some samples showed extensive cracking while others delaminated substantially. The delamination resulted in the print head to crash into some tablets, damaging or moving their position on the print bed.*

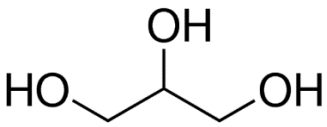



*Figure 3.5 - Molecular structure of glycerol* [105].

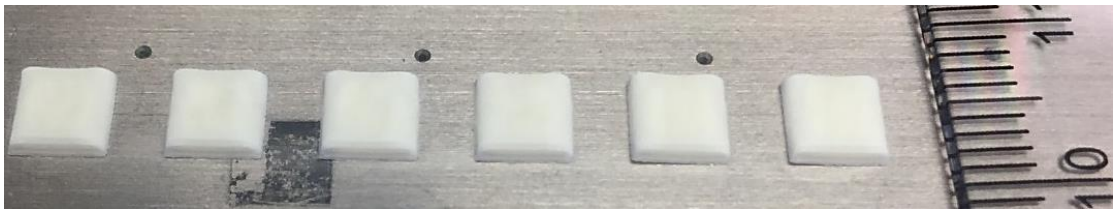


*Figure 3.6 - 3D printed tablets with glycerol.*

The final ink composition is shown in Table 3.2**.** Table 3.3 displays the ink's surface tension and viscosity (both in the recommended range for the Dimatix printer [96]) and the *Z* value of the ink was calculated to be 5.0, which is well within the printable range (1-10). Over the course of a few days, the ink did show a change in colour, initially from a pale yellow to a darker yellow. This was attributed to the oxidation of PVP (blank inks without the drug showed similar changes), a common occurrence reported in literature. This turbidity has no negative effects on the formulation and its effect on pH is negligible [106].

*Table 3.2 - Final ink formulation for tablet.*

| **Component** | **Content (wt %)** |
|---|---|
| PVP | 14 |
| Thiamine HCl | 10 |
| Polysorbate 20 | 1 |
| Glycerol | 1 |
| Deionised water | 74 |

*Table 3.3 - Ink and printer properties.*

| | |
|---|---|
| **Surface tension (mN·m$^{-1}$)** | 37.05 ± 0.67 |
| **Viscosity (mPa·s)** | 6.100 ± 0.074 |
| **Density (g·mL$^{-1}$)** | 1.2 ± 0.001 |
| **Nozzle diameter (µm)** | 21 |
| **Z factor** | 5.0 |

### 3.3.2 Jetting parameters

Standard jetting parameters were used for printing the ink. This included a jetting voltage and frequency of 16 V and 5 kHz respectively. A waveform for model fluids (Figure 3.7) for the printer was also used. The cartridge and substrate temperature were kept at 28 °C, to illustrate the ability to print drug containing formulations at lower temperatures. The resultant jetting had stable and reliable droplet formation **(**Figure 3.8). It should be noted that the presence of polysorbate 20 did cause a significant amount of bubbles to form in the ink, as it was filtered into the printer cartridge. To address this issue, the ink was left to 'sit' in the cartridge for a prolonged time and purging cleaning cycles were applied to remove the bubbles.

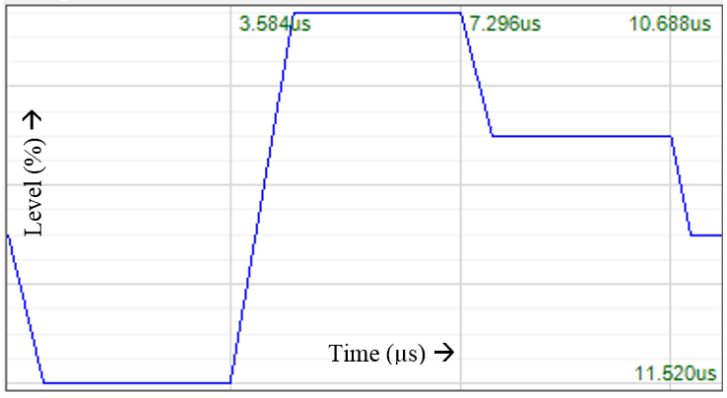



*Figure 3.7 - The standard and selected waveform applied during the jetting process.*

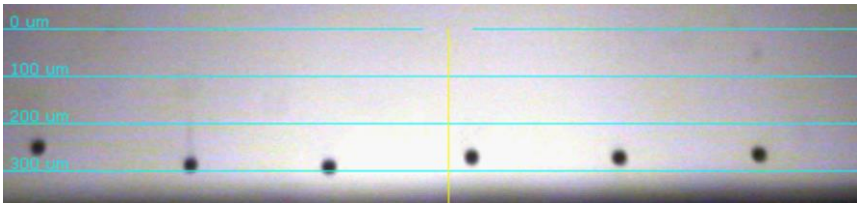



*Figure 3.8 - The jetting of droplets. Here, 6 of the 16 nozzles of the printer are jetting simultaneously. Spherical droplets were seen consistently.*

### 3.3.3 Substrate selection

The choice of substrate was an important manufacturing decision. It was important to illustrate the ability to inkjet print the entire tablet without it remaining stuck on the substrate as many previous investigations had shown through solvent inkjet printing. An ink must adhere well to the substrate during the printing process as well as being easily removable once printing is completed. A 5 x 5 mm square was printed (100 layers) on both glass slides and PET films. The tablets on glass were extremely difficult to remove and often resulted in the fracture of the tablet. Conversely, the removal of tablets from the PET film were possible with no observable damage. This difference in behaviour was attributed to the contact angle and in turn its work of adhesion of the ink on the substrates (Table 3.4). A smaller contact angle (caused by more ink spreading, thus a larger work of adhesion) means more force is required to remove the ink from the substrate. The larger contact angle seen on PET was attributed to this material's hydrophobicity [107].

*Table 3.4 - Measured contact angle and calculated work of adhesion of the ink on glass and PET substrates (n=5).*

| Substrate | Contact angle (°) | Work of adhesion ($mN \cdot m^{-1}$) |
|---|---|---|
| Glass slide | 29.1 ± 2.6 | 69.4 ± 0.8 |
| PET | 53.4 ± 1.8 | 59.1 ± 0.9 |

### 3.3.4 Print formation

Substrate temperature was maintained at 28 °C. Initially, individual droplets were jetted on the PET substrate (Figure 3.9). The printed drops were well-defined with a mean diameter of 30 ± 2 µm (n = 9). Common problems associated with solvent inkjet

printing such as the coffee-ring effect, build-up of solid material on edges of the drop [108], were not observed.

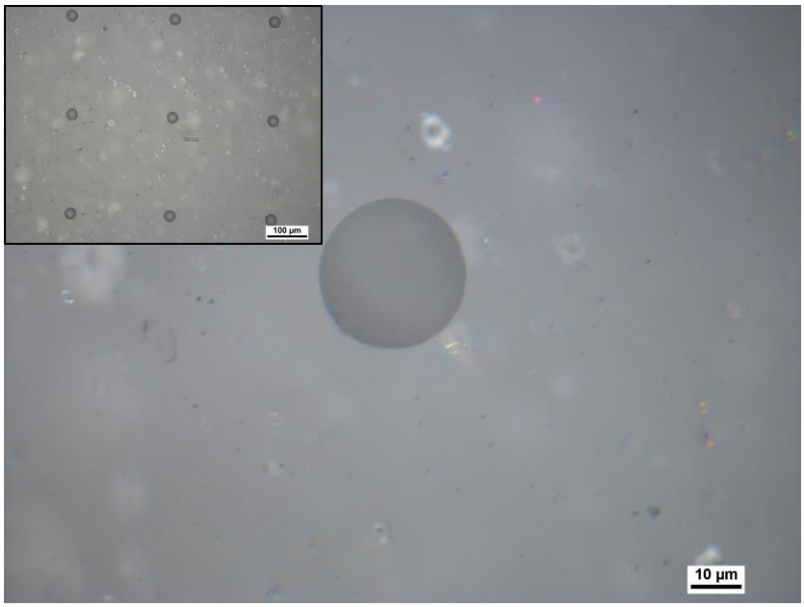



*Figure 3.9 - Individual drops of the ink printed on PET film.*

Following this, line and film formation were investigated with different drop spacings. As noted in Figure 3.10, using a 40 µm drop spacing it was not possible to form both uniform lines and films - as the distance between droplets was significantly larger than their diameter. With 20 and 30 µm drop spacings, complete lines were formed, but some bulging was observed, more so with 20 µm drop spacing. The film formation for 20 µm drop spacing showed a complete film with no gaps, in contrast to the 30 µm drop spacing film, which exhibited patchier coverage. The 20 µm drop spacing for the printing of tablets was used based on this ability to produce a uniform two-dimensional film.

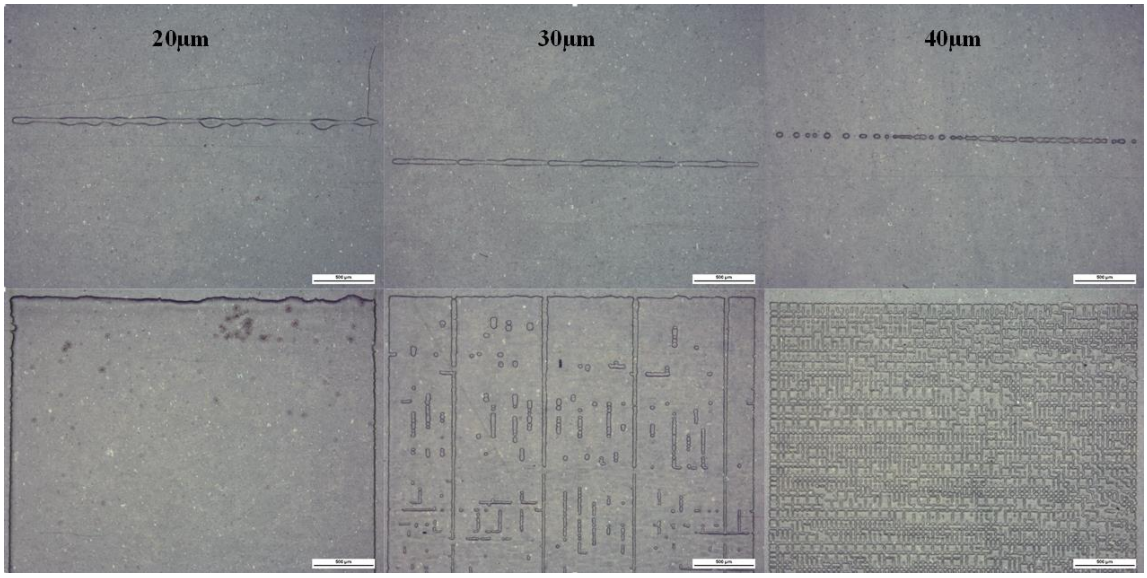



*Figure 3.10 - Single line (top) and film (bottom) formation of the formulation. Scale bar = 500 µm*

### 3.3.5 Observed phase separation

Two occurrences of phase separation in the printed films were observed during the printing and drying process. The first process could be seen as time progresses after the printed films have dried. This process was seen as crystal growth, which we attribute to thiamine HCl, being the only crystalline component in the formulation. Figure 3.11 shows a single layer of the formulation printed on a glass slide. The optical images in reflection clearly show that crystals nucleate with time, ultimately forming a suspension of thiamine HCl crystals in PVP, confirmed in the cross-polarised images in transmission.

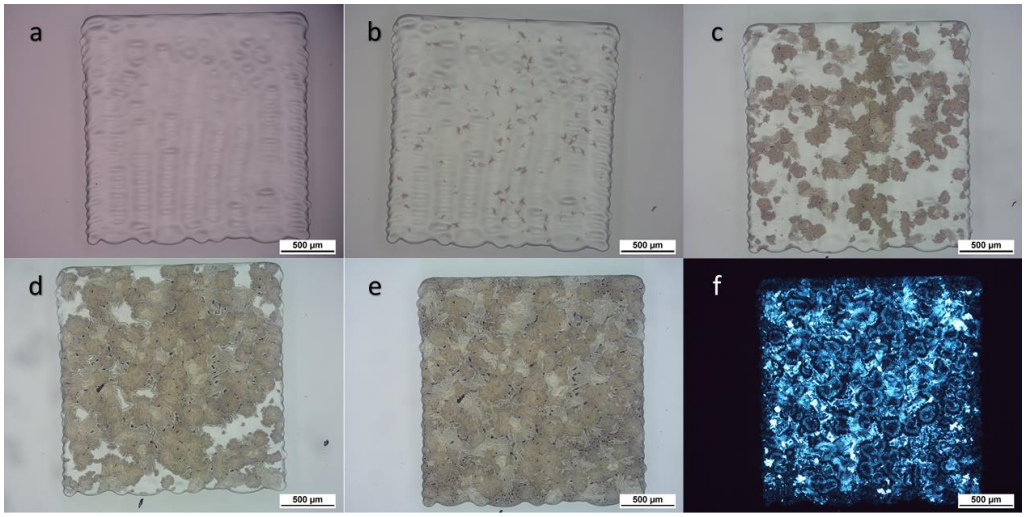



*Figure 3.11 - Optical reflection images of printed films on glass slide. a) 30 minutes after printing, b) 1 day, c) 4 days, d) 8 days, e) 12 days, f) 12 days after orienting confirm the formation of a crystalline phase (cross polarised transmission OM). Scale bar = 500 µm.*

The second occurence of phase separation was observed as additional layers were printed. Initially, films were uniformly clear, but as more material was added, white grains were seen to form, as shown in Figure 3.12. As more layers were printed, the white grains grew, eventually leading to a uniformly white tablet, as seen in Figure 3.6. The most likely explanation for this is a solvent mediated recrystallisation process [109]. The addition of a solvent (in this case, water from the ink), dissolves the previously printed drug, increasing the total concentration of drug available in the liquid phase, resulting in the nucleation and growth of additional crystals.

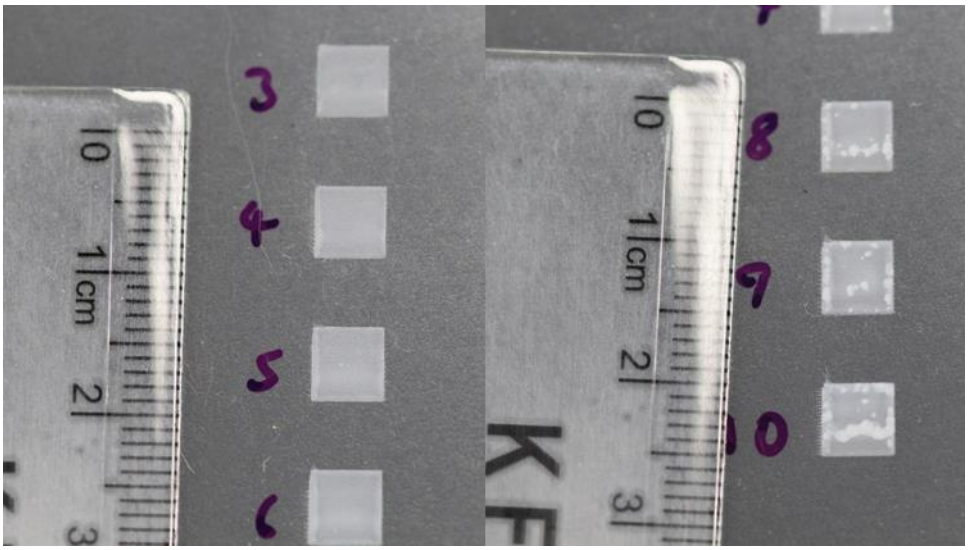


*Figure 3.12 - Films of thiamine HCl formulation printed with varying number of layers. As additional layers are printed regions of white growth are observed.*

AFM imaging provided useful information regarding the phase separation occurrences. Figure 3.13 shows the height sensor image of 10 printed layers (clear region) after phase separation has occurred. In comparison, 100 layers of the formulation shown in Figure 3.14 show are higher density of crystals. Both images indicate what was seen with the optical microscope - that thiamine HCl crystals exist in suspension in the PVP. The difference between crystal amount is attributed to the solvent mediated recrystallisation process that occurs as additional layers are printed.

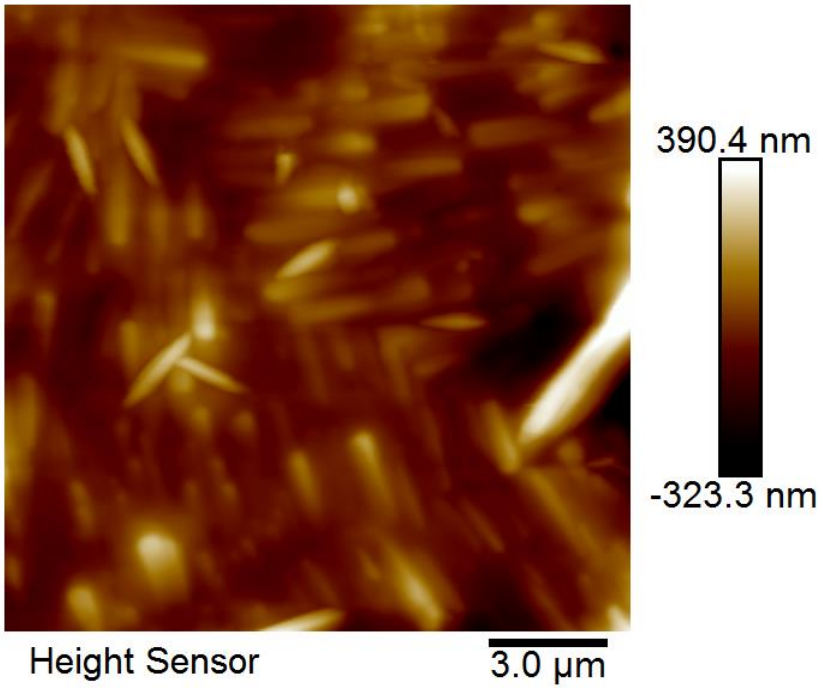



*Figure 3.13 - AFM height sensor image of the top surface of 10 layers of the printed thiamine formulation. The 'clear' region with no white crystal growth was scanned.*

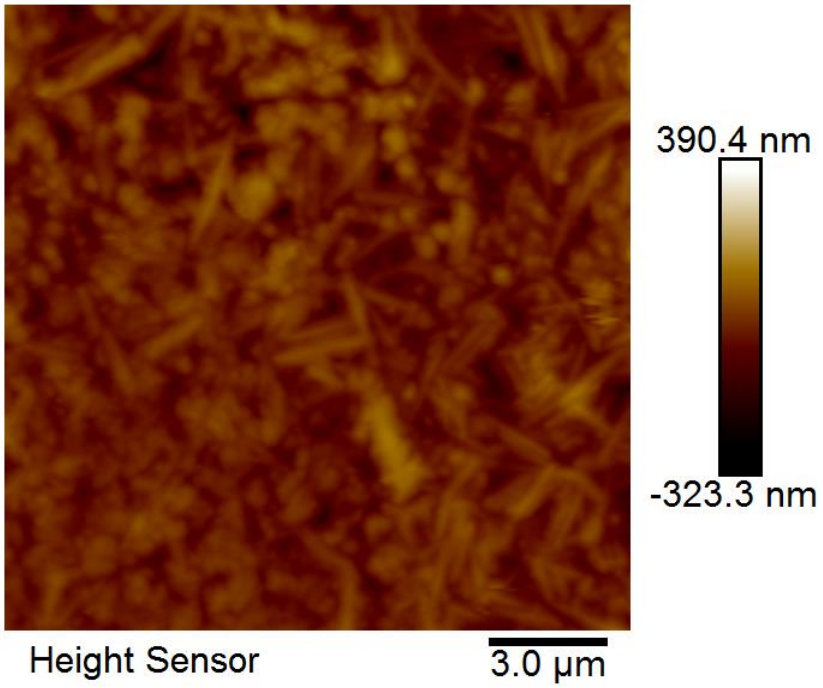



*Figure 3.14 - AFM height sensor image of the top surface of a 100 layer printed tablet. A greater density of crystals was observed.*

ToF-SIMS analysis was performed to compare the thiamine HCl content between the clear regions and white regions. Using the ion $HS^-$ (ion mass (u) = 33), which was seen in pure thiamine HCl but not in pure PVP, Figure 3.15 shows the mapped ion across a single layer and 10 layers printed on PET film. There is no evidence suggesting the white regions have a significant richer or poorer drug content as the intensity of the ion appears to be uniform.

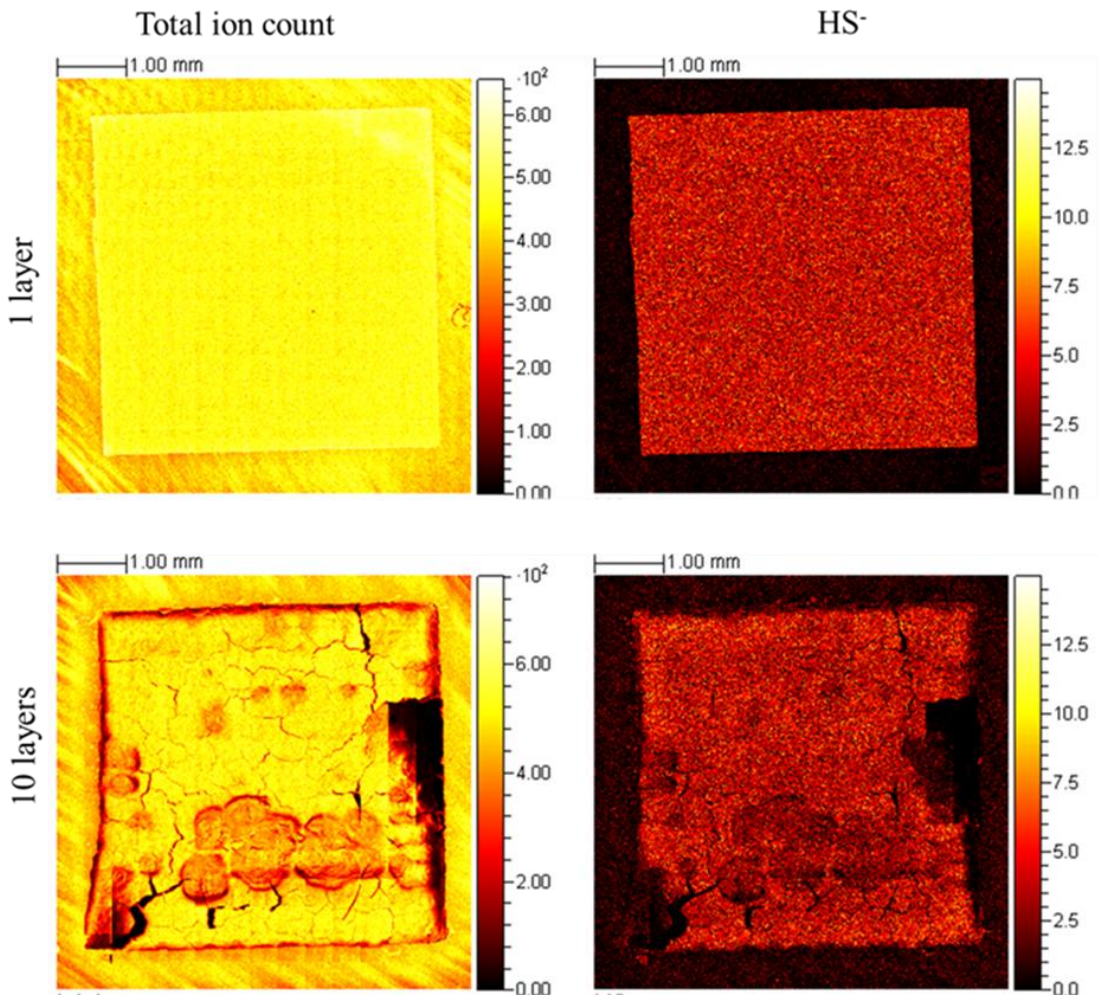



*Figure 3.15 - ToF-SIMS maps of 1layer (top) and 10 layers (bottom). The total ion intensity (left) is shown and compared to the HS- ion (right) indicative of the drug.*

There are however darker regions around the white regions' edges. This is more likely to be a result of the topography as the white regions have a roughness profile associated with them. This is shown in Figure 3.16. The fact that the total ion count also shows this behaviour further suggests that it is caused by a topographical issue, rather than the lack of material.

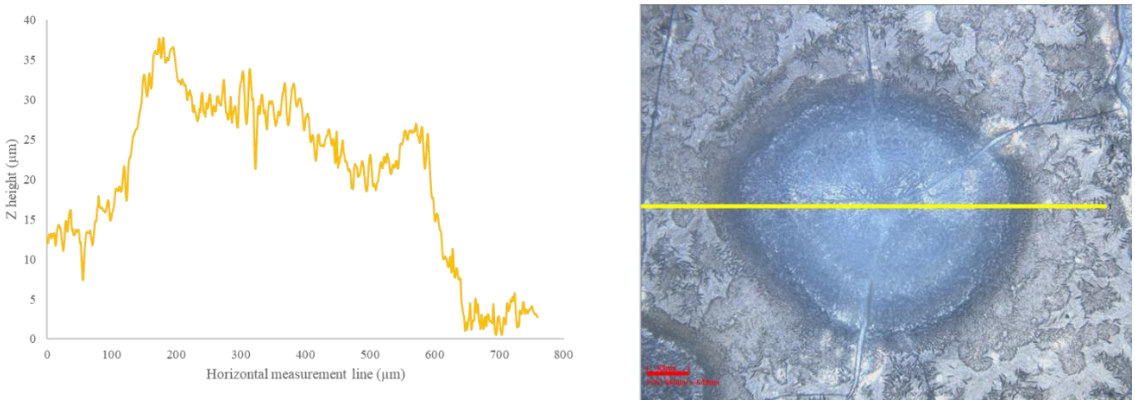



*Figure 3.16 - Optical profile (left) in reference optical image (right). The yellow line indicates the horizontal measurement line (from left to right) along which a Z height was measured. Scale bar (red) = 69 µm*

### 3.3.6 Investigation of ink jet printing's reliability

To illustrate inkjet printing as a reliable method of producing tablets, it was important to show that the printed tablet had a drug composition that is commensurate to the expected drug loading based on the ink formulation, elemental analysis by combustion was conducted. As thiamine HCl is the only sulphur containing component of the formulation, this element was used to quantify the content of thiamine HCl in the tablets. Table 3.5 shows the sulphur content (based on mass %) of the drug powder and printed tablet.

*Table 3.5 - Sulphur content (based on mass %) measured through elemental analysis by combustion (n=3)*

| Sample | Mean sulphur content (%) |
|---|---|
| Thiamine HCl | 10.11 ± 0.10 |
| Tablet | 4.03 ± 0.06 |

Using the values measured, it was determined that the thiamine HCl content in the tablet was 39.8 % (i.e. 4.03 / 10.11). This value is close to the expected value of 38.4% thiamine HCl content calculated from the composition of the solid components of the formulation of the ink and thus the jetted material corresponded reliably to the formulated ink composition. Blank tablets (tablets without any thiamine HCl) were also analysed and all readings gave values lower than the detection limit of the analyser (-0.09 ± 0.01 %) [110].

Another way to illustrate the reliability of ink jet printing, was to measure the relationship between drug content and the number of printed layers. As expected, Figure 3.17 shows a highly linear correlation between the dose and printed layers. This would suggest that there is high homogeneity in drug content in each printed and subsequent layers. Small standard deviations were calculated, highlighting ink jet printing's ability to consistently deposit a fixed dose.

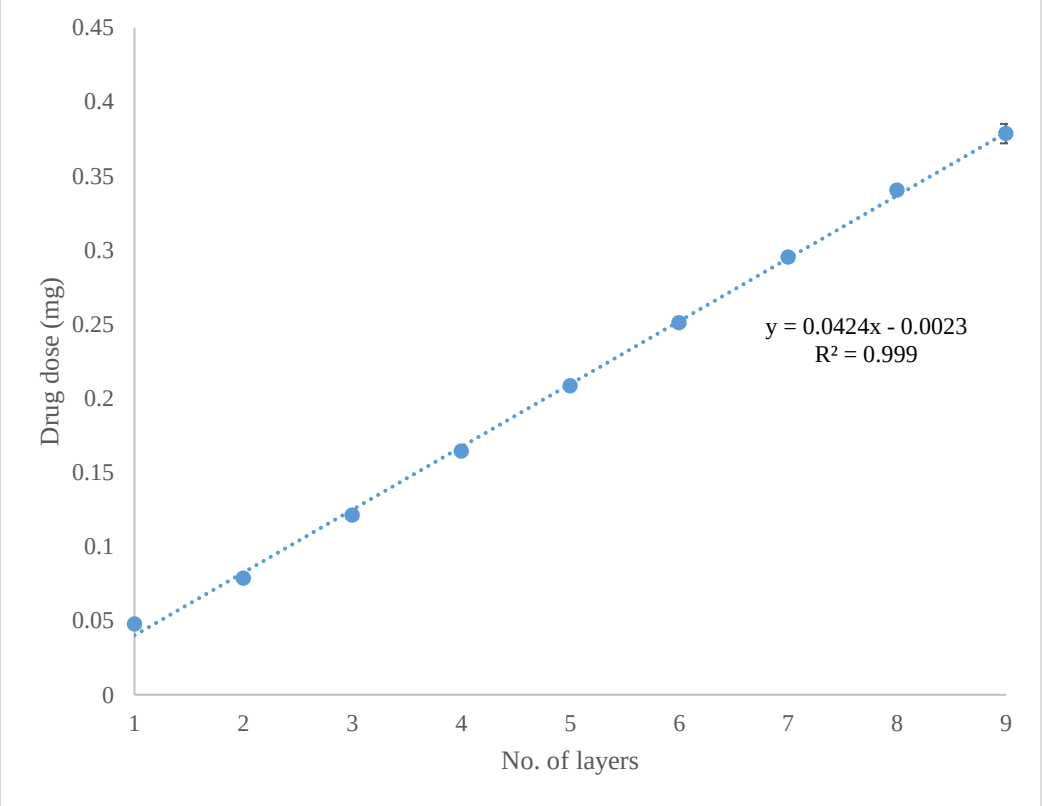



*Figure 3.17 - Relation between the number of printed layers and dose of drug detected with UV-Vis spectroscopy (n=3, for layer 7 n=2).*

### 3.3.7 Polymorph investigation

Raman spectroscopy was definitive in identifying the phase of thiamine HCl. For NSH, a single peak associated with a C=C stretching vibration from the aromatic group of the drug is seen at 1607 $cm^{-1}$ [111], whereas for HH, two closely spaced peaks at 1594 and 1614 $cm^{-1}$ are observed. An additional peak at 1332 $cm^{-1}$ is also noted in the Raman spectrum of the HH form [111]. As can be clearly seen from Figure 3.18, the tablet – like the parent powder – was found to exist in the NSH polymorphic phase based on the spectra collected from random points on both its the top and bottom faces. Similarly, the Raman spectra of a single tablet which was placed overnight in a

vacuum oven to remove all moisture, broken and subsequently ground to a powder, was also consistent with the NSH phase. This suggested that the NSH phase of thiamine HCl is ubiquitous within the bulk tablet. Thiamine HCl tablets produced by conventional means are known to undergo a phase change over time [112]. Therefore, to confirm the time-dependent stability of thiamine HCl in both the tablet and parent ink, analysis of (i) tablets printed and kept in an ambient environment for two months and (ii) tablets printed with an ink kept in an ambient environment for one month was conducted, respectively. Critically, no differences in the Raman spectra were observed relative to those obtained from fresh formulations, suggesting that thiamine HCl remains in the NSH phase in a stable manner at least over these time frames. Thiamine HCl powder that was exposed to the ambient environment for a prolonged time did undergo a phase change to the HH phase (as expected) with the peak at 1332 $cm^{-1}$ clearly forming, as well as peaks at 1594 and 1614 $cm^{-1}$.

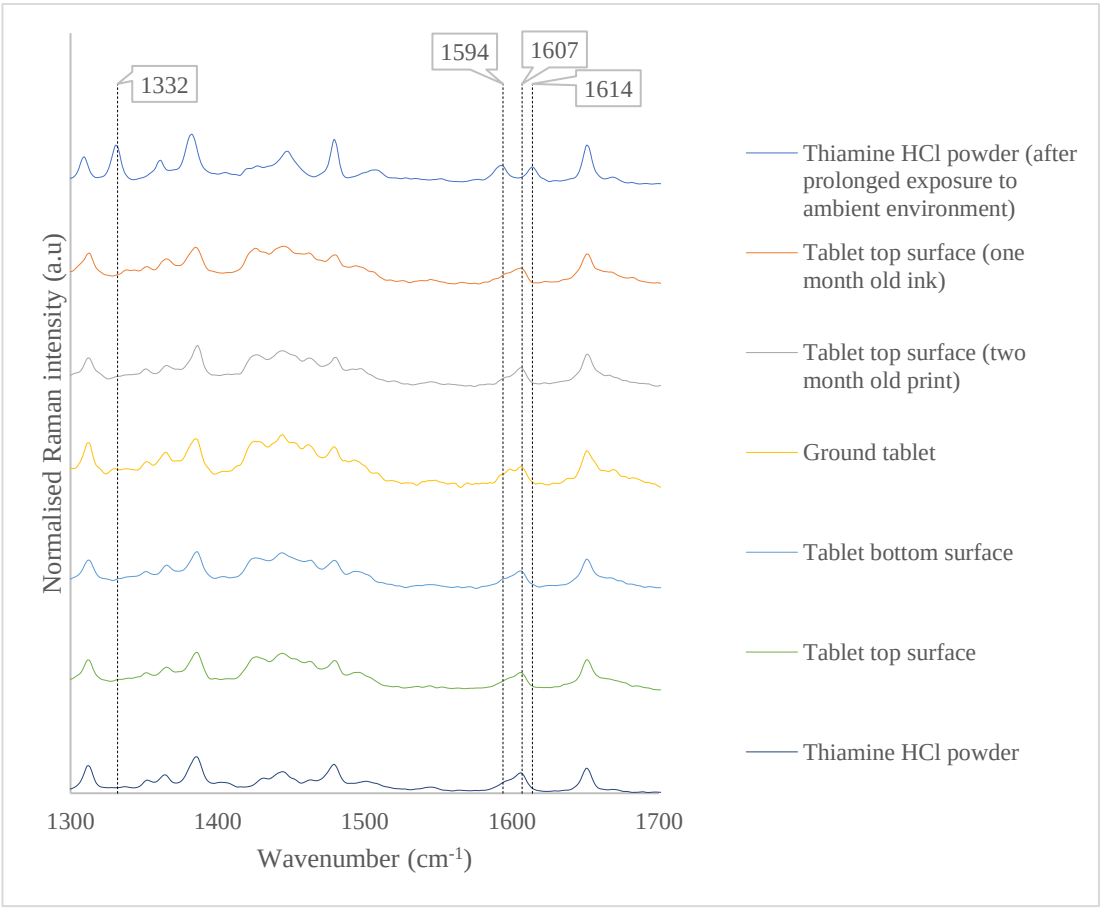



*Figure 3.18 - Raman spectra of the thiamine HCl powder and different printed samples all showing peak positions indicative of the NSH phase. Also shown is the drug powder exposed to the ambient environment with features of the HH phase.*

### 3.3.8 Drug spatial distribution

Through confocal Raman microscopy, the distribution of thiamine HCl was investigated. Three areas of the printed tablet were analysed: (i) the top surface, (ii) the bottom surface and (iii) the cross section. For the top and bottom surfaces, false colour maps of the of the components were constructed using the Raman spectra generated from the raw components of the formulation and through CLS regression analysis. Through this method, each spectrum is expressed as a linear combination of the raw component spectra. Scores are then calculated through least square regression, which are plotted to generate the map. For the cross section of the tablet (cut with a scalpel), a single line map was generated. It should be noted that since the Raman spectra are sensitive to certain conditions (e.g. temperature, wavelength shifts and non-linearity), the scores generated are not expected to accurately match the content of individual components based on the ink formulation. The scores generated are semi-quantitative and are used to illustrate only the relative amounts of materials.

Figure 3.19 shows the optical image of the areas scanned and the CLS score map of thiamine HCl for the top and bottom surfaces of the tablet. Both maps show a relatively uniform distribution of the drug across their surfaces. The top surface shows some small areas lacking in slight amounts of drug, but this has been attributed to the greater roughness associated with this surface. Evidence of high homogeneity of thiamine HCl across the two surfaces is also provided by the CLS scores generated: 55.5 ± 6.1 % (11 %, N = 576) and 55.3 ± 4.3 % (8 %, N = 576) from the top and bottom surfaces, respectively. The fact that both scores are very close with low standard deviations, suggests that thiamine HCl is uniformly found across these surfaces. Further indications of high homogeneity of the drug throughout the tablet is provided with the scores generated from the cross-section line map. A mean thiamine HCl CLS score of 54.5 ± 10.8 % (20 %, N = 968) was obtained. For all three surfaces, clear indications of the NSH phase was seen, with no evidence of the HH phase (Figure 3.20). This provides additional evidence that thiamine HCl remains in its desired NSH phase throughout the tablet.

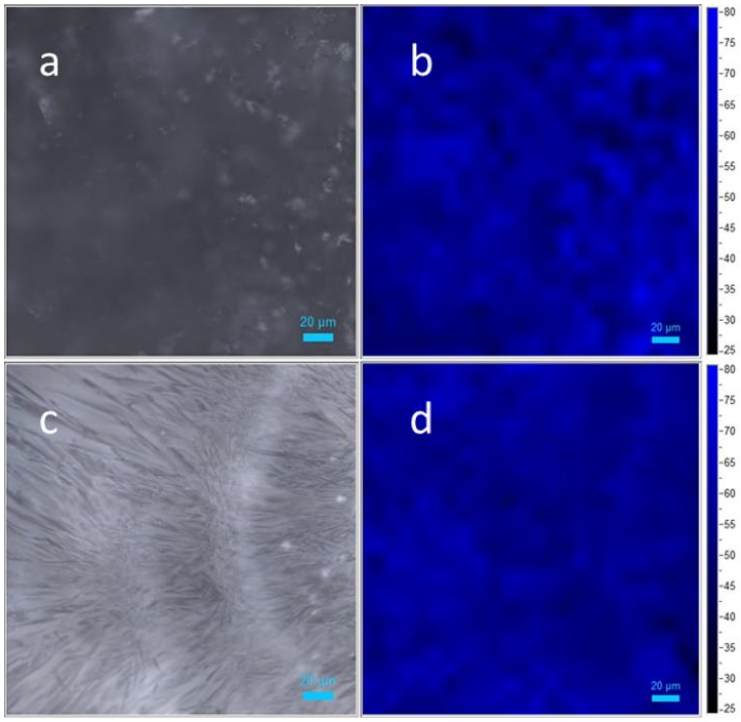



*Figure 3.19 - Optical image (a) and CLS score map for thiamine HCl (b) from the top surface. Optical image (c) and CLS score map for thiamine HCl (d) from the bottom surface. Scale bar = 500 µm.*

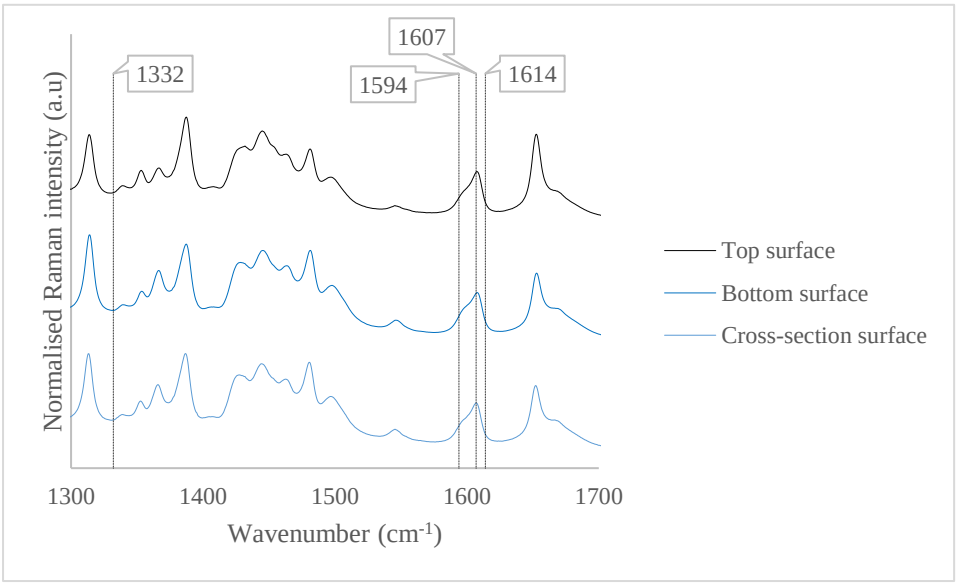



*Figure 3.20 – Mean spectra generated from the top and bottom surface lateral maps and the cross-section line measurement.*

### 3.3.9 Investigating the hygroscopic nature of the tablet

The formulation developed in this chapter contains components that are known to be hygroscopic in nature. As such, water absorption was briefly investigated. All tablets printed were weighed within 15 minutes after printing had been complete and had a mean mass of 10.0 ± 0.1 mg (n = 15). Tablets were then stored in each of the three

stated environment and weighed every hour for three hours. After this point, tablets were weighed sequentially over a period of 21 days (Figure 3.21). For the initial three hours, all batches showed a discernible reduction in weight, with the oven showing the greatest reduction followed by the desiccator and then the ambient environment. This suggests that some water had been retained after the printing process. This is an important point to note, as if the theoretical dose were to be calculated through tablet mass the additional mass due to the water would distort this value. Over the following weeks, the oven and desiccator tablet batches seem to eventually reach a relatively stable mass, with the oven tablets showing the most weight reduction, due to the elevated temperatures. There is some variation possibly caused by moisture uptake during the weighing process Tablets stored in the ambient environment showed significant fluctuation over time. This may have been caused by the higher humidity that changed over the course of three weeks, leading to moisture uptake and loss over time.

It should be noted that there would be some variation in mass caused by individual samples, but the objective of this experiment was to show that there is some moisture uptake and trapped water present in samples after printing.

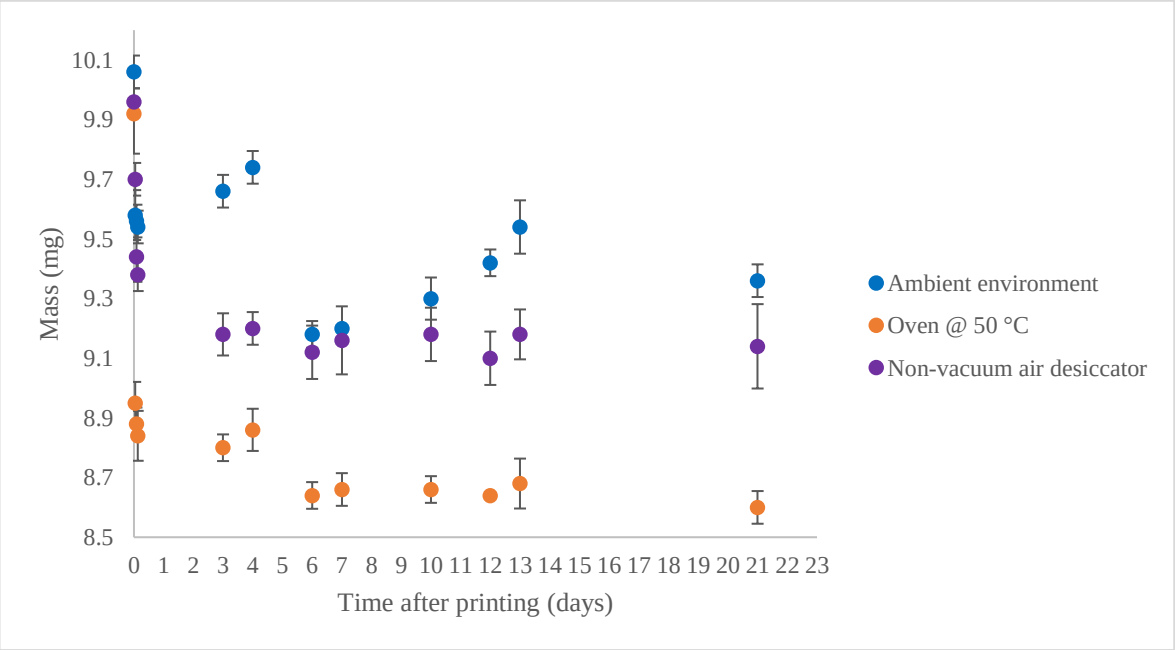



*Figure 3.21 - Mass variation over time of tablets in three different batches (i) an ambient uncontrolled environment, (ii) non-vacuum oven at 50 °C and (iii) a non-vacuum desiccator (n=5, for each batch, n=4 for samples in non-vacuum oven at 50 °C for day 21.).*

### 3.3.10 Drug release studies

Table 3.6 contains the dimensions and theoretical dose of the samples printed and tested for dissolution. The theoretical dose was calculated using the number of drops jetted per layer and per tablet. Using this data and ImageJ data where the in-flight droplet diameter was calculated to be 22 ± 1 µm (n = 4), the theoretical dose for each tablet was determined.

*Table 3.6 - The pattern dimensions, number of layers and the theoretical doses of tablets printed.*

| 2D pattern dimensions (mm) | No. of printed layers | Theoretical dose (mg) |
|---|---|---|
| 5 x 5 | 125 | 5 |
| 5 x 5 | 250 | 10 |
| 5 x 5 | 375 | 15 |
| 2.5 x 5 | 250 | 5 |
| 10 x 5 | 250 | 20 |

From Figure 3.22 and Figure 3.23, all batches of tablets showed a rapid drug release with all reaching 90 % within seven minutes. On varying the number of printed layers, no clear trend can be seen with respect to the time required for complete dissolution highlighting the rapid dissolution of the formulation. With samples that have varied pattern dimensions, a subtle trend can be seen possibly due to differences in the amount of material required to print these samples being greater. However, the error bars (standard deviation associated with repeat measurements) are large and thus definitive conclusions cannot be drawn, except that the amount of drug released varied rapidly compared to the time-frame of the measurements taken.

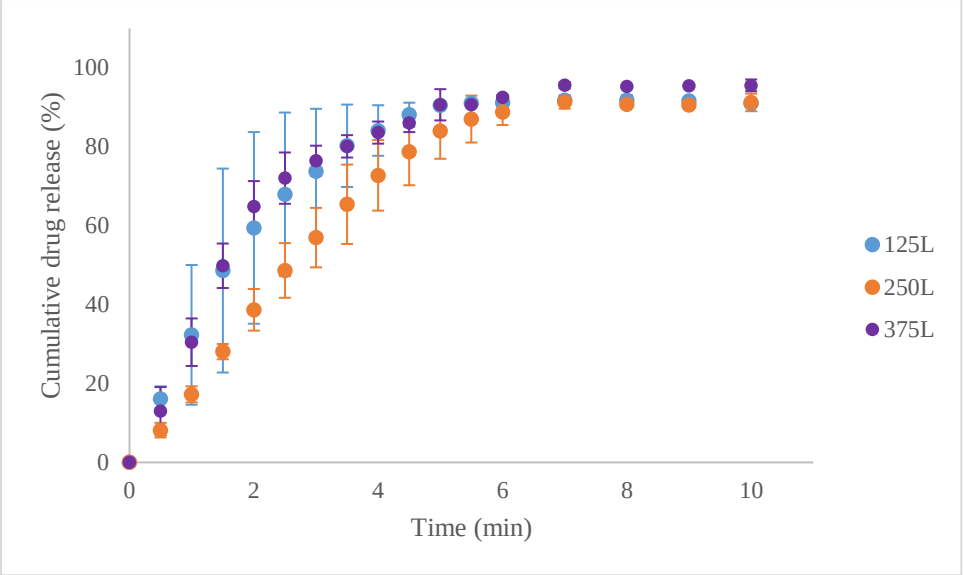



*Figure 3.22 - Release profiles of tablets with varying printed layers. The printed pattern's dimensions were set at 5 x 5 mm (n=3 except for 375L where n=2).*

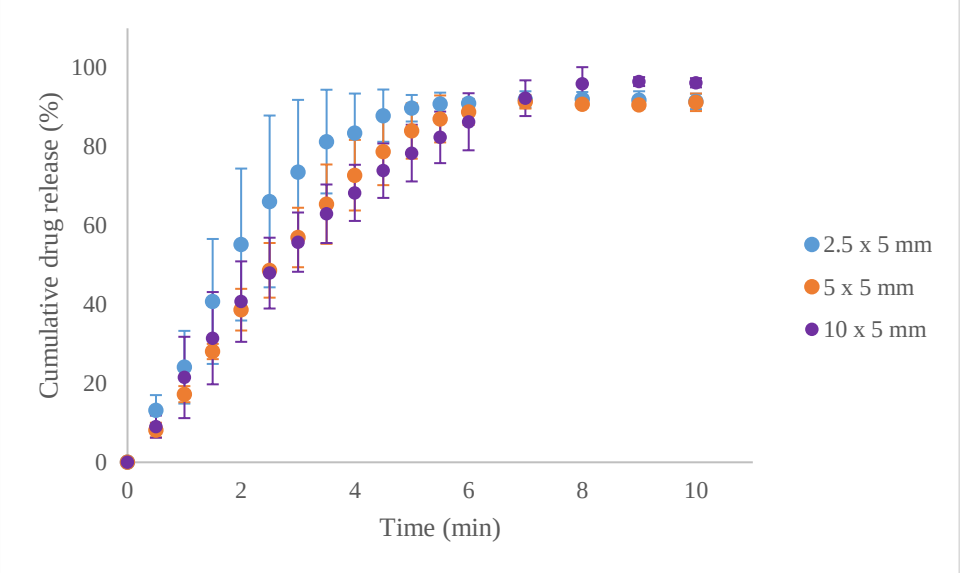



*Figure 3.23 - Release profiles of tablets with varying pattern dimensions. The number of layers for each print were kept at 250 layers (n=3).*

There is a small apparent discreprancy between the theoretical and measured dose for tested samples (± 5 – 10 %). However, the USP for thiamine HCl tablets allows drug release to be between 90 – 110 % of the theoretical dose, hence all results reported here are acceptable [98]. The differences between the theoretical and measured dose could be caused by a number of reasons. These include errors made in the printing process (e.g blocked nozzles), incorrect assumptions associated with the printing process (e.g all droplets are spherical) or due to the lack of accuracy of the drop watcher camera. There is however good correlation between the measured doses and

the sample details (e.g. halving the pattern size or number of layers leads to halving of the dose), suggesting good consistency of the printing process.

## 3.4 Conclusions

The following conclusions can be made from this chapter:

- A water-based ink formulation has been developed using thiamine HCl as a model API. Through the addition of glycerol and polysorbate 20, very effective jetting behaviour and 3D printing was seen. Tablets can be removed from the PET substrate resulting in free-standing tablets rather than dosing drug-loaded material onto edible substrates. Since water is the main solvent in this ink, this formulation illustrates inkjet printing as a manufacturing process for tablets, without the use of toxic solvents, potential for uncured material or the need of high temperatures. It can also potentially be used as a 'universal' ink for water-soluble APIs.
- Occurrences of phase separation were observed and investigated. Using optical microscopy and AFM, it was clear that thiamine HCl crystals exists as a suspension in the PVP. ToF-SIMS analysis suggested that the content of drug in the first and initial few layers exist uniformly across the top surface of the printed material.
- Elemental analysis by combustion, using sulphur as an elemental marker, showed that the inkjet printed tablet had a drug loading commensurate with the ink formulation. By dissolving prints with varying layers in small volumes of water and calculating drug content with UV-Vis spectroscopy, a strong linear correlation was seen between the number of layers and drug content. This proved that the same amount of drug was deposited in each layer consistently, illustrating inkjet printing as a reliable method for tablet manufacture.
- Through Raman spectroscopy, the desired polymorph of thiamine HCl (NSH) was seen to exist in the printed tablet. No indication of the undesired HH phase was seen even in prints after being exposed to the ambient environment over a prolonged period.
- Thiamine HCl was homogenously distributed throughout the tablet, measured with confocal Raman microscopy.

- The tablets were observed to be hygroscopic as samples that were stored in less-controlled environments were shown to have significant fluctuations in mass over time, when compared to samples stored with a degree of control.
- Drug release from the tablets was rapid, with 90% of drug being released within seven minutes.

## 3.5 Chapter Appendix: Supplementary Information

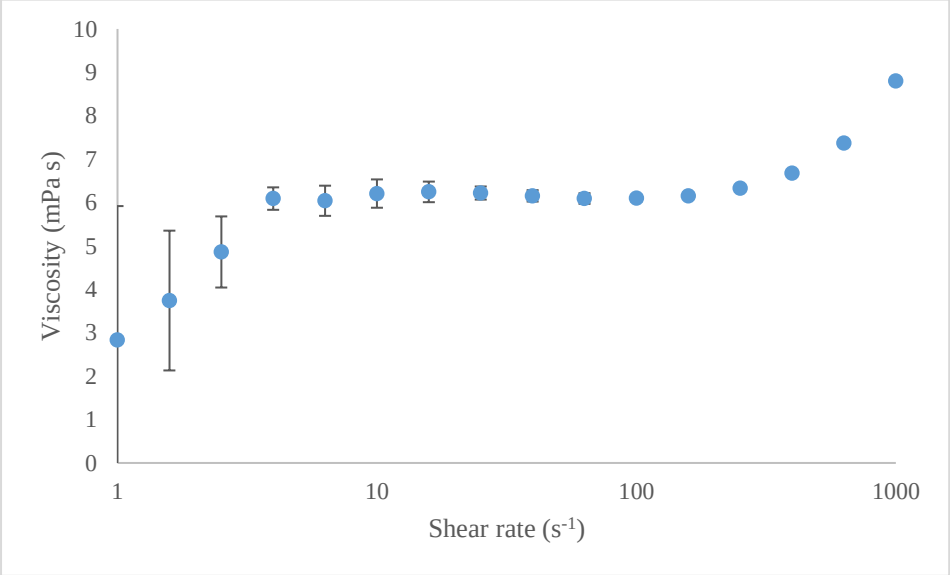



*Figure S3.24 - Rheological flow curve of the final formulated ink (n=3). Newtonian behaviour is seen from 10 to 100 $s^{-1}$. Measurements below 3.981 $s^{-1}$ did not achieve steady state and the increase in viscosity seen at shear rates above 100 $s^{-1}$ was caused by the geometry used for measuring viscosity* [113].

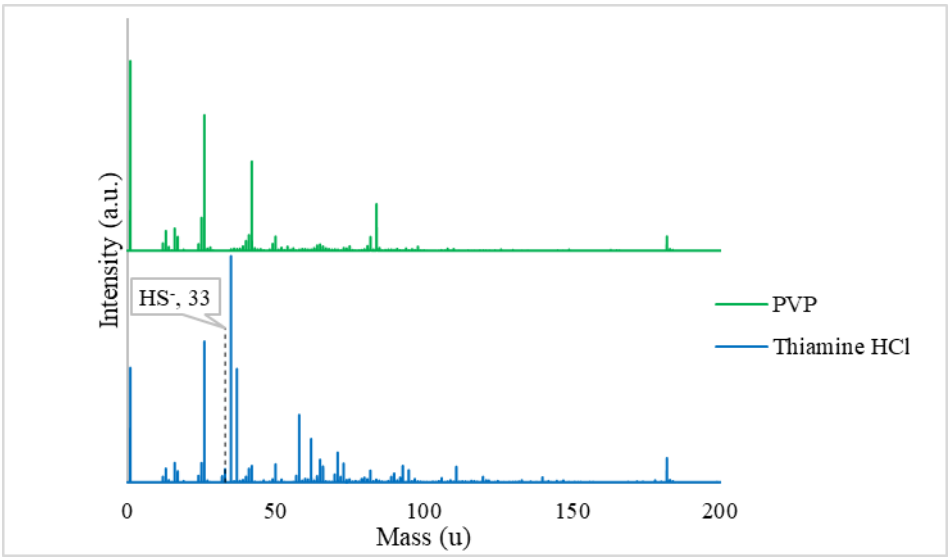



*Figure S3.25 - ToF-SIMS spectra of pure thiamine HCl and PVP.*

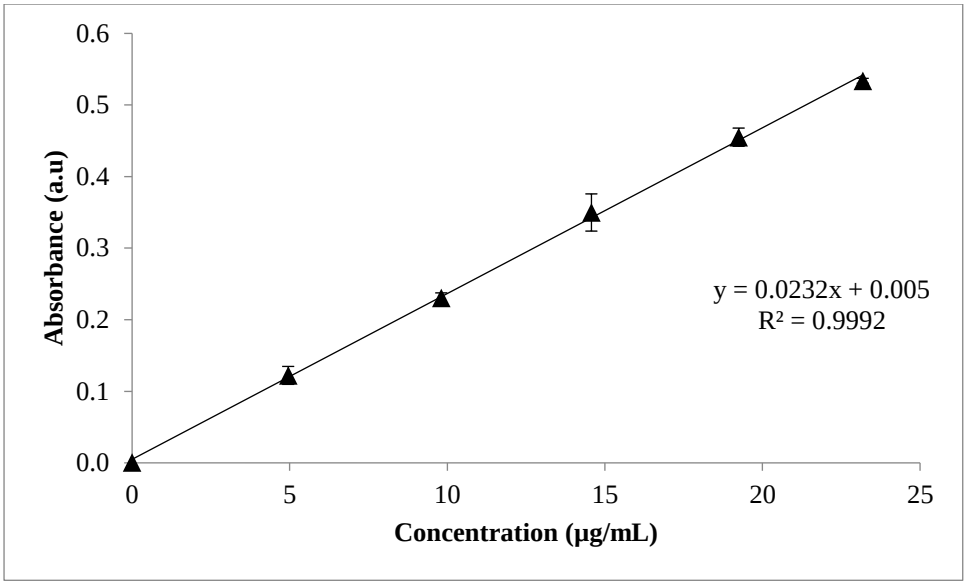



*Figure S3.26 – UV-Vis spectroscopy calibration line for thiamine dissolved in deionised water (n=3).*

*Table S3.7 - Sample details and drug release data.*

| Dimensions (mm) | No. of printed layers | No. of drops per layer | Mean thickness (mm) | Theoretical dose (mg) | Measured (experimental) Mean dose (mg) |
|---|---|---|---|---|---|
| 5x5 | 125 | 63001 | 0.49 ± 0.01 | 5 | 4.5 |
| 5x5 | 250 | 63001 | 0.91 ± 0.01 | 10 | 9 |
| 5x5 | 375 | 63001 | 1.43± 0.03 | 15 | 14 |
| 2.5x5 | 250 | 31626 | 0.96 ± 0.01 | 5 | 4.5 |
| 10x5 | 250 | 125751 | 0.95 ± 0.003 | 20 | 19 |

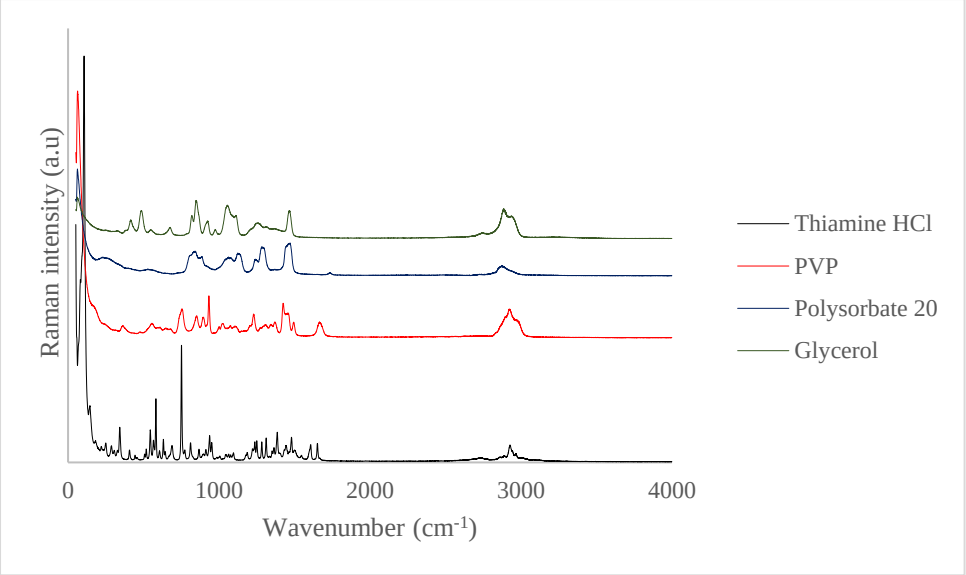



*Figure S3.27 - Raman spectra of the individual components of the formulation.*

*Table S3.8 - CLS fitting values for components from lateral maps and line cross-section.*

| Component | CLS score from the lateral surface maps (%) | | CLS score from the cross-sectional line map (%) |
|---|---|---|---|
| | Top | Bottom | |
| PVP | 38.1±3.7 | 38.0±3.2 | 36.4±8.6 |
| Thiamine HCl | 55.5±6.1 | 55.3±4.3 | 54.5±10.8 |
| Polysorbate 20 | 1.6±1.0 | 1.3±0.7 | 1.2±1.1 |
| Glycerol | 4.7±2.3 | 5.4±1.6 | 7.9±3.0 |

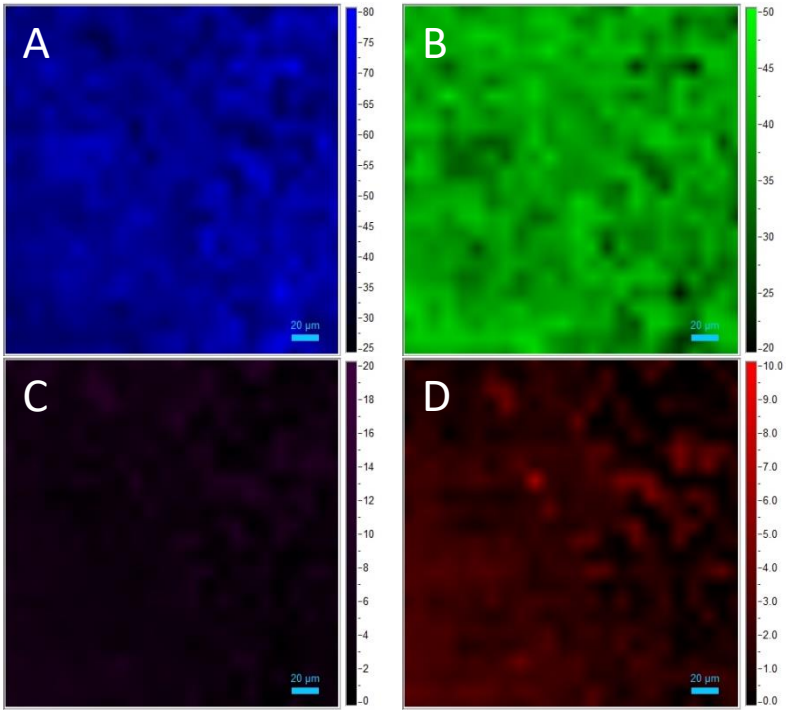



*Figure S3.28 – Top surface of tablet CLS score map for thiamine (A), PVP (B), glycerol (C) and polysorbate 20 (D). Scale bar = 20µm.*

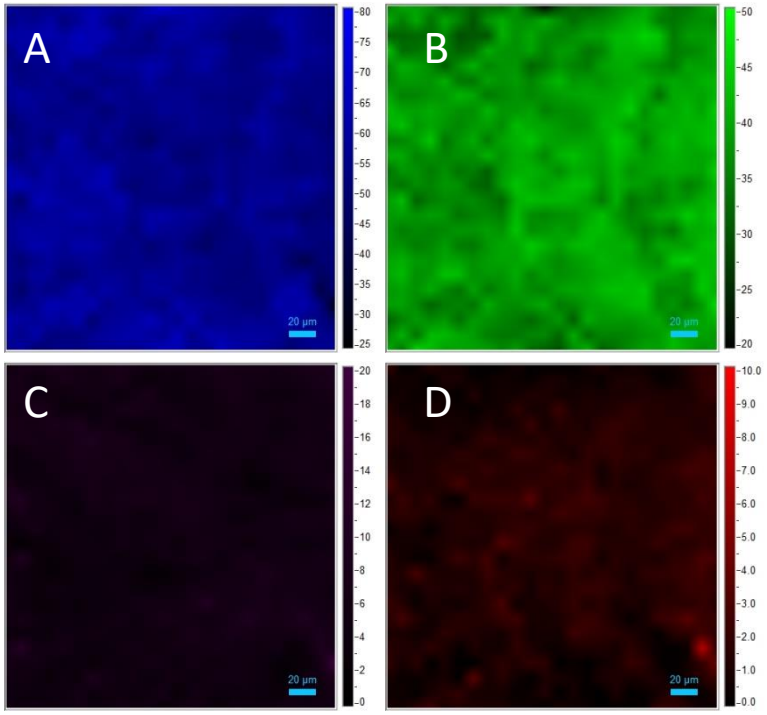



*Figure S3.29 - Bottom surface of tablet CLS score map for thiamine (A), PVP (B), glycerol (C) and polysorbate 20 (D). Scale bar = 20µm.*

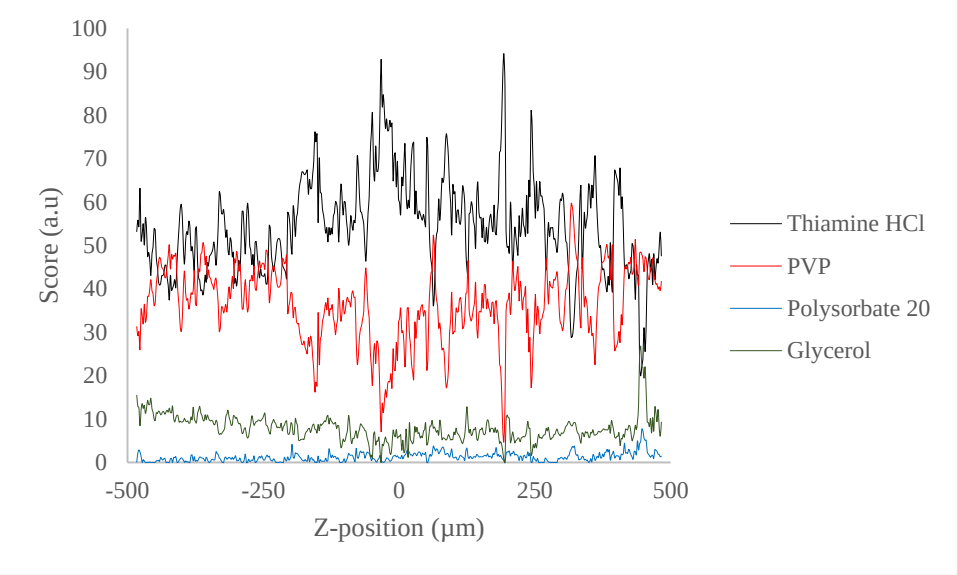



*Figure S3.30 - Raman scores generated with the CLS analysis method to show the relative location of individual components of the tablet across its cross-section. Mid-point of tablet at 0 µm.*

# 4 Inkjet Printing of a Reservoir System: The Impermeable Shell

## 4.1 Introduction

### 4.1.1 Aims of chapter

- Design a reservoir system for a controlled drug releasing tablet
- Formulate and develop a printable ink for the impermeable shell of a reservoir system
- Illustrate functionality of an impermeable shell of a reservoir system

### 4.1.2 Background

#### *4.1.2.1 Polycaprolactone*

PCL is a highly hydrophobic semi-crystalline polymer. Due to its good biocompatibility it has been used in a wide range of biomedical applications such as tissue engineering [114] and drug delivery, where it has shown particular, predominantly through degradation [115]. The mechanism of PCL degradation is through the random hydrolytic chain scission of ester linkages and is split into two stages. Initially, molecular weight decreases without any mass loss or deformation until a molecular weight of 5000 is reached. Following this, mass loss occurs [116]. The degradation of PCL can be a long process, so the material is often used for drug delivery applications that require long term delivery. It can however be blended or synthesised with other polymers to control the degradation process by changing the hydrophobicity of the material (e.g. PEG) [117].

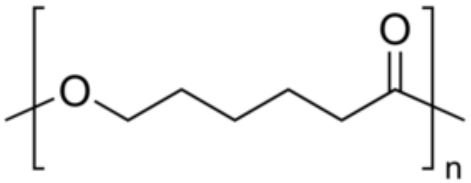



*Figure 4.1 - Molecular structure of PCL* [118].

Due to the long degradation times of this materials, PCL was the chosen to be investigated for its suitability as an impermeable material for a reservoir system tablet.

Although degradation is a common process for drug release, release can also occur through diffusion at smaller time scales.

Perez *et al.* 2000 evaluated hydrophilic and lipophilic drug release from PCL microparticles. DSC and XRD showed the microparticles had maintained their semi-crystalline properties. As significant release for both drugs occurred in a matter of hours, it was thought that diffusion was the predominant drug release mechanism due to PCL's high hydrophobicity and long degradation time. Water was thought to have penetrated the material through the amorphous regions of the matrix [119].

Jeong *et al.* 2003 investigated drug release from PCL microspheres. Different processing conditions (drug/polymer ratio, PCL solution concentration and PCL molecular weight) were used to create different microparticle batches. Using DSC, similar levels of crystallinity for different PCL concentrations (65 % – 70 %) were calculated. Small angle X-ray scattering (SAXS) showed that a long period length, referring to the repeating distance of the layers of lamellar crystals in a stacked structure [120], of samples were near identical. This suggested the length of the crystalline lamellar and amorphous phase were the same, concluding that varying polymer concentration does not affect crystallinity (although an increase in particle size was observed). With increasing molecular weight, crystallinity was seen to decrease according to DSC. SAXS, however, showed an increase in long period length, suggesting that as the molecular weight of PCL increases the amorphous regions increases. It was thought that the presence of the greater amorphous regions was a reason for the coarse morphology of the particles that was observed. The annealing of particles at different temperatures was investigated and crystallinity remained at similar values. However, it was observed that the onset of melting increased as the annealing temperature increased along with a slight shift to higher melting temperature. This was attributed to smaller and imperfect crystals forming at lower temperatures. SAXS showed a slight increase in long period length of crystals with increasing annealing temperatures, suggesting the size of the lamellae increases with annealing temperature. However, it was concluded that since DSC resulted in similar crystallinity values, the long period length should be assumed to be identical to the size of crystals. With the knowledge of the PCL microparticles crystal properties, their drug release behaviour was better understood. As in Perez *et al.* 2000,

the authors deduced that diffusion was the only mechanism of drug release as degradation would have taken significantly more time. Instead, water penetrated the material through an amorphous pathway, through which drug then diffuses through into the dissolution medium. When comparing molecular weight of PCL used, the highest weight showed the quickest release. As the material would have a lower crystallinity and greater long period length, drug can diffuse more rapidly through the coarse microstructure. When examining the effect of different annealing temperatures, samples annealed at 25 °C showed the fastest drug release. At this lower temperature, the crystals were less perfect and had the shortest crystalline lamellae. With samples annealed at 50 °C, the opposite was observed. At the higher annealing temperatures, the perfect crystals and larger lamellae act as a more effective barrier for diffusion, resulting in a slower and sustained drug release [121].

Diffusion controlled release has also been seen to occur in larger delivery devices. Holländer *et al.* 2016 investigated the release of indomethacin through PCL processed through 3D printing (material extrusion) for T-shaped implantable devices. Drug release was determined to be diffusion controlled based on the relatively short time period release observed and the mathematical fitting of the drug release profiles. PCL degradation had occurred but it only played a minor role in drug release [122].

PCL has been processed through different additive manufacturing technologies including material extrusion [122], binder jetting [69], selective laser sintering [123] and inkjet printing [124]. Yun *et al.* 2009 [125] and He et al. 2016a [124] used a solvent-based PCL formulation to conduct a systematic investigation of the printing behaviour of the material. The authors illustrated that PCL was a material capable of being processed through inkjet printing, building from individual droplets, lines and finally to a film. Both investigations showed the coffee-ring effect occurring, where there is a build-up of material at the edges of individual droplets. However, Yun *et al.* 2009 showed that the local segregation of PCL could be avoided by repeatedly jetting droplets at the same position. The multiple jetting caused the partial redissolution of PCL which eventually led the reversal of the coffee-ring effect [125]. He *et al.* 2016b used a UV-curable PCL dimethylacrylate formulation to construct 3D printed structures. The authors proved that the formulation was biocompatible with mammalian cells in a cytotoxicity assay [126]. Varan *et al*. 2017 used inkjet printing

to create bio adhesive films for cervical cancer treatment using a PCL based formulation [49].

N, N-dimethylacetamide (DMAC) is an organic solvent that has been used for a variety of applications including agrochemicals, fine chemicals and pharmaceuticals [127]. It is however a Class 2 solvent (by the European Medicines Agency), meaning the solvent can be present in a pharmaceutical formulation, but needs to be limited [128]. PCL is soluble in a wide range of solvents and with DMAC it is described as partially soluble (when PCL has a molecular weight of 14,000) [129]. DMAC was used as a solvent in the formulation of the impermeable shell of the designed reservoir system.

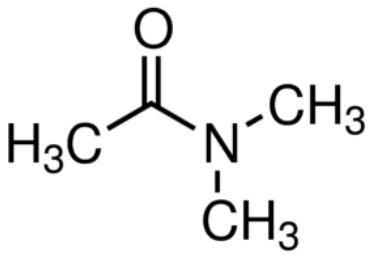



*Figure 4.2 - Molecular structure of DMAC* [130].

## 4.2 Materials and Methods

### 4.2.1 Materials

Polycaprolactone ($M_w$ ~ 14,000) and N, N-dimethylacetamide (ReagentPlus, 99%) were ordered from Sigma Aldrich. PET film, polyvinylpyrrolidone, thiamine HCl, polysorbate 20 and glycerol were also used (see Section 3.2.1 for further details)

### 4.2.2 Methods

#### *4.2.2.1 Design of reservoir system*

Bitmap files were created using the Dimatix pattern editor software. A reservoir system capable of delivering a drug dose in one direction was designed. Figure 4.3 shows the cross-section structure of the proposed reservoir system.



*Figure 4.3 - Cross-sectional schematic of the proposed reservoir system. Black represents the impermeable shell (base and walls of device). Yellow represent the rapid releasing core of the system. Blue represents the release controlling membrane through which drug release would occur.*

The above design required three bitmap patterns to be created. The first was the impermeable base of the device (also used for the release controlling membrane top surface). This was generated as an 8 x 8 mm square pattern. For the impermeable wall, an 8 x 8 mm square with a void space of 5 x 5 mm was generated. A 5 x 5 mm square used in Chapter 3 was then used for the core of the device.

For the purpose of this chapter, the entire core would be encapsulated with the presumed impermeable PCL.

#### *4.2.2.2 Ink preparation*

PCL and DMAC were weighed and placed into glass vials. Solutions were heated (60 °C) and stirred with a magnetic stirrer until all components were dissolved.

The core of the dosage form was formulated as shown in Section 3.2.2.2.

#### *4.2.2.3 Ink characterisation*

Surface tension was measured with a Krüss Drop Shape Analyser (DSA100).

Viscosity was measured with Malvern Instruments Kinexus Pro Research Rheometer. Measurements were taken at 28 °C and 60 °C.

Density was measured by calculating the ratio between the mass measured and volume of ink syringed into a glass vial.

See Sections 3.2.2.3, 3.2.2.4 and 3.2.2.5 for exact experimental procedure.

#### 4.2.2.4 Printing

Printing was done with a Fujifilm Dimatix Materials Printer DMP-2850. See Section 3.2.2.6 for further experimental details.

#### 4.2.2.5 Optical microscopy

A Nikon Eclipse LV100ND Optical Microscope was used to analyse the printed materials.

#### 4.2.2.6 Differential scanning calorimetry

DSC was conducted with a PerkinElmer DSC8000. Aluminium pans were manually crimped. The procedure consisted of four steps: (i) heating from 20 °C to 80 °C, (ii) cooling from 80 °C to 0 °C, (iii) heating from °0 C to 80 °C and (iv) cooling from 80 °C to °0 C. Heating and cooling rate was set at 10 °C/min. Nitrogen gas flow was set at 20 mL/min. A baseline run was conducted with empty pans and applied to the following experimental heat curves. Sample masses varied from 2 to 6 mg.

Pyris Data Analysis software was used to process and analyse data.

Crystallinity ($X_c$) was calculated using Equation 4.1 [131], where the experimental values for heat of fusion from melting ($\Delta H_f(T_m)$) and the heat of fusion of PCL with 100% crystallinity ($\Delta H_f^0(T_m^0)$). This was taken as 139.3 J/g [132].

$$X_c = \frac{\Delta H_f(T_m)}{\Delta H_f^0(T_m^0)} \qquad 4.1$$

#### 4.2.2.7 Layer thickness

A certain number of layers were printed and measured with a micrometer. The thickness of individual layers was calculated by dividing the thickness of the printed structure by the number of printed layers.

#### 4.2.2.8 Dissolution testing

Dissolution testing was conducted with a Copley dissolution tester (DIS 8000). 200 mL of deionised water was used as the dissolution media. Additional experimental information can be found in Section 3.2.2.17.

#### 4.2.2.9 *Scanning electron microscopy*

Scanning electron microscopy (SEM) was conducted with a Hitachi TM3030. A voltage of 15 eV was set and the composition (COMPO) imaging mode was used. Samples were observed in charge-reduction mode to avoid the need of coating samples.

## 4.3 Results and Discussion

### 4.3.1 Ink formulation

As in the previous chapter, investigation of an ink's properties was conducted. So that this ink would have similar jetting parameters to the rapid release formulation, it was formulated to have similar ink properties. This would allow similar printing parameters to be applied. The final formulation and its properties are shown in Table 4.1 and

Table 4.2.

*Table 4.1 - Ink formulation for the impermeable component.*

| Component | Content (wt %) |
|---|---|
| PCL | 10 |
| DMAC | 90 |

*Table 4.2 - Ink properties of the impermeable component. Surface tension was taken at room temperature (23 °C) and the viscosity value presented below was taken at 28 °C.*

| | |
|---|---|
| **Surface tension ($mN \cdot m^{-1}$)** | 35.65 ± 0.07 |
| **Viscosity (mPa·s)** | 5.494 ± 0.074 |
| **Density ($g \cdot mL^{-1}$)** | 1.1 ± 0.01 |
| **Nozzle diameter (µm)** | 21 |
| **Z factor** | 5.1 |

It was not required to develop this formulation any further as an appropriate Z factor value had been calculated.

### 4.3.2 Selection of printing parameters

Similar to the previous formulation (Section 3.3.2), as a result of acceptable ink and printability values, the standard Dimatix jetting parameters were used. Spherical droplets were consistently generated, similar to what was seen in Figure 3.8. The ink's temperature was maintained at 28 °C initially.

#### *4.3.2.1 Substrate temperature*

PET film was used for the initial stages of printing this material as a substrate. Through preliminary printing, it became clear that the temperature at which the substrate was heated to was critical in terms of morphology (Figure 4.4) and film formation. Thus, the behaviour of this material was investigated at three different temperatures: (i) 28 °C, (ii) 40 °C and (iii) 60 °C. These temperatures were selected as 28 °C and 60 °C were the minimum and maximum controlled temperatures respectively on the Dimatix printer. 40 °C was selected as a temperature between the maximum and minimum temperatures. For this part of the investigation, other film forming parameters such as drop spacing, single drop and line formation were not immediately investigated. The main objective here was to identify which temperature would yield the most effective 3D structure. Hence, a total of 100 layers was printed.

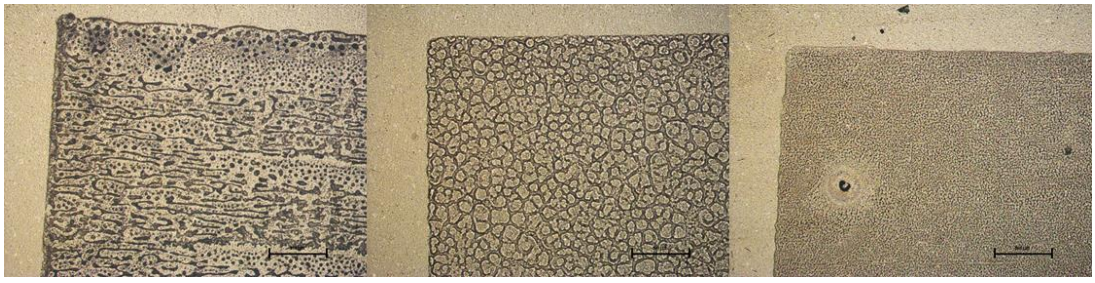


*Figure 4.4 - Optical images of the three morphologies observed when printing the PCL ink at different temperatures: 28 °C (left), 44 °C (40 °C was not observed with optical microscopy) (centre) and 60 °C (right). Scale bar = 500 µm.*

An important parameter for solvent inkjet printing was the time required for solvent to be evaporated before the following layer can be deposited. With the substrate maintained at 28 °C, an eight minute delay after each layer was required to ensure most of the DMAC had evaporated. At the end of the printing process, the resulting

material was soft with a coarse ‘powder-like’ texture (shown in Figure 4.5). The structures were easily removed from PET but would easily disintegrate with gentle rubbing. It was clear that this material would not be a viable option of a tablet due to its apparent weakness. Printing at 40 °C provided an improvement on film morphology, with a smooth texture. However, film cracking was an issue (Figure 4.6). Several methods of preventing this behaviour were attempted, including changing the delay between layers and printing on different substrates, however, this failed. Handling of this printed material proved to be very weak, often disintegrating during removal from the substrate.



*Figure 4.5 - The weak, 'powder-like' structure that from when 100 layers of PCL was printed at 28 °C.*

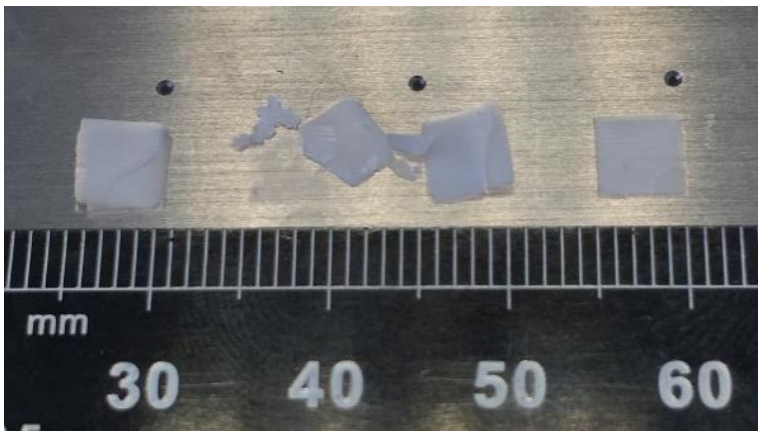



*Figure 4.6 - PCL films printed at 40 °C. Cracking and delamination occurs during the printing process.*

Printing at 60 °C resulted in molten PCL forming on the substrate. Film formation was unusual as the first layer yielded a uniform film but with additional layers ‘islands’ of PCL would form (Figure 4.7). However, after printing a certain number of layers

(usually around 50 layers on PET) a uniform but molten structure forms (Figure 4.8). When turning off the heat and allowing the substrate to cool over time in the ambient environment, the molten structure solidifies into a uniform film as shown in Figure 4.9 (this occurs around 40 °C). Removal from the PET substrate was possible with no damage to the print and handling resulted in no fracture. Although not the ideal choice, it was sufficient to create an impermeable shell.

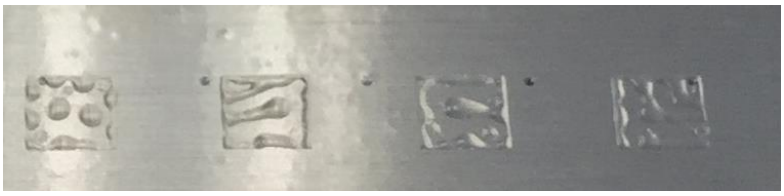


*Figure 4.7 - PCL ink being printed at 60 °C. A single layer showed good film forming characteristics but as additional layers are printed, 'islands' of molten PCL form.*

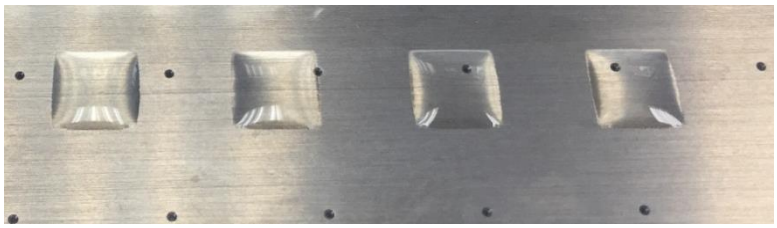


*Figure 4.8 - 100 layers of PCL ink printed at 60 °C. After a certain number of layers (approximately 50) uniform films of molten PCL form.*

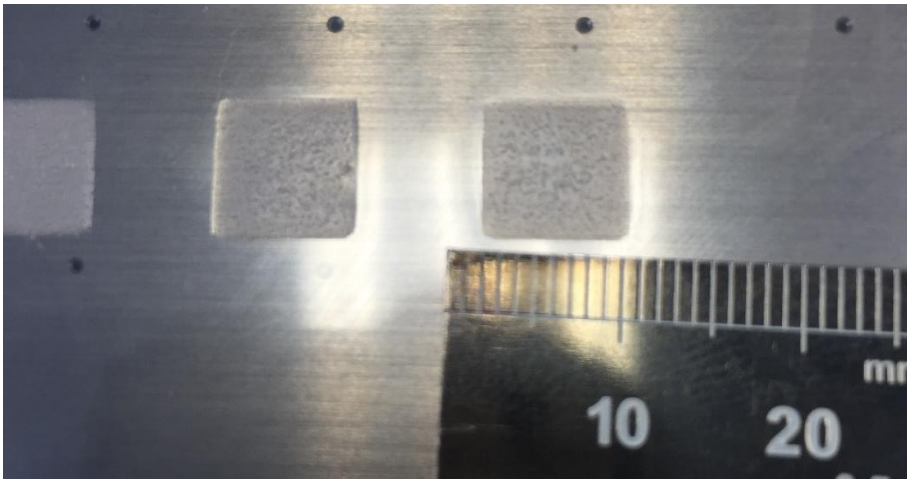



*Figure 4.9 - 100 printed layers of PCL after the substrate temperature was reduced from 60 °C to 28 °C. Uniform solid films were formed.*

The crystallisation of PCL after printing at 60 °C was observed with cross-polarised optical microscopy as shown in Figure 4.10. As is common for melt crystallised semi-crystalline polymers, spherulites are seen to form and grow. They nucleate at different points in the film and continue to grow until they impinge on one another [133].

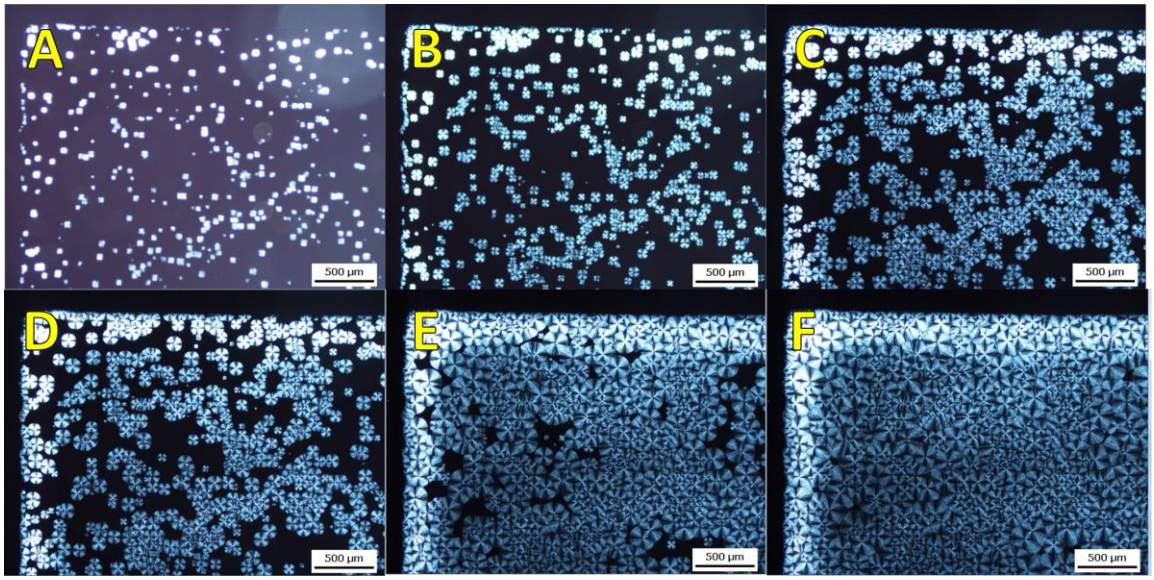



*Figure 4.10 – Single layer of PCL film printed at 60 °C crystallising (from melt) at room temperature over time: (A) immediately removed from heated print bed, (B) 30 s, (C) 60 s, (D) 90 s, (E) 120 s, (F) 180 s. Spherultic growth was clearly observed. Scale bar = 500 µm.*

The various behaviour of printed PCL seen in this section was further understood with their studied thermal behaviour through DSC. Figure 4.11 shows the melting behaviour of samples while Figure 4.12 illustrate their crystallisation behaviour. Melting of raw PCL begins at approximately 58 °C and its melting peak is seen at 65 °C. Printing of PCL with the substrate heated at 60 °C resulting in molten material forming is therefore an obvious result. Crystallisation of PCL occurs at around 40 °C, backing up what was seen experimentally (when the molten PCL is cooled and begins to solidify).

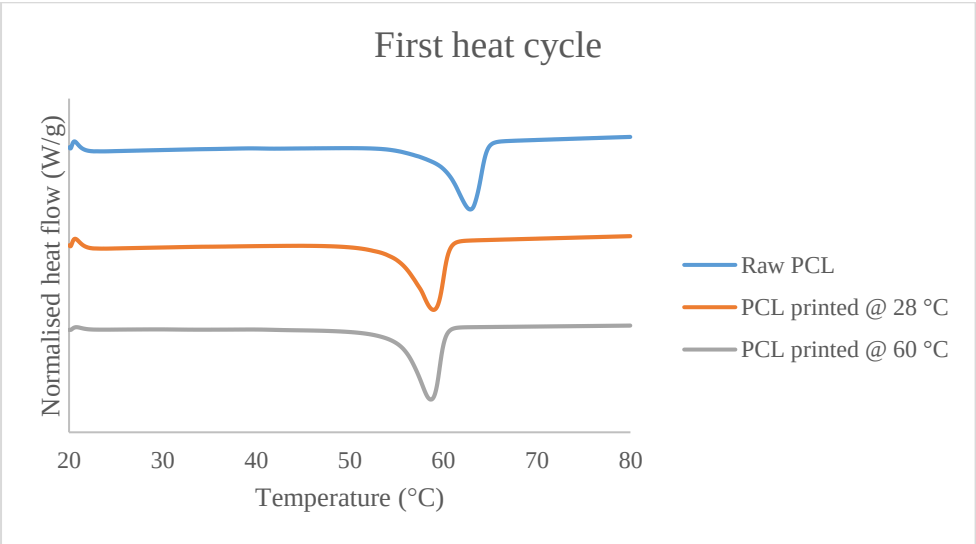



*Figure 4.11 - First heating cycle DSC thermographs (endo down). The melting peak of PCL is observed.*

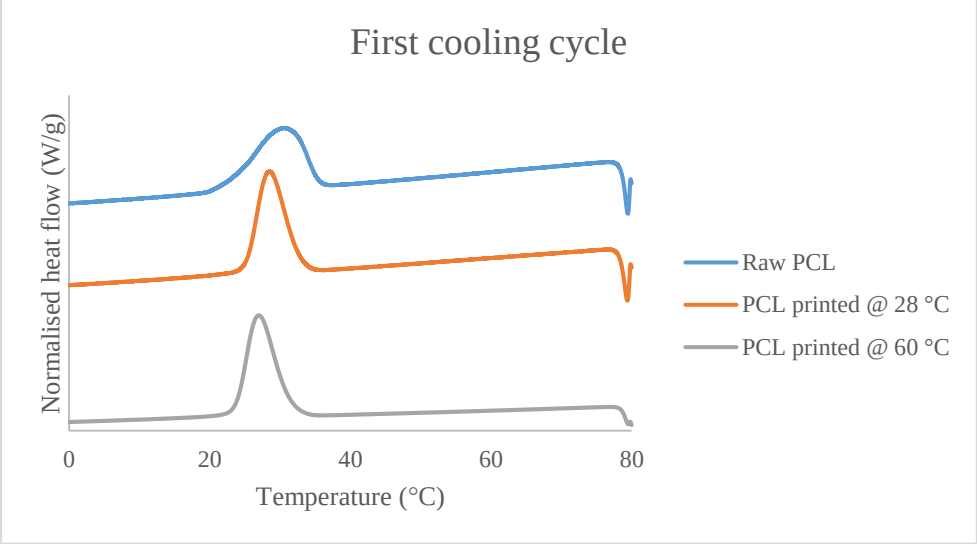



*Figure 4.12 - First cooling cycle DSC thermographs (endo down). The crystallisation peak of PCL is observed.*

Table 4.3 shows the calculated values of crystallinity from each heating cycle. A crystallinity level of 59.38 % was calculated for PCL printed at 28 °C – only slightly higher than PCL printed at 60 °C (56.23 %), suggesting no major difference in crystallinity. There was a slight shift to a higher temperature for the onset of melting and melting temperature, similar to what has been previously reported [121]. It may be possible that crystallinity was not the main reason for why different morphologies existed. The method of printing at 28 °C and 60 °C differ significantly. Printing at 28 °C, each layer solidifies (through DMAC evaporation) before the following layer is printed. In contrast, printing at 60 °C requires solidification to occur not when DMAC evaporates (a delay between layers is controlled to allow for this), but when the substrate temperature was allowed to return to room temperature. Another reason for the change in morphology is that at 60 °C, crystallisation occurred from the melt, whereas at 28 °C, evaporative crystallisation is the mechanism. There was also the possibility for PCL being re-dissolved when additional layers were deposited when the substrate was at 28 °C.

*Table 4.3 - Crystallinity values calculated from DSC (n=1).*

| Heating cycle | $X_c$ (%) | | |
|---|---|---|---|
| | Raw PCL | PCL printed @ 28 °C | PCL printed @ 60 °C |
| 1 | 66.51 | 59.38 | 56.23 |
| 2 | 45.98 | 44.47 | 43.65 |

Further experimentation for a more conclusive answer regarding the printed PCL morphologies were required, but since this was not the main aim for this investigation,

they were not pursued. No significant difference in thermal behaviour between PCL printed at 28 °C and PCL printed at 60 °C was seen. However, additional repeats may allow for more conclusive results. Table S4.5 presents a summary of the thermal properties of PCL (raw and printed samples).

For the actual printing of the reservoir system, PCL was printed at 60 °C (substrate temperature) and then allow it to solidify as the substrate temperature returned to room temperature. This was done as it allowed for a solid, crack and delamination free method of printing a potentially impermeable material.

#### *4.3.2.2 Jetting temperature*

The result of printing PCL at this elevated substrate temperature had an impact on the choice of jetting temperature (the temperature at which the ink in the reservoir was heated to). It was observed during initial printing at 60 °C, a heat transfer event between the substrate (at 60 °C) and the nozzles (at the time was set to 28 °C). As the patterns being printed were relatively large, jetting time was significant. As time progressed, nozzle temperature was seen to increase above 40 °C. If a larger pattern or greater number of samples were being printed, this temperature increase could potentially increase even more. Using the Dimatix drop watcher system, it was possible to see the effect increasing temperature had on drop formation and jetting behaviour (Figure 4.13). As the temperature increased, the initial spherical drops gain a tail. The tail grows larger as temperature increases until a stream of material was being jetted, instead of consistent spherical drops. The increase in temperature resulted in a decrease in viscosity that resulted in more material being jetted. This was confirmed when the viscosity experiment was repeated at 60 °C where viscosity was measured at 3.239 ± 0.134 mPa·s.

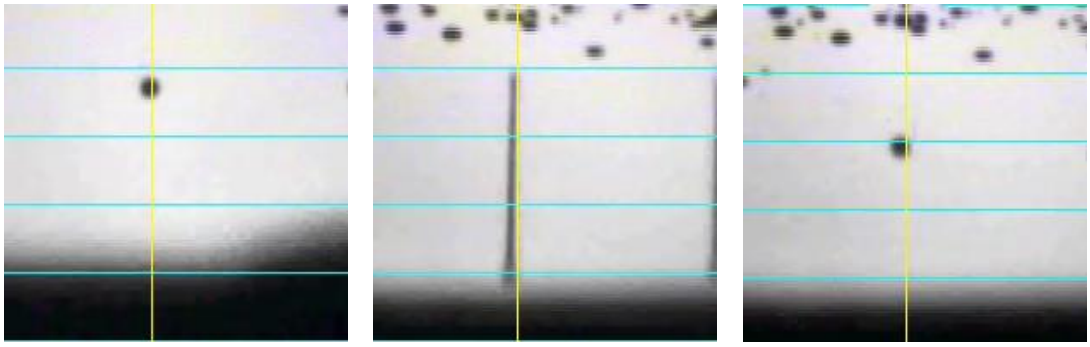


*Figure 4.13 - The PCL ink jetted at 28 °C (left), ink jetted at 70 °C (centre) and ink jetted at 70 °C with an edited waveform (right).*

To control this phenomenon, the waveform that is applied to the printed method was edited. The initial stage of jetting (the taking up of ink in the reservoir) magnitude was lowered. Its effect resulted in a return to reliably jetted spherical drops. The exact amount adjusted for each print session varied (and was noted). When printing a large number of samples over long periods of time, jetting parameters were occasionally further adjusted to ensure consistent jetting. Figure 4.14 shows the waveform used and the editing action that took place.

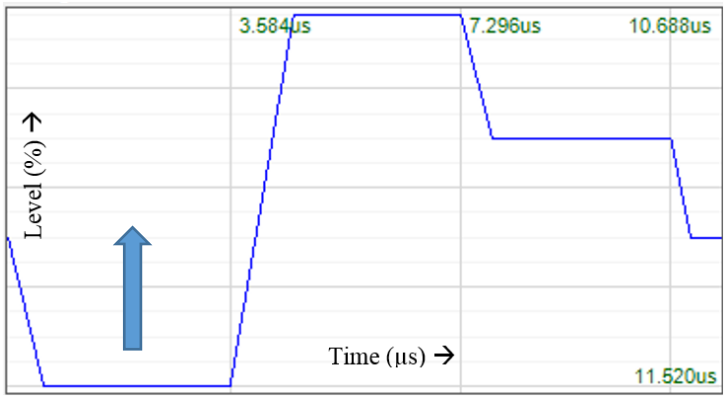



*Figure 4.14 - The general waveform applied during the printing process. To prevent tailing and satellite drops that occur due to the higher temperatures, the initial stage of the jetting process, which relates to ink uptake before jetting, is reduced.*

From this point on, the was jetted at 60 °C with the edited waveform. This would prevent the substrate (at 60 °C) from influencing the jetting behaviour.

### 4.3.3 Printing an impermeable reservoir system

Before moving on to developing the release controlling membrane, it was critical to illustrate that the base and walls of the device would be impermeable to drug release. To do this, a reservoir system consisting of a PVP-thiamine HCl core completely

surrounded by PCL alone was printed. Before printing the entire device, inks were individually printed to a set number of layers. Layer thickness was then calculated using a micrometre. The PCL ink printed on PET at 60 °C with a 20 µm drop spacing had a layer thickness of 1.94 ± 0.04 µm (n = 3) and the PVP-thiamine HCl formulation printed on PET at 28 °C had a thickness of 3.94 ± 0.01 µm (n = 3).

First, 100 layers of PCL were printed on PET with its substrate and nozzles heated to 60 °C. An 8 x 8 mm square pattern was selected. After completion of this component, the substrate temperature was lowered to 28 °C allowing for solidification of PCL. On top of this structure, the PVP-thiamine HCl formulation was printed (100 layers of a 5 x 5 mm square pattern). Lowering the substrate temperature to 28 °C was also necessary for the stable jetting of the PVP-thiamine formulation. As discussed in the previous section, the heat from the substrate can affect jetting behaviour. With the water-based ink, the effect of temperature from the substrate can eventually lead to another problem. Using the drop watcher system again, the jetting behaviour of the ink was observed as temperature increased. Initially, similar behaviour was seen with consistent spherical droplets. Significant tailing was then observed with the formation of satellite droplets as temperature increased (Figure 4.15). Eventually, jetting stopped completely. The increased temperature in the nozzles led to greater evaporation of water of the ink formulation, leading to blocking of the nozzles. This behaviour is attributed to the vapour pressure of water.

Vapour pressure refers to how easily a liquid partitions to the atmosphere [134] (i.e. its tendency to evaporate). At 20 °C, water's vapour pressure is at 2.3 kPa and increases to 19.9 kPa at 60 °C [135]. This significant increase means that water would have a greater tendency to evaporate at this higher temperature. This in turn led to the blocking of nozzles. This behaviour was not seen for the DMAC solvent. This was because DMAC has a significantly lower vapour pressure of 0.176 kPa at 20 °C. Even though the vapour pressure of DMAC is known to increase as temperature increases [136] (at 40 °C, DMAC vapour pressure is reported to be 0.652 kPa [137]), it does not presumably reach a point where the nozzles blocks.

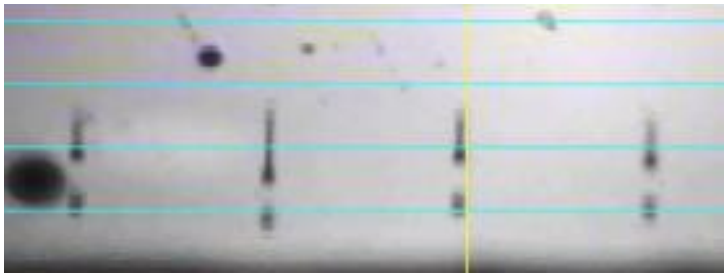


*Figure 4.15 - Satellite drops and tailing of droplets that were seen while printing the water-based ink at elevated temperatures, before the nozzles completely block and stop working.*

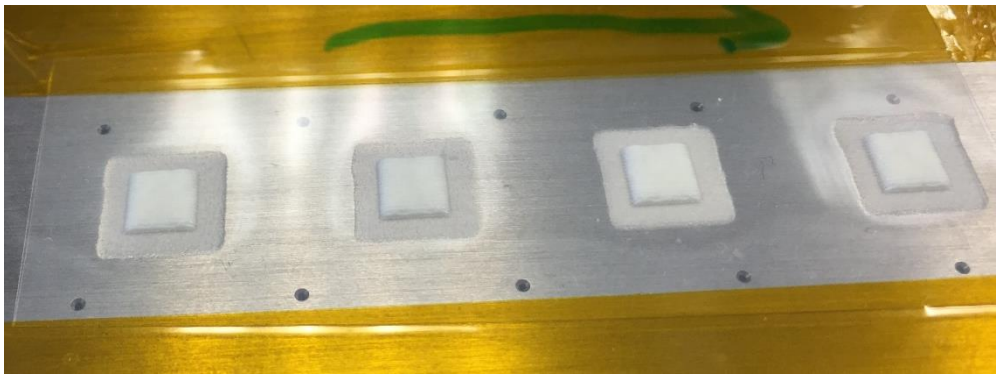


*Figure 4.16 - Printed PVP-thiamine formulation on the PCL printed base of the reservoir system.*

Following the printing of the core, the walls of the device were printed, using the same ink formulation of the base of the device with the same printing conditions. Based on the layer thickness 200 layers of PCL were needed to encapsulate the core on the edges. As the PCL being printed was molten (due to the substrate heat), printing a large number of layers led to some spreading and partial loss of shape however, it was clear that the edges were covered.

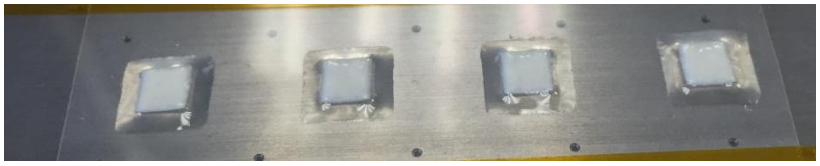


*Figure 4.17 - Reservoir devices after the PCL walls were printed at 60 °C. Some loss of shape is observed due to the spreading of the molten PCL, but closer visual examination showed the edges were sufficiently encapsulated.*

The top of the device was then capped off with 100 layers of an 8 x 8 mm square pattern. The substrate was then cooled down to room temperature, which allowed the molten components to solidify. The tablets were then 'popped' off the substrate through bending of the PET. Some residual material was seen to remain on the PET, but only at the edges.



*Figure 4.18 - Completed reservoir systems with PVP-thiamine completely encapsulated in printed PCL.*

Figure 4.19 summarises the printing process for this reservoir system.

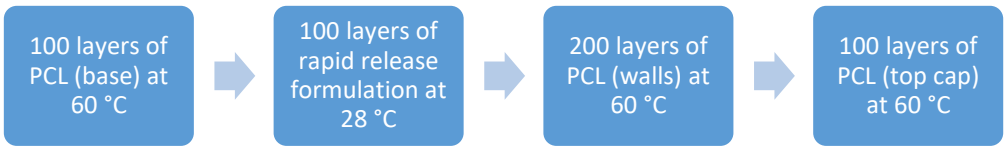



*Figure 4.19 - The manufacturing process for inkjet printed reservoir systems.*

### 4.3.4 Illustrating the impermeable nature of the material

Dissolution studies were conducted to investigate the effectiveness of the PCL material. Reservoir devices where the PVP-thiamine HCl formulation is completely encapsulated by the highly hydrophobic material were tested. Before carrying out the dissolution test, optical microscopy was used to examine the top and bottom surfaces of the reservoir tablets primarily to make sure there were no cracks or other flaws present. An example is shown in Figure 4.20 where the PVP-thiamine HCl core was clearly encapsulated and no evidence of cracking was observed on either surface. The top surface did appear to have a rougher profile in contrast to the bottom and smoother surface. This was attributed to the homogeneous interaction the print had with the PET substrate on the bottom, in contrast to the top surface exposed to the air environment. Evaporation of DMAC may have also had an impact on the surface morphology.

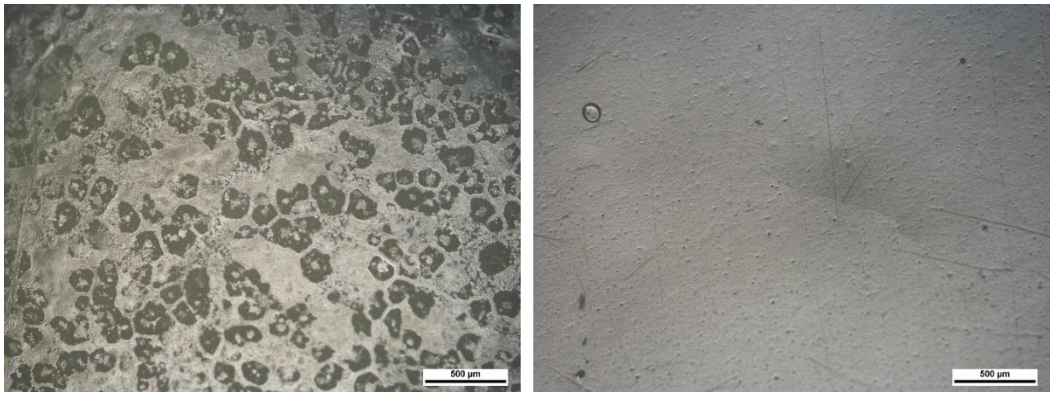



*Figure 4.20 - Optical images of one the reservoir devices. The top surface (left) appeared to be rough in contrast to the bottom surface (right), where a very flat and smooth surface was observed. Scale bar = 500 µm.*

Two of the three devices did show significant drug release (74.1 % and 51.7 %), but one device showed only a negligible amount of drug released (2.5 %) after five hours. Figure 4.21 shows the release profiles of the reservoir tablets tested. Before any conclusions were made, inspection of these samples after dissolution (e.g. Figure 4.22) were needed and conducted.

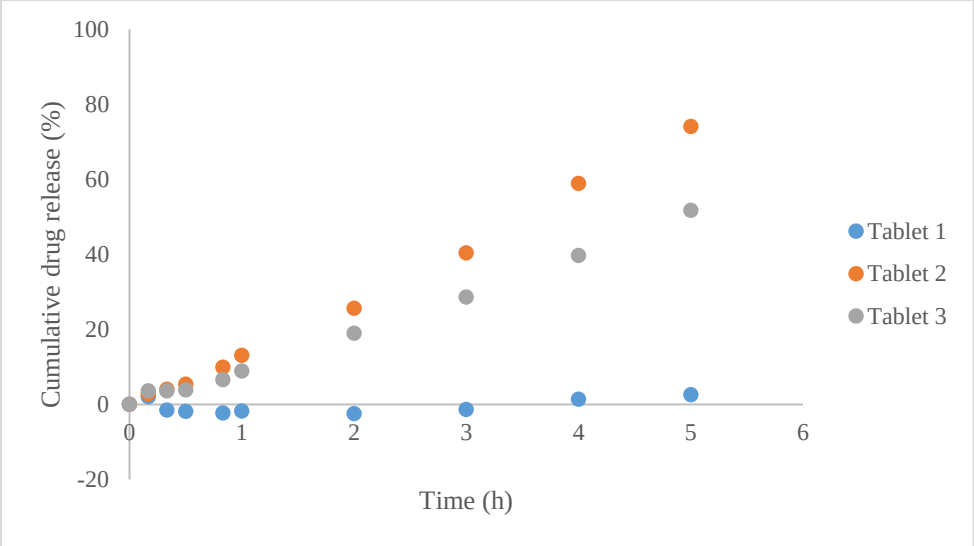



*Figure 4.21 - Release profile of PCL encapsulated reservoir tablets.*

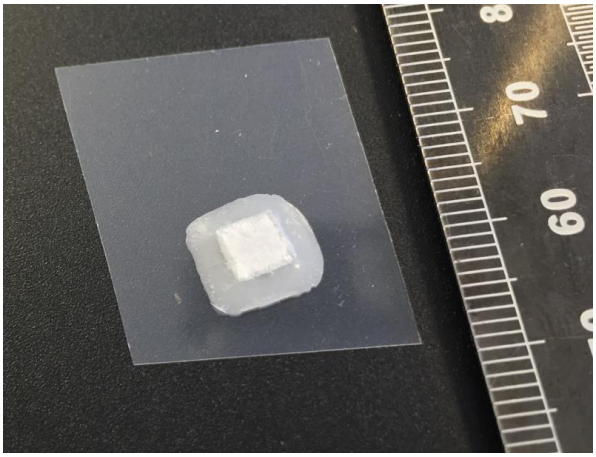



*Figure 4.22 - Tablet after dissolution.*

Figure 4.23 shows the SEM image of the top surface of the device that has not undergone dissolution. Although the core of the device is not seen, holes or gaps are observed. It was not thought that these holes played a direct role in drug release. When compared to the device that did not show significant drug release (Tablet 1 in Figure 4.21) similar features are observed on the top surface (Figure 4.24). In contrast, the bottom surface showed a high degree of smoothness, probably due to the uniform interaction of the PET substrate rather than the air atmosphere the top surface encounters. At this point it was still not clear why release had occurred. Through analysis of one of the samples that did show release (e.g. Tablet 2 in Figure 4.21), it became clear why release had occurred in this sample. Figure 4.24 shows the top surface of the tablet after dissolution with a region of physical loss of the membrane. The bottom surface did not show any clear indication of physical loss. By using both SEM imaging and release data it was concluded that drug release does not occur through PCL in the time scale investigated. Drug release was seen only when a physical loss of membrane occurred. It was thought that the top surface has a weaker morphology in contrast the base due to the different surface interactions (consistent and uniform interaction with the PET substrate).

PCL was proven to be an appropriate material choice for the base and walls of the device and a new formulation was developed for the release controlling membrane (Chapter 5).

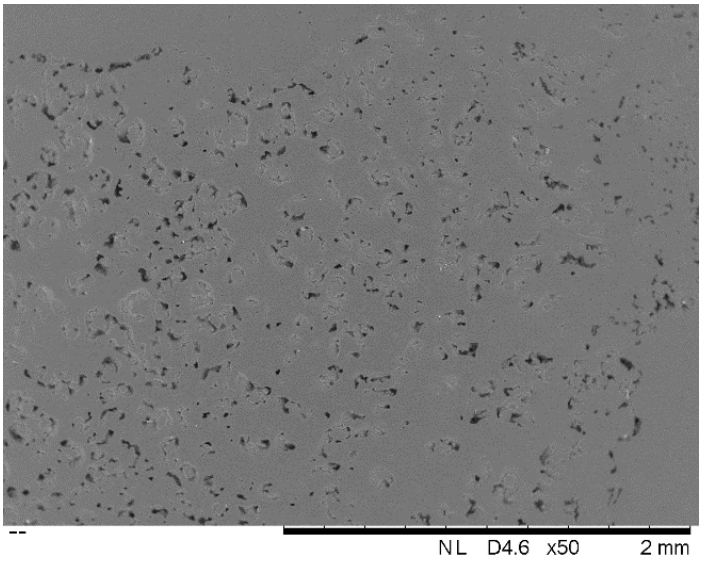



*Figure 4.23 - The top surface of the tablet (PCL only) that has not undergone dissolution*

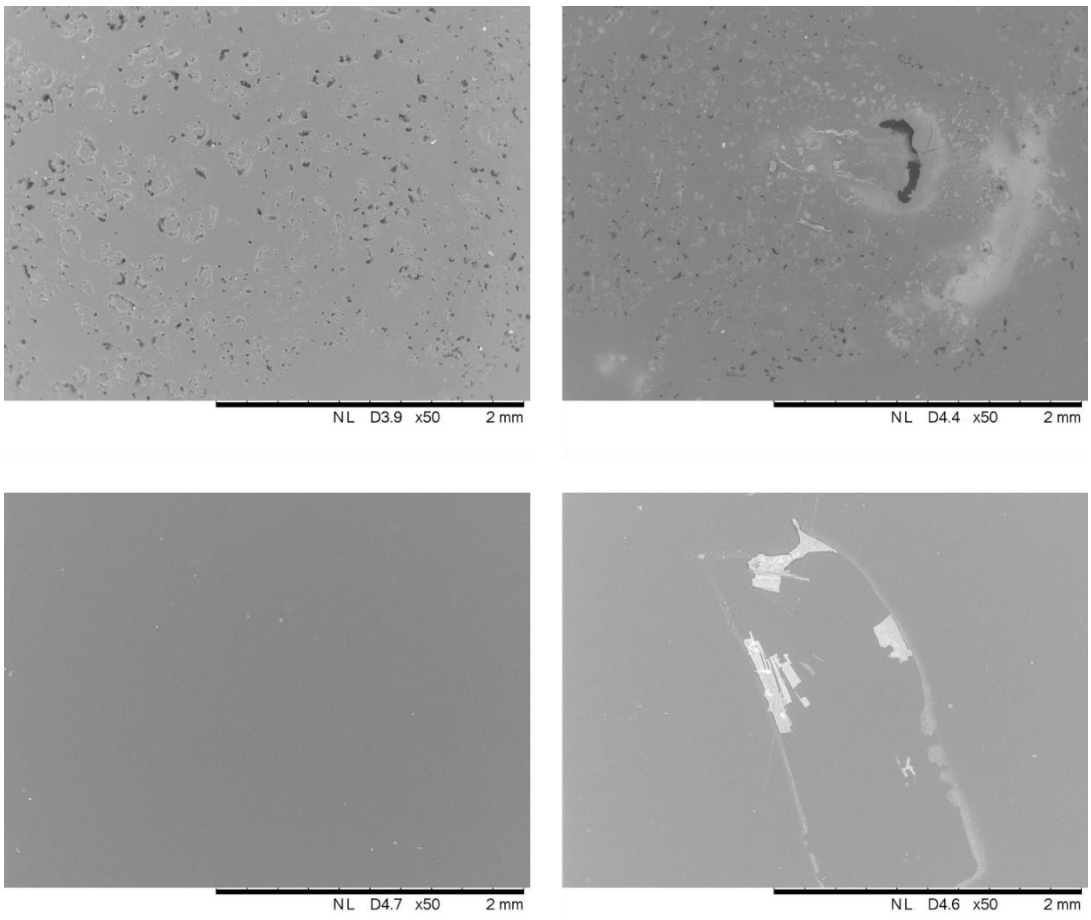



*Figure 4.24 - SEM images of tablets that underwent dissolution. The tablet that showed no significant drug release (left) showed no indication of physical loss of membrane on the top (top) or bottom (bottom) surfaces. The tablet that did show a release (right) clearly showed a significant physical loss on the top surface. No indication of mass loss was seen on the bottom surface (although some dirt is seen).*

## 4.4 Conclusions

The following conclusions can be made from this chapter:

- PCL is a semi-crystalline polymer that is well established for its use in the medical and pharmaceutical industry. Due to its hydrophobic nature and long degradation times it was investigated as a potential material for the impermeable shell for the reservoir system. It is partially soluble in DMAC, which was the selected solvent in this investigation.
- The formulated ink (10 wt% PCL) showed to have an appropriate Z printability factor based on its viscosity, surface tension, density and nozzle diameter of the printer. Printing on the Dimatix with the standard settings proved to be consistent and reliable.
- The morphologies that formed varied depending on the substrate temperature. Printing 3D structures at 28 °C was possible but resulted in a coarse 'powdery' structure which was very weak. Printing at 40 °C was more challenging due to the material's tendency to crack and delaminate. For both printing at 28 °C and 40 °C, the slow evaporation of DMAC required that there be a significant delay between layers – slowing down the entire manufacturing process. Printing at 60 °C, molten PCL forms after DMAC evaporation. A solid 3D structure then forms as the substrate heating was turned off and allowed to return to room temperature. The resulting structure appeared to have a uniform surface with no indication of cracking and delamination. This substrate temperature would be used when it came to printing the entire reservoir system.
- DSC was conducted to compare crystallinity of the PCL structures printed at 28 °C and 60 °C. The level of crystallinity for both samples appeared to be quite close, suggesting crystallinity was not affected by the substrate temperature. The reason for the contrasting morphologies could be attributed to the method of printing the two structures and the effect substrate temperature has on the crystallisation process.
- As 60 °C was selected for the substrate temperature, the effect of temperature on the jetting behaviour of ink was observed. Heat transfer was seen to occur from the substrate to the nozzles resulting in the spherical drops to tail and have satellite droplets, ruining the consistency and precision inkjet printing is

known for. The heat in nozzles had decreased the viscosity of the PCL ink from 5.494 mPa·s to 3.239 mPa·s. This decrease caused significant tailing. To address this, the waveform applied to the jetting process was edited, reducing the initial uptake of ink before the actual jetting mechanism. This resulted in consistent and spherical drops to be generated allowing the ink to be maintained at 60 °C to prevent uncontrolled heat transfer from the substrate. Similar behaviour was observed with the PVP-thiamine HCl ink. Initially tailing and satellite droplets appear as temperature increases, but after a greater duration, the nozzles stop jetting. This was attributed to the greater evaporation of water, due to its higher vapour pressure. The evaporation of water had caused the blocking of nozzles. It was because of this problem the substrate temperature would be maintained at 28 °C when printing the PVP-thiamine HCl component for the reservoir system.

- To prove that PCL was an appropriate material for an impermeable shell, a reservoir system was designed and printed consisting of a PVP-thiamine HCl core surrounded by printed PCL. Dissolution studies showed that when the reservoir system was not damaged, only a negligible amount of drug was detected (2.5 %) after five hours. The top surface of the PCL reservoir system was susceptible to damage and mass loss resulting in drug release. No damage was observed for any sample on the base of the system. As the top surface would be replaced with a permeable release controlling membrane, this was not deemed to be a major issue. Since the sample that was not damaged showed negligible release, it was concluded that PCL would be an appropriate impermeable shell for the base and walls of a reservoir system.

## 4.5 Chapter Appendix: Supplementary Information

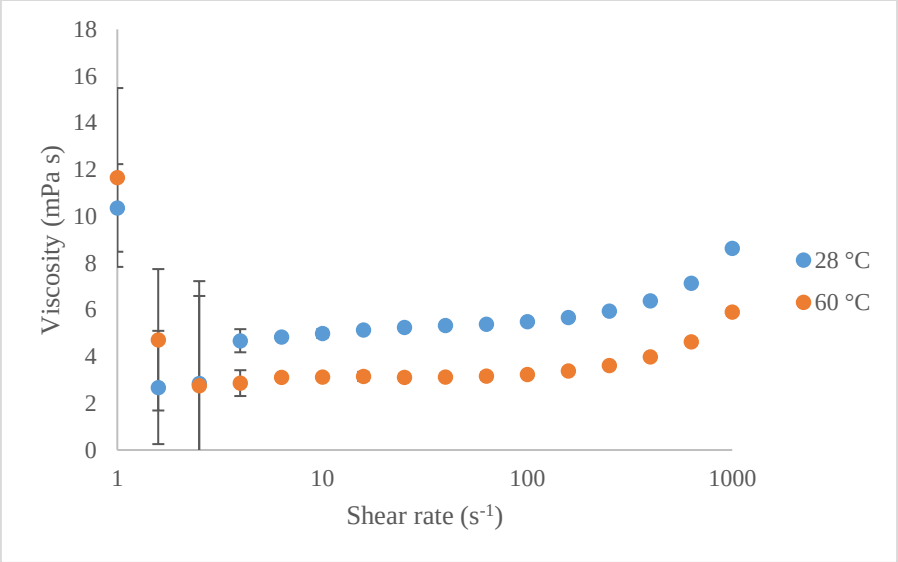



*Figure S4.25 - Rheological flow curves of the PCL-DMAC ink measured at 28 °C and 60 °C.*

*Table S4.4 - Additional information regarding thickness of the PCL printed structures (n = 4). PET thickness was 0.110 ± 0.001 mm.*

| No. of layers printed | Thickness of total structure (mm) | Individual layer thickness (µm) |
|---|---|---|
| **100** | 0.194 ± 0.004 | 1.94 ± 0.04 |

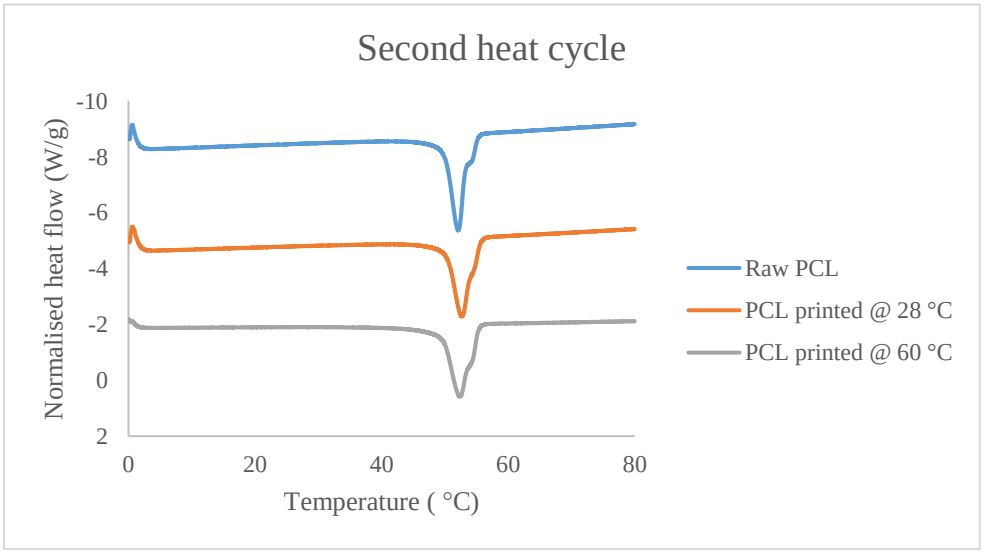



*Figure S4.26 - The second heating cycle DSC thermographs (endo down). Melting peak of PCL is observed.*

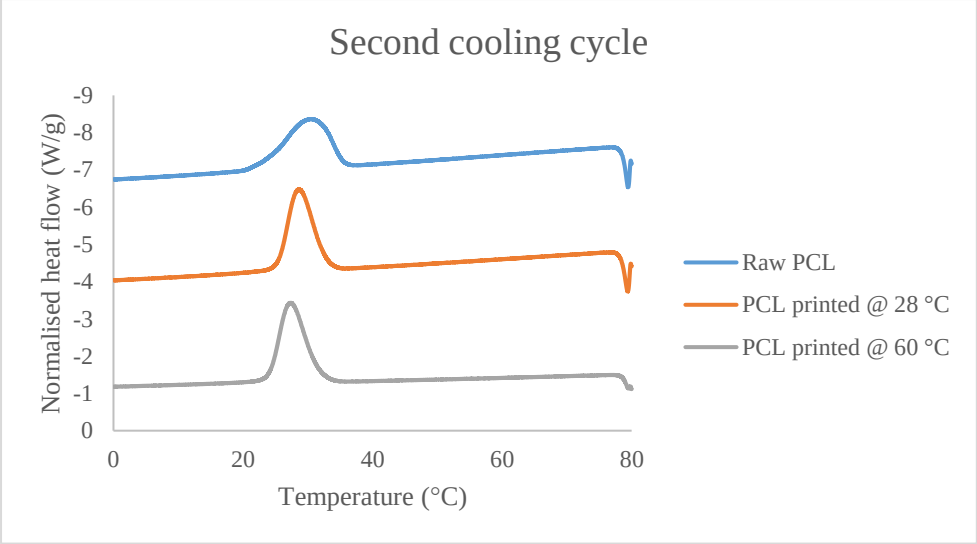



*Figure S4.27 - Second cooling cycle DSC thermographs (endo down). Crystallisation peak of PCL is observed.*

*Table S4.5 - Thermal properties of samples analysed with DSC.*

| | | Raw PCL | PCL printed @ 28 °C | PCL printed @ 60 °C |
|---|---|---|---|---|
| First heating cycle | Tm (°C) | 65.55 | 61.58 | 61.63 |
| | Onset (°C) | 61.80 | 57.99 | 58.35 |
| | End (°C) | 67.39 | 63.27 | 63.18 |
| | Area (mJ) | 259.40 | 272.98 | 485.61 |
| | Delta H (J/g) | 92.64 | 82.72 | 78.32 |
| First cooling cycle | Tc (°C) | 33.49 | 31.52 | 30.32 |
| | Onset (°C) | 38.51 | 35.90 | 34.84 |
| | End (°C) | 25.59 | 28.27 | 27.06 |
| | Area (mJ) | -184.73 | -199.17 | -396.63 |
| | Delta H (J/g) | -65.98 | -60.35 | -63.97 |
| Second heating cycle | Tm (°C) | 54.70 | 55.28 | 55.29 |
| | Onset (°C) | 52.47 | 52.73 | 52.46 |
| | End (°C) | 56.14 | 57.30 | 58.26 |
| | Area (mJ) | 179.35 | 204.41 | 377.02 |
| | Delta H (J/g) | 64.05 | 61.94 | 60.81 |
| Second cooling cycle | Tc (°C) | 33.45 | 31.66 | 30.68 |
| | Onset (°C) | 38.53 | 35.90 | 35.13 |
| | End (°C) | 26.24 | 28.45 | 27.46 |
| | Area (mJ) | -182.76 | -208.15 | -391.86 |
| | Delta H (J/g) | -65.27 | -63.08 | -63.20 |

# 5 Inkjet Printing Reservoir Systems with a Controlled Drug Release

## 5.1 Introduction

### 5.1.1 Aims of chapter

- Formulate and develop a printable ink for the drug release controlling membrane a reservoir system
- Characterise the formulated membrane
- Investigate the influence printing and ink parameters have on drug release behaviour
- Create specific drug release profiles

### 5.1.2 Background

#### *5.1.2.1 Polymer blends*

A polymer blend is a mixture of two or more polymers. Blends are often created to develop new materials with different physical properties and characteristics than the constituent polymers, so that each polymer can offer its own advantages in a single structure [138]. The blend structures are highly dependent on the miscibility between the phases present. This is influenced by the individual characteristics of the polymers, their respective amounts and the method of mixing employed [139].

Polymer blends are often defined in three categories: (i) miscible blends that are thermodynamically stable with a single glass transition temperature, (ii) immiscible blends that are thermodynamically unstable and eventually separate and (iii) compatible blends where an additive or interaction between functional groups of the phases prevent immiscibility [140]. In context of this investigation, immiscible blends will be discussed.

A simplistic way to illustrate the tendency for a blend to phase separate (i.e. be immiscible) is by determining the polymer system's Gibbs free energy ($\Delta G_m$) (Equation 5.1). The Gibbs free energy is influenced by the enthalpy of mixing in the

system ($\Delta H_m$), the entropy (a measurement of disorder) of mixing ($S_m$) and temperature ($T$) [141].

$$\Delta G_m = \Delta H_m - TS_m \quad 5.1$$

For a system to be miscible, the Gibb's free energy is negative – meaning heat is generated ($\Delta H_m < 0$) during mixing. As mixing is exothermic, the enthalpic term will mean that the Gibb's free energy is negative. As a system favours disorder, the entropy of mixing will always be positive. For a system to be immiscible, the opposite is required (i.e. $\Delta G_m > 0$, $\Delta H_m > 0$) [138]. The molecular weight of the polymers can also have an impact on the tendency of phase separation. For low molecular weight systems the entropy of mixing is the dominant factor, whereas in higher molecular weight systems, the entropy of mixing is usually a small value and miscibility is controlled by the sign of the enthalpy of mixing [142].

There are two common phase separation mechanisms. Spinodal decomposition occurs if a system is unstable to small concentration fluctuations within the system. This results in phase separation occurring continuously and spontaneously [143]. From a homogenous mixture, two distinct phases form by macromolecules moving against a diffusion gradient. In the second occurrence – nucleation and growth – the system remains a continuous phase until a significant fluctuation occurs [138]. Once a stable nucleus has formed (assuming the surface energy barrier has been overcome), a thermodynamically favourable phase separation process can occur [143]. Polymer chains will then diffuse to the surface of the nucleus allowing the nucleation site to grow in size [138].

The resulting morphology of a polymer blend is often described as one dispersed phase in a continuous morphology. Whether a component is the dispersed or continuous phase is often determined by the amount of each polymer. Lower loadings of one polymer will usually mean it will be the dispersed phase. Increasing its concentration or loading of this polymer, can transition it into the continuous phase [138]. A common feature seen in blends, is the dispersed phase appearing as spherical regions in the continuous matrix. This is due to the system's tendency to minimise its free surface

energy. It is possible for other geometries to form, often caused by stresses that may be applied during processing [138].

When used in the context of drug delivery applications, the versatility of polymer blends and their properties can be utilised to create more complex drug delivery systems [144]. They can help address issues such as poor film formation and storage stability. More importantly, they can be used to create very specific drug release profiles that can be used for site specific drug delivery [145].

PCL and PVP have been blended and synthesised previously, through different methods and for various applications. Chung *et al.* 2004 synthesised PCL and PVP micelles block copolymers as potential carriers for pharmaceutical applications [146]. Xing and Yang 2009 investigated PCL and PVP blends made via successive *in situ* polymerisation steps to investigate changes in material behaviour including crystallinity, which was seen to decrease [147]. The creation of blended fibres has also been investigated. Mary *et al.* 2013 , Kim *et al.* 2014, Lee *et al*. 2014 prepared their fibres by dissolving PCL and PVP in a solvent system before electrospinning [148] [149] [150]. The resulting fibres had a morphology of PVP domains dispersed in a PCL matrix. The PVP was removed by solvents to create highlight porous fibres for applications such as drug delivery and tissue engineering. Jin *et al*. 2014 used side-by-side dual-electrospinning of PCL and PVP to create aligned fibres with different geometries. Exposure to water of these fibres resulted in swelling of the PVP to volumetrically expand the fibres as well as forming porous structures [150]. Wang *et al.* 2017 used electrohydrodynamic printing to create 3D film patches with antibiotics, highlighting this approach as a method of manufacturing dosage forms for personalised release by controlling printing and formulation parameters [151].

With this well-established behaviour of blending PCL and PVP, this material would be used as the basis of a release controlling membrane for the reservoir system. It was hypothesised that PVP domains would be dispersed in a PCL matrix. When exposed to water, it was thought that the PVP would dissolve, providing water with a pathway to the core of the system and for drug molecules to diffuse out the newly porous membrane.

## 5.2 Materials and Methods

### 5.2.1 Materials

Polycaprolactone, polyvinylpyrrolidone, thiamine HCl, polysorbate 20, glycerol and N, N–dimethylacetamide were used. See Section 3.2.1 and 4.2.1 for additional details.

### 5.2.2 Methods

#### *5.2.2.1 Ink preparation*

PCL, PVP and DMAC components were weighed and placed into glass vials. Solutions were heated (60 °C) and stirred with a magnetic stirrer until all components were dissolved.

For the impermeable shell and core formulation preparation, see Sections 4.2.2.2 and 3.2.2.2 respectively

#### *5.2.2.2 Ink characterisation*

Surface tension was measured with a Krüss Drop Shape Analyser (DSA100).

Viscosity was measured with Malvern Instruments Kinexus Pro Research Rheometer. Measurements were taken at 28 °C and 60 °C.

Density was measured by calculating the ratio between the mass measured and volume of ink syringed into a glass vial.

See Sections 3.2.2.3, 3.2.2.4 and 3.2.2.5 for exact experimental procedures.

#### *5.2.2.3 Printing*

Printing was done with the Fujifilm Dimatix Materials Printer DMP-2850. See Section 3.2.2.6 for further experimental details.

#### *5.2.2.4 Investigation and highlighting phase separation*

##### 5.2.2.4.1 Raman mapping

Raman mapping was done with a Horiba Jobin Yvon LabRAM HR Raman spectrometer. The method was similar to what was done in Section 3.2.2.15 with some differences.

Raman microscopy was done with a 50 µm confocal hole and a 300 lines $mm^{-1}$ grating. Individual components of the formulation and mapping (100 x 100 µm, in 1 µm steps, 10,201 total spectra) were acquired with a spectrum over the range of 400 – 1800 $cm^{-1}$, with an acquisition time of 2.5 seconds and 2 accumulations. Total map time was 16 hours. Spectral resolution was 1.6 $cm^{-1}$. ViewSharp™ and AutoFocus were used to correct for topography.

Raman experimental and data processing in this section was conducted by Dr. Graham Rance (University of Nottingham).

##### 5.2.2.4.2 Time-of-flight secondary ion mass spectrometry

ToF-SIMS was conducted with a ToF-SIMS IV instrument (ION-TOF GmbH). ToF-SIMS was conducted on reservoir samples and a cross-section of the release controlling membrane.

Map sizes of 2 x 2 mm (500 x 500 pixels, 1 scan), 500 x 500 µm (256 x 256 pixels, 30 scans) and 50 x 50 µm (256 x 256 pixels, 30 scans) were generated. For drop and line maps, a 150 x 150 µm map (256 x 256 pixels, 35 scans) and a 3 x 0.4 mm map (480 x 60 pixels, 1 scan) were generated respectively.

PCL was mapped (in green) using the $C_6H_{11}O_3^-$ fragment (u = 131) [152] and PVP was mapped (in blue) using the $CN^-$ fragment (u = 26) [153]. Pure PCL and PVP materials were analysed with these peaks identified.

To prepare cross-sectioned samples, samples were embedded in Araldite epoxy resin. Samples were cut using a glass blade with a microtome (PowerTome RMC).

Additional experimental details can be found in Section 3.2.2.9.

ToF-SIMS experimental work was done by Dr. David Scurr and Dr. Long Jiang (University of Nottingham). Samples were microtomed by Dr. Elisabeth Steer (University of Nottingham)

#### *5.2.2.5 Optical microscopy*

A Nikon Eclipse LV100ND Optical Microscope was used to analyse the printed materials.

#### *5.2.2.6 Micro computed tomography scanning*

Micro computed tomography (CT) scanning was conducted with a Skyscan 1174 Micro CT. Samples were placed in an Eppendorph$^{TM}$ centrifuge tube as a sample holder during scanning. Voltage and current were set to 50 kV and 800 µA respectively. A scanning resolution of 12.2 µm with 0.4° rotating step were used. An averaging frame of 6 was used. The transmission images generated from the scans were reconstructed using NRecon software.

Scanning and reconstruction was done with assistance from Dr. Jane McLaren (University of Nottingham).

#### *5.2.2.7 Layer thickness*

A certain number of layers were printed and measured with a micrometer. The thickness of individual layers was calculated by dividing the thickness of the printed structure by the number of printed layers.

#### *5.2.2.8 Dissolution testing*

Dissolution testing was conducted with a Copley dissolution tester (DIS 8000). 200 mL of deionised water was used as the dissolution media. Additional experimental information can be found in Section 3.2.2.17.

#### *5.2.2.9 Pore size analysis*

Scanning electron microscopy (SEM) was conducted with a Hitachi TM3030 (see Section 4.2.2.9 for additional experimental details.)

SEM images with a 100 X magnification to loaded to ImageJ software. An appropriate scale was set, and a threshold limit was applied. Despeckling was done to remove noise particles. Pore area was then measured on individual particles by using the 'analyse particles' function.

## 5.3 Results and Discussion

### 5.3.1 Ink formulation and printing parameters

To help ensure the resultant morphology would result in PVP domains dispersed in a PCL matrix, an ink with a higher loading of PCL than PVP was formulated. The starting composition of the ink is presented in Table 5.1.

*Table 5.1 - Formulation of the release controlling membrane.*

| Component | Content (wt %) |
|---|---|
| PCL | 10.5 |
| PVP | 6.4 |
| DMAC | 83.1 |

As in previous chapters, ink properties were measured and presented in Table 5.2. Surface tension (at ambient temperature, 23 °C) and viscosity (at 28 °C) were in the acceptable limits for the Dimatix printer resulting in an appropriate Z printability factor.

*Table 5.2 - Ink properties of the release controlling membrane.*

| | |
|---|---|
| **Surface tension ($mN \cdot m^{-1}$)** | 36.54 ± 0.30 |
| **Viscosity (mPa·s)** | 10.407 ± 0.038 |
| **Density ($g \cdot mL^{-1}$)** | 1.1 ± 0.02 |
| **Nozzle diameter (µm)** | 21 |
| **Z factor** | 4.8 |

Similar to the impermeable formulation (see Section 4.3.2.1), printing the PCL-PVP ink was initially done with the standard Dimatix settings but film formation at lower temperatures resulted in poor morphologies, cracking and delaminating films (e.g.

Figure 5.1). Therefore, the ink would be printed while the substrate heated to 60 °C. Even though the PCL phase appeared to be molten after printing, the PVP component seemed to hold the molten material in place. This made it easier to print additional layers (islands of material were not seen). No ink spreading was observed, even with a larger number of layers (100 layers).

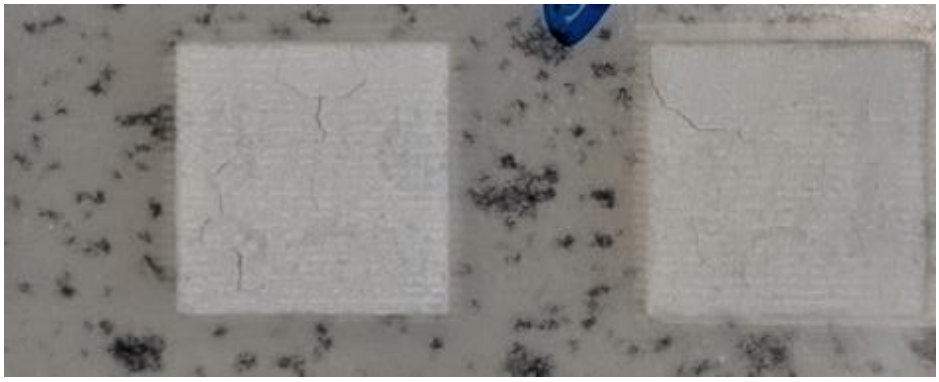


*Figure 5.1 – Films of PCL-PVP ink printed on PET at 40 °C with cracking.*

To prevent heat transfer from the substrate to the nozzles, jetting temperature was set to the same temperature of 60 °C. Initially, there was no need to edit the waveform for this formulation when jetting at higher temperatures due to the higher viscosity compared to the PCL only ink, therefore the standard waveform was used (see Figure 3.7). Similar to the impermeable formulation, the jetting parameters was occasionally adjusted to ensure spherical drops with limited tailing and no satellite drops would be jetted. Viscosity measurements were repeated at 60 °C, resulting in a viscosity of 5.918 ± 0.188 mPa·s (within the acceptable viscosity range for the Dimatix printer).

Different parameters such as PVP loading and drop spacing were not investigated at this point, but their influence on drug release is discussed in later sections.

### 5.3.2 Initial characterisation of the release controlling membrane

To gain an initial understanding of the printed morphologies of the release controlling membrane, Raman and ToF-SIMS mapping was conducted on the reservoir system with an emphasis on its PCL-PVP components.

Figure 5.2 shows an image of the top surface of a reservoir system generated through Raman mapping. As expected, regions of PVP are dispersed in a PCL continuous matrix. The tablet was then exposed to water for one hour. Analysis of the same region

showed the PVP regions no longer being present. PCL remains and appears unchanged. CLS scores for PVP decreased from 28.4 ± 32.0 % to 1.0 ± 4.4 %. This supports the theory that PVP would act as a pore forming agent in the release controlling membrane.

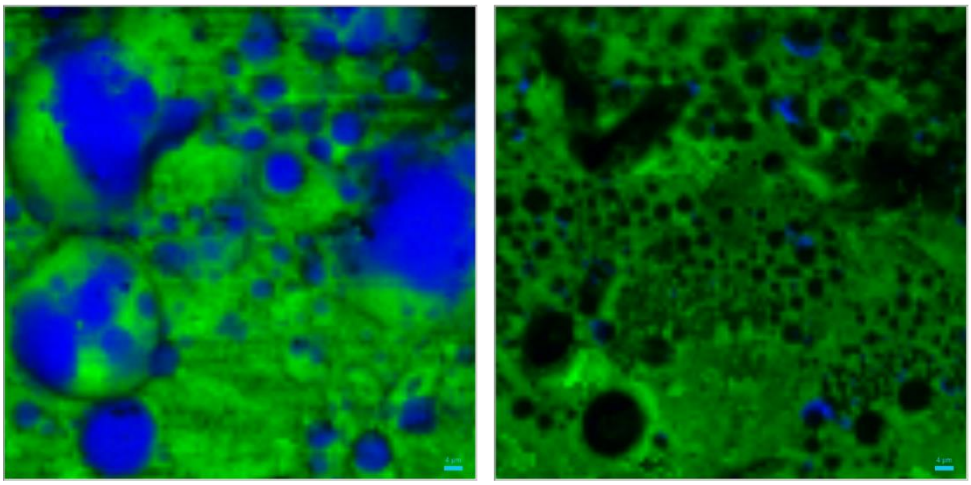


*Figure 5.2 - Raman image mapping of the top surface of a reservoir device. Regions of PVP (blue) are seen as individual domains in a continuous phase of PCL (green) (left). After the device was exposed to water for 1 hour (right), the same region was mapped. Nearly all indication of PVP was removed, suggesting PVP would act as a pore-forming agent in the printed reservoir systems. Scale bar = 4 µm.*

To gain a further understanding of the resultant porous nature of the film, a PCL-PVP film was cross-sectioned. As Figure 5.3 shows, regions of PVP appeared to be embedded in the PCL matrix, similar to what was seen with Raman mapping. It does not appear that a direct path of PVP through the PCL membrane exists. This suggests that a highly tortuous network of pores form after exposure to water [20].

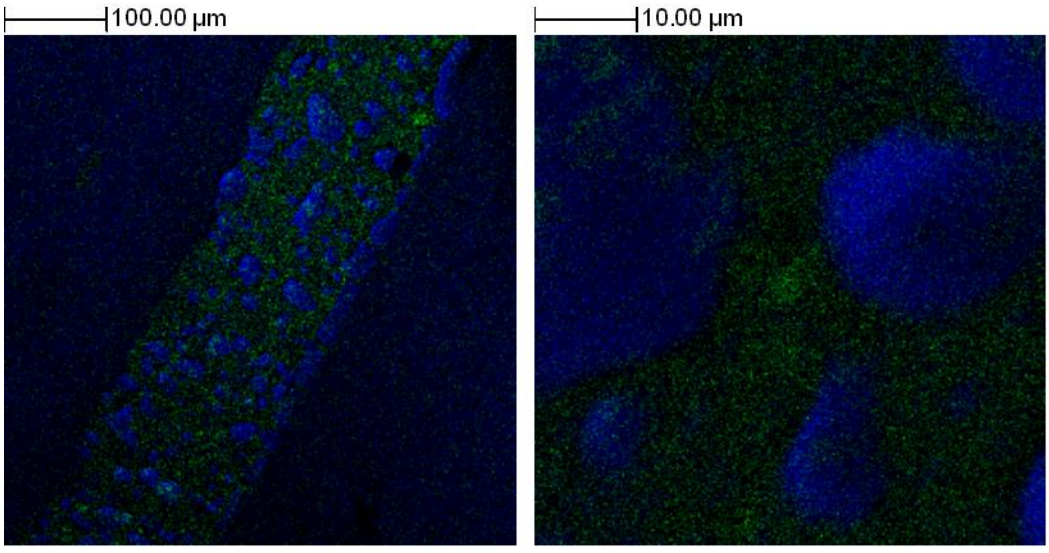



*Figure 5.3 - ToF-SIMS map of a PCL (green) – PVP (blue) film's cross section.*

An interesting phenomenon was observed with the ToF-SIMS maps of individual drops and lines of the PCL-PVP formulation (Figure 5.4). For an individual drop, PVP rich regions tended to form at the edge of the drop while PCL is richer in the centre and appears to be crystallise outwards, illustrated by the dendritic structure that formed. Similar behaviour was seen in a single line of the formulation, where the edge of the line was richer in PVP than anywhere else. A possible reason for this could be attributed to the so-called 'coffee-ring' effect [154]. It was thought that as PCL is described as only partially soluble in the DMAC solvent [129], it comes out of solution faster than the dissolved PVP. As the coffee ring effect progresses, DMAC and the still-in-solution PVP moves to the edge of the drop where the remaining DMAC begins to evaporate. It is here that PVP rich regions form. The dendritic structure that was seen may be a result of PCL crystallisation from melt [155].

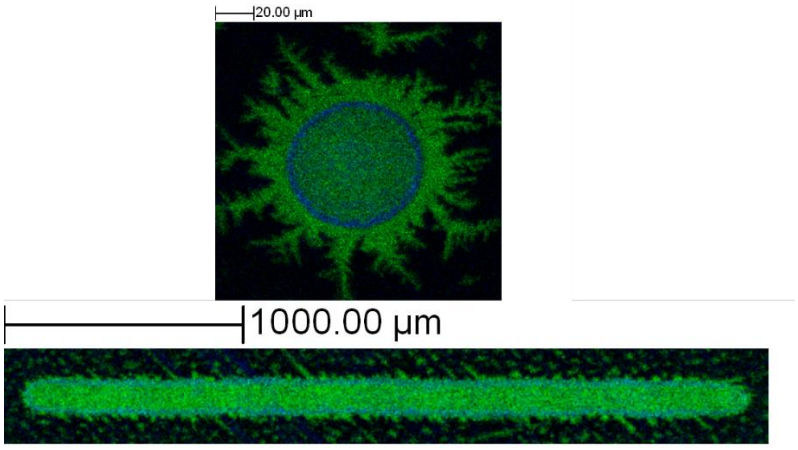



*Figure 5.4 – ToF-SIMS drop and line of the PCL (green) – PVP (blue) formulation printed on PET substrate.*

### 5.3.3 Testing the functionality of the release controlling membrane

To fully illustrate the functionality of the release controlling membrane, a reservoir system with 25 layers of the release controlling membrane was printed. The same manufacturing process summarised in Figure 4.19 was used, with the exception of the final step where 25 layers of the PCL -PVP ink was printed (Figure 5.5). All reservoir systems would have a theoretical drug dose of 4 mg.

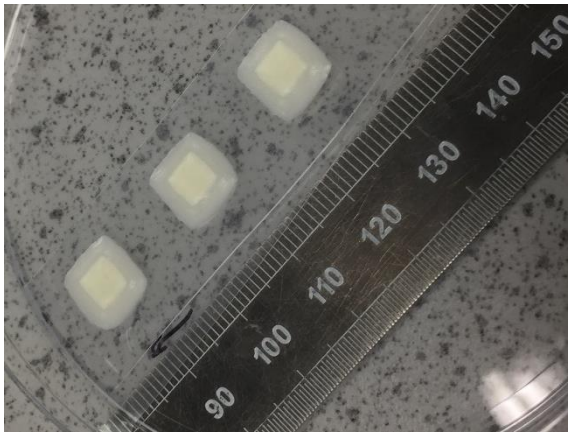



*Figure 5.5 - Completed reservoir system tablets*

Figure 5.6 shows the top and bottom surface of the tablets before dissolution testing. On the top surface no cracks or other types of flaws were observed, suggesting a uniform jetting and film formation of the PCL-PVP release controlling membrane. On the base of one of the tablets, some scratches were observed. It was not clear how deep these scratches penetrated the reservoir system. The extent of this flaw and its effect on dissolution, at this point, was not known.

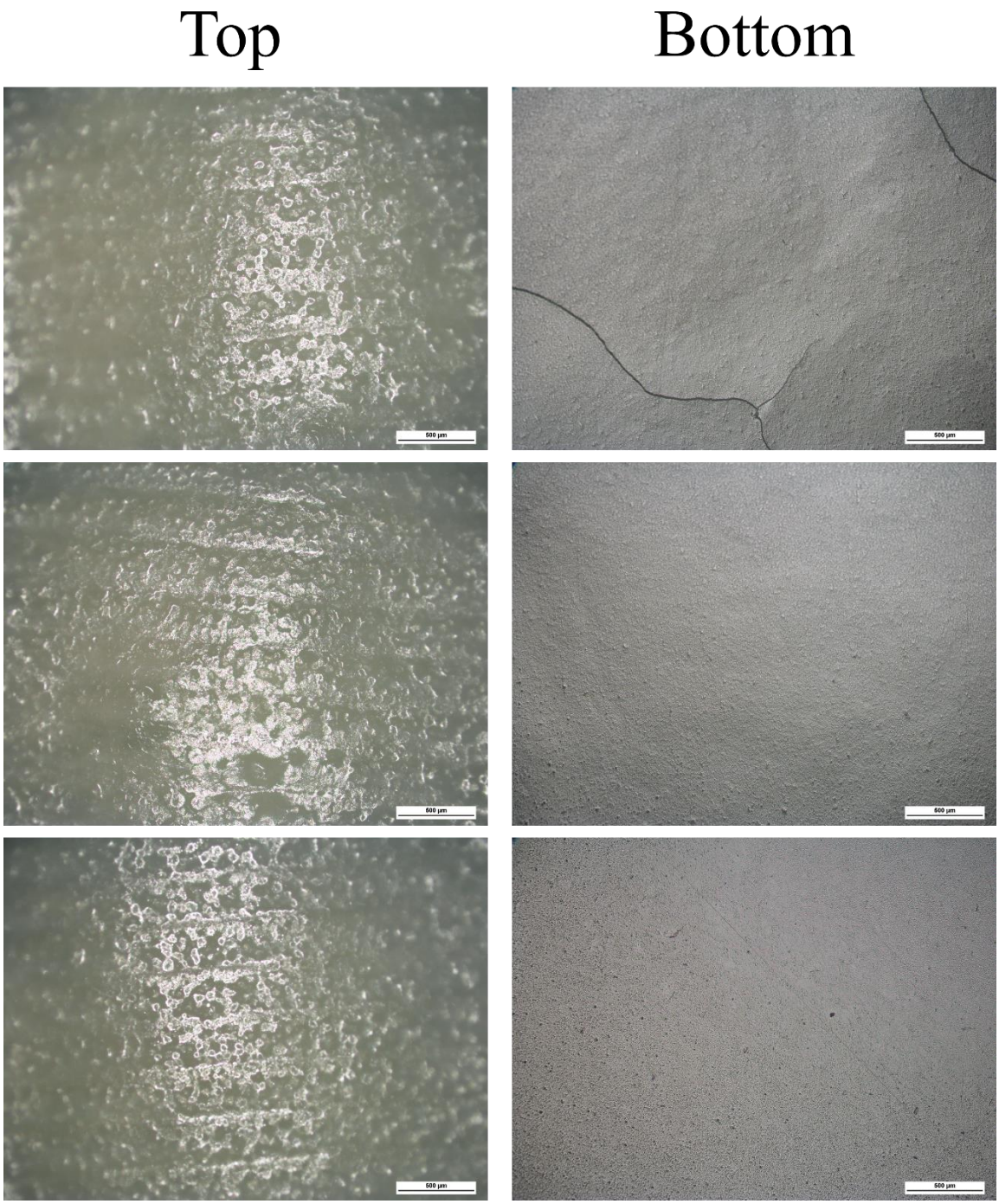



*Figure 5.6 - Optical microscope images of the tablets (25 L release controlling membrane). The top and bottom surfaces of the tablets were inspected for flaws. Scale bar = 500 µm.*

Figure 5.7 illustrates the drug release profile of the tested reservoir systems. Drug release appeared to steadily occur for approximately 1 hour, after which release slows down and plateaus. 100 % drug release was not achieved (this is further discussed in Section 5.3.5.1), but it appeared that no more additional drug would be released. The small variation between the samples suggested that the release controlling membrane

worked effectively, introducing a degree of control for the reservoir system. It was also concluded that the scratches observed before dissolution on the base of one of the tablets did not have a significant effect on drug release due to the consistency of the release profile.

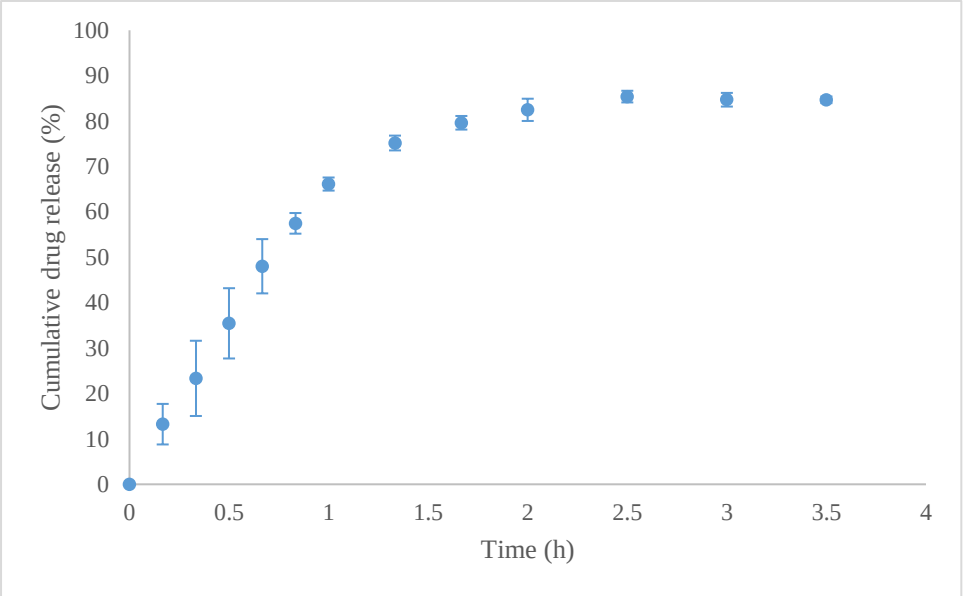



*Figure 5.7 - Release profile of a reservoir system with a 25 layer release controlling membrane (n=3).*

Analysis of the tablets after dissolution was also conducted (Figure 5.8). On the top surface, only one of the tablets had a clear indication of fracture (Figure 5.9). It was thought that this fracture may have been caused after drug release had occurred, as the apparent loss of the internal core had made the structural integrity of the tablet weaker. Damage may have occurred during handling and storage after dissolution. The fact that no damage was observed on the other tablets and all tablets had similar release behaviour, further supports the claim that the damage did not have a significant effect on drug release. Examination of the bottom surfaces also showed no significant mass loss, although similar scratch features to what was observed before dissolution was seen again.

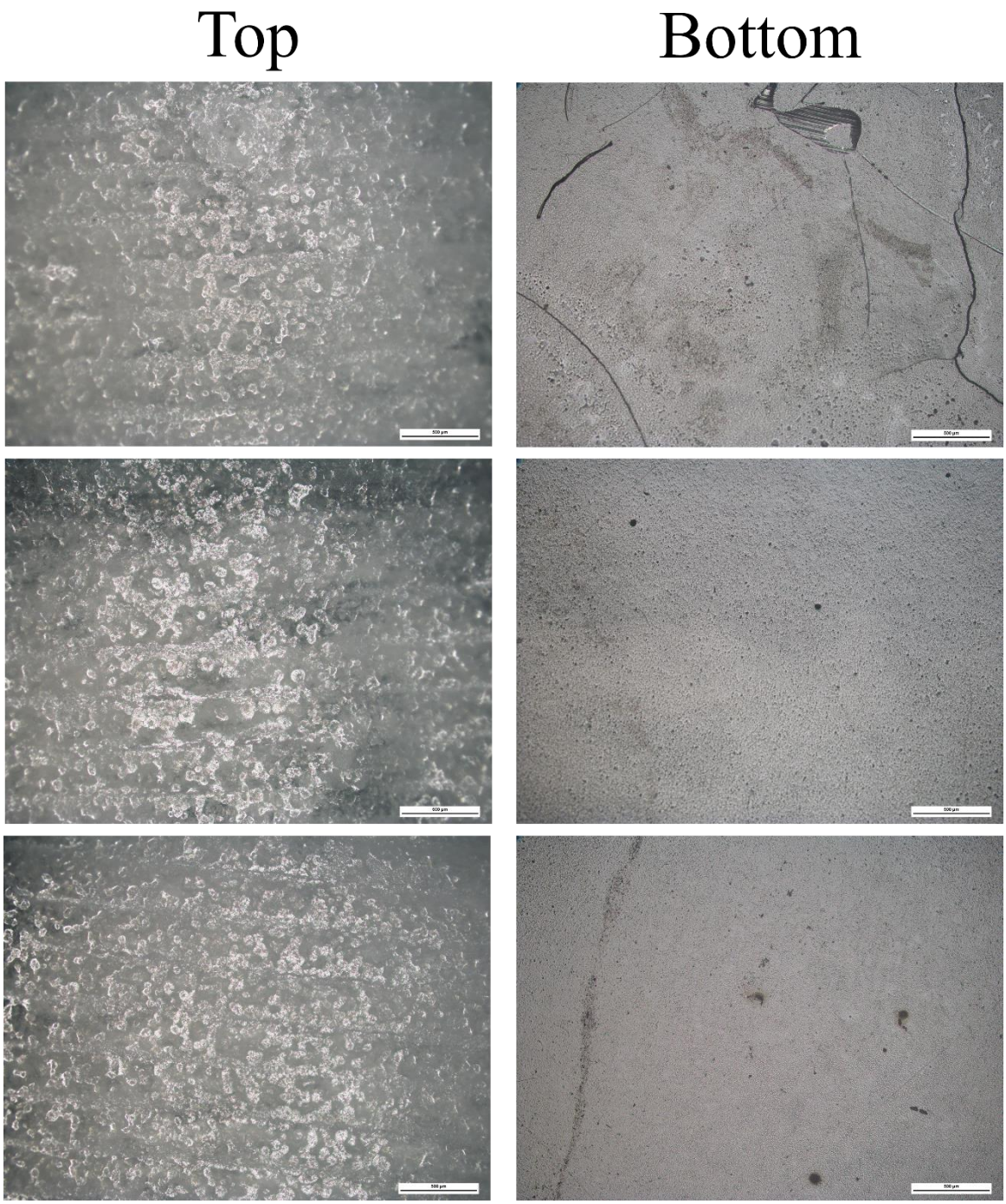



*Figure 5.8 - Top and bottom surfaces (centre region) of tablets after dissolution. Scale bar = 500 µm.*

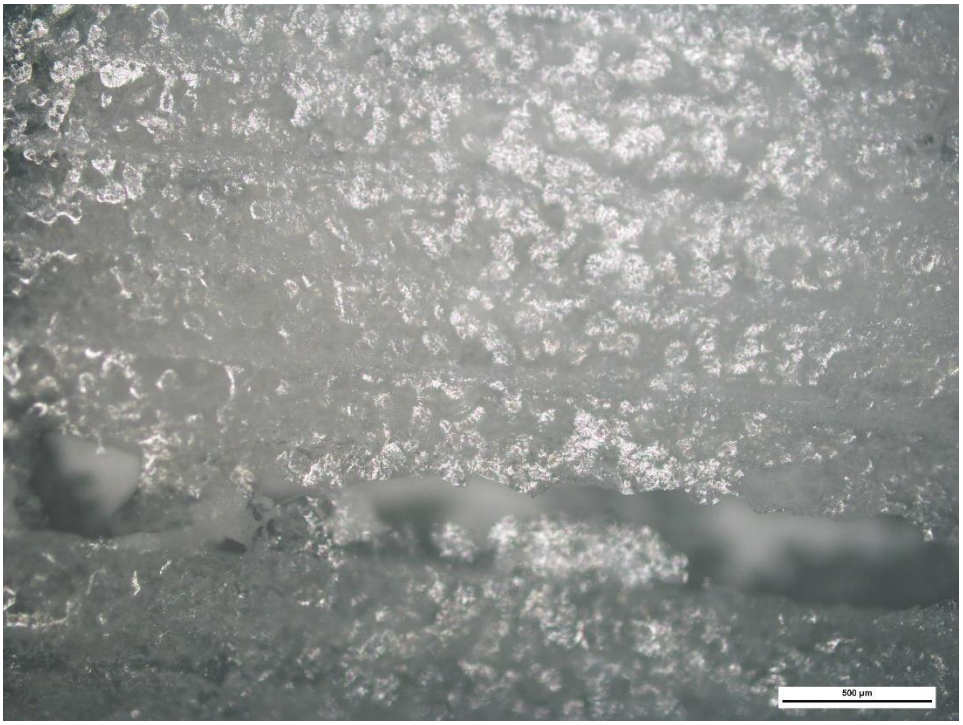



*Figure 5.9 - Possible fracture of the release controlling membrane (at the edge of the core region). Since no similar features were seen on the tablets tested, it was thought that it did not play a significant role in drug release. Damage may have been caused during handling of the tablet post-dissolution. Scale bar = 500 µm.*

To understand the drug release mechanism, different mathematical models were applied to the dissolution data. Depending on the fits calculated from these different kinetic models, it was possible to determine the likely release mechanism [156]. This is presented Table 5.3 with graphical illustrations in Figure S5.37.

Zero-order kinetics are often seen in drug release systems that do not break apart with a slow drug release. It is assumed that no change in area or equilibrium of conditions occurs. Zero-order kinetics are achieved when the same amount of drug is released in every unit of time [156]. Systems with a zero-order release kinetic are often described as having a constant activity source. This means the drug concentration in the system is greater than the solubility of the drug. When water penetrates into the core (in context of a reservoir system), not all the drug is dissolved due to a saturated drug solution being rapidly created in the core. The diffusion process through the membrane is assumed to be significantly slower than the dissolution of drug from its polymer matrix. The drug molecules that have diffused across the membrane are then rapidly replaced by the partial dissolution of drug remaining in the matrix core [21]. In contrast, first order kinetics describe drug release where release is proportional to the amount of drug in the dosage form. The amount of drug that is released decreases with

time [156]. First order systems are described as having a non-constant activity source. With reference to a reservoir system, this means that when water penetrates the core, all drug molecules rapidly dissolved. The diffusion process that follows is much slower than drug dissolution. As there is no excess drug remaining in the core, drug molecules are not replaced, therefore the concentration of drug in the core decreases over time [21]. With the Higuchi model, drug release is described as a diffusion process, which follows Fick's first law and is dependent on the square root of time [156]. The Korsmeyer-Peppas model is used to determine whether drug release follows anomalous behaviour (i.e. non-Fickian or Fickian diffusion) [157]. The model is often used when more than one type of release mechanism is potentially involved [156].

*Table 5.3 - Correlation values of the different kinetic models applied to dissolution data (the first 60% of drug release) of the 25 layer reservoir system.*

| **Mathematical fit** | Zero-order | First-order | Higuchi | Korsmeyer-Peppas |
|---|---|---|---|---|
| **$R^2$** | 0.9983 | 0.9797 | 0.9235 | 0.9970 |

The highest correlation was the zero-order fit, but it should be noted that there is also a high correlation for the Korsmeyer-Peppas model. The release exponent calculated (which is the gradient of the line shown in Figure S5.37) was 0.93. This value (which is used to characterise different release mechanisms) suggests that a non-Fickian process, approaching Case II transport (a time independent zero-order release), occurs [158]. This means that drug release was strongly influenced by polymer relaxation and dissolution [159]. Based on these models, we can further elucidate the drug release behaviour. First, water dissolved the PVP in the release controlling membrane and moved towards the core. As the PVP-thiamine HCl core's surface was wetted, the polymer hydrated to form a gel layer, transitioning from a glassy (or solid) state to a rubbery state. As the drug is highly soluble, the drug on the surface passed into the surrounding solution (still within the reservoir system). With time, the gel layer grows due to the fluid penetrating the dosage's core. Eventually, the outer layer is fully hydrated leading to polymer chain relaxation causing the weakening of the gel layer. The continued fluid penetration leads to complete dissolution of the core [160]. As zero order release has been suggested to have occurred, the initial dissolved drug molecules have likely saturated the solution within the device. These drug molecules

then diffuse through the membrane into the dissolution medium into sink conditions. Only then do additional thiamine HCl molecules dissolve from the PVP, which then diffuse through the membrane again. This leads to the same amount of drug to be released at each unit of time (i.e. zero-order release).

Zero-order release is often the preferred kinetic behaviour for drug delivery. This is because it can compensate for drug removal out of a patient, allowing for constant drug concentrations at the intended therapeutic site [161].

### 5.3.4 Controlling drug release behaviour

As it has been proved that the reservoir system designed and manufactured has the ability to deliver its dose consistently, the effect of different printing and ink parameters were investigated.

#### *5.3.4.1 Varying the number of printed layers*

The simplest way to control drug release of the reservoir system is to vary the thickness of the release controlling membrane. This was achieved by printed additional layers of the PCL-PVP ink. Figure 5.10 shows the release profiles of three batches of tablets with a different number of printed layers for the release controlling membrane (25, 50 and 100). Through printing an additional 25 layers, it was possible to extend drug release – increasing drug release duration from two hours to seven hours. This is likely the result of a greater distance required for the water to move through the membrane and for the drug molecules to diffuse out. With 100 total layers printed, a delay is introduced, suggesting even greater time was required for water ingression and drug diffusion. Most importantly, a pathway for drug diffusion must form before diffusion can begin, highlighted by the delay.

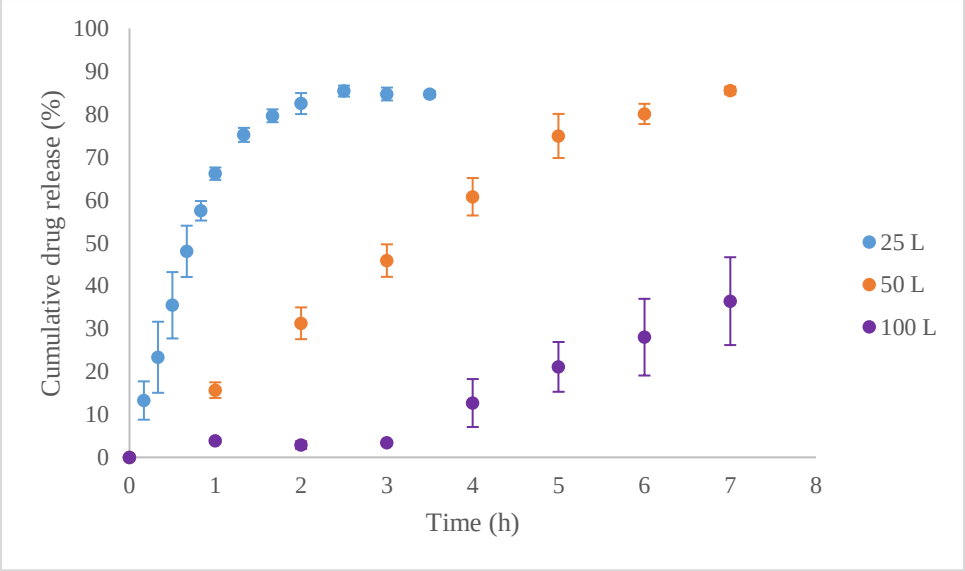



*Figure 5.10 - Release profiles of reservoir systems with different number of printed layers for the release controlling membrane. (n=3)*

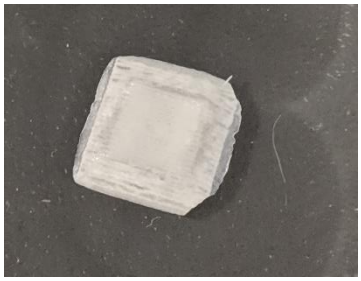


*Figure 5.11 - 100 layer reservoir system after dissolution.*

It should be noted that the tablets presented in Figure 5.10 were all made in the same print batch (i.e. these prints should be identical with the exception of the release controlling membrane component). It was thought that as tablets with a 50 layer release controlling membrane reach a similar drug release level after seven hours, compared to a 25 layer release controlling membrane at three hours, all available drug in the system that could be released had been released (even though approximately 85 % of drug had been calculated to have been released). To investigate this claim, CT scanning of tablets before and after dissolution were conducted. As Figure 5.12 shows, before dissolution the PVP-thiamine HCl core can be clearly seen (bright region in Figure 5.12). A tablet with a 50 layer release controlling membrane was examined after dissolution as well. In contrast, the bright region was replaced by what appeared to be a void region. This suggested that the entire PVP-thiamine HCl core dissolves over time during dissolution. The final reading of 85 % drug release may be due to the

inaccuracy of the theoretical dose or that some drug is trapped in the tablet reservoir (this is further discussed in Section 5.3.5.1).

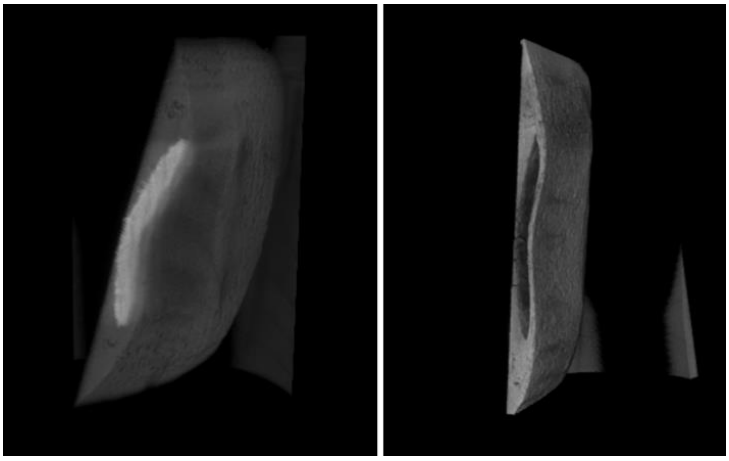
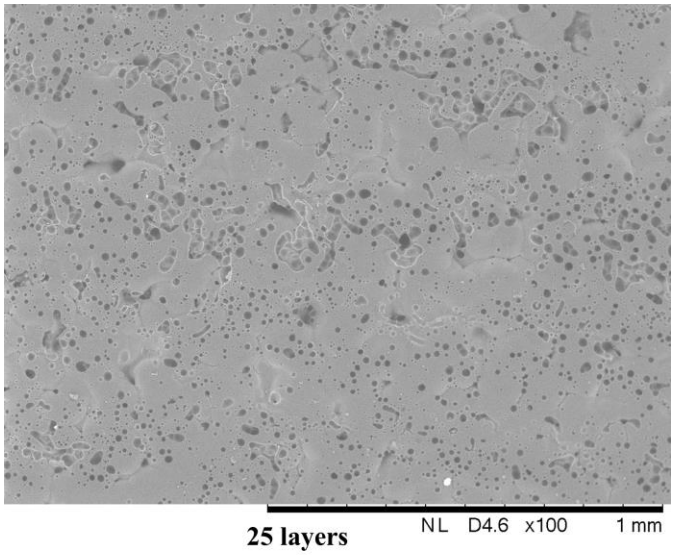
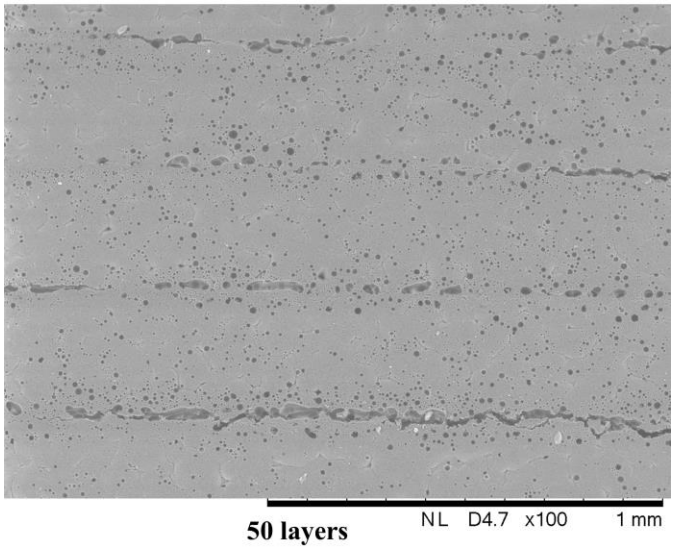


*Figure 5.12 - CT scan of a reservoir system before dissolution (left) and after dissolution (right). Before dissolution the PVP-thiamine HCl core was distinctively seen, in contrast to the sample after dissolution where a void space was observed.*

Based on the SEM images of the reservoir systems after dissolution (Figure 5.13), there appeared to be a trend where, as the number of printed layers increased, the size of pores decreased. Pores also appeared to separate into specific regions of the print tracks. This may be where the print tracks overlapped during the printing process. PVP tended to agglomerate near the edge of print tracks (see Figure 5.4). It was possible to measure the size (area) of pores present in the system using the SEM images and ImageJ software. Mean and median pore areas decreased from 21 $\mu m^2$ and 83 $\mu m^2$ respectively (25 layers) to 7 $\mu m^2$ and 24 $\mu m^2$ respectively (100 layers). Total pore area (sum of all pores measured) also decreased from $3.27 \times 10^5$ $\mu m^2$ (25 layers) to $1.15 \times 10^5$ $\mu m^2$ (100 layers). Additional details are presented in Table S5.7.



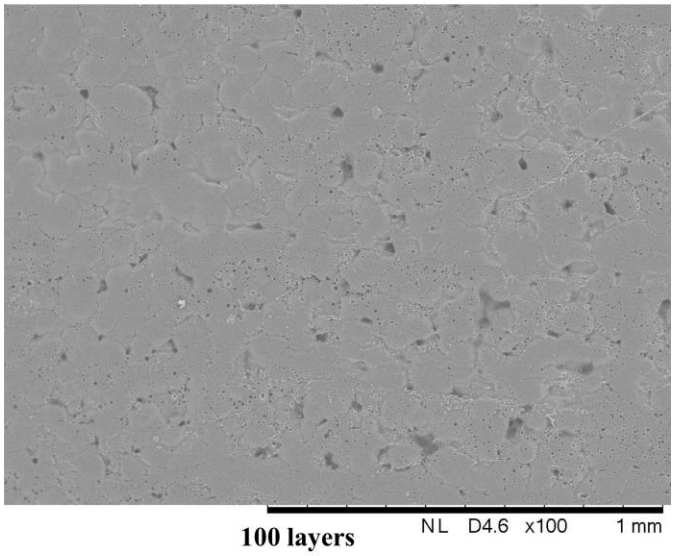




*Figure 5.13 - SEM images of the top surface of the reservoir system. As the number of printed layers increased, the size of pores appeared to decrease.*

Changes in pore size may have been caused by the partial re-dissolving of material, a result of jetting subsequent ink. This however would require further experimentation to confirm. It should be noted that only the surface pores have been analysed. Investigating if there had been any change in the PVP distribution or size of domains within the release controlling membrane's internal structure would allow for a more complete understanding of drug release.

### *5.3.4.2 Varying PVP loading*

The effect of PVP loading in the release controlling membrane was investigated. A new ink was formulated with a greater PVP content, resulting in 43 wt% PVP in the release controlling membrane. New reservoir systems were printed with 100 layers of the new ink. Figure 5.14 shows the release profile of the higher PVP loading reservoir systems compared to reservoir systems with 100 layers of 38 wt% PVP loading. With a higher PVP loading, drug release occurred significantly faster with a plateau being reached at approximately hour four, in contrast to 38 wt% PVP where drug release just appears to begin at hour four. It was assumed that the layer thickness for both inks were similar (similar solid loadings of polymers were used - see Table S5.5).

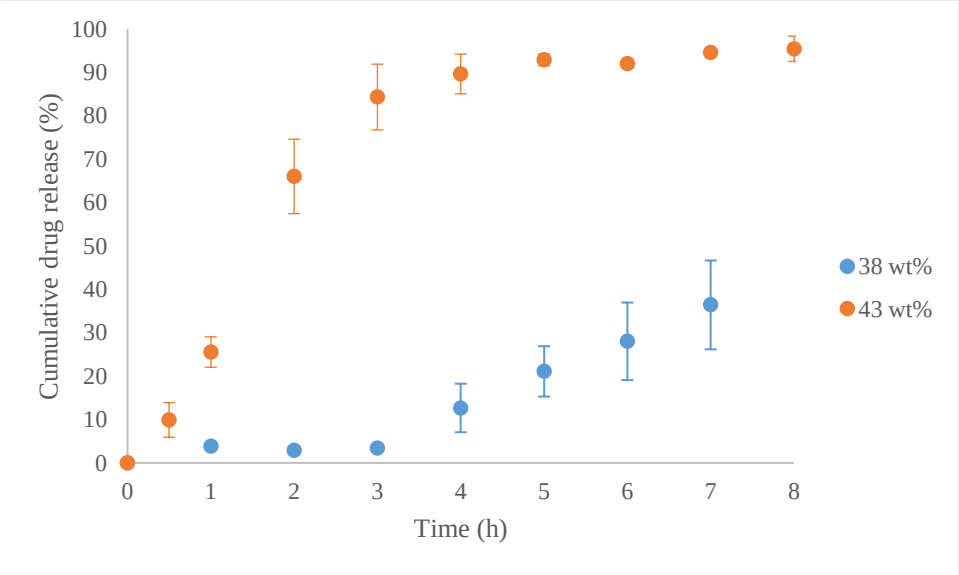



*Figure 5.14 - Release profile of reservoir systems with different PVP loadings in the release controlling membrane. (n = 3 for 38 wt% and n = 2 for 43 wt%)*

Examination of one of the samples after dissolution showed the presence of a large crack on the top surface (Figure 5.15). Analysis on the second sample was not possible as it broke during handling after dissolution. It was therefore not conclusive if the

crack played a role in drug release. It would be possible, since the entire core dissolved (see Section 5.3.4.1), the entire reservoir system's structural integrity would have weakened. The meant that the crack may have formed after all drug had been released or during handling.

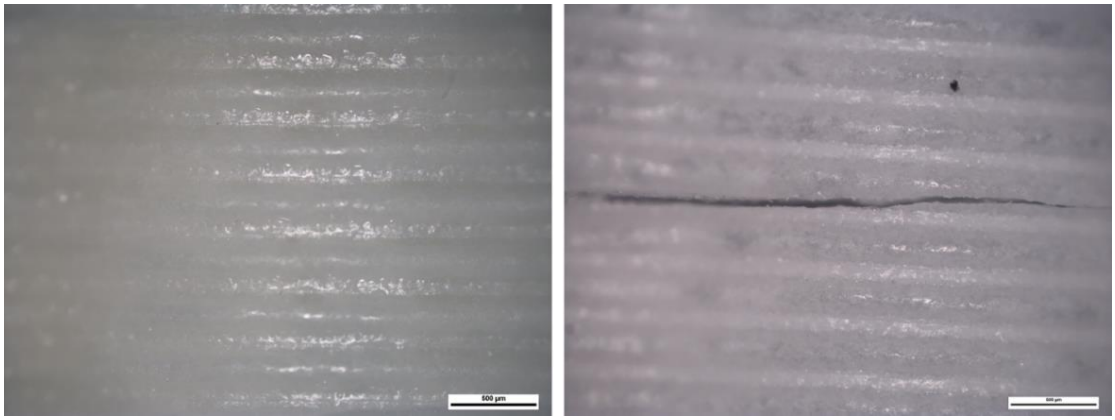


*Figure 5.15 – Optical microscope images of one of the reservoir tablets tested before (left) and after (right) dissolution. Scale bar = 500 µm.*

Comparison of SEM images (Figure 5.16) to 38 wt% samples, suggested that with higher PVP loadings, pore size increases significantly. Mean, median and total pore area increased from 7 $\mu m^2$, 24 $\mu m^2$ and 1.15 x $10^5$ $\mu m^2$ (38 wt%) respectively to 17 $\mu m^2$, 77 $\mu m^2$ and 1.68 x $10^5$ $\mu m^2$ (43 wt%) respectively (the sample presented in Figure 5.16 was not used for the actual image analysis, see Figure S5.39 for the used image).

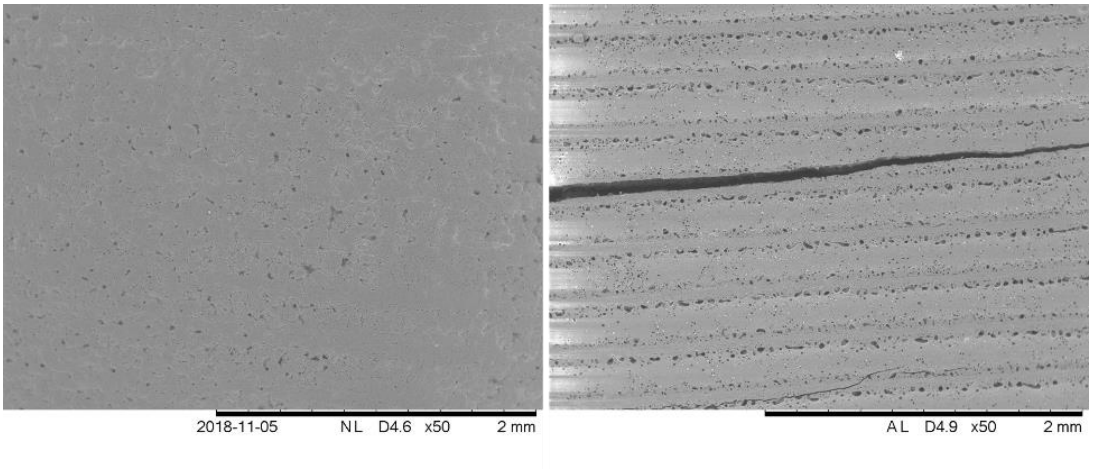



*Figure 5.16 - SEM images of the release controlling membrane of reservoir systems with 100 layers and a 38 wt% (left) and 43 wt% (right) PVP loading. A large crack was observed with the 43 wt% membrane.*

ToF-SIMS was able to highlight again the reason for the increased rate of release with a higher PVP loading. As Figure 5.17 shows, a reservoir system with a higher loading of PVP resulted in larger regions of PVP forming. The increased pore size (area

determined with SEM imaging) after PVP dissolved potentially allowed easier access for water to move through the membrane and into the core of device. The growth in size of PVP domains was expected as it is a common occurrence in polymer blends when the loading of one of components increases.

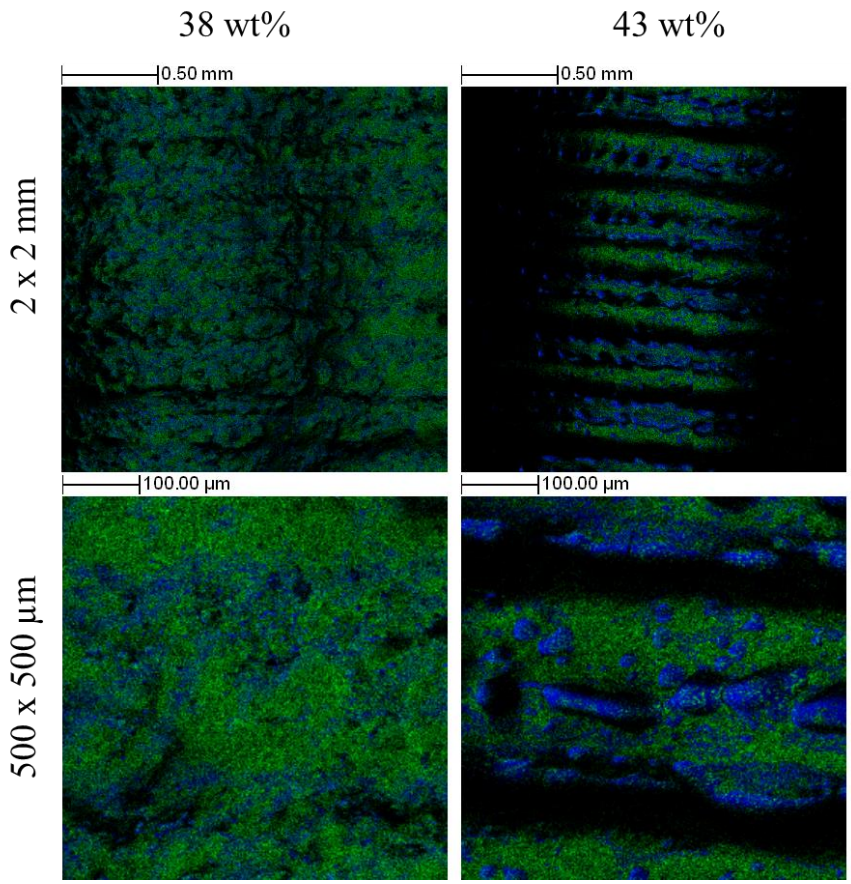



*Figure 5.17 - ToF-SIMS maps of the top surface of reservoir systems that did not undergo dissolution. With a higher PVP loading, the PVP domains appear to be larger, which would account for the faster drug release observed. PCL is mapped in green and PVP is mapped in blue.*

### *5.3.4.3 Varying drop spacing*

Drop spacing refers to the distance between each droplet in a pattern. The smaller the drop spacing, the greater the overlap. This also means a greater number of droplets are required to complete a pattern. This could potentially change the thickness of individual layers. An example is illustrated in Figure 5.18 where the number of drops and their overlap increases as drop spacing decreases.




*Figure 5.18 - Illustration of the effect of varying the drop spacing has on drop overlap and the number of drops required to complete a single layer of an 8 x 8 mm square pattern.*

The effect of drop spacing of the release controlling membrane on drug release was investigated. Figure 5.19 shows single layers of the PCL-PVP ink (38 wt% PVP) on a glass slide. With a lower drop spacing, more material and greater overlap of droplets occurred. This resulted in a greater number of PVP domains as well as a clear increase in size of the regions. The hypothesis was that as drop spacing increases drug release would be slower (due to the smaller pores). However, this was not the case.

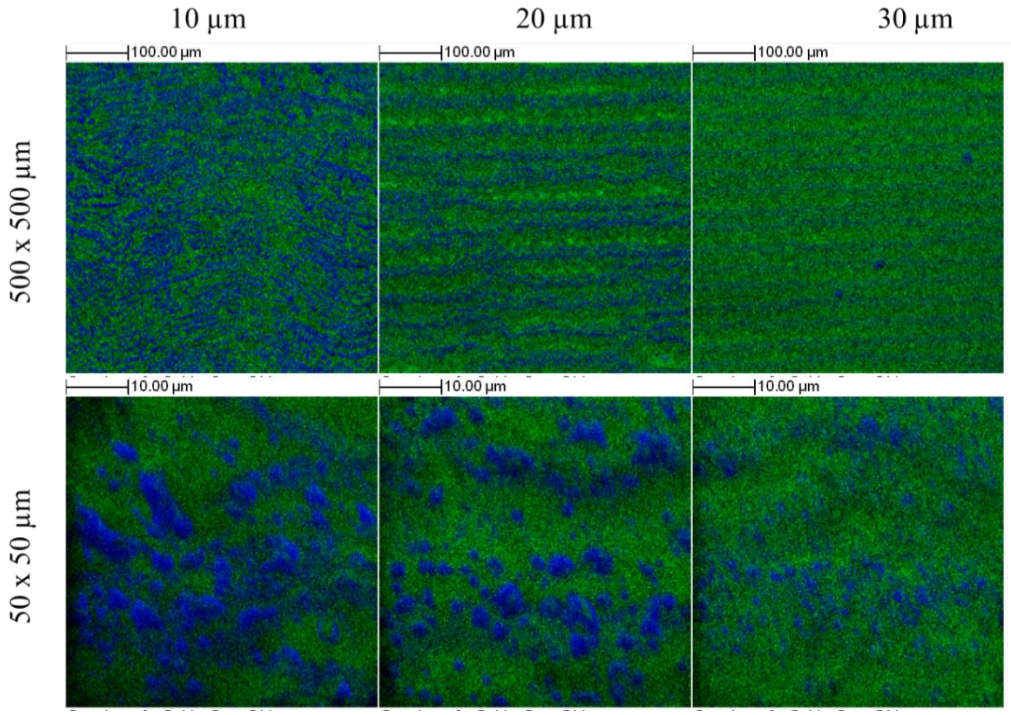



*Figure 5.19 - ToF-SIMS maps of single layer prints of the PCL-PVP ink on a glass slide. As drop spacing increases, PVP regions appear to be smaller in size. PCL is mapped in green and PVP is mapped in blue.*

Figure 5.20 shows the release profiles of 50 layer reservoir system tablets with its release controlling membrane printed with a 20 µm and 30 µm drop spacing. With a 30 µm drop spacing, release plateaus after four hours in contrast to the 20 µm drop spacing that presumably plateaus after hour seven (see Section 5.3.5.1). As Figure 5.21 shows, smaller pores are seen with a 30 µm membrane when compared to samples

with a 20 µm membrane. Mean, median and total pore area decreased from 47 $\mu m^2$, 18 $\mu m^2$ and 1.69 x $10^5$ $\mu m^2$ (20 µm) respectively to 23 $\mu m^2$, 9 $\mu m^2$ and 1.50 x $10^5$ $\mu m^2$ (30 µm) respectively. A potential reason for the different release profile was another variable that changing drop spacing introduces, which is layer thickness. Table 5.4 presents the mean values for layer thickness of the PCL-PVP ink. A lower drop spacing resulted in a thicker layer. This would be a result of the greater amount of material that is deposited onto the substrate. As the reservoir system printed with a 30 µm release controlling membrane resulted in a thinner structure, the distance water molecules had to move through the membrane and drug molecules to diffuse out was significantly shorter compared to the reservoir system with a thicker 20 µm drop spacing membrane (approximately 70 µm versus 120 µm). For the systems presented in Figure 5.20, it would appear that the thickness of the release controlling membrane played a greater role in influencing drug release than pore size.

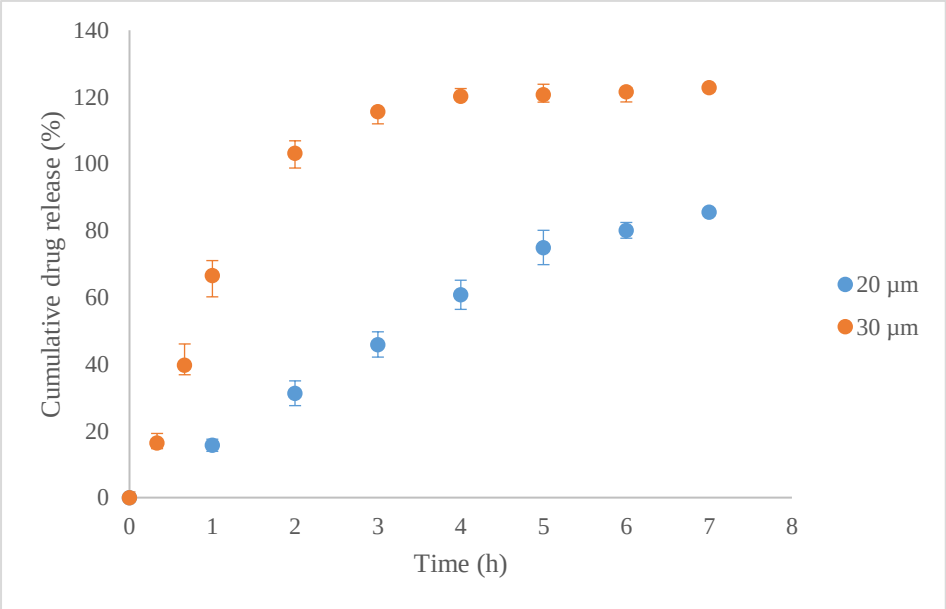



*Figure 5.20 - Drug release profiles of reservoir systems with 50 printed layers of the release controlling membrane, with varied drop spacing. (n=3)*

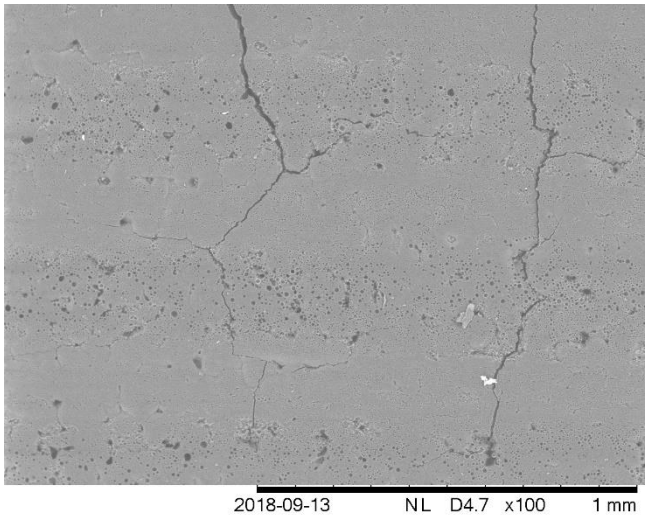



*Figure 5.21 - 50 layers of the release controlling membrane printed with a 30 µm drop spacing.*

*Table 5.4 - Average layer thickness of the PCL-PVP ink (38 wt% PVP). Films were printed on PET substrate and their layer thickness was calculated based on the number of layers printed (n =3).*

| Drop spacing | Thickness (µm) |
|---|---|
| 10 | 5.3 ± 0.58 |
| 20 | 2.4 ± 0.01 |
| 30 | 1.4 ± 0.02 |

Samples with different drop spacings but with comparable amounts of material deposited (i.e. the number of drops jetted) were compared. Figure 5.22 shows the release profile of reservoir systems with a 30 µm, 90 layer release controlling membrane. After a short delay (approximately 80 minutes) drug release appears to steadily occur over seven hours. Comparable samples were reservoir systems with a 10 µm, 10 layer release controlling membrane ($10 \times 3^2$). Extremely different release behaviour was observed for these samples with significant variation between individual samples and complete release occurring just after 40 minutes. The exact number of drops vary slightly as drop spacing can affect the resolution of the prints as well.

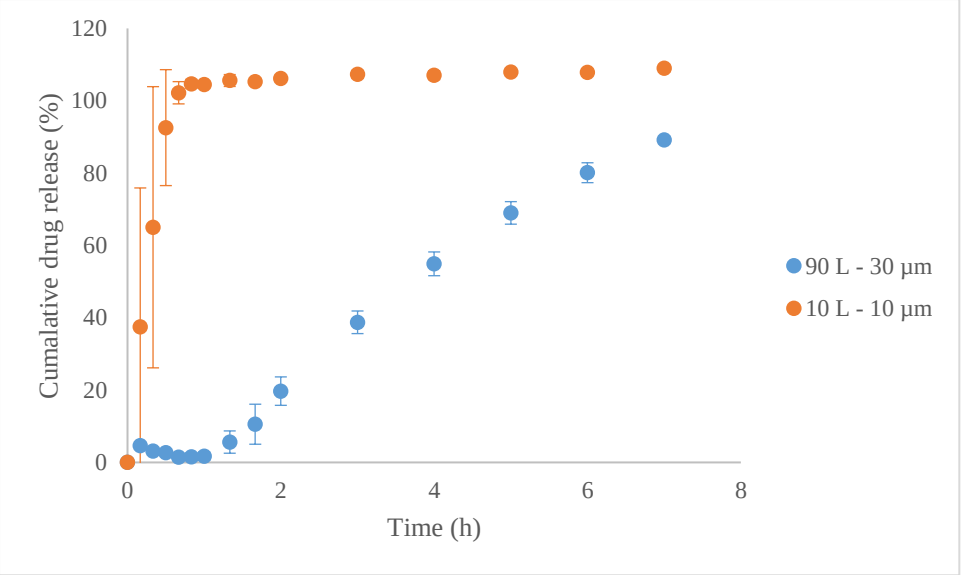



*Figure 5.22 - Release profiles of reservoir systems with a different number of layers and drop spacing. The amount of material and drop density were comparable. (n=3)*

Optical microscopy (Figure 5.23) and ToF-SIMS (Figure 5.24) allowed a better understanding of the release profiles seen in Figure 5.22. The 10 µm reservoir system had significantly larger areas of PVP domains. This would have been caused by the greater overlap of drops and amount of material present in the system. These large areas would account for the significantly more rapid and variable release observed. In contrast to the 30 µm reservoir system where PVP domains appear more uniform and homogenously dispersed across the surface on the release controlling membrane. This resulted in a more controlled and sustained release. The lag phase was probably a result the greater time required for a pathway to be created, caused by the smaller pore areas (similar to what was seen for samples with a 100 layer / 20 µm drop spacing membrane). Quantification of pore areas was not done for these samples due to the significant loss of material (loss of PVP) after dissolution of the 10 µm sample.

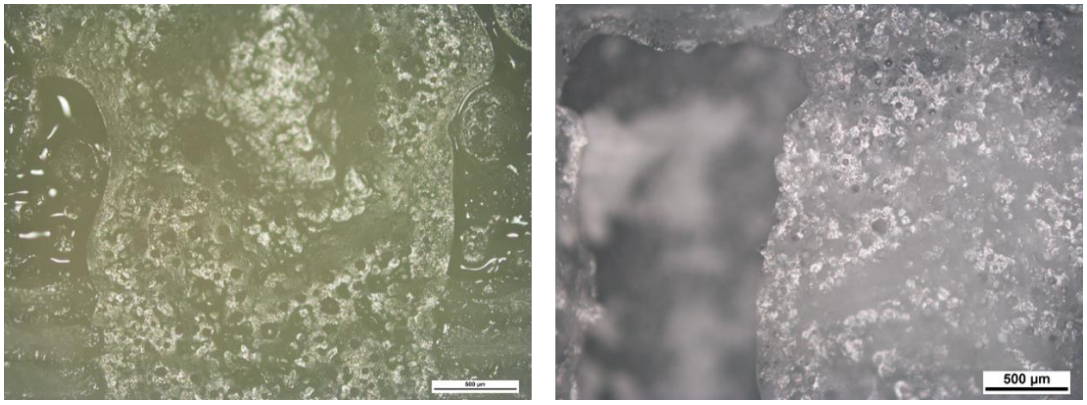



*Figure 5.23 - Optical microscope images of a 10 layer and 10 µm drop spacing reservoir system before (left) and after (right) dissolution.*

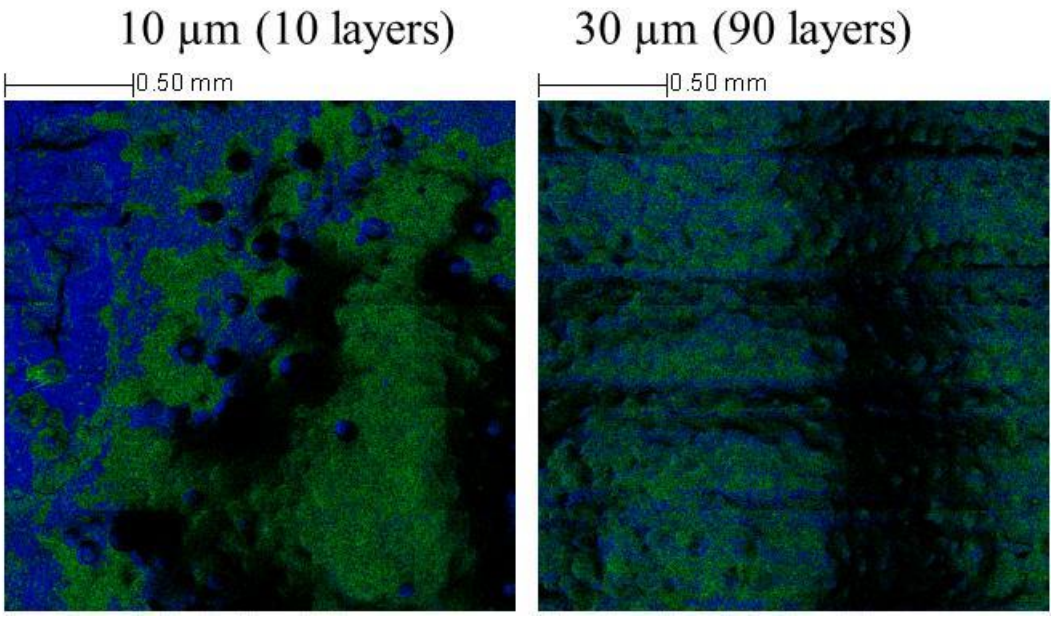



*Figure 5.24 - ToF-SIMS maps of a 10 layer, 10 µm drop spacing (left) and a 90 layer, 30 µm drop spacing (right) reservoir system. PCL is mapped in green and PVP is mapped in blue.*

The larger and seemingly non-homogenous distribution of PVP regions seen in the 10 µm sample may have been due to the drop spacing choice for the ink. Due to the large overlap and amount of material in addition to the molten PCL component of the ink, bulging or spreading of the ink may have had occurred. Visual examination of the tablets printed did suggest that the release controlling membrane component had not formed a very homogenous film in terms of a well-defined printed pattern (Figure 5.25), in comparison to other printed samples (e.g. Figure 5.5).

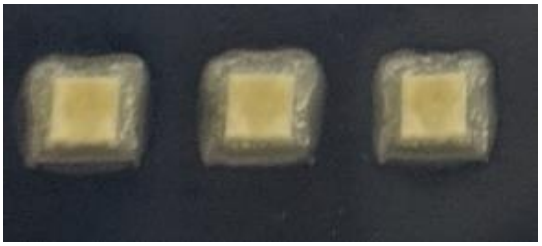


*Figure 5.25 - Reservoir system tablets with 10 layers, 10 µm and 38wt% PVP release controlling membrane.*

#### *5.3.4.4 Bimodal drug release*

Bimodal drug delivery devices are capable of producing release profiles where the release rates change over time (i.e. initial fast drug release followed by a slower release or the opposite) [162]. This can be advantageous as drug release rates can be made to vary as the delivery system moves through the body. For some diseases, increased drug release rates prevent more intense symptoms that can be caused by circadian rhythms (e.g. nocturnal asthma) [163]. For many drugs, absorption is slow in the stomach, fast in the proximal intestine and slow again in the distal segment of the intestine. For there to be a constant concentration of drug in the blood, a controlled delivery device must be able to compensate for the changes in absorption throughout the GI tract (e.g. increase drug release rate in parts of the tract where absorption is slow) [164]. The key aim of any bimodal drug delivery device would be to maintain the therapeutic drug level throughout its presence in the body [165].

To achieve a bimodal drug release profile, where an initial fast release transitions to a slower and sustained release, a multi-core reservoir system was printed. Here, two cores (total dose of 8 mg) were adjacent to each other with one core printed with a 25 layer release controlling membrane and a second core with an additional 75 layers (total 100 layers) printed. A cross-sectional schematic is presented in Figure 5.26 and the actual print is shown in Figure 5.27.



*Figure 5.26 - Cross sectional schematic of a multi-core reservoir system. Black represents the impermeable PCL shell, yellow represents the PVP-thiamine HCl core and blue represents the PCL-PVP release controlling membrane.*

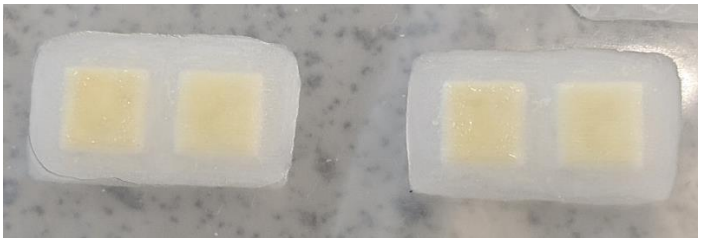


*Figure 5.27 - Printed multi-core reservoir systems.*

The release profile is presented in Figure 5.28, where 53 % drug release has occurred at minute 100 (near complete drug release for single reservoir system with 25 layers of the membrane was achieved at a similar time, see Figure 5.7). After this point, a clear change in gradient of the drug release profile occurs suggesting release from the second core begins or at least becomes more dominant as the first core has released all its drug, extending drug release for an additional 10 hours.

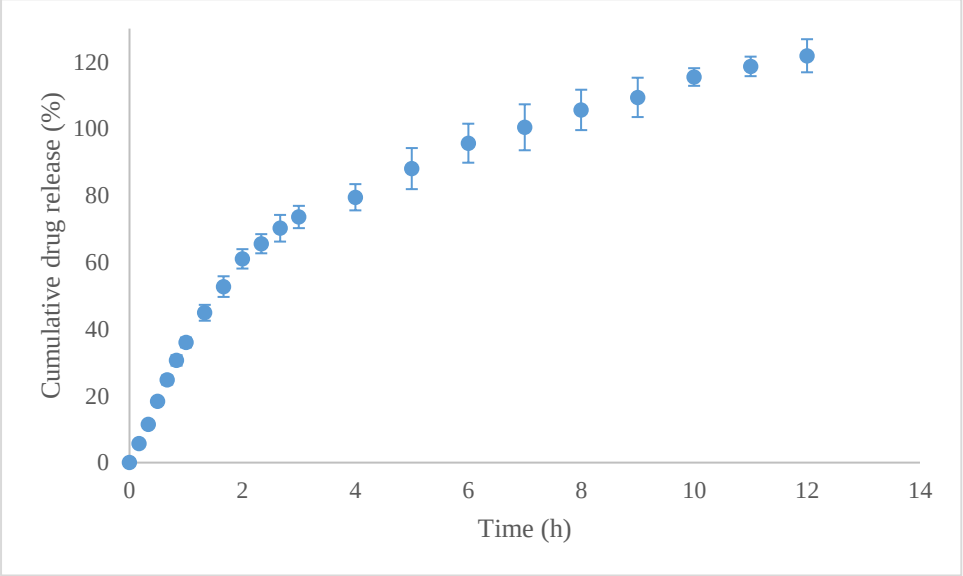



*Figure 5.28 - Release profile of a multi-core reservoir system. Initial drug release occurs at a faster rate and transitions into a more sustained drug release.*

### 5.3.5 Limitations of the current reservoir system

#### *5.3.5.1 Calculation of theoretical drug content*

For some of the release profiles presented in this chapter, drug release was seen to plateau before reaching the theoretical 100 % drug release or to continue for significant levels after drug release (i.e. beyond 100 %). These were clear indications that there was a significant difference in drug content between what was calculated and what

was actually printed. The method of calculating drug release was explained in Section 3.2.2.11.

One of the reasons for the drug content errors could be attributed to the lack of accuracy of the drop watcher system. The actual function of this system is not to accurately determine drop volume and in turn drug content in each drop. Its function is to observe droplet formation – i.e. making sure droplets are spherical and are consistently produced. Only a small number of droplets (n = 4) were used to derive a mean value of drug content in each drop (for a 100 layer core component, 6300100 drops were required). In addition, a small change in the measured drop diameter would result in a significant change in the total drug content of a tablet (e.g. with the used 22 µm diameter, 100 layers has a calculated drug mass of 4 mg, whereas if diameter was changed to 21 µm, drug mass is reduced to 3.4 mg – a 15 % difference). Calculation of drug content for each batch of tablets created was done with their specific ink loadings of the PVP-thiamine HCl formulation – limiting any variation between batches.

For samples where significantly less than 100 % drug release was calculated, it's possible that blocked nozzles may have also been the cause for a reduced amount of drug. In contrast to samples where larger than expected drug content was calculated, tailing or satellite droplets may have increased the overall drug content. It is, however, more likely that variation in droplet diameter would have been the predominant cause for the inaccurate drug content. This is because using the stated printing parameters (see Section 3.3.2), no indication of tailing or satellite droplets were observed when using the drop watcher system. Before every print run, the drop watcher system was used to confirm this. Often, printing was paused, and the drop watch system was used to investigate jetting. In most observations, jetting continued to be effective and reliable. On some occasions, one or two nozzles were seen to be not jetting but a standard cleaning cycle was able to return the nozzle to effective use. Furthermore, a cleaning cycle is automatically conducted by the printer after each layer was printed, to avoid potential blockages. It was observed while printing the PVP-thiamine HCl component that the ink could block the nozzles after an extended period of no jetting, and that a cleaning cycle would easily clear out the blockages. No evidence of the nozzles becoming blocked was observed (i.e. the blocking process was not seen).

Jetting was observed for over a minute with no blocking or significant change in jetting behaviour. It should be noted that there was not much variability between samples that were made in the same batch (small error bars towards the end of the dissolution profile would suggest this). There was greater variability in dose for samples created from different batches, further suggesting that there may have been changes in droplet size between batches that were not measured, leading to inaccuracy for calculating the theoretical dose.

The main reason why the drop watcher system was used to calculate the theoretical amount of drug in the printed tablet was to prevent any distortion caused by water absorption (hygroscopicity) (see Section 3.3.9). If drug content was calculated using the printed tablet's mass, the hygroscopic nature of the tablet may have resulted in a very different drug mass either due to residual water in the printed tablet from the ink and by any water absorbed during storage.

#### *5.3.5.2 Replacing PCL*

To significantly improve the reservoir system presented in this investigation, it would have been beneficial to replace PCL both as the impermeable shell and as a component of the release controlling membrane. The main issue was printing PCL at its melting temperature resulted in molten material being formed on the substrate. For printing the impermeable shell, film formation was poor for the initial layers (e.g. forming islands of PCL, Figure 4.8). Additionally, there is a slight loss of shape when printing a large number of layers. This was exasperated when printing larger multi-layer reservoir systems were attempted. This meant that with PCL involved, the reservoir system was limited in the z-direction.

The weakness observed of PCL when printed on the top surface of the reservoir system also proved to be a problem. It was attempted to investigate the surface area of the release controlling membrane as a parameter to control release, but the weakness of PCL (discussed in Section 4.3.4) prevented this to be an effective investigation. Figure 5.29 shows the schematic of reservoir systems with a smaller pattern for the release controlling membrane. Instead of the usual 8 x 8 mm pattern, a 3 x 3 mm and 4 x 4 mm pattern were used (25 layers). Additional layers of the impermeable material were printed on the edges (25 layers) of the release controlling membrane.



*Figure 5.29 - Reservoir systems with a reduced surface area for the release controlling membrane. Black represents the impermeable PCL shell, yellow represents the PVP-thiamine HCl core and blue represents the PCL-PVP release controlling membrane.*

Figure 5.30 shows the release behaviour of the two new systems printed. It was expected that due to the lower surface area of the release controlling membrane, release would be extended when compared to the regular 8 x 8 mm samples. Instead release was faster with drug release for both batches of tablets plateauing after only one hour, in contrast to the standard 8 x 8 mm system (plateau begins after two hours, see Figure 5.7). Overlapping errors bars suggested that the difference between these two batches were not significant.

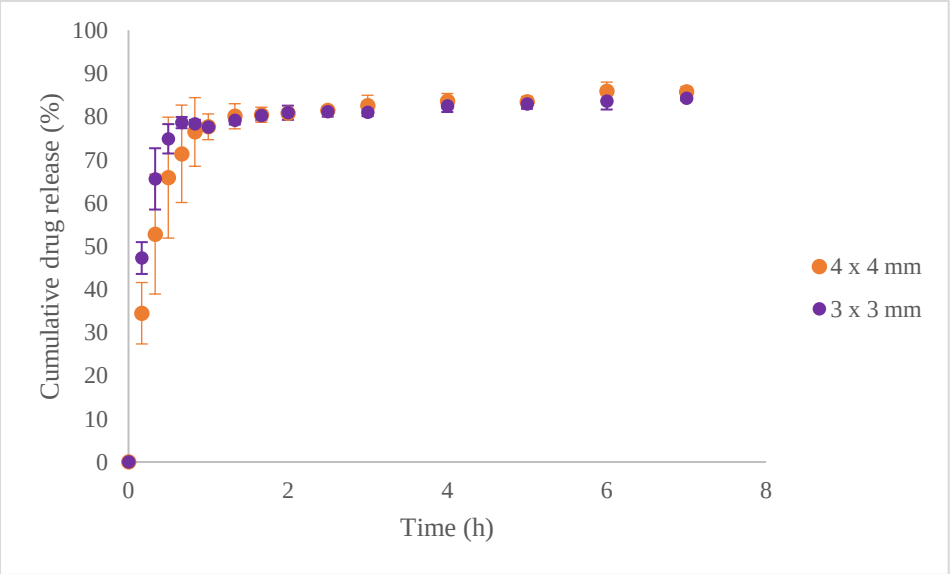



*Figure 5.30 - Experimental release profile of reservoir systems with a reduced surface area for the release controlling membrane.*

Optical microscopy after dissolution (Figure 5.31) showed significant damage on the top surface of the system with more damage at the interface between the PCL-PVP material and the PCL only material. Significant parts of the release controlling membrane had also been damaged. At this point it was unclear if the damage had been due to the potential brittleness of PCL (see Figure 4.23) or if the release controlling

membrane printed had been weak and caused the fracture (optical microscope analysis before dissolution showed no clear flaws, see Figure 5.31).

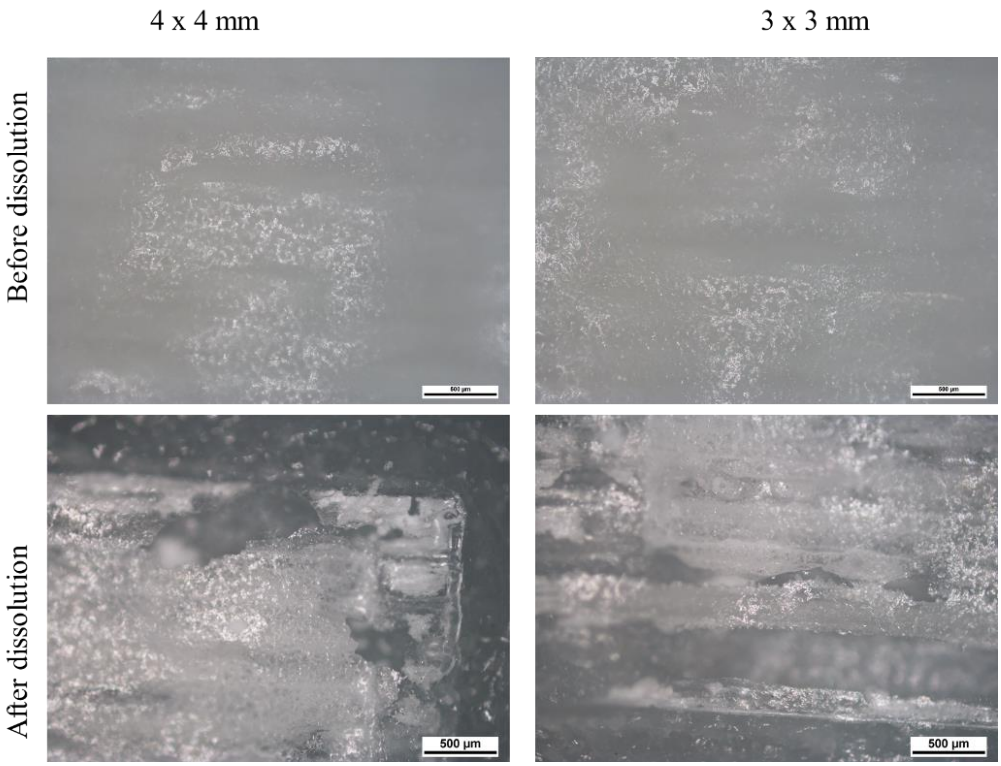



*Figure 5.31 - Optical microscope images of samples before and after dissolution. Scale bar = 500 µm.*

Therefore, additional (multi-core) samples were printed with a reduced surface area but with more printed layers to ensure material thickness had not played a role in the damage caused (50 layers of PCL-PVP and 100 layers of PCL on the edge). Post-dissolution examination of these tablets showed the PCL component had delaminated from the rest of the reservoir system (Figure 5.32). Optical microscopy showed that the actual release controlling membrane component had not suffered any clear damage (Figure 5.33).

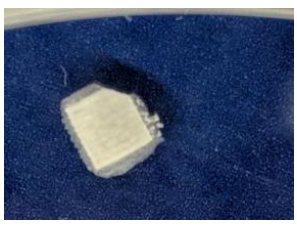


*Figure 5.32 - Delaminated PCL with the release controlling membrane printed on top.*

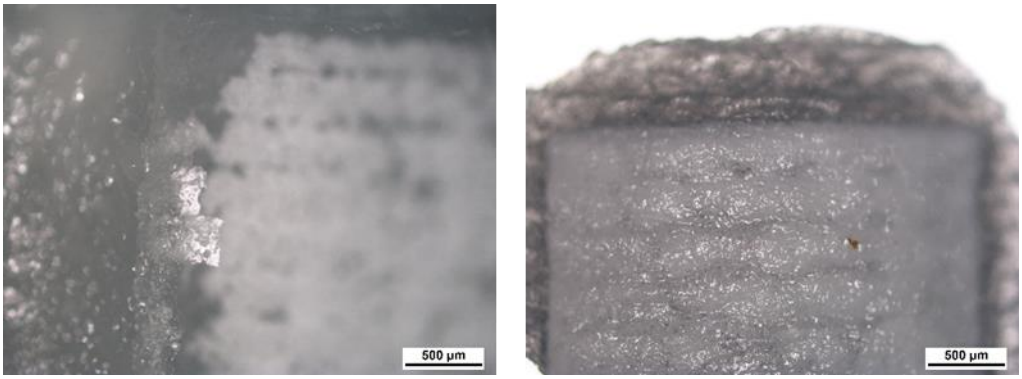



*Figure 5.33 - Damaged and exposed reservoir system (left) and the delaminated release controlling membrane with a reduced pattern area (right). Scale bar = 500 µm.*

Ideally, PCL should be replaced with another highly hydrophobic material with better film forming properties and mechanical integrity.

## 5.4 Conclusions

The following conclusions can be made from this chapter:

- An ink formulation consisting of hydrophobic PCL, hydrophilic PVP and DMAC was developed to be printed as a release controlling membrane. Ink characterisation was conducted and showed that the formulation had properties that would be effective for printing using the Dimatix printer. Substrate parameters were investigated, and similar issues were encountered when printing the PCL only impermeable material. Substrate temperature was set at 60 °C to ensure the best morphology for the resultant material.
- Raman spectroscopy had shown that PCL and PVP phase separate after printing. When exposed to water, PVP dissolves and near zero amounts remain in the film. PCL remained unchanged. This suggested that PVP would act as a pore forming agent in the release controlling membrane, allowing the creation of a path for water molecules to move through, dissolve the drug in the core of the reservoir system, which would then diffuse out.
- ToF-SIMS of the cross-section of the blended membrane suggested that a tortuous network of pores would form when the system is exposed to water.
- A reservoir system was printed with a 25 layer release controlling membrane and release occurred in a controlled manner over two hours. Comparing samples before and after dissolution suggested that the release occurred

through the pores that form. Although one sample appeared to be damaged after dissolution, the similar release profiles of the other samples tested which showed no damage indicated the resultant PCL-PVP film had the mechanical integrity to be an effective release controlling membrane. Application of different kinetic models on the dissolution data suggested that zero-order release was achieved.

- The effect of additional printed layers of the release controlling membrane showed that drug release could be extended (50 layers, over seven hours) and a delay could be introduced into the system (100 layers). In addition to making the membrane thicker, the size of pores on the top surface reduce in size. Examining samples before and after dissolution with CT scanning also showed that the entire core of the device dissolves over time.
- The loading of PVP on the release controlling membrane formulation was also investigated. With a greater loading, the surface pores were larger (imaged by ToF-SIMS and SEM) resulting in faster drug release. Cracking was seen in one of the samples after dissolution and the breaking of other samples prevented a fair comparison and would need repeating.
- The effect of drop spacing of the PCL-PVP ink was initially investigated with ToF-SIMS. Chemical maps generated showed that as drop spacing increases, PVP regions decrease in size – initially suggesting that if drop spacing increases, drug release rate would decrease. When comparing two batches of 50 layer reservoir systems with different drop spacings (20 µm and 30 µm) it was found that the 30 µm samples had a faster drug release. This was attributed to the thinner membrane that was printed when using a 30 µm drop spacing, which had a bigger impact on drug release than pore size (even though SEM analysis showed smaller surface pores). When comparing samples with different drop spacings, but with comparable amounts of material (number of drops) drug release behaviour was seen to be drastically different, highlighting another method where drop spacing could be used to produce matrices which control drug release.
- A multi-core reservoir system was printed to create a drug delivery device capable of delivering a bimodal drug release, where release transitions from a faster to a slower release. Using a different number of layers on each of the

two cores, approximately 50 % of drug released in two hours and the remainder was released over an additional 10 hours.

- Different release profiles have been created with the system discussed in this chapter including: extended, delayed and bimodal. In addition to varying the ink formulation of the membrane, these release profiles were created by varying printing parameters (drop spacing, number of layers, geometry) using a single formulation for the membrane ink.
- One limitation that was observed was the method to calculate the theoretical drug content. It was thought that the most likely reason is the variation in droplet size when printing the PVP-thiamine HCl formulation and the lack of accurate method of measuring the droplet. Even a small variation in diameter of the droplet could result in significant changes in the calculated drug content of tablets.
- To improve the reservoir system, it would be beneficial to replace PCL with another hydrophobic and impermeable material. Printing this material proved challenging at 60 °C (its melting temperature) as molten material would form. Printing larger and multilayer tablets were not possible due to the significant loss of shape. The top surface of the material appeared to be susceptible to fracture (as was seen in the previous chapter as well), which made it a challenge to investigate the influence the surface area of the release controlling membrane would have on drug release due to the damage and delamination that occurred.

## 5.5 Chapter Appendix: Supplementary Information

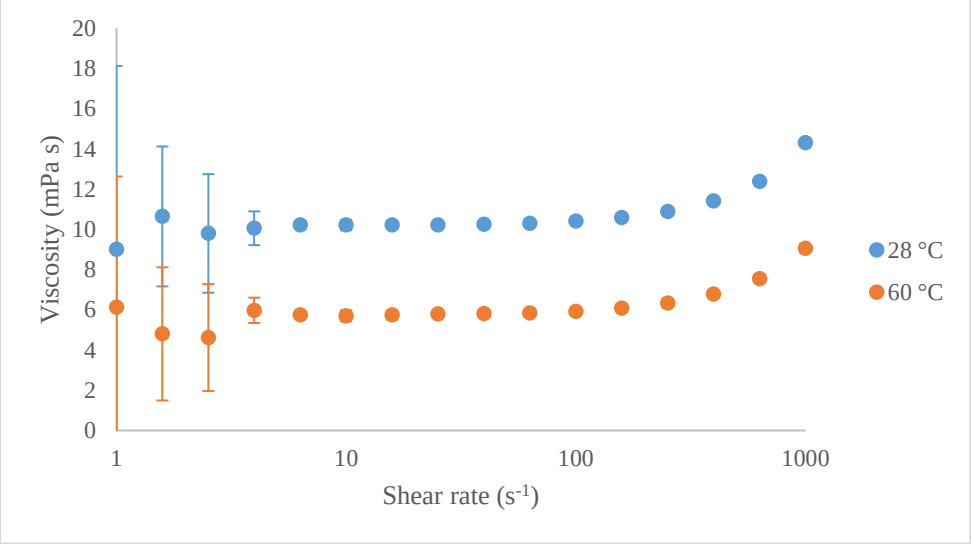



*Figure S5.34 - Rheological flow curves of the release controlling membrane formulation.*

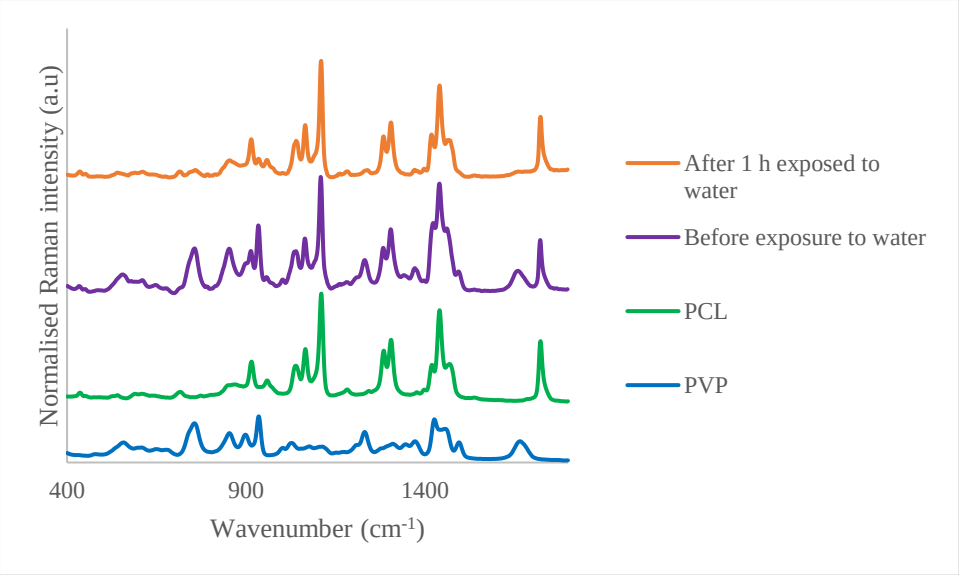



*Figure S5.35 - Raman spectra of pure PVP, PCL, the mean spectra for the surface of the release controlling membrane before and after exposure to water.*

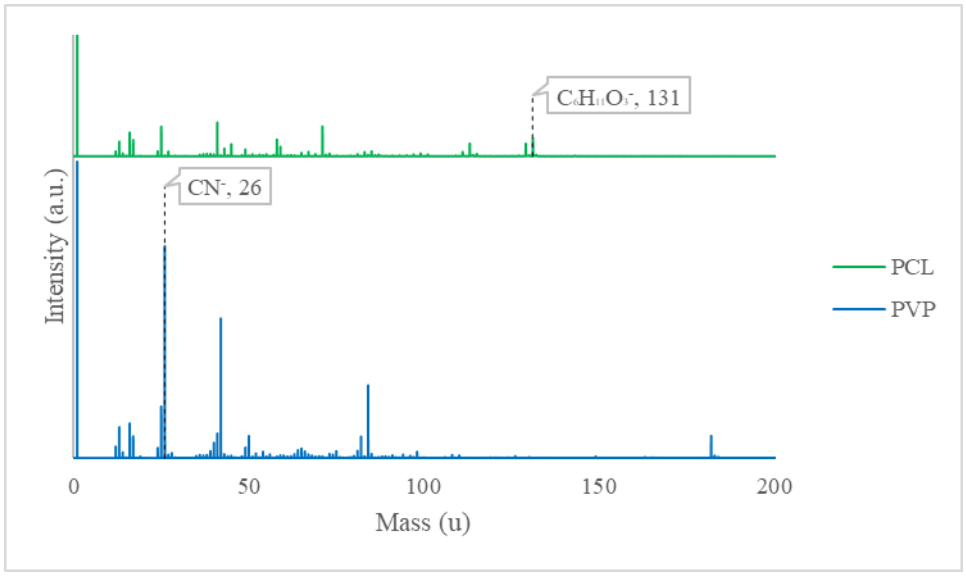



*Figure S5.36 - ToF-SIMS spectra of pure PCL and PVP material.*

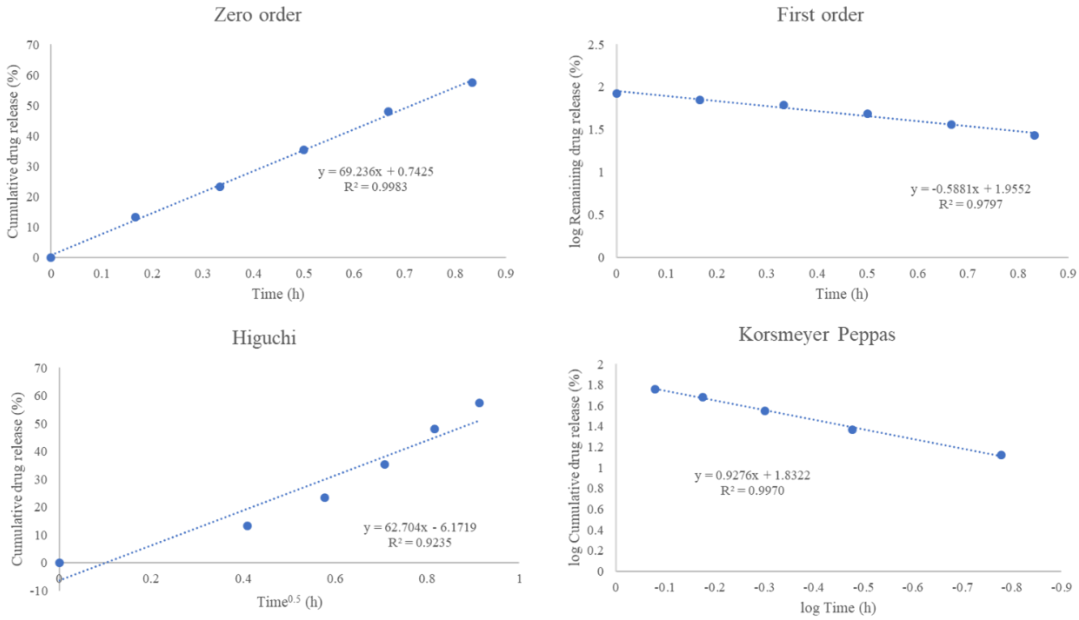



*Figure S5.37 - Dissolution models applied to data of drug release for a 25 layer reservoir system.*

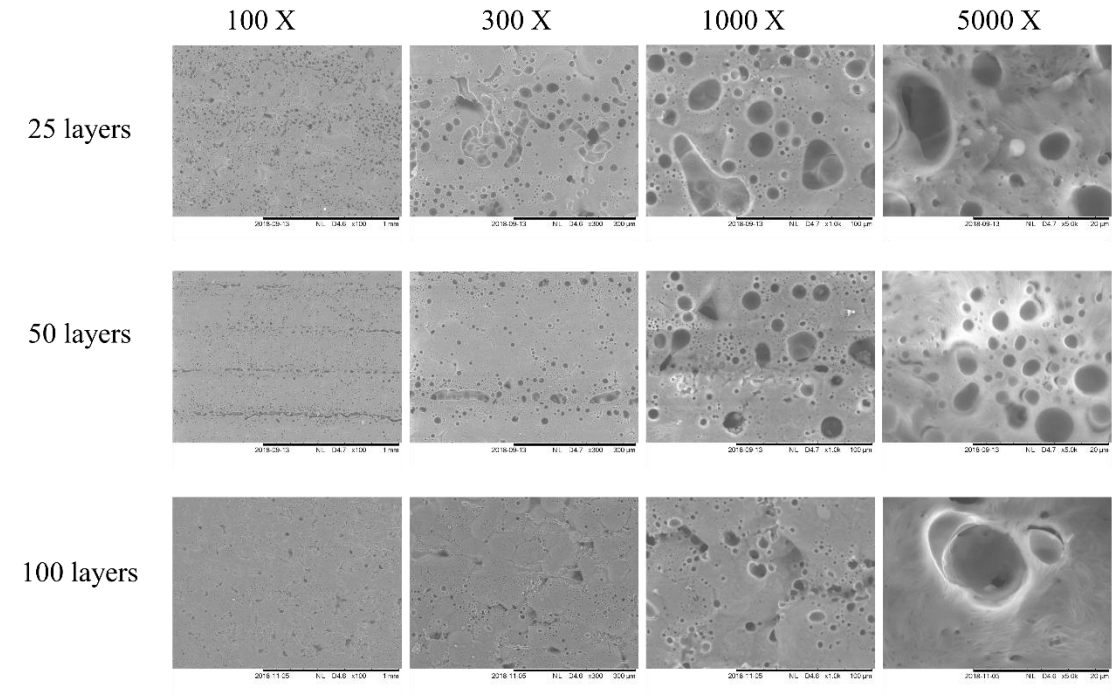



*Figure S5.38 - SEM images of different number of printed layers of the release controlling membrane of reservoir systems at different magnifications after dissolution. A 20 µm drop spacing and 38 wt% PVP loading was used for all samples.*

*Table S5.5 - Ink formulation for a release controlling membrane with an increased PVP loading (43 wt% in release controlling membrane).*

| Component | Content (wt %) |
|---|---|
| PCL | 10.0 |
| PVP | 7.5 |
| DMAC | 82.5 |

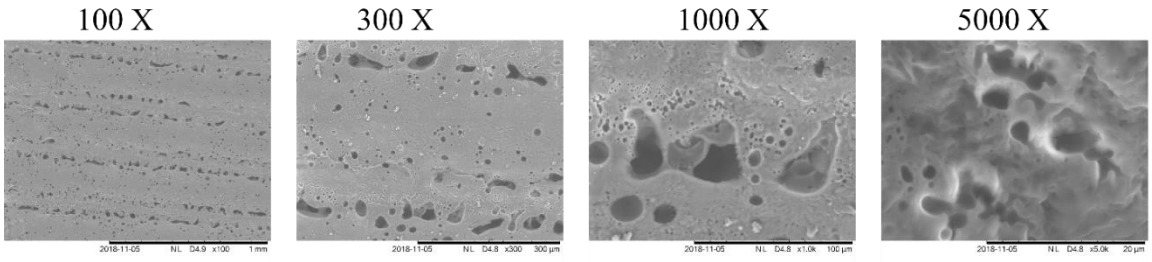



*Figure S5.39 - SEM images of 100 layers of the release controlling membrane (20 µm drop spacing and 43 wt% PVP loading). This specific sample was not used in actual dissolution testing but used to measure pore sizes. This specific sample was however made in the exact same batch of tablets used in dissolution testing.*

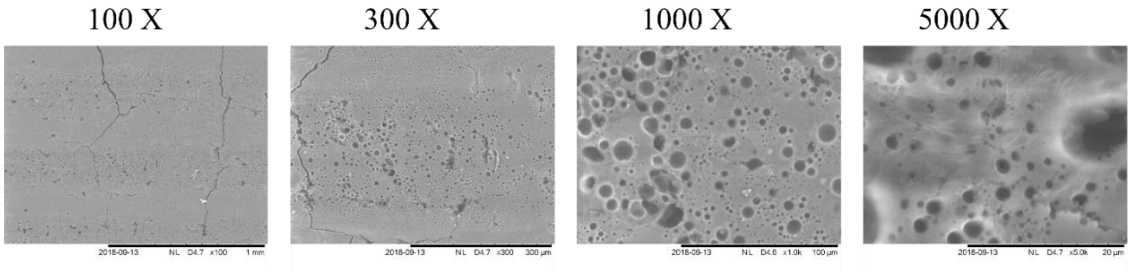



*Figure S5.40 - SEM images of 50 layers of the release controlling membrane (30 µm drop spacing and 38 wt% PVP loading).*

*Table S5.6 – Additional information regarding thickness of the PCL-PVP (38 wt%) printed structures (n = 3). PET thickness was 0.136 ± 0.0 mm.*

| Drop spacing | No. of layers printed | Thickness of printed structure (mm) | Individual layer thickness (µm) |
|---|---|---|---|
| 10 | 1 | 0.005 ± 0.0006 | 5.3 ± 0.58 |
| 20 | 100 | 0.243 ± 0.001 | 2.4 ± 0.01 |
| 30 | 90 | 0.125 ± 0.002 | 1.4 ± 0.02 |

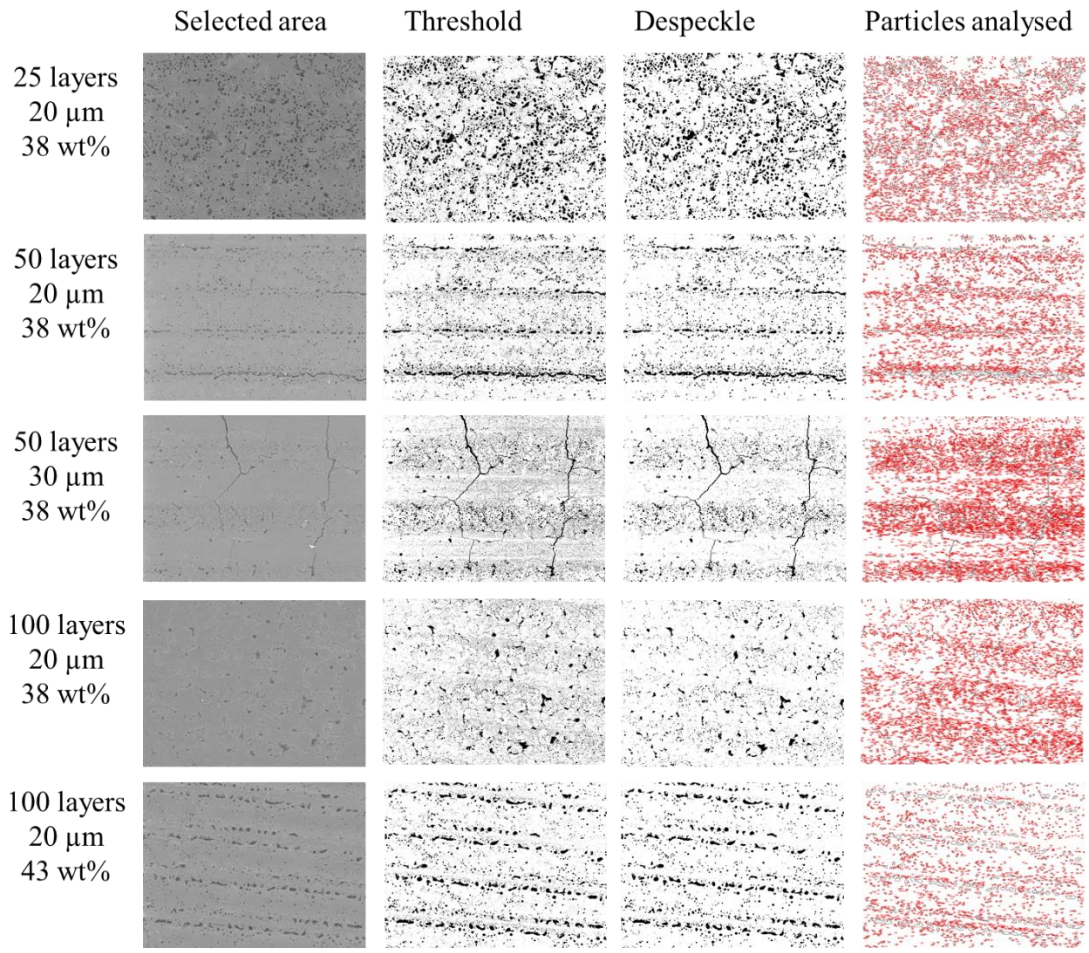



*Figure S5.41 - Areas of SEM images analysed, thresholded images, with despeckling and the outlines of particles analysed at a 100 X magnification.*

*Table S5.7 - Analysis of particles from Figure S5.41.*

| No. of layers | Drop spacing (µm) | PVP loading (wt%) | Total pore area (x $10^5$ µm$^2$) | Median pore area (µm$^2$) | Mean pore area (µm$^2$) | Standard deviation (µm$^2$) | No. of particles analysed | Threshold value |
|---|---|---|---|---|---|---|---|---|
| 25 | 20 | 38 | 3.27 | 21 | 83 | 184 | 3927 | 121 |
| 50 | 20 | 38 | 1.69 | 18 | 47 | 200 | 3592 | 149 |
| 50 | 30 | 38 | 1.50 | 9 | 23 | 113 | 6589 | 149 |
| 100 | 20 | 38 | 1.15 | 7 | 24 | 89 | 3000 | 141 |
| 100 | 20 | 43 | 1.68 | 17 | 77 | 217 | 2176 | 137 |

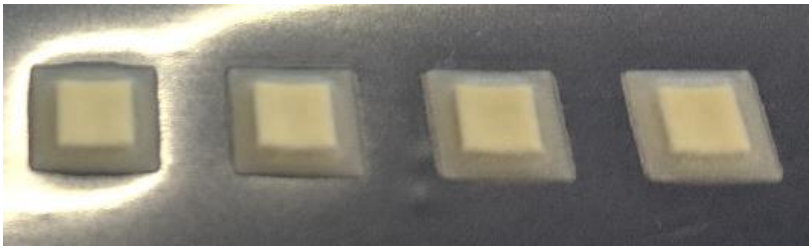


*Figure S5.42 - Reservoir system tablets with 50 layer, 30 µm and 38wt% PVP release controlling membrane.*



*Figure S5.43 - Reservoir system tablets with 50 layer, 30 µm and 38wt% PVP release controlling membrane after dissolution.*



*Figure S5.44 - Reservoir system tablets with 10 layers, 10 µm and 38wt% PVP release controlling membrane after dissolution.*



*Figure S5.45 - Multi-core reservoir system after dissolution.*

# 6 Conclusions and Future Work

## 6.1 Conclusions

The main aim of this research, to inkjet print a solid oral dosage form capable of a controlled drug release, has been achieved. The novelty of this work lies in the two different systems created.

With reference to the rapid releasing tablet in Chapter 3, we have illustrated a method of using solvent based inkjet printing to wholly manufacture tablets from non-toxic materials. Previous work had used solvent inkjet printing to create dosage forms with the use of edible substrates or preformed tablets or with solvents that would require content tracking. Wholly inkjet printed tablets have been made before, however the work used a UV-curable system and a hot melt inkjet system. In Chapters 4 and 5, we developed additional materials to create a multi-material inkjet printed reservoir system capable of delivering controlled drug release. Controlling release was not only achieved by varying ink formulation of the release controlling membrane. By using one single formulation, we were able to vary the physically structure of the release controlling membrane. This thesis demonstrated the following drug release profiles:

- Rapid
- Extended
- Delayed
- Bimodal (fast to slow)

### 6.1.1 Rapid releasing tablets

The first component of the reservoir system to be formulated was the core of the dosage form, which on its own would act as a rapid releasing tablet, with no degree of control.

Using thiamine HCl as a model API for a water-soluble drug, a water-based formulation was created. Using water soluble PVP and the use of additives (polysorbate 20 to reduce surface tension and glycerol to improve film forming behaviour), consistent and effective jetting behaviour was observed. By printing the ink on a PET substrate, the 3D printed tablets were easily removed with no signs of

damage. The use of high temperatures was avoided (since printing was performed at 28 °C), as was the use of toxic solvents and the potential of uncured materials – highlighting this method as a safe and toxic-free method of printing tablets with a potentially 'universal' ink for water soluble drugs.

During the printing process, occurrences of phase separation were observed. Over time, we observed thiamine HCl crystallisation and growth in the PVP matrix resulting in a solid-suspension of crystals. In addition to this, when layers were subsequently printed on top of each other, a potential solvent mediated recrystallisation process occurred. White regions nucleated and grew until the entire film was covered. These regions were seen to have a rougher surface profile in comparison to the 'clearer' regions. AFM and cross-polarised optical microscopy confirmed this phase separation processes. ToF-SIMS showed that the drug content across the layers was uniform at the micron scale.

The reliability of the inkjet process was shown by elemental analysis by combustion. Using sulphur as an elemental marker, the drug content of the printed tablet corresponded accurately with the theoretical drug loading based on the ink formulation. Using UV-Vis spectroscopy, the amount of drug deposited in each layer was shown to be uniform (where a high linear correlation was calculated between drug content and the number of printed layers).

Raman spectroscopy proved that thiamine HCl existed in its desired NSH polymorphic form. The undesirable HH phase was not observed even in prints that had been exposed to the ambient environment for prolonged periods or in tablets that were printed from older inks. Confocal Raman microscopy again showed the drug to be homogenously distributed throughout the tablet.

One potential limitation with the printed tablet was its hygroscopic nature. By tracking the masses of tablets, tablets were seen to have residual water after printing and when stored in environments with little or no control, fluctuations in mass were measured.

Drug release was successfully rapid, with 90 % of drug being released within seven minutes.

With the stated conclusions, this tablet formulation could be used as a polymer-drug core of a reservoir system. Potential flaws in the system would be highlighted by the rapid and uncontrolled release of the core formulation.

### 6.1.2 Controlled release tablets

To create a reservoir system with a single direction for drug release, an impermeable shell for the base and walls of the system needed to be developed. PCL was chosen due to its hydrophobicity and long degradation times. DMAC was selected as the solvent. With 10 wt% PCL, effective jetting behaviour was seen.

The PCL morphologies were shown to be greatly affected by the substrate temperature. While printing at low temperatures (28 °C and 40 °C) films were weak and susceptible to cracking and delamination. It was decided to print the PCL ink with the substrate at 60 °C, meaning molten PCL would form on the substrate. The substrate heating was then turned off, allowing PCL to solidify from the melt into a solid 3D structure. To prevent heat transfer from the substrate to the nozzles (which was seen to change jetting behaviour), the nozzle temperature was also set to 60 °C and the waveform adjusted to maintain good jetting behaviour.

To prove that PCL would be an effective material to act as an impermeable shell, a reservoir system where the PVP-thiamine HCl core was fully encased in PCL was printed. Dissolution testing showed that when the top surface of the system was not damaged only 2.5 % of drug was released after five hours. This suggested that PCL would be a suitable material for the impermeable base and walls for the reservoir system.

For the release controlling membrane, a blend of PCL and PVP was created. A higher loading of PCL was used to promote small regions of PVP domains dispersed in a PCL matrix. DMAC was used again as a solvent. Similar printing parameters were used as for the PCL only formulation (e.g. jetting at 60 °C, substrate temperature at 60 °C).

Using Raman mapping, phase separation between PCL and PVP was observed. With smaller PVP domains distributed throughout a PCL matrix. When the material was exposed to water, the PVP regions appeared to have dissolved while PCL remained

unchanged. The dissolution of PVP had shown its potential to act as a pore forming agent, allowing a path for water ingression and drug diffusion. ToF-SIMS of the cross-section suggested a highly tortuous network of pores would form after water had dissolved the PVP in the membrane.

To first illustrate the functionality of the release controlling membrane, a reservoir system with a 25 layer membrane was printed. Drug release was seen to occur over two hours (extended from seven minutes with no surrounding material). Optical microscopy of the tested samples before and after dissolution suggested that the membrane had acted effectively providing a degree of control. Dissolution kinetic models applied to the dissolution data showed that a zero-order drug release was the predominant mode for release. Micro-CT scanning of samples before and after dissolution suggested that the entire PVP-thiamine HCl core dissolves as drug release progresses.

Through the investigation of differing printing and ink parameters, their influence on drug release was determined. By printing a greater number of layers, drug release was extended and at one point a delay was introduced (100 layers of the PCL-PVP ink). The increase in distance required for water molecules and drug molecules to move and the apparent decrease in pore size is a proposed reason for slower drug release.

By increasing the content of PVP in the release controlling membrane, drug release rate was seen to increase. ToF-SIMS and SEM image analysis showed that by increasing the PVP content in the ink for the release controlling membrane, larger regions of PVP form (leading to larger pores), which is a common behaviour for polymer blend systems.

Drop spacing during printing was shown to also influence the drug release profile. With increasing drop spacing, ToF-SIMS analysis illustrated a reduction in size of PVP domains, suggesting that drug release could be extended by increasing drop spacing alone. However, when comparing two batches of reservoir systems with 50 printed layers of the release controlling membrane (20 µm and 30 µm), drug release duration was significantly shorter in the batch with a higher drop spacing. This was because drop spacing caused a change in thickness of the printed layers (i.e. higher drop spacing led to thinner structures). This was seen to have a more significant

influence on drug release than pore size. By investigating samples with comparable amounts of material (number of drops, 90 layers with 30 µm drop spacing vs 10 layers with a 10 µm drop spacing), drug release was seen to be significantly different. With 10 layers / 10 µm, ToF-SIMS analysis showed very large domains of PVP dispersed in the PCL matrix, with no consistency or homogeneity. In contrast, 90 layers / 30 µm had much smaller regions of PVP and these were uniformly dispersed throughout the PCL matrix. This was attributed to the poor choice of drop spacing (10 µm) which may have caused poor film formation where large amounts of material and overlap may have led to significant bulging and ink agglomeration. This in turn caused very fast drug release with no real degree of control.

By creating reservoir systems with more than one core, it was possible to create a dosage form capable of delivering drug with a transition in drug release rate. With two cores printed in a single system, each with a different thickness (25 and 100 layers) for the release controlling membrane, it was possible to have approximately 50 % of drug released in two hours and the remaining drug released over an additional 10 hours.

## 6.2 Future work

### 6.2.1 Short term considerations

Suggested work in this section focuses on the immediate gaps in the thesis that could be addressed. Most are specific to the reservoir system presented in this thesis.

#### *6.2.1.1 Drug degradation*

One area that this thesis has not investigated is the potential degradation of thiamine HCl in the printed tablets. Although the formulation and printing method is well below the drug's degradation temperature [166], it should still be conclusively proved that thiamine HCl does not degrade with the current system. HPLC [167] and nuclear magnetic resonance (NMR) spectroscopy [168] are two potential characterisation methods that could be used to investigate drug degradation.

#### 6.2.1.2 Detection limits of thiamine HCl

UV-Vis spectroscopy was used to detect and quantify thiamine HCl content for drug uniformity and dissolution tests. To strengthen the reliability of these results, the limits of detection and quantification of thiamine HCl should be determined. It would clearly identify what signal is actually the drug, and what is noise [169]. This is particularly important for the initial stages of drug release where very small amounts of thiamine HCl would be detected (e.g. during the delay of a 100 layer reservoir system).

#### 6.2.1.3 Investigating residual DMAC solvent

Due to the hazardous potential of DMAC, it would be critical to measure and quantify the amount of any remaining solvent. As DMAC is a Class 2 solvent, its residual amounts are required to be identified and quantified. It has a permitted daily exposure of 10.9 mg/day (concentration limit of 1090 ppm) [170]. There are numerous methods to investigate the presence of residual solvents including loss on drying, thermogravimetric analysis and gas chromatographic methods [171].

#### 6.2.1.4 Influence of PVP loadings on the release controlling membrane

It was seen that by increasing PVP loading in the release controlling membrane, larger PVP domains form. This would explain why faster drug release was seen for samples printed with a 43 wt% PVP loading in the release controlling membrane. The samples tested in Section 5.3.4.2 did not, however allow for a conclusive proof that the larger pores were the main reason for the faster drug release. This was because one of the samples tested did show the presence of a large crack after dissolution, while the other sample was broken during handling before it could be analysed. This experiment should therefore be repeated to determine or prove that it was the increased size of pores that caused the quicker release.

#### 6.2.1.5 Effect of drop spacing on drug release with similar membrane thicknesses

Drop spacing was seen to change two properties of the release controlling membrane (PVP domain size and layer thickness). Reservoir systems should therefore be printed with varying drop spacings, but the exact same thickness for the release controlling membrane (this would mean a difference in the number of printed layers). Further

work in this area could help proving that a single formulation can be used to control pore size to influence drug release.

#### *6.2.1.6 Further characterisation of PCL and PVP phase separation*

To gain a deeper understanding of the phase separation between PCL and PVP, it would be advantageous to conduct hot-stage microscopy. This method would allow the visualisation of the phase separation occurrence. Hot stage microscopy would also be useful in observing the effects of adding more material on previous depositions (see Section 5.3.5.1) for changes in pore size due to the number of printed layers).

#### *6.2.1.7 Further investigation of porous network*

SEM imaging and ToF-SIMS analysis conducted on reservoir systems in Section 5.3.5 allowed characterisation of only the surface pores that form with different ink and printing parameters. The level of tortuosity based on PCL and PVP phase separation has not been fully investigated (only one sample was studied with ToF-SIMS). Different printing parameters may have affected the tortuosity of the resulting porous network and would allow for a fuller understanding of drug release behaviour.

#### *6.2.1.8 Finding at alternative to PCL*

There were numerous setbacks when using PCL in this system. Poor film formation, weak structures and printing molten material are just some of the limitations. It would be possible to improve the system (e.g. addition of surfactants to prevent the coffee ring effect [154] or addition of water-insoluble plasticisers to prevent cracking at lower temperatures [172]) or replace PCL altogether. A good candidate would be ethyl cellulose, which is known to have very low drug permeability. It can also be processed with an aqueous dispersion [173] or with organic solvents [174]. It has been used in numerous investigations as a component for a reservoir device [175]. Ethylcellulose inks have also been processed with flexographic printing for oral drug delivery applications [55].

### 6.2.2 Long term considerations

Suggestions discussed in this section focus more on the long term considerations for the additive manufacturing of tablets.

#### *6.2.2.1 Phase separation of thiamine HCl*

As shown in Section 3.3.5, thiamine HCl was seen to phase separate via two occurrences. Although through polymorphic investigations in Section 3.3.7, the drug remains in its desired form, if other drugs are used with this system, phase separation in the form of crystallisation can have potential negative effects (e.g. poorer solubility). Printing strategies or the ink additives to prevent or minimise this occurrence should be investigated if inkjet printing is to be a viable manufacturing route for pharmaceutical products.

#### *6.2.2.2 Calculation of the theoretical drug content in tablets*

Section 5.3.5.1 explains in more depth the potential reasons for distortion in calculating the theoretical drug content in the printed tablets. Inkjet printing can be an accurate manufacturing process, only when however, its behaviour is consistent identical. Small variations in droplet diameter for example can have significant consequences such as dosing strength of printed tablets. For this investigation, it would have been more effective to have measured the diameters of droplets with a much larger sample size (instead of just four drops). An alternative method of calculating the theoretical drug amount (e.g. measuring drug content in individual drops, similar to the drug content in layers seen in Section 3.3.6) may have resulted in more accurate theoretical doses. Storing samples in dry and controlled environments and using mass to determine the theoretical drug content would also be an effective alternative (see Section 3.3.9 for moisture uptake of the tablets). Although this would not address the problem of printing a tablet with a predetermined dose.

In context of large scale manufacturing systems, a more accurate and reliable drop watcher system should be incorporated in printing systems. There has been some work to develop self-detecting inkjet print heads for jetting failure such as the work done by Kim *et al.* 2011 with the use of a scanning device capable of detecting poor jetting signals in their early stages [176]. More traditional printing companies, such as Mutracx International B.V., use a technology that can predict when a single nozzle is about to fail due to air entrapment. Nozzles can then be switched during printing to prevent the image from being printed poorly [177].

#### 6.2.2.3 *Simulating the human body for dissolution studies*

Dissolution studies carried out in this thesis used deionised water as the dissolution medium, as instructed in thiamine HCl's pharmacopeia [98]. If controlled drug release is to be realistically illustrated, the dissolution media must simulate the physiological environment of the human body. This would mean the use of dynamic dissolution testing where pH levels can be controlled during the dissolution tests. There are additional factors such as fluid composition and hydrodynamics that should also be considered [178]. This would be the first step for moving towards *in vivo* testing of inkjet printed tablets.

#### 6.2.2.4 *Optimising manufacturing efficiency*

The optimisation of inkjet printing for tablet manufacturing would be very advantageous to investigate. This would include ways of optimising the large print times as well as making efficient use of the space available on the print bed. For example, printing a row of tablets with an inter-layer delay would be less efficient than printing two rows of tablets, which would allow for a greater number of samples produced with the same time. The speed of tablet manufacture with inkjet printing can be controlled by a range of printing settings including jetting frequency, number of nozzles used, drop spacing, size of the pattern, orientation of pattern, spacing between patterns and number of pattern repeats (x and y direction). Substrate heating could also influence printing time by changing the rate at which solvent would evaporate.

#### 6.2.2.5 *Incorporating additional materials for greater functionality*

The ease at which additional inks can be incorporated for inkjet printing is one of this method's biggest advantages. This investigation has successfully used three different functional materials (rapid release, release controlling membrane, impermeable shell) to create modified release profiles. Incorporating another material that would surface erode over time would allow for a pulsatile or a fast-to-slow bimodal drug delivery device [162]. The surface eroding component would prevent drug release until it has completely degraded at which point drug release would begin through the release controlling membrane printed beneath it. It would also be advantageous to incorporate a gastroretentive component into the 3D printed device. If the oral devices printed are for long-term use, it would be critical that they survive in the body in a stable manner.

There are numerous physiological factors that can affect gastric retention. These include the presence or absence of food, posture of the patient, gender, age, emotional state and the presence and nature of the ailment. These highly individualised factors can be addressed by the personalised nature of 3D printing for drug delivery devices. Different mechanisms for gastroretention of the device include expanding, floating, mucoadhesion, magnetic and high density sinking [160].

# 7 References


[1] ASTM International, “F2792-12a - Standard Terminology for Additive Manufacturing Technologies,” *Rapid Manufacturing Association*. 2013.

[2] C. K. Chua and K. F. Leong, *3D Printing and Additive Manufacturing: Principles and Applications*. 2015.

[3] I. Gibson, D. W. Rosen, and B. Stucker, *Additive Manufacturing Technologies*. 2010.

[4] A. Cox, “Power, value and supply chain management,” *Supply Chain Manag. An Int. J.*, vol. 4, no. 4, pp. 167–175, 1999.

[5] S. Magdassi, *The Chemistry of Inkjet Inks*. 2009.

[6] B. Derby, “Inkjet Printing of Functional and Structural Materials: Fluid Property Requirements, Feature Stability, and Resolution,” *Annu. Rev. Mater. Res.*, vol. 40, no. 1, pp. 395–414, 2010.

[7] G. D. Martin, S. D. Hoath, and I. M. Hutchings, “Inkjet printing - the physics of manipulating liquid jets and drops,” in *Journal of Physics: Conference Series*, 2008, vol. 105, p. 012001.

[8] G. Cummins and M. P. Y. Desmulliez, “Inkjet printing of conductive materials: a review,” *Circuit World*, vol. 38, no. 4, pp. 193–213, 2012.

[9] H. Wijshoff, “The dynamics of the piezo inkjet printhead operation,” *Phys. Rep.*, vol. 491, no. 4–5, pp. 77–177, 2010.

[10] S. D. Hoath, *Fundamentals of Inkjet Printing*. 2016.

[11] A. Hudd *et al.*, *Chemistry of Inkjet Inks*. 2010.

[12] M. E. Aulton and K. M. G. Taylor, *Aulton’s Pharmaceutics: The Design and Manufacture of Medicines*, 4th ed. 2013.

[13] M. Gibson, *Pharmaceutical Preformulation and Formulation*, 2nd ed., vol. 199. 2009.

[14] H. Loth, *Modern Pharmaceutics*. Marcel Dekker, 2002.

[15] G. G. Z. Zhang, D. Law, E. A. Schmitt, and Y. Qiu, “Phase transformation considerations during process development and manufacture of solid oral dosage forms,” *Adv. Drug Deliv. Rev.*, vol. 56, no. 3, pp. 371–390, 2004.

[16] M. Saifee, N. Inamdar, D. L. Dhamecha, and A. a. Rathi, “Drug polymorphism: A review,” *Int. J. Heal. Res.*, vol. 2, no. December 2009, pp. 291–306, 2009.

[17] Y. Cui, “A material science perspective of pharmaceutical solids,” *Int. J. Pharm.*, vol. 339, pp. 3–18, 2007.

[18] H. Wen and K. Park, *Oral Controlled Release Formulation Design and Drug Delivery*. John Wiley & Sons, 2010.

[19] T. Perrie, Yvonne; Rades, *Pharmaceutics: Drug Delivery and Targeting*, 2nd ed. 2012.

[20] J. Siepmann, R. A. Siegal, and M. J. Rathbone, *Fundamentals and Applications of Controlled Release Drug Delivery*. 2012.

[21] J. Siepmann and F. Siepmann, “Modeling of diffusion controlled drug delivery,” *J. Control. Release*, vol. 161, no. 2, pp. 351–362, 2012.

[22] P. Láng *et al.*, “Polymorph screening of an active material,” *J. Pharm. Biomed. Anal.*, vol. 84, pp. 177–183, 2013.

[23] C. L. Ventola, “Medical Applications for 3D Printing : Current and Projected Uses,” *Pharm. Ther.*, vol. 39, no. 10, pp. 704–711, 2014.

[24] A. Goyanes, P. Robles Martinez, A. Buanz, A. W. Basit, and S. Gaisford, “Effect of geometry on drug release from 3D printed tablets,” *Int. J. Pharm.*, vol. 494, no. 2, pp. 657–663, 2015.

[25] J. Ledesma-Fernandez, “Jetting of multiple functional materials by Additive Manufacturing,” 2018.

[26] S. A. Khaled, J. C. Burley, M. R. Alexander, J. Yang, and C. J. Roberts, “3D

printing of five-in-one dose combination polypill with defined immediate and sustained release profiles," *J. Control. Release*, vol. 217, pp. 308–314, 2015.

[27] R. Daly, T. S. Harrington, G. D. Martin, and I. M. Hutchings, "Inkjet printing for pharmaceutics – A review of research and manufacturing," *Int. J. Pharm.*, vol. 494, no. 2, pp. 554–567, 2015.

[28] C. Voura *et al.*, "Printable medicines: a microdosing device for producing personalised medicines," *Pharm. Technol. Eur.*, vol. 23, pp. 32–36, 2011.

[29] N. Scoutaris, M. R. Alexander, P. R. Gellert, and C. J. Roberts, "Inkjet printing as a novel medicine formulation technique," *J. Control. Release*, vol. 156, pp. 179–185, 2011.

[30] D. O'Connell, "Early-stage Development, Xcelodose & Clinical Phases," *J. Clin. Stud.*, vol. 9, no. 5, pp. 53–54, 2017.

[31] D. Phillips, "DiffCORE ™ Accelerating the Development of controlled Release Products."

[32] D. Radulescu, N. Schwade, and D. Wawro, "Uniform Paclitaxel-Loaded Biodegradable Microspheres Manufactured by Ink-Jet Technology," in *Proc., the Winter Symposium and 11th International Symposium on Recent Advances in Drug Delivery Systems, Salt-lake City, UT*, 2003, pp. 1–5.

[33] N. Scoutaris *et al.*, "Development and Biological Evaluation of Inkjet Printed Drug Coatings on Intravascular Stent," *Mol. Pharm.*, vol. 13, pp. 125–133, 2016.

[34] M. J. Uddin, N. Scoutaris, P. Klepetsanis, B. Chowdhry, M. R. Prausnitz, and D. Douroumis, "Inkjet printing of transdermal microneedles for the delivery of anticancer agents," *Drug Deliv. Transl. Res.*, vol. 494, pp. 593–602, 2015.

[35] M. Gore, "Systems And Methods For Preparation Of Pharmaceutical Dosage Using Compositions Containing Aqueous Vesicles," US 2005/0232973 Al, 2005.

[36] P. A. Meléndez, K. M. Kane, C. S. Ashvar, M. Albrecht, and P. A. Smith,

"Thermal Inkjet Application in the Preparation of Oral Dosage Forms: Dispensing of Prednisolone Solutions and Polymorphic Characterization by Solid-State Spectroscopic Techniques," *J. Pharm. Sci.*, vol. 97, no. 7, pp. 2619–2636, 2008.

[37] S. Desai, J. Perkins, B. S. Harrison, and J. Sankar, "Understanding release kinetics of biopolymer drug delivery microcapsules for biomedical applications," *Mater. Sci. Eng. B Solid-State Mater. Adv. Technol.*, vol. 168, no. 1, pp. 127–131, 2010.

[38] A. B. M. Buanz, M. H. Saunders, A. W. Basit, and S. Gaisford, "Preparation of personalized-dose salbutamol sulphate oral films with thermal ink-jet printing," *Pharm. Res.*, vol. 28, no. 10, pp. 2386–2392, 2011.

[39] J. Pardeike *et al.*, "Nanosuspensions as advanced printing ink for accurate dosing of poorly soluble drugs in personalized medicines," *Int. J. Pharm.*, vol. 420, no. 1, pp. 93–100, 2011.

[40] N. Sandler *et al.*, "Inkjet Printing of Drug Substances and Use of Porous Substrates-Towards Individualized Dosing," *J. Pharm. Sci. Sci.*, vol. 100, no. 8, pp. 3386–3395, 2011.

[41] B. K. Lee, Y. H. Yun, J. S. Choi, Y. C. Choi, J. D. Kim, and Y. W. Cho, "Fabrication of drug-loaded polymer microparticles with arbitrary geometries using a piezoelectric inkjet printing system," *Int. J. Pharm.*, vol. 427, no. 2, pp. 305–310, 2012.

[42] N. Scoutaris, A. L. Hook, P. R. Gellert, C. J. Roberts, M. R. Alexander, and D. J. Scurr, "ToF-SIMS analysis of chemical heterogenities in inkjet micro-array printed drug/polymer formulations," *J. Mater. Sci. Mater. Med.*, vol. 23, no. 2, pp. 385–391, 2012.

[43] N. Genina, E. Maria, A. Breitenbach, J. Breitkreutz, and N. Sandler, "Evaluation of different substrates for inkjet printing of rasagiline mesylate," *Eur. J. Pharm. Biopharm.*, vol. 85, no. 3, pp. 1075–1083, 2013.

[44] N. Genina, D. Fors, M. Palo, J. Peltonen, and N. Sandler, "Behavior of

printable formulations of loperamide and caffeine on different substrates - Effect of print density in inkjet printing," *Int. J. Pharm.*, vol. 453, no. 2, pp. 488–497, 2013.

[45] L. Hirshfield, A. Giridhar, L. S. Taylor, M. T. Harris, and G. V. Reklaitis, "Dropwise additive manufacturing of pharmaceutical products for solvent-based dosage forms," *J. Pharm. Sci.*, vol. 103, no. 2, pp. 496–506, 2014.

[46] W. S. Cheow, T. Y. Kiew, and K. Hadinoto, "Combining inkjet printing and amorphous nanonization to prepare personalized dosage forms of poorly-soluble drugs," *Eur. J. Pharm. Biopharm.*, vol. 96, pp. 314–321, 2015.

[47] H. Wickström *et al.*, "Improvement of dissolution rate of indomethacin by inkjet printing," *Eur. J. Pharm. Sci.*, vol. 75, pp. 91–100, 2015.

[48] N. Scoutaris, M. Snowden, and D. Douroumis, "Taste masked thin films printed by jet dispensing," *Int. J. Pharm.*, vol. 494, no. 2, pp. 619–622, 2015.

[49] C. Varan, H. Wickström, N. Sandler, Y. Aktaş, and E. Bilensoy, "Inkjet printing of antiviral PCL nanoparticles and anticancer cyclodextrin inclusion complexes on bioadhesive film for cervical administration," *Int. J. Pharm.*, 2017.

[50] H. Vakili, R. Kolakovic, N. Genina, and N. Sandler, "Hyperspectral imaging in quality control of inkjet printed dosage forms," *Int. J. Pharm.*, vol. 483, pp. 244–249, 2014.

[51] M. Palo *et al.*, "Quantification of caffeine and loperamide in printed formulations by infrared spectroscopy," *J. Drug Deliv. Sci. Technol.*, 2016.

[52] H. Wickström *et al.*, "Colorimetry as Quality Control Tool for Individual Inkjet-Printed Pediatric Formulations," *AAPS PharmSciTech*, vol. 18, no. 2, pp. 293–302, 2016.

[53] M. Edinger, D. Bar-Shalom, J. Rantanen, and N. Genina, "Visualization and Non-Destructive Quantification of Inkjet-Printed Pharmaceuticals on Different Substrates Using Raman Spectroscopy and Raman Chemical

Imaging," *Pharm. Res.*, pp. 1023–1036, 2017.

[54] M. Edinger, D. Bar-Shalom, N. Sandler, J. Rantanen, and N. Genina, "QR encoded smart oral dosage forms by inkjet printing," *Int. J. Pharm.*, vol. 536, no. 1, pp. 138–145, 2018.

[55] N. Genina *et al.*, "Tailoring controlled-release oral dosage forms by combining inkjet and flexographic printing techniques," *Eur. J. Pharm. Sci.*, vol. 47, no. 3, pp. 615–623, 2012.

[56] D. Raijada *et al.*, "A Step Toward Development of Printable Dosage Forms for Poorly Soluble Drugs," *J. Pharm. Sci.*, vol. 102, no. 10, pp. 3694–3704, 2013.

[57] A. B. M. Buanz, C. C. Belaunde, N. Soutari, C. Tuleu, M. O. Gul, and S. Gaisford, "Ink-jet printing versus solvent casting to prepare oral films: Effect on mechanical properties and physical stability," *Int. J. Pharm.*, vol. 494, no. 2, pp. 611–618, 2015.

[58] M. Palo, K. Kogermann, I. Laidma, A. Meos, M. Preis, and J. Heina, "Development of Oromucosal Dosage Forms by Combining Electrospinning and Inkjet Printing," 2017.

[59] M. Montenegro-Nicolini *et al.*, "The Effect of Inkjet Printing over Polymeric Films as Potential Buccal Biologics Delivery Systems," *AAPS PharmSciTech*, no. 5, 2018.

[60] C. B. Fox *et al.*, "Picoliter-volume inkjet printing into planar microdevice reservoirs for low-waste, high-capacity drug loading," *Bioeng. Transl. Med.*, no. December 2016, pp. 9–16, 2017.

[61] G. F. Acosta-Vélez, C. S. Linsley, M. C. Craig, and B. M. Wu, "Photocurable Bioink for the Inkjet 3D Pharming of Hydrophilic Drugs," *Bioengineering*, vol. 4, no. 11, pp. 1–11, 2017.

[62] G. F. Acosta-Vélez, T. Z. Zhu, C. S. Linsley, and B. M. Wu, "Photocurable Poly(ethylene glycol) as a Bioink for the Inkjet 3D Pharming of Hydrophobic

Drugs," *Int. J. Pharm.*, vol. Accepted M, 2018.

[63] Y. Thabet, D. Lunter, and J. Breitkreutz, "Continuous inkjet printing of enalapril maleate onto orodispersible film formulations," *Int. J. Pharm.*, vol. 546, no. 1–2, pp. 180–187, 2018.

[64] Y. Thabet, R. Sibanc, and J. Breitkreutz, "Printing pharmaceuticals by inkjet technology: Proof of concept for stand-alone and continuous in-line printing on orodispersible films," *J. Manuf. Process.*, vol. 35, no. August, pp. 205–215, 2018.

[65] M. Alomari *et al.*, "Printing T3and T4oral drug combinations as a novel strategy for hypothyroidism," *Int. J. Pharm.*, vol. 549, no. 1–2, pp. 363–369, 2018.

[66] N. Scoutaris, M. Malamatari, A. Letellier, and D. Douroumis, "Jet dispensing of multi-layered films for the co-delivery of three antihypertensive agents," *Drug Deliv. Transl. Res.*, vol. 8, no. 1, pp. 32–42, 2018.

[67] M. Kyobula *et al.*, "3D inkjet printing of tablets exploiting bespoke complex geometries for controlled and tuneable drug release," *J. Control. Release*, vol. 261, no. March, pp. 207–215, 2017.

[68] E. A. Clark *et al.*, "3D printing of tablets using inkjet with UV photoinitiation," *Int. J. Pharm.*, vol. 529, no. 1–2, pp. 523–530, 2017.

[69] B. M. Wu, S. W. Borland, R. A. Giordano, L. G. Cima, E. M. Sachs, and M. J. Cima, "Solid free-form fabrication of drug delivery devices," *J. Control. Release*, vol. 40, pp. 77–87, 1996.

[70] C. W. Rowe, W. E. Katstra, R. D. Palazzolo, B. Giritlioglu, P. Teung, and M. J. Cima, "Multimechanism oral dosage forms fabricated by three dimensional printing.," *J. Control. Release*, vol. 66, no. 1, pp. 11–17, 2000.

[71] D. G. Yu, C. Branford-White, Z. H. Ma, L. M. Zhu, X. Y. Li, and X. L. Yang, "Novel drug delivery devices for providing linear release profiles fabricated by 3DP," *Int. J. Pharm.*, vol. 370, no. 1–2, pp. 160–166, 2009.

[72] D. G. Yu, X. L. Yang, W. D. Huang, J. Liu, Y. G. Wang, and H. Xu, “Tablets With Material Gradients Fabricated by Three-Dimensional Printing,” *J. Pharm. Sci.*, vol. 96, no. 9, pp. 2446–2456, 2007.

[73] D. Wetherhold, L. Beach, and K. Caputo, “Achieving High Drug Load With Rapid Dispersion Using 3D Printing,” 2017.

[74] Aprecia, “ZipDose Technology.” [Online]. Available: https://www.aprecia.com/technology/zipdose. [Accessed: 03-Dec-2018].

[75] S. A. Khaled, J. C. Burley, M. R. Alexander, and C. J. Roberts, “Desktop 3D printing of controlled release pharmaceutical bilayer tablets,” *Int. J. Pharm.*, vol. 461, pp. 105–111, 2014.

[76] A. Goyanes, A. B. M. Buanz, A. W. Basit, and S. Gaisford, “Fused-filament 3D printing (3DP) for fabrication of tablets,” *Int. J. Pharm.*, vol. 476, pp. 88–92, 2014.

[77] S. A. Khaled *et al.*, “Extrusion 3D Printing of Paracetamol Tablets from a Single Formulation with Tunable Release Profiles Through Control of Tablet Geometry,” *AAPS PharmSciTech*, pp. 1–11, 2018.

[78] A. Goyanes *et al.*, “3D Printing of Medicines: Engineering Novel Oral Devices with Unique Design and Drug Release Characteristics,” *Mol. Pharm.*, vol. 12, no. 11, pp. 4077–4084, 2015.

[79] A. Goyanes, M. Scarpa, M. Kamlow, S. Gaisford, A. W. Basit, and M. Orlu, “Patient acceptability of 3D printed medicines,” *Int. J. Pharm.*, vol. 530, no. 1–2, pp. 71–78, 2017.

[80] J. Wang, A. Goyanes, S. Gaisford, and A. W. Basit, “Stereolithographic ( SLA ) 3D printing of oral modified-release dosage forms,” *Int. J. Pharm.*, vol. 503, pp. 207–212, 2016.

[81] F. Fina, A. Goyanes, S. Gaisford, and A. W. Basit, “Selective laser sintering (SLS) 3D printing of medicines,” *Int. J. Pharm.*, vol. 529, no. 1–2, pp. 285–293, 2017.

[82] F. Fina, C. M. Madla, A. Goyanes, J. Zhang, S. Gaisford, and A. W. Basit, “Fabricating 3D printed orally disintegrating printlets using selective laser sintering,” *Int. J. Pharm.*, vol. 541, no. 1–2, pp. 101–107, 2018.

[83] F. Fina *et al.*, “3D printing of drug-loaded gyroid lattices using selective laser sintering,” *Int. J. Pharm.*, vol. 547, no. 1–2, pp. 44–52, 2018.

[84] J. C. Thermodynamics, S. S. Dhondge, D. W. Deshmukh, and L. J. Paliwal, “Density , speed of sound , viscosity and refractive index properties of aqueous solutions of vitamins B 1 . HCl and B 6 . HCl at temperatures ( 278 . 15 , 288 . 15 , and,” *J. Chem. Thermodyn.*, vol. 58, no. 67, pp. 149–157, 2013.

[85] Sigma-Aldrich, “Thiamine hydrochloride.” [Online]. Available: https://www.sigmaaldrich.com/catalog/product/sial/t4625?lang=en&region=GB. [Accessed: 06-Aug-2018].

[86] A. Sarkar and B. Sinha, “Effect of tetrabutylammonium hydrogen sulphate on the Solution thermodynamics of thiamine hydrochloride in aqueous solutions,” *J. Mol. Liq.*, vol. 223, pp. 321–328, 2016.

[87] M. Sharma, T. S. Banipal, and P. K. Banipal, “Molecular Interactions of Saccharides and Their Derivatives with Thiamine HCl and Pyridoxine HCl Vitamins in Aqueous Solutions: Calorimetric, Viscometric, and NMR Spectroscopic Studies,” *J. Chem. Eng. Data*, vol. 63, no. 5, pp. 1325–1351, 2018.

[88] Sigma-Aldrich, “Thiamine hydrochloride.” [Online]. Available: https://www.sigmaaldrich.com/catalog/product/sial/t4625?lang=en&region=GB. [Accessed: 11-Sep-2018].

[89] P. Chakravarty and R. Suryanarayanan, “Characterization and Structure Analysis of Thiamine Hydrochloride Methanol Solvate,” *Cryst. Growth Des.*, vol. 10, no. 10, pp. 4414–4420, 2010.

[90] P. Chakravarty, R. T. Berendt, E. J. Munson, V. G. Young JR., R. Govindarajan, and R. Suryanarayanan, “Insights into the Dehydration Behavior of Thiamine Hydrochloride (Vitamin B1) Hydrates: Part I,” *J.*

*Pharm. Sci.*, vol. 99, no. 2, pp. 816–827, 2009.

[91] K. Masuda *et al.*, “Study of the Pseudo-Crystalline Transformation from Form I to Form II of Thiamine Hydrochloride (Vitamin B1),” *Chem. Pharm. Bull. (Tokyo).*, vol. 59, no. 1, pp. 57–62, 2011.

[92] P. Chakravarty, R. Govindarajan, and R. A. J. Suryanarayanan, “Investigation of Solution and Vapor Phase Mediated Phase Transformation in Thiamine Hydrochloride,” *J. Pharm. Sci.*, vol. 99, no. 9, pp. 3941–3952, 2010.

[93] M. Teodorescu and M. Bercea, “Poly(vinylpyrrolidone) – A Versatile Polymer for Biomedical and Beyond Medical Applications,” *Polym. - Plast. Technol. Eng.*, vol. 54, no. 9, pp. 923–943, 2015.

[94] Sigma-Aldrich, “Polyvinylpyrrolidone.” [Online]. Available: https://www.sigmaaldrich.com/catalog/product/sial/pvp10?lang=en&region=GB. [Accessed: 06-Aug-2018].

[95] M. E. Schrader, “Young-Dupre Revisited,” *Langmuir*, vol. 11, no. 9, pp. 3585–3589, 1995.

[96] Fujifilm, “Dimatix Materials Printer DMP-2850 Data Sheet,” 2016.

[97] A. Rodger, *Encyclopedia of Biophysics: Concentration Determination Using Beer-Lambert Law*. Springer, 2013.

[98] U.S. Pharmacopeia, “Thiamine Hydrochloride Tablets.” [Online]. Available: http://www.pharmacopeia.cn/v29240/usp29nf24s0_m82500.html. [Accessed: 16-Apr-2018].

[99] G. Vazquez, E. Alvarez, and J. M. Navaza, “Surface tension of alcohol water+ water from 20 to 50 °C,” *J. Chem. Eng. Data*, vol. 40, no. 3, pp. 611–614, 1995.

[100] Z. Õszi and G. Pethõ, “Quantitative determination of polysorbate 20 in nasal pharmaceutical preparations by high-performance liquid chromatography,” *J. Pharm. Belg.*, vol. 53, no. 3, p. 230, 1998.

[101] W. R. Farkas *et al.*, “Polysorbate Toxicity in Neonatal Rats and Mice,” *Pharmacol. Toxicol.*, vol. 68, no. 2, pp. 154–156, 1991.

[102] Sigma-Aldrich, “TWEEN (R) 20.” [Online]. Available: https://www.sigmaaldrich.com/catalog/product/sigma/p2287?lang=en&region=GB. [Accessed: 06-Aug-2018].

[103] E. Snejdrova and M. Dittrich, *Pharmaceutically Used Plasticizers, Recent Advances in Plasticizers*. 2012.

[104] E. H. IMMERGUT and H. F. MARK, *Plasticization and Plasticizer Processes*. Advances in Chemistry; American Chemical Society, 1965.

[105] Sigma-Aldrich, “Glycerol.” [Online]. Available: https://www.sigmaaldrich.com/catalog/product/sial/g9012?lang=en&region=GB. [Accessed: 06-Aug-2018].

[106] V. Bühler, *Polyvinylpyrrolidone Excipients for Pharmaceuticals: Povidone, Crospovidone and Copovidone*. 2005.

[107] M. Parvinzadeh, S. Moradian, A. Rashidi, and M. E. Yazdanshenas, “Surface characterization of polyethylene terephthalate/silica nanocomposites,” *Appl. Surf. Sci.*, vol. 256, no. 9, pp. 2792–2802, 2010.

[108] M. Kuang, L. Wang, and Y. Song, “Controllable Printing Droplets for High-Resolution Patterns,” *Adv. Mater.*, vol. 26, no. 40, pp. 6950–6958, 2014.

[109] B. T. Cardew and R. J. Davey, “The kinetics of solvent-mediated phase transformations,” vol. 398, no. 1815, pp. 415–428, 1985.

[110] LECO Corporation, “CHN628 Series Sulfur Add-On Module - Specification Sheet,” 2012.

[111] S. Mazurek and R. Szostak, “Quantitative analysis of thiamine hydrochloride in tablets—Comparison of infrared attenuated total reflection, diffuse reflectance infrared and Raman spectroscopy,” *Vib. Spectrosc.*, vol. 62, pp. 10–16, 2012.

[112] P. Chakravarty, R. Suryanarayanan, and R. Govindarajan, “Phase Transformation in Thiamine Hydrochloride Tablets: Influence on Tablet Microstructure Physical Properties and Performance,” *J. Pharm. Sci.*, vol. 101, no. 4, pp. 1410–1422, 2012.

[113] C. Sturgess, “Fully Reactive 3D Inkjet Printing of Polydimethylsiloxane and Polyurethane,” 2018.

[114] W. Y. Yeong *et al.*, “Porous polycaprolactone scaffold for cardiac tissue engineering fabricated by selective laser sintering,” *Acta Biomater.*, vol. 6, no. 6, pp. 2028–2034, 2010.

[115] M. F. Canbolat, A. Celebioglu, and T. Uyar, “Drug delivery system based on cyclodextrin-naproxen inclusion complex incorporated in electrospun polycaprolactone nanofibers,” *Colloids Surfaces B Biointerfaces*, vol. 115, pp. 15–21, 2014.

[116] H. Sun, L. Mei, C. Song, X. Cui, and P. Wang, “The in vivo degradation, absorption and excretion of PCL-based implant,” *Biomaterials*, vol. 27, no. 9, pp. 1735–1740, 2006.

[117] C. Y. Gong *et al.*, “Biodegradable in situ gel-forming controlled drug delivery system based on thermosensitive PCL-PEG-PCL hydrogel. Part 2: Sol-gel-sol transition and drug delivery behavior,” *Acta Biomater.*, vol. 5, no. 9, pp. 3358–3370, 2009.

[118] Sigma-Aldrich, “Polycaprolactone.” [Online]. Available: https://www.sigmaaldrich.com/catalog/product/aldrich/440752?lang=en&region=GB. [Accessed: 04-Oct-2018].

[119] M. Hombreiro Pérez *et al.*, “The preparation and evaluation of poly(e-caprolactone) microparticles containing both a lipophilic and a hydrophilic drug,” *J. Control. Release*, vol. 65, no. 3, pp. 429–438, 2000.

[120] S. V. Meille *et al.*, “Definitions of terms relating to crystalline polymers (IUPAC Recommendations 2011),” *Pure Appl. Chem.*, vol. 83, no. 10, pp. 1831–1871, 2011.

[121] J. C. Jeong, J. Lee, and K. Cho, “Effects of crystalline microstructure on drug release behavior of poly(ε-caprolactone) microspheres,” *J. Control. Release*, vol. 92, no. 3, pp. 249–258, 2003.

[122] J. Holländer *et al.*, “Three-Dimensional Printed PCL-Based Implantable Prototypes of Medical Devices for Controlled Drug Delivery,” *Three-Dimensional Print. PCL-Based Implant. Prototypes Med. Devices Control. Drug Deliv.*, vol. 105, no. 9, pp. 2665–2676, 2016.

[123] J. M. Williams *et al.*, “Bone tissue engineering using polycaprolactone scaffolds fabricated via selective laser sintering,” *Biomaterials*, vol. 26, no. 23, pp. 4817–4827, 2005.

[124] Y. He, R. D. Wildman, C. J. Tuck, S. D. R. Christie, and S. Edmondson, “An Investigation of the Behavior of Solvent based Polycaprolactone ink for Material Jetting,” *Sci. Rep.*, vol. 6, no. 20852, pp. 1–10, 2016.

[125] Y. H. Yun, J. D. Kim, B. K. Lee, B. Yoo, J. H. Lee, and Y. W. Cho, “Construction of micro-patterned polymer structures by piezoelectric inkjet printing,” *Polym. - Plast. Technol. Eng.*, vol. 48, no. 12, pp. 1318–1323, 2009.

[126] Y. He *et al.*, “A new photocrosslinkable polycaprolactone-based ink for three-dimensional inkjet printing,” *J. Biomed. Mater. Res. - Part B Appl. Biomater.*, vol. 105, no. 6, pp. 1645–1657, 2017.

[127] European Chemicals Agency, “Draft background document for N,N-Dimethylacetamide (DMAC),” 2012.

[128] European Medicines Agency, “ICH guideline Q3C ( R6 ) on impurities : guideline for residual solvents,” 2017.

[129] C. Bordes *et al.*, “Determination of poly(ε-caprolactone) solubility parameters: Application to solvent substitution in a microencapsulation process,” *Int. J. Pharm.*, vol. 383, no. 1–2, pp. 236–243, 2010.

[130] Sigma-Aldrich, “N,N-Dimethylacetamide.” [Online]. Available: https://www.sigmaaldrich.com/catalog/product/aldrich/185884?lang=en&regi

on=GB. [Accessed: 04-Oct-2018].

[131] K. Phillipson, “Ageing and Crystallisation of Polycaprolactone,” 2016.

[132] M. F. Koenig and S. J. Huang, “Biodegradable blends and composites of polycaprolactone and starch derivatives,” *Polymer (Guildf).*, vol. 36, no. 9, pp. 1877–1882, 1995.

[133] R. J. Young and P. A. Lovell, *Introduction to Polymers*, 2nd ed. 1991.

[134] T. Mahnel, V. Štejfa, M. Fulem, and K. Růžička, “Recommended vapor pressures for acenaphthylene, fluoranthene, and fluorene,” *Fluid Phase Equilib.*, vol. 434, pp. 74–86, 2017.

[135] D. R. Lide, *CRC Handbook of Chemistry and Physics*, 86th ed. 2004.

[136] S. De Vrieze, T. Van Camp, A. Nelvig, B. Hagström, P. Westbroek, and K. De Clerck, “The effect of temperature and humidity on electrospinning,” *J. Mater. Sci.*, vol. 44, no. 5, pp. 1357–1362, 2009.

[137] OECD SIDS, “N,N-DIMETHYLACETAMIDE (DMAC),” in *SIDS Initial Assessment Report for 13th SIAM*, 2001, pp. 1–95.

[138] S. Thomas, Y. Grohens, and P. Jyotishkumar, *Characterization of Polymer Blends: Miscibility, Morphology and Interfaces*, 4th ed. John Wiley & Sons, 2014.

[139] C. E. Carraher Jr, *Introduction to Polymer Chemistry*, 4th ed. 2017.

[140] C. D. Reynolds, “Rheological behaviour of polymer melts and its relationship with underlying structure and topology,” 2018.

[141] S. Thomas, Y. Grohens, and P. Jyotishkumar, *Characterization of Polymer Blends*, 1st ed. 2014.

[142] H. Fruitwala, “PHASE SEPARATION IN POLYMER BLENDS AND ITS EFFECTS ON MECHANICAL PROPERTIES,” 1988.

[143] J. N. Clark, “Intermolecular interactions in polymer blends,” 1990.

[144] J. H. Guo and G. W. Skinner, “SUSTAINED RELEASE POLYMER BLEND FOR PHARMACEUTICAL APPLICATIONS,” US 6,358,525 B1, 2002.

[145] F. Siepmann, J. Siepmann, M. Walther, R. J. MacRae, and R. Bodmeier, “Polymer blends for controlled release coatings,” *J. Control. Release*, vol. 125, no. 1, pp. 1–15, 2008.

[146] T. W. Chung *et al.*, “Novel micelle-forming block copolymer composed of poly (ε- caprolactone) and poly(vinyl pyrrolidone),” *Polymer (Guildf).*, vol. 45, no. 5, pp. 1591–1597, 2004.

[147] Z. Xing and G. Yang, “Crystallization, Melting Behavior, and Wettability of Poly(e-caprolactone) and Poly(e-caprolactone)/ poly(N-vinylpyrrolidone) Blends,” *J. Appl. Polym. Sci.*, vol. 115, pp. 2747–2755, 2010.

[148] L. Amalorpava Mary *et al.*, “Centrifugal spun ultrafine fibrous web as a potential drug delivery vehicle,” *Express Polym. Lett.*, vol. 7, no. 3, pp. 238–248, 2012.

[149] Y. J. Lee, A. Elosegui-Artola, K. H. T. Le, and G. M. Kim, “Morphological cues for regulation of cell adhesion and motility with tailored electrospun scaffolds of pcl and pcl/pvp blends,” *Cell. Mol. Bioeng.*, vol. 6, no. 4, pp. 482–492, 2013.

[150] G. Jin, S. Lee, S. H. Kim, M. Kim, and J. H. Jang, “Bicomponent electrospinning to fabricate three-dimensional hydrogel-hybrid nanofibrous scaffolds with spatial fiber tortuosity,” *Biomed. Microdevices*, vol. 16, no. 6, pp. 793–804, 2014.

[151] J.-C. Wang, H. Zheng, M.-W. Chang, Z. Ahmad, and J.-S. Li, “Preparation of active 3D film patches via aligned fiber electrohydrodynamic (EHD) printing,” *Sci. Rep.*, vol. 7, no. June 2016, p. 43924, 2017.

[152] S. Roberson, A. Sehgal, A. Fahey, and A. Karim, “Time-of-flight secondary ion mass spectrometry (TOF-SIMS) for high-throughput characterization of biosurfaces,” *Appl. Surf. Sci.*, vol. 203–204, pp. 855–858, 2003.

[153] J. Feng, L. T. Weng, C. M. Chan, J. Xhie, and L. Lin, “Imaging of sub-surface nano particles by tapping-mode atomic force microscopy,” *Polymer (Guildf).*, vol. 42, no. 5, pp. 2259–2262, 2001.

[154] C. Seo, D. Jang, J. Chae, and S. Shin, “Altering the coffee-ring effect by adding a surfactant-like viscous polymer solution,” *Sci. Rep.*, vol. 7, no. 1, pp. 1–9, 2017.

[155] C. Yu, Q. Xie, Y. Bao, G. Shan, and P. Pan, “Crystalline and Spherulitic Morphology of Polymers Crystallized in Confined Systems,” *Crystals*, vol. 7, no. 6, p. 147, 2017.

[156] P. Costa and J. M. S. Lobo, “Modeling and comparison of dissolution profiles,” *Eur. J. Pharm. Sci.*, vol. 13, pp. 123–133, 2001.

[157] R. Korsmeyer and N. Peppas, “Effect of the Morphology of Hydrophilic Polymeric,” *J. Membr. Sci. 9*, vol. 9, pp. 211–227, 1981.

[158] R. W. Korsmeyer, R. Gurny, E. Doelker, P. Buri, and N. A. Peppas, “Mechanism of release from porous hydrophilic polymers,” *Int. J. Pharm.*, vol. 15, pp. 25–35, 1983.

[159] E. P. Holowka and S. K. Bhatia, *Drug delivery: Materials design and clinical perspective*. Springer Science, 2014.

[160] C. G. Wilson and P. J. Crowley, *Controlled Release in Oral Drug Delivery*. 2011.

[161] B. Dekyndt, J. Verin, C. Neut, F. Siepmann, and J. Siepmann, “How to easily provide zero order release of freely soluble drugs from coated pellets,” *Int. J. Pharm.*, vol. 478, no. 1, pp. 31–38, 2015.

[162] Y. Qui and D. Zhou, “Understanding Design and Development of Modified Release Solid Oral Dosage Forms,” *J. Valid. Technol.*, vol. 17, no. 2, pp. 23–32, 2011.

[163] A. Ghaffari, H. Abdollahi, M. R. Khoshayand, I. S. Bozchalooi, A. Dadgar, and M. Rafiee-Tehrani, “Performance comparison of neural network training

algorithms in modeling of bimodal drug delivery," *Int. J. Pharm.*, vol. 327, no. 1–2, pp. 126–138, 2006.

[164] A. C. Shah, N. J. Britten, L. S. Olanoff, and J. N. Badalamenti, "Gel-matrix systems exhibiting bimodal controlled release for oral drug delivery," *J. Control. Release*, vol. 9, no. 2, pp. 169–175, 1989.

[165] G. S. MacLeod, J. T. Fell, and J. H. Collett, "An in vitro investigation into the potential for bimodal drug release from pectin/chitosan/HPMC-coated tablets," *Int. J. Pharm.*, vol. 188, no. 1, pp. 11–18, 1999.

[166] A. Watanabe and H. Nakamchai, "Polymorphism of Thiamine Hydrochloride," *Yakugaku Zasshi*, vol. 96, no. 10, pp. 1236–1240, 1976.

[167] G. C. Ceschel, R. Badiello, C. Ronchi, and P. Maffei, "Degradation of components in drug formulations: A comparison between HPLC and DSC methods," *J. Pharm. Biomed. Anal.*, vol. 32, no. 4–5, pp. 1067–1072, 2003.

[168] R. M. Maggio, N. L. Calvo, S. E. Vignaduzzo, and T. S. Kaufman, "Pharmaceutical impurities and degradation products: Uses and applications of NMR techniques," *J. Pharm. Biomed. Anal.*, vol. 101, pp. 102–122, 2014.

[169] D. A. Armbruster and T. Pry, "Limit of blank, limit of detection and limit of quantitation," *Clin. Biochem. Rev.*, vol. 29, no. i, pp. 49–52, 2008.

[170] USP-NF, "General Chapter <467> Residual Solvents."

[171] K. Grodowska and A. Parczewski, "Analytical methods for residual solvents determination in pharmaceutical products," *Acta Pol. Pharm. - Drug Res.*, vol. 67, no. 1, pp. 13–26, 2010.

[172] E. Snejdrova and M. Dittrich, *Pharmaceutically Used Plasticizers, Recent Advances in Plasticizers*. 2012.

[173] B. Oshlack, M. Chasin, and F. Pedi Jr., "CONTROLLED-RELEASE FORMULATIONS COATED WITH AQUEOUS DISPERSIONS OF ETHYLCELLULOSE," 5,472,712, 1995.

[174] L. F. Siew, A. W. Basit, and J. M. Newton, “The properties of amylose-ethylcellulose films cast from organic-based solvents as potential coatings for colonic drug delivery,” *Eur. J. Pharm. Sci.*, vol. 11, no. 2, pp. 133–139, 2000.

[175] S. Muschert, “POLYMERIC COATINGS FOR SOLID DOSAGE FORMS : CHARACTERIZATION AND OPTIMIZATION,” 2008.

[176] B. H. Kim *et al.*, “A study of the jetting failure for self-detected piezoelectric inkjet printheads,” *IEEE Sens. J.*, vol. 11, no. 12, pp. 3451–3456, 2011.

[177] Mutracx, “Predict - Why does every drop count?” [Online]. Available: http://www.mutracx.com/index.php/english/lunaris/predict/. [Accessed: 17-Nov-2018].

[178] M. McAllister, “Dynamic dissolution: A step closer to predictive dissolution testing?,” *Mol. Pharm.*, vol. 7, no. 5, pp. 1374–1387, 2010.